



Textron Aviation
Raytheon Missile Systems
AIAA Foundation

The 2018-19 AIAA/Textron Aviation/Raytheon Missile Systems Design/Build/Fly Competition Flyoff was held at TIMPA Field in Tucson, AZ on the weekend of April 11-14, 2019. This was the 23rd year for the competition. Of the 138 proposals submitted and judged, 113 teams were invited to submit a formal report for the next phase of the competition. 104 teams submitted design reports to be judged, and 77 teams attended the flyoff (21 international). About 800 students, faculty, and guests were present. Of the 77 teams, 65 successfully completed tech inspection. The weather was mild and allowed for non-stop flying. Of the 255 official flight attempts, 93 resulted in a successful score with 38 teams achieving a successful flight score and 26 teams successfully completing all four missions (one ground and three flight). The quality of the teams, their readiness to compete, and the execution of the flights continues to improve each year.

The contest theme this year was Aircraft Carrier Operations. Each aircraft was required to have a 4 foot minimum wing span. To simulate the transition from the hanger to the flight deck, the aircraft were required to roll through a 3 foot x 2 foot box necessitating wing folding and locking mechanisms which had to operate remotely and without external assistance. The aircraft were required to complete three flight missions, each taking off from a 4 foot by 10 foot “carrier flight deck”. The first mission was a Delivery Flight with no payload for three laps within five minutes. The second mission was a Reconnaissance Flight with the addition of a radome which was required to be fixed during take-off and landing but rotating during cruise. The final mission was an Attack Flight which included the dropping of foam “attack stores”. During this mission, ten minutes were provided to complete as many laps as possible while dropping only one store per lap. Teams were also required to complete a timed ground mission demonstrating full carrier operations. As usual, the total score is the product of the total mission score and design report score. More details on the mission requirements can be found at the competition website: <http://www.aiaadbf.org>.

First Place went to the University of Ljubljana, Second Place went to the Georgia Institute of Technology and Third Place went to the FH JOANNEUM University of Applied Sciences. A full listing of the results is included below. The Best Paper Award, sponsored by the Design Engineering TC for the highest report score, went to the University of Southern California with a score of 93.13.

We owe our thanks for the success of the DBF competition to the efforts of many volunteers from Textron Aviation, Raytheon Missile Systems, and the AIAA sponsoring technical committees: Applied Aerodynamics, Aircraft Design, Flight Test, and Design Engineering. These volunteers collectively set the rules for the contest, publicize the event, gather entries, judge the written reports, and organize the flyoff. Thanks also go to the Premier Sponsors: Raytheon Missile Systems and Textron Aviation, and also to the AIAA Foundation for their financial support as well as our Gold sponsors this year – AeroVironment, Aurora Flight Sciences, General Atomics, Mathworks, and Honeywell Aerospace. Special thanks go to Raytheon Missile Systems for hosting the flyoff this year.

Finally, this event would not be nearly as successful without the hard work and enthusiasm from all the students and advisors. If it weren't for you, we wouldn't keep doing it.

Matt Angiulo
For the DBF Organizing Committee

UNIVERSITY OF SOUTHERN CALIFORNIA
PRESENTS

ExS Calibur



AIAA DESIGN-BUILD-FLY
2018-2019
DESIGN REPORT

Table of Contents

ACRONYMS, ABBREVIATIONS, AND SYMBOLS	3
1.0 EXECUTIVE SUMMARY	4
2.0 MANAGEMENT SUMMARY	5
2.1 TEAM ORGANIZATION.....	5
2.2 MILESTONE CHART.....	6
3.0 CONCEPTUAL DESIGN.....	6
3.1 MISSION REQUIREMENTS	7
3.2 DESIGN REQUIREMENTS	9
3.3 CONFIGURATION SELECTION	11
3.4 AIRCRAFT COMPONENTS SELECTION, PROCESSES AND RESULTS	13
3.5 FINAL CONCEPTUAL DESIGN.....	16
4.0 PRELIMINARY DESIGN	16
4.1 DESIGN METHODOLOGY.....	16
4.2 MISSION MODEL	17
4.3 DESIGN TRADE STUDIES	19
4.4 AERODYNAMICS.....	21
4.5 STABILITY AND CONTROL	25
4.6 PREDICTED AIRCRAFT PERFORMANCE	27
5.0 DETAIL DESIGN.....	27
5.1 DIMENSIONAL PARAMETERS TABLE	27
5.2 STRUCTURAL CHARACTERISTICS AND CAPABILITIES.....	28
5.3 SUB-SYSTEM DESIGN	28
5.4 WEIGHT AND MASS BALANCE	36
5.5 FLIGHT AND MISSION PERFORMANCE	37
5.6 DRAWING PACKAGE	37
6.0 MANUFACTURING PLAN	42
6.1 MANUFACTURING PROCESSES INVESTIGATED	42
6.2 MANUFACTURING PROCESSES SELECTED	43
6.3 MANUFACTURING MILESTONES.....	46
7.0 TESTING PLAN	46
7.1 TEST OBJECTIVES	47
7.2 SUBSYSTEM TESTING	47
7.3 FLIGHT TEST SCHEDULE AND FLIGHT PLAN	53
7.4 FLIGHT CHECKLISTS	54
8.0 PERFORMANCE RESULTS.....	55
8.1 DEMONSTRATED PERFORMANCE OF KEY SUBSYSTEMS	55
8.2 DEMONSTRATED FLIGHT PERFORMANCE OF COMPLETED AIRCRAFT	58
9.0 BIBLIOGRAPHY.....	60

ACRONYMS, ABBREVIATIONS, AND SYMBOLS

α	Aircraft angle of attack	L/D	Lift to drag ratio
δ_e	Elevator deflection	$(L/D)_{cruise}$	Lift to drag ratio in cruise
δ_{flap}	Flap deflection	$(L/D)_{max}$	Maximum lift-to-drag ratio
μ_s	Rolling resistance coefficient	M_1	Mission 1 Flight Score
η_b	Battery efficiency factor	M_2	Mission 2 Flight Score
ω_n	Natural frequency	M_3	Mission 3 Flight Score
ζ	Damping coefficient	MAC	Mean Aerodynamic Chord
AIAA	American Institute of Aeronautics and Astronautics	MDO	Multidisciplinary design optimization
AR	Aspect Ratio	N	Number of laps
AVL	Athena Vortex Lattice	NiCd	Nickel-Cadmium
b	Wingspan	NiMH	Nickel-Metal Hydride
c	Wing chord	RAC	Rated Aircraft Cost
C_d, C_D	Drag coefficient (2D, 3D)	R/C	Remote-controlled
C_{D0}	Zero-lift drag coefficient	Re	Reynolds number
$C_{D,i}$	Induced drag coefficient	S, S_w	Wing planform area
$C_{D,P}$	Parasite drag coefficient	$S_{horizontal}$	Horizontal stabilizer planform area
C_f	Coefficient of friction	S_{ref}	Reference Area
C_l, C_L	Coefficient of lift (2D, 3D)	$S_{vertical}$	Vertical stabilizer planform area
$C_{L,max}$	Maximum lift coefficient	T	Time
$C_{m\alpha}$	Change in pitching moment coefficient due with α	τ	Dynamic mode's time constant
C_P	Coefficient of power	T_{USC}	USC Time
C_T	Coefficient of thrust	TOFL	Take Off Field Length
CG	Center of Gravity	USC	University of Southern California
D	Drag	V	Voltage
d	Diameter	V_{stall}	Stall velocity
DBF	Design/Build/Fly	V_H	Horizontal tail volume coefficient
e	Oswald efficiency factor	V_V	Vertical tail volume coefficient
ESC	Electronic Speed Controller	W/S	Wing loading
EW	Empty Weight	WS	Wingspan
FEA	Finite Element Analysis	y	Lateral spacing of stores on wing
FoM	Figures of Merit		
GM	Ground Mission Score		
I	Current		
Kv	Speed Constant		
L	Lift		
l_t	Tail moment arm		
l/d	Fineness ratio		

1.0 EXECUTIVE SUMMARY

The objective of the 2018-19 American Institute of Aeronautics and Astronautics (AIAA) Design/Build/Fly (DBF) competition is to simulate the design of a multi-purpose aircraft to support carrier operations [1]. The aircraft must be able to fit within a 3 ft (0.9 m) wide by 2 ft (0.6 m) tall box. All moving components must be able to remotely transition from a stowed to a flight configuration and mechanically lock without assistance. The aircraft must be able to complete three flight missions and a Ground Mission that simulates flight deck operations and maintenance. The flight missions require the plane the takeoff from a 10 ft (3 m) long ramp that is inclined at 5°. The payloads include a team-built radome and attack stores provided by DBF.

The first flight mission consists of flying three laps in 5 minutes or less without any payloads. The second flight mission requires the plane to complete three laps as fast as possible while carrying a team-built radome. The radome must start rotating after the first 180° turn and stop rotating after the final 180° turn prior to landing. The third flight mission consists of flying as many laps as possible within ten minutes while carrying a team-specified number of attack stores. During this mission, one store must be dropped per downwind leg. The Ground Mission demonstrates the plane's remote transition from stowed to flight configuration as well as the attachment and actuation of the payloads. The flight missions must be completed in order while the Ground Mission can be attempted before or after any flight mission.

Analysis of the mission scoring was conducted during the preliminary design phase and indicated that maximizing the number of Mission 3 laps flown was critical to this year's design. Performance trade studies estimated that 13 was the maximum number of laps the plane could fly in 10 minutes; thus, carrying 13 attack stores would give the highest score.

During the conceptual design phase, a monoplane configuration was selected for its favorable stability characteristics and attack store arrangement. An H-tail was selected as the empennage due to spatial constraints and to minimize flow interference from the radome onto the tail control surfaces. The wing and tail were balsa and plywood built-up. Their loads were carried through spars constructed of balsa shear webbing and carbon spar caps. The wing area and tail sizing were first determined analytically and then validated through extensive takeoff field length (TOFL) testing using a team-built ramp. A tricycle landing gear configuration was utilized to improve load dispersion and ground handling. The fuselage was built from Kevlar and featured a carbon tube and foam stringers that transfer flight and landing loads.

The radome structure utilized plywood ribs in a waffle-pattern with a solite skin and was placed directly aft of the wing to minimize moments during flight. The rotation and braking of the radome was controlled by a servo. 13 attack stores were attached directly under the wing with zip ties and were released using servos. The stores were placed in tandem to reduce drag while a single store was not in tandem. Additionally, payload and wing folding mechanisms were designed for quick installation to reduce Ground Mission time. All components were designed to survive flight loads and validated through in-lab, wind tunnel, and flight testing. Data was collected at flight tests to validate theoretical performance and drag models.

University of Southern California's aircraft, *ExSCalibur* (Figure 1), is designed to maximize score by maximizing flight performance while also minimizing drag and weight. *ExSCalibur* will take off at 20 ft/s (6.1 m/s) before climbing to cruise altitude and velocity. With a top flight speed of 110 ft/s (33.5 m/s), *ExSCalibur* will complete three laps for Mission 2 in 116 s while carrying a rotating radome. With 13 attack stores, *ExSCalibur* will complete 13 laps in ten minutes for Mission 3. *ExSCalibur* will be able to complete the Ground Mission in 30 s. At an empty weight of 7.4 lb (3.4 kg) with a 6.5 ft (2.0 m) wingspan, *ExSCalibur* is estimated to have a final score of 1,843.

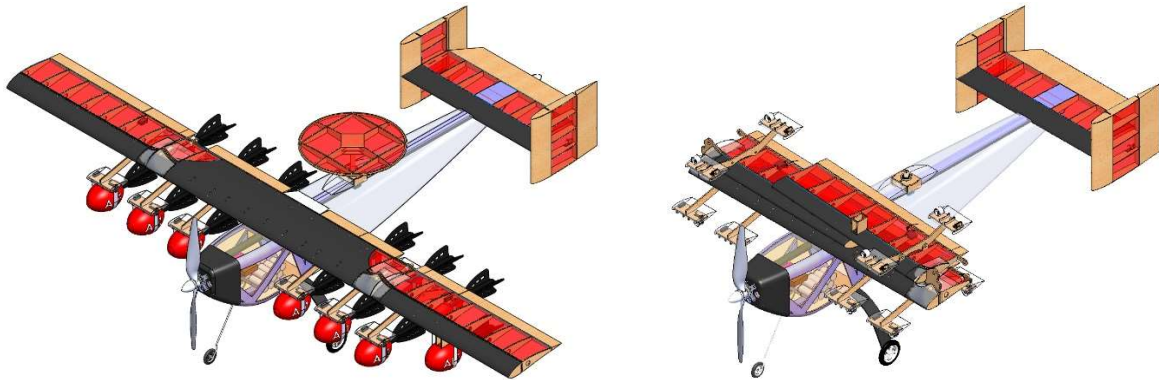


Figure 1: *ExSCalibur* with Mission 2 & 3 payloads (left) and in stowed configuration (right)

2.0 MANAGEMENT SUMMARY

The 2018-19 AeroDesign Team of USC consists of 35 students that participate on an extracurricular basis. Six team members are seniors while the remainder are juniors and underclassmen. The team is entirely student-led but receives guidance and suggestions from industry advisors, USC alumni, and faculty members at weekly meetings and design reviews.

2.1 TEAM ORGANIZATION

The AeroDesign Team of USC employs a matrix structure of leadership, similar to the management hierarchy of most aerospace firms. The team leadership for this competition year is shown in Figure 2.

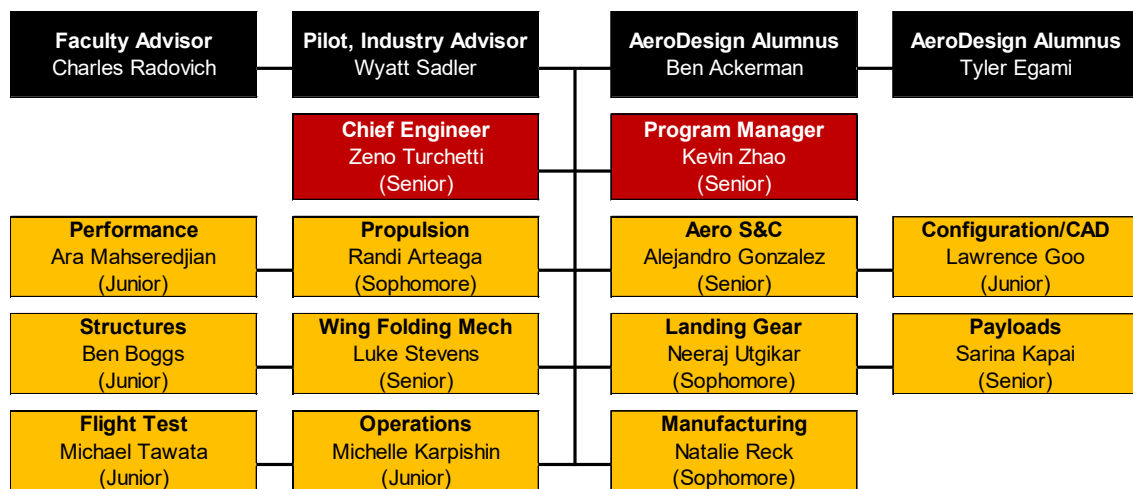


Figure 2: Organization Chart of the USC AeroDesign Team



Team leaders, as shown in **red**, receive suggestions from team advisors (**black**) and coordinate the design effort among sub-team leaders (**gold**). The Chief Engineer and Program Manager divide tasks such that the Chief Engineer supervises design, build, and test efforts while the Program Manager sets major milestones, ensures adherence to the master schedule, and works with the Operations Manager to obtain funding and manage team logistics.

2.2 MILESTONE CHART

The Program Manager maintains a schedule, shown in Figure 3, that is used to plan workflow, allocate resources, and track tasks to completion. An unplanned task (indicated by ***) was required in November and December due to complexity associated with the motor configuration downselect. The manufacturing schedule set at the beginning of the year was adjusted accordingly as shown by “Actual Timing”. Note that actual timing is not shown for future tasks.

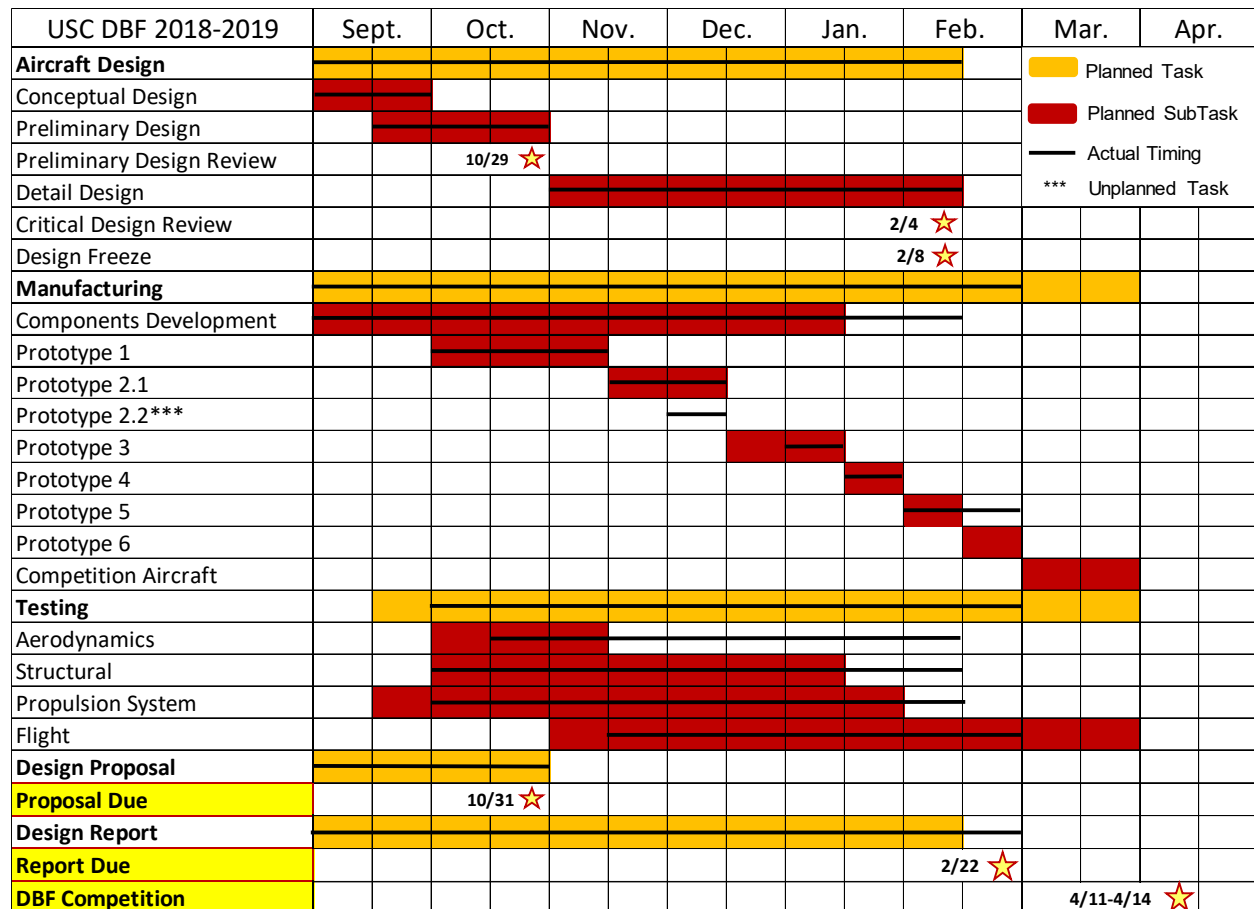


Figure 3: Master schedule showing the planned and actual timing for team tasks

3.0 CONCEPTUAL DESIGN

In the conceptual design phase, the team analyzed the competition requirements and scoring equations to set design objectives for the competition year. Numerous aircraft configurations were evaluated to identify the highest scoring configuration. The final conceptual design is presented in Section 3.5.

3.1 MISSION REQUIREMENTS

The rules for the 2018-19 American Institute of Aeronautics and Astronautics (AIAA) Design/Build/Fly (DBF) contest simulate the design of a multi-purpose aircraft to support carrier operations [1]. This requires the aircraft to fit inside of a 3 ft (0.9 m) wide and 2 ft (0.6 m) tall box while having a 4 ft (1.2 m) minimum wingspan. The aircraft was designed to complete the contest's three flight missions and Ground Mission, which can be completed before or after any of the flight missions.

Each flight mission requires the aircraft to take off from a 10 ft (3 m), 5° inclined ramp parallel to the runway and then fly competition laps, consisting of two 1,000 ft (300 m) straightaways, two 180° turns, and one 360° turn in the opposite direction of the 180° turns. The flight course requires that the aircraft make right-hand and left-hand turns and land within the bounds of the runway, thereby demonstrating flight stability and handling characteristics of the aircraft. A schematic of a competition lap is shown in Figure 4. Prior to each flight, the flight crew must arrive at the flight line with the aircraft in stowed configuration. The crew will then have 5 minutes to remotely transition the aircraft to flight configuration and then attach the payloads: a rotating radome for Mission 2 and attack stores for Mission 3.

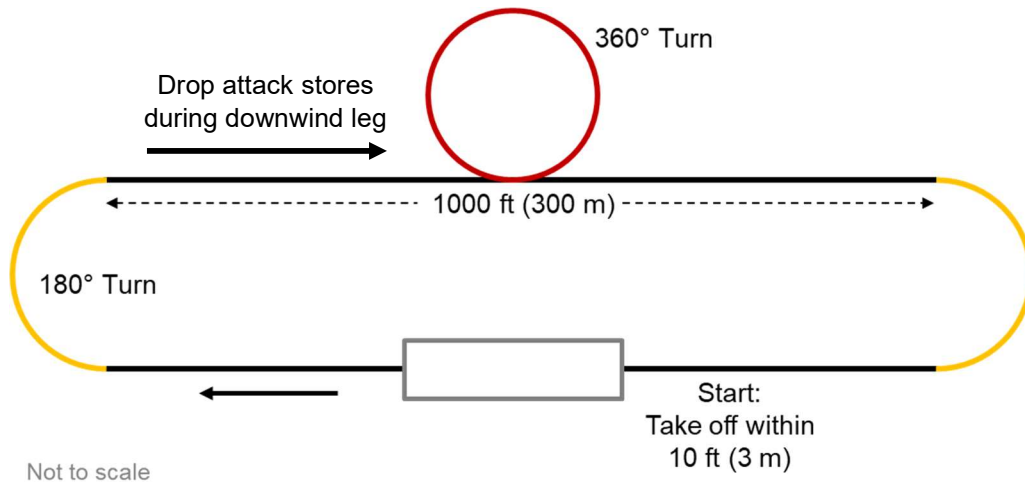


Figure 4: AIAA Competition Lap Layout

3.1.1 SCORING SUMMARY

The overall score for the 2019 AIAA DBF contest is given by Eq. 1.

$$\text{Score} = \text{Written Report Score} \cdot \text{Total Mission Score} \quad \text{Eq. 1}$$

The *Written Report Score* is based on the quality of the design report, and the *Total Mission Score* is the sum of each flight and Ground Mission score given by Eq. 2.

$$\text{Total Mission Score} = M_1 + M_2 + M_3 + GM \quad \text{Eq. 2}$$

M_1 , M_2 , M_3 , and GM denote the scores for Mission 1, Mission 2, Mission 3, and Ground Mission respectively.

3.1.2 MISSION SCORING

Fight Mission 1 – Delivery Mission

The objective of Mission 1 is to successfully complete 3 competition laps within a 5-minute flight window without any payloads. Time starts when the throttle is initiated for takeoff. The score for this mission is binary with $M_1 = 1$ for a successful mission and $M_1 = 0$ for an unsuccessful mission.

Flight Mission 2 – Reconnaissance Mission

The objective of Mission 2 is to complete 3 laps as quickly as possible while carrying a team-built rotating radome. Time starts when the throttle is initiated for takeoff. The score for this mission is given by Eq. 3,

$$M_2 = 1 + \frac{(T_{M2})_{BEST}}{(T_{M2})_{USC}} \quad \text{Eq. 3}$$

where $(T_{M2})_{BEST}$ is the fastest successful time of any team for Mission 2 and $(T_{M2})_{USC}$ is the time USC takes.

Flight Mission 3 – Attack Mission

The objective of Mission 3 is to complete as many laps as possible within a 10-minute flight window while carrying a team-determined number of attack stores. One store must be dropped per downwind leg of the course shown in Figure 4 to be considered a successful scoring lap. A minimum of 4 stores must be carried under the wing. Additional stores can be carried under either the wing or the fuselage. The score for this mission is given by Eq. 4,

$$M_3 = 2 + N_{scoring\ laps} \quad \text{Eq. 4}$$

where $N_{scoring\ laps}$ is the number of successful laps.

Ground Mission – Flight Deck Maintenance and Operations Mission

The objective of the Ground Mission is to remotely transition the aircraft from stowed to flight configuration, install and show rotation of the radome, and install and show deployment of 4 attack stores. The Ground Mission can be completed before or after any flight mission. The score for this mission is given by Eq. 5,

$$GM = \frac{(T_{GM})_{BEST}}{(T_{GM})_{USC}} \quad \text{Eq. 5}$$

where $(T_{GM})_{BEST}$ is the fastest successful time of any team for the Ground Mission and $(T_{GM})_{USC}$ is the time USC takes. Note that everything listed above is counted towards $(T_{GM})_{USC}$ except for the activation of the radome and the deployment of the stores.

3.1.3 AIRCRAFT CONSTRAINTS

In addition to the flight missions described above, the aircraft must meet the following requirements:

Stowed Configuration

- The wing span must be a minimum of 4 ft (1.2 m).

- The aircraft must fold and fit inside a space 3 ft (0.9 m) wide and 2 ft (0.6 m) tall.
- The nose and all landing gear must fit within a distance of 2 ft (0.6 m).
- The aircraft must remotely transition from stowed to flight configuration and mechanically lock without assistance.

Takeoff

- The aircraft must have a “tail hook” on its centerline for a crew member to hold while the aircraft throttles up.
- The aircraft must takeoff from a ramp that is 4 ft (1.2 m) wide and 10 ft (3.0 m) long, inclined at 5°.

Propulsion

- Batteries must be Nickel-Cadmium (NiCd) or Nickel-Metal Hydride (NiMH).
- Components used for the propulsion package must be commercially available.

Payloads – Rotating Radome

- The radome must have a minimum diameter of 12 in. (30.5 cm) and a thickness of 1 in. (2.5 cm) at the center.
- The radome must be mounted on the aircraft centerline.
- The radome must be 3 in. (7.6 cm) away from any part of the aircraft, excluding mounting structure.

Payloads – Attack Stores

- A minimum of 4 attack stores must be carried under the wing; additional stores can be carried under either the wing or the fuselage.
- There must be at least a 0.5 in. (1.3 cm) clearance between stores and any part of the fuselage.

3.2 DESIGN REQUIREMENTS

Design requirements were developed from the scoring equations and competition guidelines in order to guide the design process. By analyzing the scoring equations, an aircraft configuration and design approach were selected to maximize the total score. Mission requirements and score equations were translated into design parameters, as shown in Table 1.

Table 1: Design parameters

Mission	Objective	Design Parameter
2 – Reconnaissance	Maximize flight speed to minimize flight time for 3 laps	$(T_{M2})_{USC}$
3 – Attack	Maximize endurance, flight speed, and payload storage to fly maximize number of scoring laps	$N_{scoring\ laps}$
GM – Flight Deck Maintenance and Operations	Optimize wing actuation and payload attachment to minimize transition/loading time	$(T_{GM})_{USC}$

3.2.1 FLIGHT SCORE SENSITIVITY ANALYSIS

The scoring equations, Eq. 1 - Eq. 5, were analyzed to set design objectives by identifying mission objectives and design parameters, shown in Table 1, that were most important in maximizing the score. Analysis began by estimating the top mission performance of any competitor in each of the three missions and performance for a baseline USC competition aircraft, as shown in Table 2. The assumptions guiding these estimates are detailed in the following paragraphs.

Table 2: Estimates for top performance (competitors) and baseline aircraft parameters (USC)

Top Competitor Mission Performances	Assumption
$(T_{M2})_{BEST}$	90 s
$(T_{GM})_{BEST}$	15 s
Top USC Mission Performances	Assumption
$(T_{M2})_{USC}$	120 s
$(T_{GM})_{USC}$	30 s
$N_{scoring\ laps}$	12

Competitor Assumptions

Competitor score assumptions were based on top competitor aircraft performances over the past 20+ DBF competitions that had similar payload, weight, and speed configurations. At the 2017 DBF contest, a competitor flew 3 laps in 93 s, which was the fastest time that year. From this, performance lap times can be approximated at around 30 s, giving a $(T_{M2})_{BEST}$ of 90 s for a top performance plane at this year's contest. In the 2015 contest, a similar loading and unloading Ground Mission was performed. Averaging the fastest three competitors times, $(T_{GM})_{BEST}$ was approximately 15 s.

USC Mission Performances

The baseline assumptions for USC's aircraft are estimated based on the team's performance in previous competitions. In 2013, USC flew 6 laps in 3.5 minutes and had a shortened takeoff field length (TOFL) of 30 ft, giving an average lap time of 35 s [2]. The assumed USC time for Mission 2 was 120 s to account for the larger aircraft this year. In 2017, USC flew 6 laps in 5 minutes, averaging 50 s laps [3]. When extrapolated to a 10 minute flight, the total laps flown would be 12. This would require 12 attack stores, which is similar to the payload weight of 1.5 lb (0.7 kg) in 2017 [3]. Based on team-built prototypes and the assumed competitor Ground Mission time, the USC Ground Mission time was doubled as a conservative estimate. Sensitivity of each score variable was plotted in Figure 5 to observe the effect on the final score.

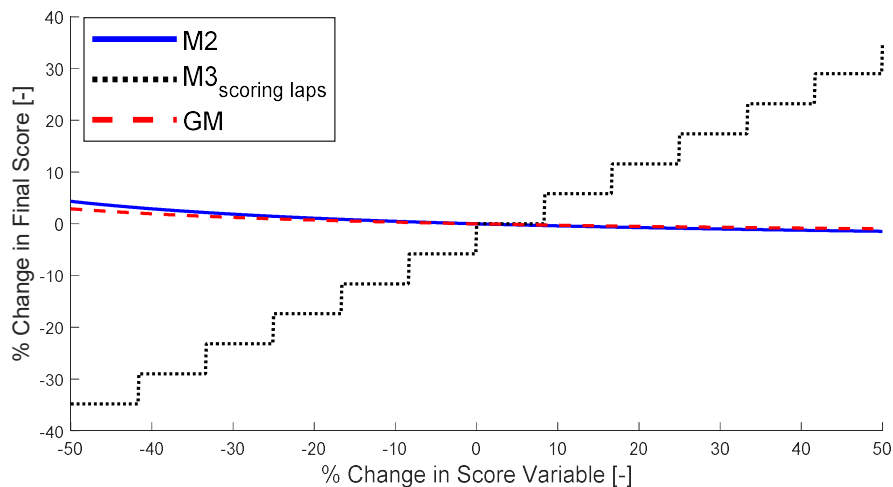


Figure 5: Score analysis representing impact of score parameters

The score analysis studied individual parameters' effect on overall score. The step pattern to Mission 3 sensitivity is because only completed, integer laps are counted. From the analysis, it was shown that the number of laps completed in Mission 3 has the greatest impact on the total mission score. Further analysis showed that a plane that flies the fastest on Mission 2 and flies 11 laps on Mission 3 would lose to a plane that has a poor Mission 2 time but flies 12 laps on Mission 3. Therefore, the primary objective was set to focus on optimizing and designing a plane for Mission 3 performance.

3.3 CONFIGURATION SELECTION

Once the design requirements were determined, a configuration downselect process was used to select a preliminary aircraft configuration. After the aircraft configuration was selected, concepts for each individual component were selected.

3.3.1 AIRCRAFT CONFIGURATION

The configuration downselect method used a series of estimates and assumptions that allows for a quantitative comparison of configurations across a range of design parameters. Figures of Merit (FoM) were derived from the design parameters as shown in Table 1. Each FoM was assigned a score factor and was used to identify the most competitive aircraft configuration.

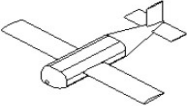
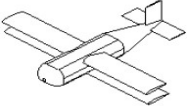

Table 3: Figures of Merit and corresponding design parameters for aircraft configuration selection

Figures of Merit	Design Parameters	Score Factor
Flight Speed	$(T_{M2})_{USC}, N_{scoring\ laps}$	0.4
Payload Storage	$N_{scoring\ laps}$	0.3
Stability and Control	$(T_{M2})_{USC}, N_{scoring\ laps}$	0.2
Wing Folding Complexity	$(T_{GM})_{USC}$	0.1

The score factor for each FoM was derived qualitatively by assigning relative importance to each factor based on the design parameters for the aircraft. The score factors were weighted such that the sum of the score factors equaled one and are shown in the third column of Table 3. Next, the configurations were scored for each FoM (independent of the other FoMs). The monoplane was used as the baseline to which all other configurations were compared; and so, it was assigned a 0 for each FoM. For the other configurations, a value of 0 implied that the configuration scored as well as a monoplane for the given FoM, a value of -1 indicates a worse score, and a value of 1 meant it would be expected to perform better. The final step was to multiply each configuration evaluation with the corresponding FoM Score Factor, and then sum the values for each configuration. The Total Score for each configuration, shown at the bottom of Table 4, provides the basis for the quantitative comparison, with the highest score being most favorable.

The aircraft configuration downselect compared the baseline monoplane to the biplane and blended wing body (BWB) in an effort to generate more lift for the short TOFL and carry more payload, respectively. The results of this comparison is shown in Table 4.

Table 4: Aircraft configuration downselect

				
Figures of Merit	Score Factor	Monoplane	Biplane	BWB
Flight Speed	0.4	0	-1	-1
Payload Storage	0.3	0	-1	1
Stability and Control	0.2	0	-1	-1
Wing Folding Complexity	0.1	0	-1	0
Total Score		0	-1	-0.3



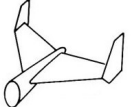
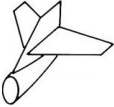
As shown in Table 4, there were several disadvantages to the biplane and BWB configurations. A lower flight speed and worse stability characteristics were the main factor that eliminated both configurations. Additionally, the biplane would have added wing folding complexity and carry less stores since it would have a shorter span; and so, the monoplane configuration was selected.

3.3.2 TAIL CONFIGURATION

With a monoplane configuration selected, an empennage was required to maintain longitudinal stability. The main factors governing empennage selection were staying within spatial constraints, maximizing stability, and minimizing drag. The conventional configuration was set as the baseline and the following designs were compared with the downselect shown in Table 5:

- **Conventional:** The conventional design is simple to design and implement, while providing necessary stability and control requirements.
- **V-Tail:** Two lifting surfaces form a V-shape and, through mixed servo action, provide both pitch and yaw control, which can contribute to less pitch and yaw authority [6].
- **H-Tail:** Two vertical stabilizers are attached to the ends of the horizontal stabilizer to reduce the height of the vertical stabilizers, but maintains similar lateral stability as the conventional tail
- **Cruciform:** Similar to conventional tail but part of the vertical stabilizer is shifted below the tail cone in order to reduce overall height

Table 5: Empennage downselect

					
Figures of Merit	Score Factor	Conventional	V-Tail	H-Tail	Cruciform
Spatial Constraint	0.4	0	1	1	0
Stability & Control	0.2	0	-1	0	-1
Drag	0.2	0	1	-1	0
Design & Build	0.1	0	-1	0	-1
Assembly	0.1	0	0	0	-1
Total Score		0	-0.3	0.2	-0.4

The results from Table 5 were used to select the H-Tail empennage design. The lower height for Ground Mission requirement of 2 ft (0.6 m), ease of construction, and effective control made it the favorable tail configuration for this aircraft.

3.4 AIRCRAFT COMPONENTS SELECTION, PROCESSES AND RESULTS

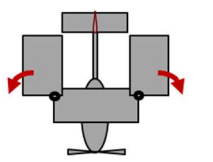
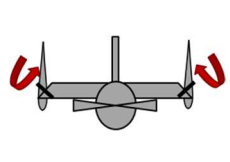
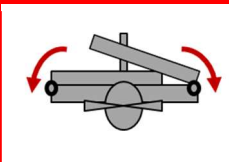
Following the aircraft and tail configuration selection, individual wing folding, payload configuration, propulsion, and landing gear components were chosen. Each configuration choice was quantified using downselect tables similar to those detailed in Sections 3.3.1 and 3.3.2. The highest scoring components were selected for the preliminary design.

3.4.1 WING FOLDING

The aircraft must roll through a 2 ft (0.6 m) tall and 3 ft (0.9 m) wide box, requiring the wing to fold or rotate. Before each flight, the aircraft must transition from stowed to flight configuration and mechanically self-lock without assistance. This deployment is timed as a part of the Ground Mission score. Three folding methods were prototyped based on the wing configuration selected in Section 3.3.1. Each mechanism was evaluated based on weight, integration with wing structure, simplicity, and deployment speed. The trailing edge hinge was set as the baseline for its mechanism simplicity as shown in Table 6.

- **Trailing Edge Hinge:** Rotates tip section backwards in-plane with the wing using a hinge on the aft-spar. Lift loads transfer through the hinge point, requiring stronger structure that was heavier.
- **E-2 Sto-Wing:** Northrop Grumman's patented aft-folding method allowing the wing to fold backwards and rotate 90° [7]. Alignment is crucial; thus, reliable manufacturing was an issue.
- **Turbo:** Folds upwards and on top of the fuselage and root section of the wing. Simple design but needs to resist all lift loads from tip section when in flight.

Table 6: Wing Mechanism Downselect

				
Figure of Merit	Score Factor	Trailing Edge Hinge	E-2 Sto-Wing	Turbo
Weight	0.5	0	1	1
Structural Integration	0.2	0	0	1
Simplicity	0.2	0	-1	0
Deployment Speed	0.1	0	0	0
Total Score		0	0.3	0.7

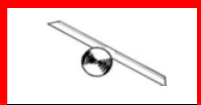
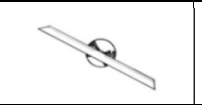
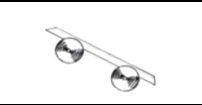
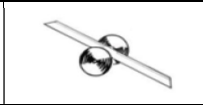
The “Turbo” design was chosen for its lightweight and favorable flight load transfer characteristics.

3.4.2 PROPULSION

A motor configuration was chosen based on weight, power, efficiency, and minimization of interference with landing gear and payload. These FoM all play crucial roles in the aircraft being able to maximize the design parameter $N_{scoring\ laps}$. The tractor configuration was set as the baseline for the downselect. The following motor configurations were compared and a downselect is shown in Table 7.

- **Tractor:** Single motor located at the front of the aircraft
- **Pusher:** Single motor aft of the fuselage
- **Wing-Mounted Twin:** Twin motors mounted on the wings
- **Pull/Push:** Twin motors mounted in-line, fore and aft of the fuselage

Table 7: Motor configuration downselect




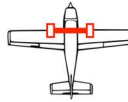

					
Figures of Merit	Score Factor	Tractor	Pusher	Wing-Mounted Twin	Pull/Push
TOFL	0.3	0	0	-1	-1
Efficiency	0.3	0	-1	1	0
Weight	0.2	0	0	-1	-1
Component Interference	0.2	0	-1	0	-1
	Total Score	0	-0.5	-0.2	-0.7

The tractor and the wing-mounted twin motor configurations yielded the highest score; therefore, both configurations were built and flight tested with their results shown in Section 8.1.2. Ultimately, the tractor configuration was selected because the wing-mounted twin configuration failed to meet the TOFL requirement due to a reduction of dynamic pressure (less prop wash) over the horizontal stabilizer. The wing-mounted twin motor configuration also weighed more and pulled more current for the same cruise speed than the tractor configuration, which would have resulted in a lower flight score.

3.4.3 LANDING GEAR

The goal for choosing the landing gear configuration was to meet takeoff requirements and landing loads while minimizing drag and weight to adhere to the design parameters in Table 1. The landing gear is also spatially constrained with a 2 ft (0.6 m) maximum distance between the nose and the aft-most landing gear. Five configurations were selected for comparison, as shown in Table 8. The tricycle gear served as the baseline. The FoM of wheelbase was weighed the most as the team would be disqualified if dimensional constraints were not met. Integration and drag were weighed the second most as they contribute to vertical spatial constraints and flight speed, respectively. The weight and ground handling were weighed the least since the weight differences are minimal and the aircraft only needs to track straight for 10 ft (3.0 m).

Table 8: Landing Gear downselect

Figures of Merit	Score Factor					
		Tricycle	Tip Tricycle	Bicycle	Tail Dragger	Tip Tail Dragger
Wheelbase	0.4	0	0	0	-1	-1
Integration	0.2	0	-1	-1	0	-1
Drag	0.2	0	0	1	0	0
Weight	0.1	0	0	1	0	0
Ground Handling	0.1	0	0	-1	0	0
Total Score		0	-0.2	0	-0.4	-0.6

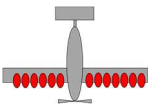
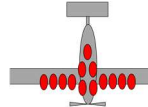
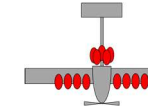
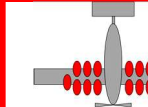
Configurations that feature wing-tip wheels would increase the overall height of the plane and exceed the vertical height limit of 2 ft (0.6 m) when using the wing folding mechanism chosen in Section 3.4.1. Both tail dragger configurations would extend the wheelbase out of the 2 ft (0.6 m) maximum limit. Although, the bicycle configuration scored the same as the tricycle configuration, it was not chosen due to unfavorable ground handling characteristics. Therefore, the tricycle gear was selected.

3.4.4 PAYLOAD

The location of the attack stores has a major impact on the total drag of the aircraft which directly affects $N_{scoring\ laps}$ for Mission 3. Viscous and pressure drag were estimated in Section 4.4.3 for the four different attack store arrangements. They were each prototyped and evaluated for ease of structural integration and weight as shown in Table 9. The adjacent-under-wing placement was used as the baseline.

- **Adjacent-under-wing:** All 13 stores placed side by side on the wing
- **Fuselage Stores:** Carry some stores under the fuselage in tandem to reduce frontal area/drag (but are in the wash of the propeller) and carry the rest side by side on the wing
- **Revolver:** 8 stores side by side on the wing and 5 stores in tandem with the main fuselage using a revolver-like mechanism; the design lacks a fairing since a fairing was not allowed by the rules
- **Tandem-under-wing:** 12 stores all on wing but in tandem of each other to reduce drag; 1 odd store stands along on one side of the wing

Table 9: Store Placement Downselect

Figures of Merit	Score Factor				
		Adjacent-under-wing	Fuselage Stores	Revolver	Tandem-under-wing
Drag	0.8	0	0	-1	1
Integration	0.1	0	-1	1	-1
Weight	0.1	0	0	1	-1
Total Score		0	-0.1	-0.6	0.6

When compared to the baseline, the revolver had a 28% increase in total drag when using hand-calculations as further discussed in Section 4.4.3. This was because stores in the propeller wash saw a significant drag increase, which also eliminated the fuselage stores configuration. The tandem on wing configuration places stores behind one another to reduce total drag, while also keeping more stores out of the propeller wash. While not naturally integrated into the wing structure, this configuration had a 35% reduction in drag when compared to the adjacent on wing configuration. For this reason, the tandem on wing configuration was selected.

3.5 FINAL CONCEPTUAL DESIGN

The final configuration consists of a single motor, high wing conventional aircraft with a H-tail designed to carry 13 attack stores and a rotating radome in separate missions as shown in Figure 1. The aircraft is stowed by folding the wing along a chord-wise hinge and locking it on top of the root section of the wing.

4.0 PRELIMINARY DESIGN

The team collaborated to design all aircraft components to meet the three design objectives: maximize $N_{scoring\ laps}$ for Mission 3 by optimizing for endurance and flight speed and minimize time required for Mission 2 and the Ground Mission. Additionally, meeting the 10 ft (3.0 m) takeoff field length (TOFL) is critical to receiving flight mission scores. Numerous trade studies were conducted using software simulations and models to size all components of the aircraft. Computer models and prototypes allowed for further development of the structural elements of the team's design.

4.1 DESIGN METHODOLOGY

The preliminary design was developed through an iterative and collaborative process that required the input of numerous sub-team leaders and team members across multiple disciplines. The critical components in the preliminary design phase and their corresponding design requirements are described as follows:

Wing

- Wing planform area (S): The wing produces the lift required to support the aircraft and its payload. This year's wing must produce enough lift (using high-lift devices) to meet the 10 ft (3.0 m) TOFL.
- Aspect Ratio (AR): High AR wings reduce induced drag, offering better takeoff and cruise performance than low AR wings. AR is limited by structural and spatial limitations.
- Airfoil: The team used the Eppler E560 airfoil designed to operate efficiently at low Reynolds numbers. The minimum allowable Reynolds number for this airfoil is $Re_c = 100,000$, below which unfavorable stability characteristics can exist. The airfoil is designed to generate the required lift at takeoff and then optimized for $(L/D)_{cruise}$ to improve lifting efficiency and minimize power required at cruise.
- Ground Mission: Wing actuation from stowed to flight configuration was designed to minimize $(T_{GM})_{USC}$.

Structures

- Wing Spars: The wing spars were designed to withstand the maximum in-flight and landing loads (8g) expected for the wing.
- Fuselage: The fuselage connects all the aircraft components, thus requiring efficient load paths from internal components to the ground. The fuselage must also have both minimal weight and drag contributions.

Propulsion

- Motor, propeller, and battery pack: These components were selected to meet TOFL requirements and the designed performance goals of the aircraft while minimizing overall package weight.

Payloads

- The radome and attack store mounting structures are designed to have minimal drag and handle aerodynamic forces from 8g turns to reduce lap times for Missions 2 and 3.
- Ground Mission: Attachment and removal mechanisms were all designed to be quick to minimize $(T_{GM})_{USC}$.

4.2 MISSION MODEL

A series of simulation packages and multidisciplinary design optimization (MDO) software were used to determine the highest scoring aircraft design. The MDO and simulation packages were implemented via PlaneTools, a first-order MATLAB simulation developed by the team that modeled all flight missions. PlaneTools simulated missions by modeling four phases of the competition course: takeoff, climb, cruise, and turns. Each of the four course segments is detailed in Figure 6.

1. Takeoff – Assumed to be performed at maximum throttle using a 20° flap deflection. The model accounted for the motor ramp-up time and ensured that the airplane started to accelerate once the propeller was delivering full static thrust, simulating the effect of the aircraft being held by the tail hook. Once full thrust had been achieved, the model simulated the acceleration of the aircraft up a ramp inclined by 5° with respect to the horizontal. The model accounted for the rolling resistance (μ_s) coefficient of the team-built testing ramp, which was experimentally determined to be 0.01 as described in Section 7.2.4.
2. Climb – The aircraft was assumed to climb to 25 ft (7.6 m) above the 2600 ft (800 m) altitude (ground level) of Tucson, AZ [3]. The rate of climb was calculated via the difference in thrust and drag on takeoff and multiplied by the proportion of the takeoff speed to the plane's weight. The model accounted for the drag due to the radome during Mission 2 and the drag due to each attack store during Mission 3.
3. Cruise – This phase of flight assumed steady level flight with equal thrust and drag. The cruise model accounted for drag due to the radome during Mission 2 and each individual attack store

during Mission 3. Drag due to stores was modeled as if each store was exposed to the free-stream velocity during climb and cruise; hence, a conservative estimate was used that did not account for a reduction in drag when stores are in a tandem configuration. The Mission 3 simulation iterated each lap, accounting for the reduction in drag and weight after the release of an attack store. For each mission, an optimum cruise throttle setting was selected so the aircraft did not exceed its nominal battery capacity by the end of the mission.

4. Turn – A coordinated level turn with constant speed and radius was assumed for both types of turning maneuvers (two 180° turns and one 360° turn). The load factor in the simulation was limited to 8g by the structural components of the aircraft. This load factor was used to calculate a representative turn radius.

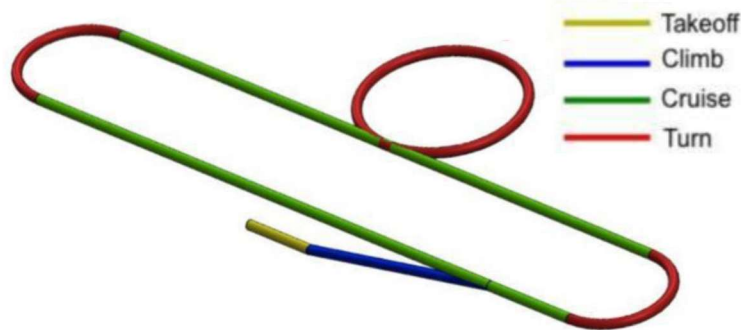


Figure 6: Flight course model in PlaneTools

Fundamental aircraft performance and aerodynamic equations were used to calculate output parameters such as rate of climb, cruise speed, and turn radius. The mission model also included the following uncertainties and assumptions:

- **Winds** – A headwind of 10 ft/s (5.8 m/s) was assumed for takeoff and cruise based on historical weather patterns during competition weekend (Mid-April) in Tucson, AZ [8].
- **Battery performance** – Battery resistance and capacity were based on in-lab bench tests and flight tests. Battery voltage decay is modeled iteratively and is assumed to drop by 5% each lap.
- **Propeller performance** – Thrust (C_T) and power (C_p) coefficients used for thrust calculations were based on values provided by the manufacturer and verified via static and flight testing [9].

The mission model neglected interference drag and compressibility. The propulsion model accounted for variations in internal temperature, which affect the resistance and voltage of the system. Nevertheless, lab testing deemed these parameters negligible.

The mission model was programmed within PlaneTools as an object-oriented class with several operations to simulate missions on any user-defined aircraft. The role of the mission model in PlaneTools is represented by Figure 7. The simulations help determine the initial design parameters (such as wing area and span) for the aircraft by selecting those that result in a higher flight score.

This object-oriented approach allowed the team to isolate each component of the aircraft and perform trade studies more effectively. Uncertainties are propagated throughout the mission model; uncertainty values are quantified based on results from laboratory testing and flight tests. Figure 7 provides a simplified schematic of the process that PlaneTools uses to simulate the entire mission. Note that while this figure shows a linear progression to output values, iteration is used within the tool to ensure convergence.

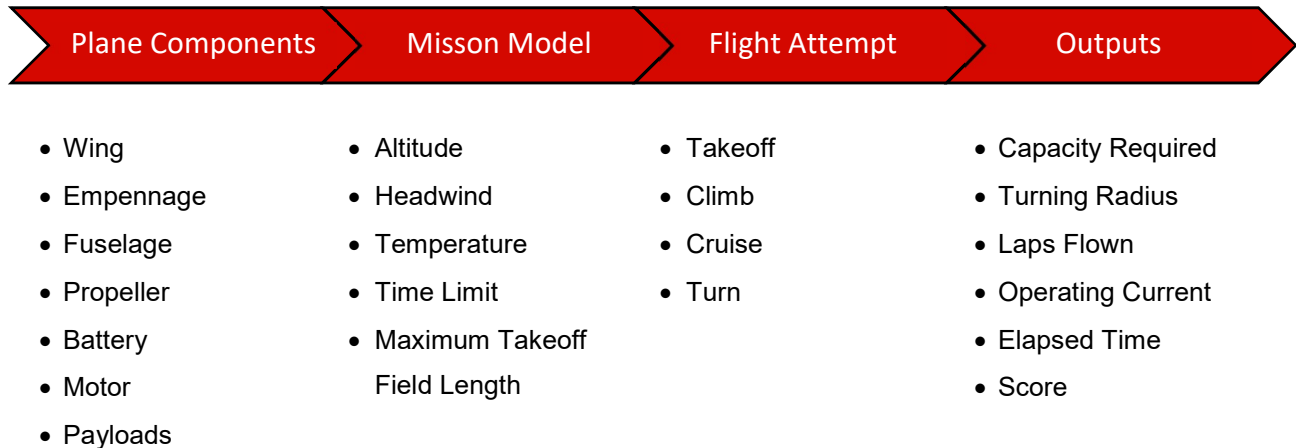


Figure 7: PlaneTools Simulation Components

4.3 DESIGN TRADE STUDIES

4.3.1 WING GEOMETRY

The wing area that maximized wing loading, W/S , was determined by modelling the change in velocity of the aircraft as it accelerated up the ramp. The takeoff model assumed that the AR -adjusted $C_L = C_{L,max}$ with 20° flaps deployed. This assumption was made because the airplane has full elevator authority on takeoff; thus, it rolls up the ramp with $\alpha \cong \alpha_{C_{L,max}}$. The model assumed that changes in dynamic thrust during acceleration up the ramp were negligible due to the short TOFL. The trajectory of the airplane was then plotted. The wing area chosen (4.5 ft^2) allowed the aircraft to droop off the end of the ramp by 0.8 ft before climbing. The results of the takeoff model are presented in Figure 8.

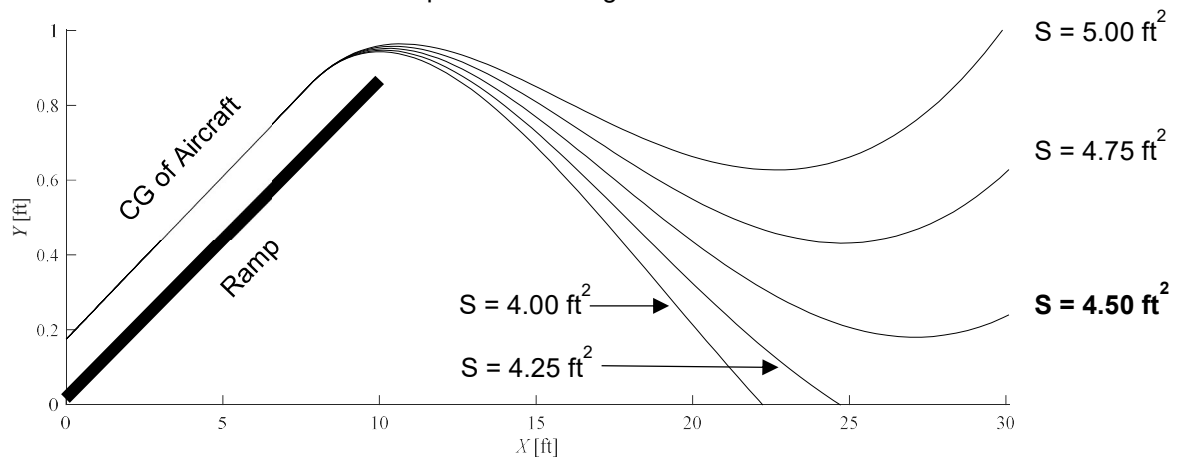


Figure 8: Trajectory of the aircraft's CG with varying wing area

The takeoff model indicated that a minimum wing area of 4.5 ft² (0.4 m²) was required for a successful takeoff after the aircraft droops off the ramp. A wing geometry trade studies were then performed to determine the effect of S , AR , and span (b) on final score. Results of the trade study are shown on a carpet plot in Figure 9. Multiple carpet plots for aircraft were generated with varying propellers, battery packs (cell capacity and number), and motors.

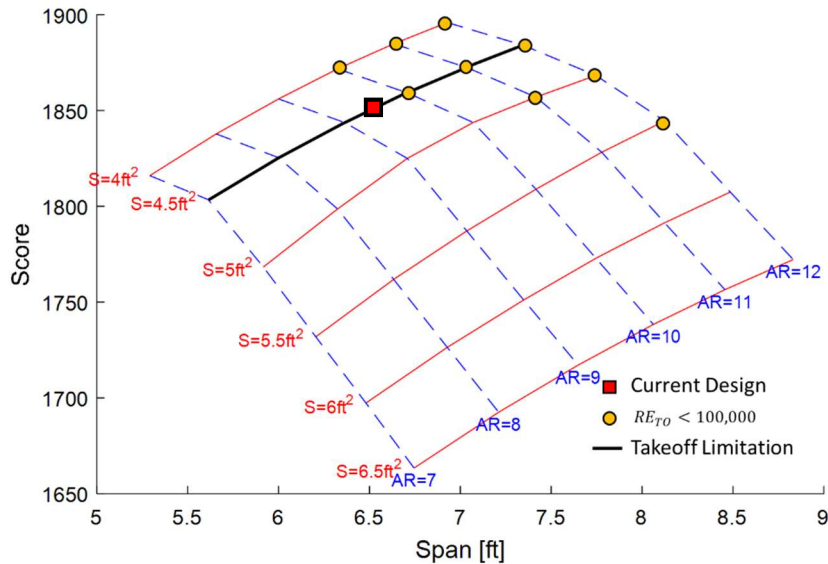


Figure 9: Score as a function of wing geometry

The wing geometry that maximizes score minimizes S and maximizes AR . This is because there are no upper constraints on wing span in the form of a Rated Aircraft Cost (RAC) metric. Therefore, score increases with AR in a concave-down fashion because the relative contribution of induced drag to total drag increases. This reduction in drag allows the aircraft to fly faster in Mission 2 and fly longer in Mission 3. The optimal wing geometry is bounded by minimum wing area of 4.5 ft² (0.4 m²) that allows a ramp droop takeoff at maximum takeoff weight during Mission 3 and by an AR of 9.5, ensuring that $RE_{TO} \geq 100,000$ for stability.

4.3.2 PROPULSION SIZING

Preliminary sizing for the propulsion system was focused first on maximizing the number of laps flown in Mission 3 then on minimizing the time required to complete Mission 2. Mission 3 was the limiting case as it consisted of maximizing the number of laps flown in 10 minutes, starting with 13 stores and dropping 1 each lap. The propulsion system also needed to provide enough thrust to takeoff in 10 ft (3.0 m).

NiMH cells were chosen over NiCd cells due to their higher energy density and lack of memory effect. For preliminary sizing, Tenergy 4200mAh cells were chosen for Mission 2 and Elite 5000mAh were chosen for Mission 3 due to their measured performance during static and flight tests when compared to other high-capacity batteries. From prior propulsion-analysis, a properly sized propulsion system can achieve about 80% efficiency, η_b , from the power supplied from its battery pack, calculated by Eq. 6 [5].

$$P = \eta_b * P_{battery} = \eta_b * V * I \quad \text{Eq. 6}$$

Because score is most sensitive to Mission 3, the propulsion system was designed for speed and endurance. An electrical power loading $P/W = 120 \text{ W/lb}$ was targeted, which is common for planes seeking high performance capabilities such as basic aerobatics and increased speed [10]. While not the highest power loading in terms of endurance, 120 W/lb still allows the plane to meet the TOFL requirement. The total power required of 1,092 W is determined using Eq. 7 with a maximum weight of 9.1 lb (4.1 kg).

$$P_R = W * P/W \quad \text{Eq. 7}$$

The minimum power required from the battery pack is 1,365 W, calculated by using Eq. 8

$$P_{battery} = P_R/\eta_b \quad \text{Eq. 8}$$

Both the Tenergy 4200mAh and the Elite 5000mAh have a nominal voltage of 1.2 volts per cell, V_c . The target pack size for Mission 2 ($n_{c,M2}$) is 23 cells and $n_{c,M3} = 21$ cells for Mission 3. Using those parameters, a maximum static current for Mission 2 is calculated to be 49 A, using Eq. 9.

$$I_{max,M2} = \frac{P_{battery}}{V_c * n_{c,M2}} \quad \text{Eq. 9}$$

and the maximum static current for Mission 3 was calculated to be 54 A using Eq. 10.

$$I_{max,M3} = \frac{P_{battery}}{V_c * n_{c,M3}} \quad \text{Eq. 10}$$

The specifications above were used to determine the required Kv [RPM/V]. The Neu 1415/2Y with a 4.2:1 gearbox was identified as the highest-scoring motor, balancing Kv, power rating, and weight. PlaneTools was used to identify the highest-scoring propeller that would produce enough static thrust to satisfy the TOFL requirement and be able to successfully complete each mission. The preliminary package for each mission is shown in Table 10.

Table 10: Preliminary Propulsion Package by Mission

Mission	Motor	Battery Pack	Propeller
1 & 2	Neu 1415/2Y (1100 Kv*)	23x Tenergy 4200mAh	APC 18x12E
3		21x Elite 5000mAh	APC 20x10E

*Effective Kv = 262 with the addition of the gearbox

4.4 AERODYNAMICS

The aerodynamics of the aircraft were designed and analyzed primarily with XFLR5 [11] and Athena Vortex Lattice (AVL) [12]. XFLR5 is a graphically oriented program that utilizes the lifting line theory capabilities of XFOIL to predict lift and drag characteristics of an airfoil. Similarly, AVL employs an extended vortex lattice model to capture aerodynamic characteristics of the full aircraft configuration, allowing for static and dynamic stability to be analyzed.

4.4.1 AIRFOIL SELECTION

Using XLFR5, several airfoils were analyzed at the takeoff and cruise Reynolds numbers (Re) of 100,000 and 250,000, respectively. By prioritizing the need for a large maximum lift coefficient, $C_{l,max}$, while still minimizing drag, the Eppler 560 (E560) and BA527Is (a team-designed airfoil) were found to be the best options of the airfoils analyzed. Figure 10 shows the lift and drag polars produced by XLFR5 for each airfoil.

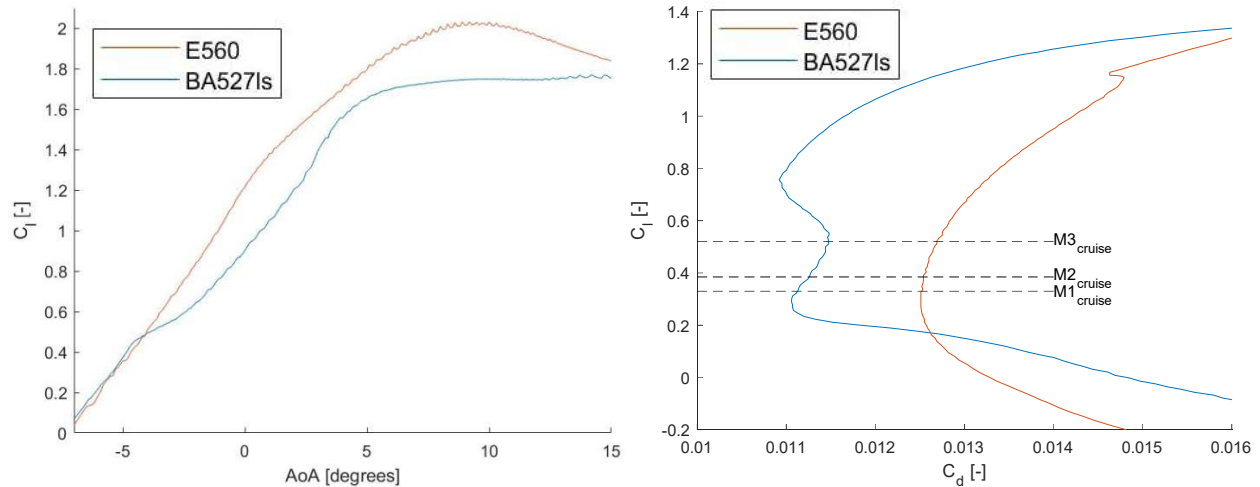


Figure 10: Lift (left) and drag (right) polars of the E560 and BA527Is airfoils at Re of 100k (takeoff) and 250k (cruise), respectively. Airfoils have 20° flaps at takeoff and no flaps during the cruise

The E560 has a $C_{l,max} = 2.0$ while the BA527Is has a $C_{l,max} = 1.7$. Additionally, it can also be seen that the BA527Is has a lower drag coefficient, C_d , for all missions due to its less cambered profile. However, due to the 10 ft (3.0 m) TOFL, PlaneTools mission simulations showed that achieving a higher $C_{l,max}$ was more important than the 10% reduction in C_d . Therefore, the E560 airfoil was selected.

4.4.2 AERODYNAMIC COMPONENT ANALYSIS

In the preliminary design phase, a model was made to predict the drag of the Missions 2 and 3 payloads. Using Hoerner, the radome could be modeled as an ellipsoid and the stores could be modeled as an ellipsoid with flat plates [13]. To describe the varying geometry of ellipsoids, the fineness ratio, l/d , was used, where l and d are the length and diameter of an ellipsoid. The fineness ratio was used to yield a drag coefficient, C_D , of an ellipsoid with Eq. 11.

$$C_D = 0.44 \frac{d}{l} + 4C_f \frac{l}{d} + 4C_f \left(\frac{d}{l}\right)^2 \quad \text{Eq. 11}$$

where C_f is the coefficient of friction for laminar flow described by,

$$C_f = \frac{0.664}{\sqrt{Re}} \quad \text{Eq. 12}$$

and Reynolds number, Re_{l_c} , is,

$$Re_{l_c} = \frac{U\rho l_c}{\mu} \quad \text{Eq. 13}$$

where l_c is the characteristic length of a given ellipsoid or flat plate. Additionally, the drag coefficient for a flat plate is described as,

$$C_D = 2C_f \quad \text{Eq. 14}$$

The equations above were used to model drag due to payloads.

4.4.3 DRAG ANALYSIS

XFLR5 data with 3-D conversions [11][12] and Eq. 11-14 were used to estimate the drag for each component of the aircraft during cruise of each mission. The estimated drag of each component can be visualized in Figure 11 as a percentage of the aircraft's total drag.

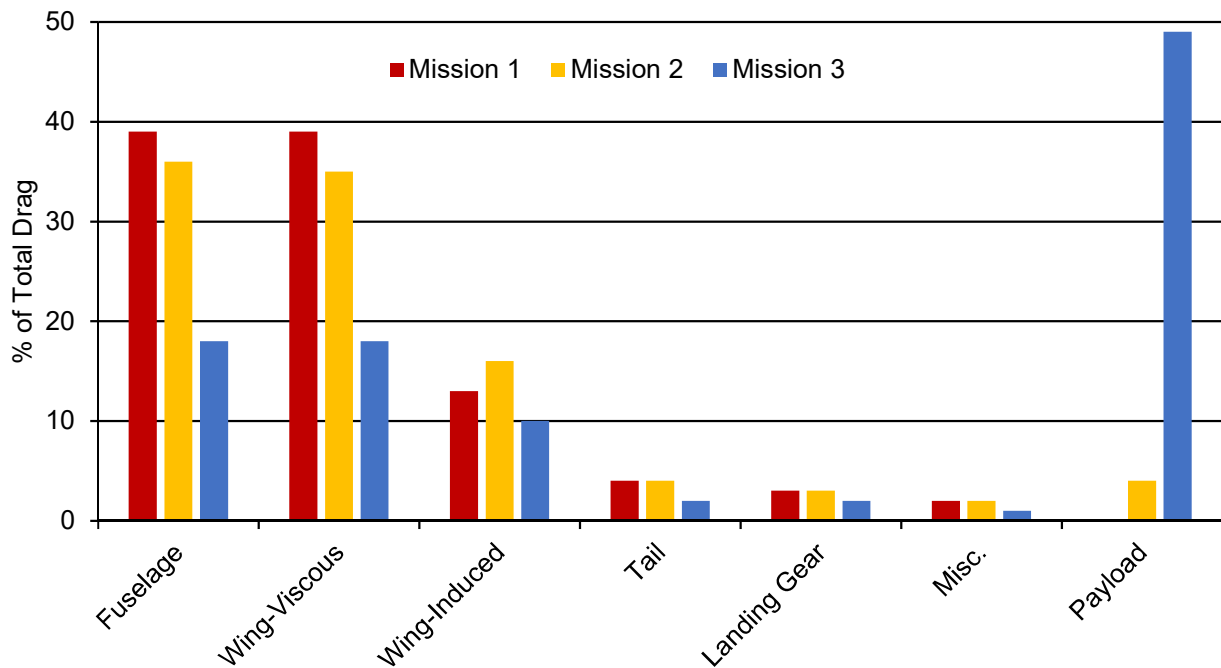


Figure 11: Drag breakdown of aircraft during cruise of each mission

In Missions 1 and 2, the aircraft drag was dominated by the wing and fuselage. For Mission 3, the aircraft drag was dominated by the stores so additional considerations were taken into store placement on the aircraft as previously mentioned in Section 3.4.4. To minimize drag, pairs of stores would be placed in tandem on the wing with a lateral spacing of one store diameter while maximizing vertical spacing from the wing. This is further explained and tested in Sections 7.2.1 and 8.1.1, respectively. Even with these considerations, the store drag still dominated the aircraft's total drag for Mission 3 as shown in Figure 11.

The drag buildup shown in Figure 12 for each mission was used to create a lift to drag ratio (L/D) versus coefficient of lift (C_L) plots to visualize the efficiency of the aircraft during cruise and turns. The expected C_L values for cruise and turns were obtained through AVL analysis for each mission.

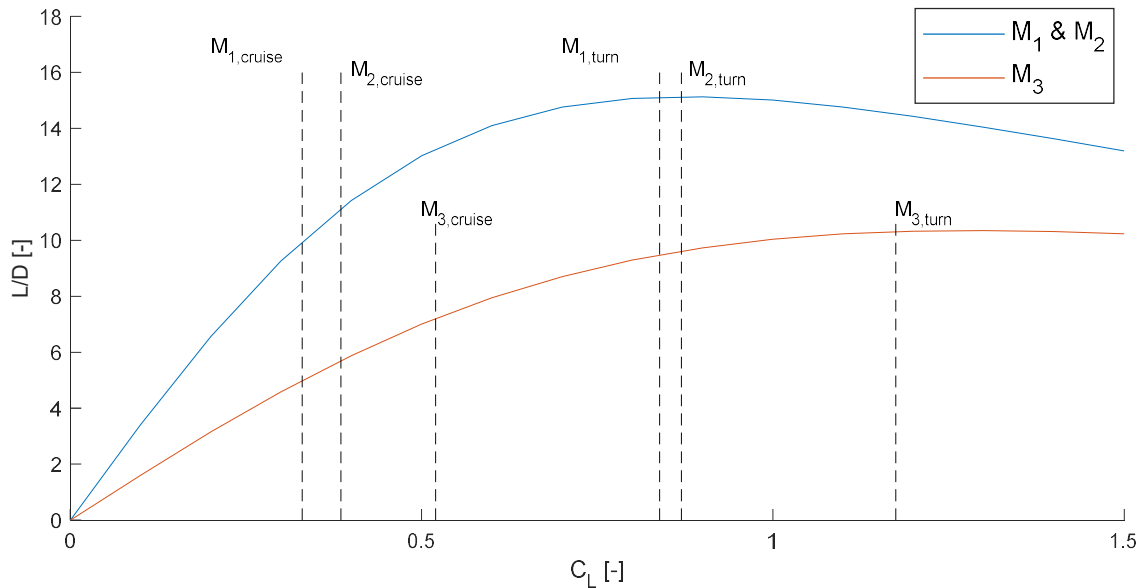


Figure 12: L/D plot to visualize aircraft efficiency. Missions 1 and 2 have different L/D curves than Mission 3 due to the large drag effect of the stores

The aircraft operates near peak efficiency in turns while operating around 70% of the maximum lift-to-drag ratio, $(L/D)_{max}$, during cruise.

AVL was also used to perform Trefftz plane analysis on the aircraft to determine the angle of attack, α , and trim elevator deflection, δ_e , for the aircraft during all the missions. The acceptable bound for both of these was $\pm 3^\circ$ to reduce trim drag and was achieved for all mission simulations as seen in Table 11.

Additionally, the Trefftz plane analysis in Figure 13 allowed for the span efficiency of the wing, e , to be quantified as well as for the lift distribution of the aircraft to be visualized.

Table 11 (left): Trim deflections with lift and drag coefficients for each mission during cruise

	Mission 1	Mission 2	Mission 3
e [-]	0.49	0.55	0.70
α [°]	-1.68	-1.09	0.44
δ_e [°]	0.81	0.51	-0.18
C_L [-]	0.33	0.39	0.52
C_D [-]	0.080	0.095	0.134
$C_{D,i}$ [-]	0.008	0.009	0.013
$C_{D,p}$ [-]	0.075	0.089	0.130

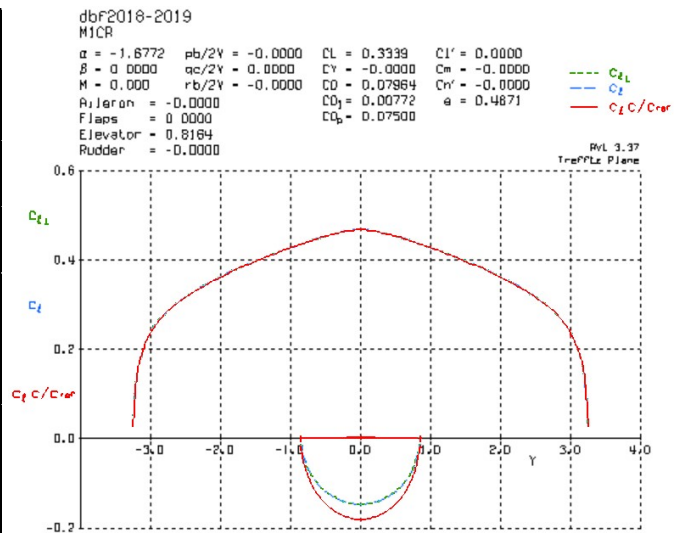


Figure 13 (right): Trefftz plane analysis of aircraft during Mission 1 cruise

4.5 STABILITY AND CONTROL

4.5.1 STATIC STABILITY ANALYSIS

Sizing of the aircraft for stable flight started by sizing and locating the tail of the aircraft based off a typical horizontal tail volume, V_H , of 0.9 and a typical vertical tail volume, V_V , of 0.07, using Eq. 15-16 [15].

$$V_H = \frac{l_t * S_{horizontal}}{c * S_w} \quad \text{Eq. 15}$$

$$V_V = \frac{l_t * S_{vertical}}{b * S_w} \quad \text{Eq. 16}$$

Here $S_{horizontal}$ and $S_{vertical}$ are the planform areas of each respective surface, while c , b , and l_t are the wing chord, wing span, and tail moment arm. Tail volume coefficients were used since they are common metrics for a tail's effectiveness in both longitudinal and lateral-directional stability. Additionally, as a baseline, the center of gravity (CG) of the aircraft was initially placed at the quarter chord of the wing where the center of pressure was located. The tail volumes and CG location were iterated throughout the preliminary design of the aircraft using flight test data and AVL analysis until the aircraft was deemed sufficiently stable by the team and aircraft pilot. The final tail has horizontal and vertical tail volumes of 1.27 and 0.11, respectively, while having a CG location that results in a static margin of 25%. This tail configuration and static margin allowed the aircraft to be statically stable as indicated by the static stability derivatives for Mission 1 in Table 12.

Table 12: Static stability derivatives of aircraft during Mission 1 cruise

$C_{L\alpha}$	5.40	$C_{m\alpha}$	-1.24	$C_{Y\beta}$	-0.418	$C_{Y\delta_r}$	-0.005	C_{Y_p}	-0.033	C_{Y_r}	0.329
$C_{L\delta_e}$	0.011	$C_{m\delta_e}$	-0.04	$C_{l\beta}$	-0.028	$C_{l\delta_r}$	-0.0002	C_{l_p}	-0.567	C_{l_r}	0.108
C_{Lq}	10.10	C_{mq}	-26.58	$C_{n\beta}$	0.079	$C_{n\delta_r}$	0.002	C_{n_p}	-0.010	C_{n_r}	-0.126

The aircraft was also statically stable during Missions 2 and 3 simulations in AVL. For Mission 2, the location of the radome was investigated to determine its effect on the stability of the aircraft. The radome location was varied from the trailing edge of the main wing to the leading edge of the tail in AVL and only a 7% change was seen in the pitching moment coefficient for a given change in angle of attack, $C_{m,\alpha}$, while all other static stability derivatives were mostly unchanged. Since $C_{m,\alpha}$ was less than zero for all locations, the radome location was chosen to be near the aerodynamic center to reduce in flight moments but aft of the wing to avoid compromising the structure of the wing.

4.5.2 DYNAMIC STABILITY ANALYSIS

The aircraft's dynamic stability characteristics were also analyzed for all flight missions using AVL. A root locus plot was used to analyze the stability of the different dynamic modes of the aircraft, as shown in Figure 14. For a mode to be stable, it must be negative on the horizontal axis. The five dynamic modes of the aircraft are shown both during takeoff (TO) and cruise (CR) of each mission: roll (1), spiral (2), phugoid (3), dutch roll (4), and short period (5).

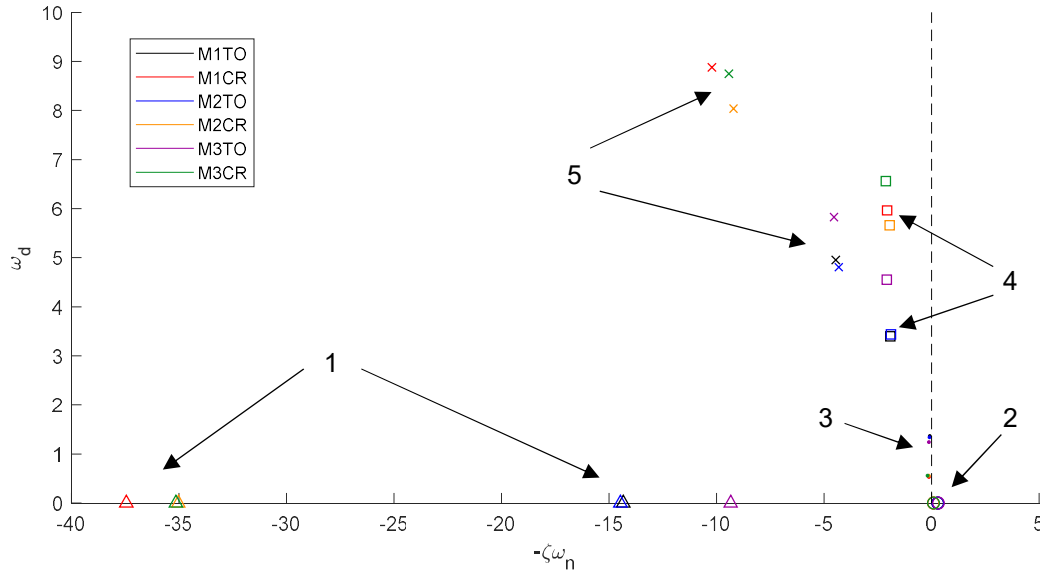


Figure 14: Root locus plot of the five dynamic stability modes during takeoff and cruise of each mission; roll (1), spiral (2), phugoid (3), dutch roll (4), and short period (5)

All modes, except spiral, are stable at takeoff and cruise of each mission. The aircraft was designed to satisfy the Level 1 flying qualities of a Class 1 (small and lightweight) aircraft, described in MIL-F-8785C [16]. In Table 13, characteristic values of the five modes are shown, with the MIL-F-8785C requirements in parentheses. Note that only Mission 2 takeoff and cruise is shown, due to the similar dynamic stability characteristics found between all the missions.

Table 13: Dynamic stability parameters of aircraft during Mission 2; values are listed as takeoff value / cruise value

	Mode	ζ [-]	ω_n [rad/s]	$\zeta \omega_n$ [rad/s]	τ [s]
1	Roll	-	-	14.47 / 35.03	0.069 / 0.029 ($\tau < 1.4$)
2	Spiral	-	-	-0.2827 / -0.079	3.54 / 12.66
3	Phugoid	0.074 / 0.237 ($\zeta > 0.04$)	1.33 / 0.573	0.0987 / 0.1357	10.13 / 7.37
4	Dutch Roll	0.483 / 0.325 ($\zeta > 0.08$)	3.93 / 5.99 ($\omega_n > 0.4$)	1.896 / 1.948 ($\zeta \omega_n > 0.15$)	0.53 / 0.51
5	Short Period	0.668 / 0.754 ($0.35 < \zeta < 2.00$)	6.46 / 12.22	4.317 / 9.214	0.23 / 0.11

The stable modes from Figure 14 all satisfy the MIL-F-8785C requirements. Spiral mode was the only unstable mode and it did not satisfy MIL-F-8785C requirements; however, MIL-F-8785C specifies that an unstable spiral mode can still satisfy the requirements if $\tau > 5.77s$ so further analysis was conducted on the mode. Adding dihedral to the wing would increase the spiral mode's time constant, τ , to satisfy MIL-F-8785C for both takeoff and cruise. However, pilot feedback from flight test deemed the change unnecessary; thus, dihedral was not added since it would have only increased complexity to the manufacturing process.

4.6 PREDICTED AIRCRAFT PERFORMANCE

ExSCalibur's performance characteristics based on PlaneTools predictions are shown in Table 14 below.

Table 14: Preliminary design performance characteristics

Performance Parameter	Mission 1	Mission 2	Mission 3
$C_{L_{max}}$	2.23	2.23	2.23
$C_{L_{cruise}}$	0.33	0.39	0.43
e	0.49	0.55	0.70
C_{D_0}	0.08	0.09	0.13
$(L/D)_{max}$	9.70	9.68	9.69
$(L/D)_{cruise}$	4.73	3.68	4.51
Rate of Climb [ft/s]	12.6 (3.9 m/s)	12.5 (3.8 m/s)	11.1 (3.4 m/s)
W/S [lb/ft ²]	1.66 (8.1 kg/m ²)	1.69 (8.3 kg/m ²)	2.05 (10 kg/m ²)
u_{cruise} [ft/s]	70 (21 m/s)	65 (20 m/s)	62 (19 m/s)
u_{stall} [ft/s]	32 (9.8 m/s)	32 (9.8 m/s)	36 (9.4 m/s)
Gross Weight [lb]	7.4 (3.3 kg)	7.5 (3.4 kg)	9.1 (4.1 kg)
Mission Score	1	1.78	15

5.0 DETAIL DESIGN

Detail design combines conceptual and preliminary design with detailed testing and analysis of individual components. Structure, weight, and mission performance were considered to refine the competition aircraft.

5.1 DIMENSIONAL PARAMETERS TABLE

Table 15 lists the characteristic parameters for ExSCalibur, USC's entrant into the 2018-19 DBF Competition. Each subsystem will be highlighted in subsequent sections.

Table 15: Characteristic components properties for ExSCalibur

Wing		Tail	
Airfoil	Eppler E560	Airfoil	NACA 0010
Span	6.5 ft (1.81 m)	Horizontal Span	1.60 ft (0.49 m)
MAC	0.7 ft (0.21 m)	Horizontal Chord	0.85 ft (0.26 m)
Planform Area	4.47 ft ² (0.42 m ²)	Vertical Span	0.73 ft (0.22 m) each
AR	9.45	Vertical Chord	0.85 ft (0.26 m)
Incidence Angle	-2°	Planform Area	1.23 ft ² (0.11 m ²)
Static Margin	23-25%	Incidence Angle	0°
Fuselage		Tail Arm	
Total Length	4.28 ft (1.30 m)	Controls	
Nose Length	8.75 in. (0.22 m)	Receiver	Futaba R7008SB
Tail Length	2.01 ft (0.61 m)	Servo	Dymond D-60s
Width	5.88 in. (0.15 m)	Battery Model	Tenergy, Elite
Height	7.5 in. (0.19 m)	Internal Resistance	0.05 Ω
Motor		Cell Count	23 (M1&M2); 21 (M3)
Model	Neu 1415/2Y	Pack Voltage	28.75V (M1&M2); 26.25V (M3)
Gearbox	P32 (4.2:1)	Pack Weight	3.4 lb (M1&M2); 3.1 lb (M3)
Effective Kv	262	Propeller	
Power Rating	2200 W	Manufacturer	APC
No-Load Current (I_0)	1.10 amps	Mission 1	18" x 12"
Internal Resistance	0.024 Ω	Mission 2	18" x 12"
Weight	0.80 lb	Mission 3	20" x 10"



5.2 STRUCTURAL CHARACTERISTICS AND CAPABILITIES

The plane structure was designed to minimize weight and drag to increase flight speed while withstanding flight and landing loads. To reduce turn times, a load factor of 8g was used to size the wing spar, allowing for a bank angle of 82.8°. The wing was also designed to pass the wingtip test. To accommodate payload and wing folding mechanisms, a light balsa built-up design with carbon spar caps was pursued for both the wing and tail. A composite fuselage with a foam truss and carbon fiber tail boom was designed to contain electronics and withstand thrust, lift, landing, and torque loads. The tail hook was also designed to withstand an axial load equal to the maximum takeoff thrust.

5.3 SUB-SYSTEM DESIGN

5.3.1 WING

The structure of the wing was driven by maximum lift loads and mechanism integration. A balsa built-up wing proved to be the easiest to design for minimum weight while easily integrating payloads and folding mechanisms. An initial spar design was conducted using SparSizer, an Excel-based program developed by former team advisor Mark Page. Spar Sizer calculates lift shear and moment loads on the spar from maximum expected weight, load factor, and wing geometry inputs. The shear web was sized to withstand 8g loads with a safety factor of 1.5. Figure 15 shows the stress distribution of the shear web along the span. The shear web starts with a width of 0.38 in. (1.0 cm) and reduces to 0.25 in. (0.6 cm) following the wing folding mechanism at 18 in. (45.7 cm).

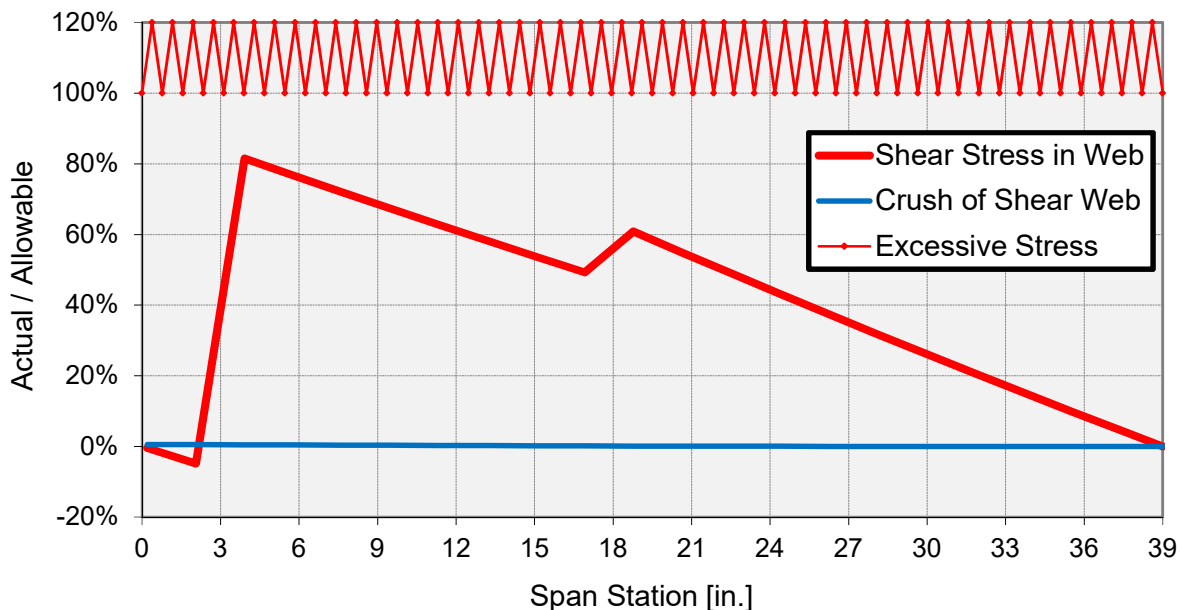


Figure 15: Expected stresses of the shear web (red) along the span. Discontinuities occur at 3 in. (7.6 cm) station for the fuselage mounting location and 18 in. (45.7 cm) station for wing folding

Unidirectional carbon fiber spar caps were sized using a MATLAB script, which optimized the number of plies per section for the same width as the shear web, as shown in Figure 16.

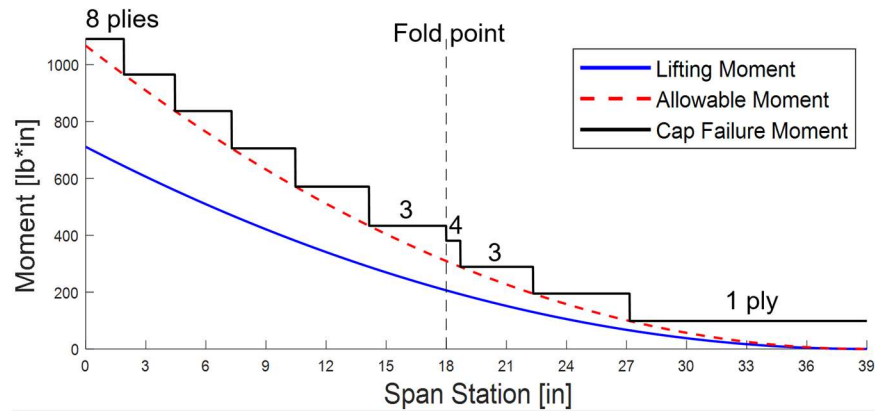


Figure 16: Spar cap thickness optimization with each step indicating a decrease in plies

A single panel wing with an integrated folding mechanism was built and tested to verify the various analysis methods used as later detailed in Sections 7.2.3 and 8.1.3.

5.3.2 WING FOLDING MECHANISM

The wing folding mechanism selected in Section 3.4.1 was designed to transfer all flight loads from tip section to root section and minimize weight, drag, and unfolding time for faster mission times. The hinge mechanism was first designed in FEA and then the full mechanism was load tested on a prototype in lab. The mechanism was ultimately sized to withstand up to 1.3 ft-lbf (1.8 N-m) of bending moment at the folding point, 1.5 ft (0.46 m) from the fuselage centerline. This wing folding location minimized load transfer as it shortens the two tip sections of the wing. The final design is shown in Figure 17.

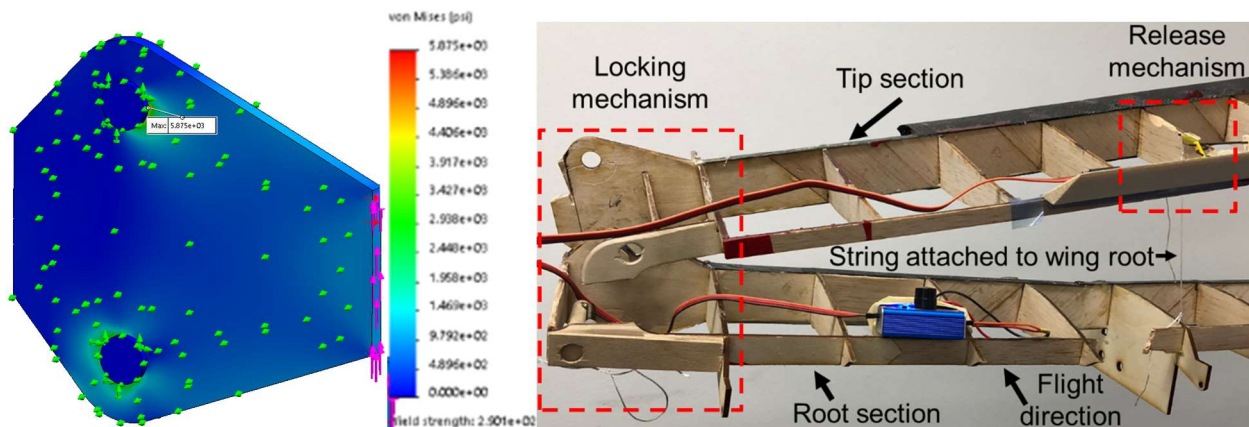


Figure 17: FEA study (left) and Wing Folding Mechanism Overview (right)

The wing folding mechanism is split into two subsystems: the release mechanism and locking mechanism, both boxed in red in Figure 17. Each subsystem is further detailed in Figure 18. When the tip sections fold on top of the root sections, the two tip sections overlap. The tip section underneath (not shown) is held down by the tip section on top. The tip section on top is held down to its root section by a string. Upon release of the string, a torsion spring rotates the tip sections into place, where the locking mechanism automatically engages the wing into flight configuration.

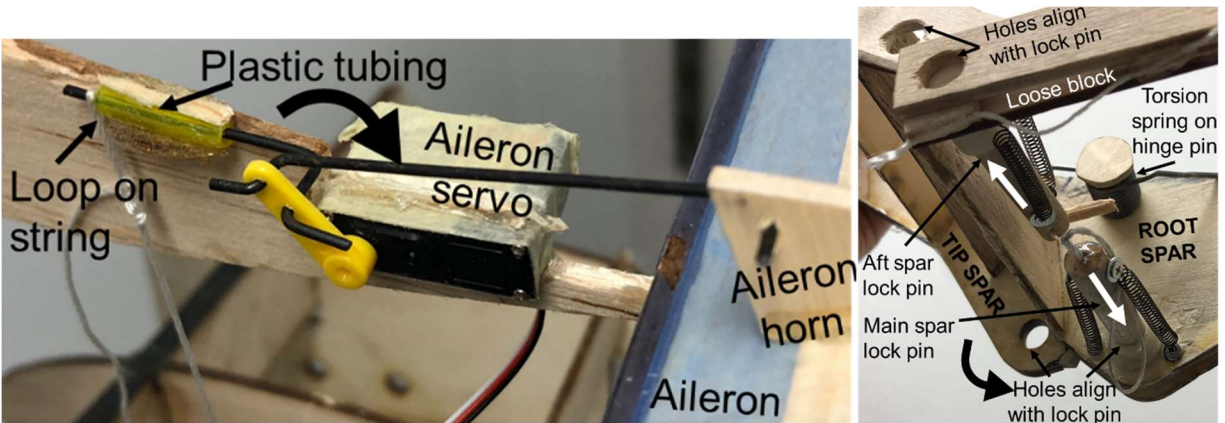


Figure 18: Release mechanism detail (left) and locking mechanism detail (right)

Since the torsion spring is constantly forcing the tip section to unfold, the release mechanism is meant to hold the tip section folded until pilot actuation. On command, the pilot actuates the aileron servo that is connected to the pushrod holding a loop on the string that is connected to the fixed root section. When the pushrod pulls through the loop, the tip section is released from the string and rotates into flight position. As the tip spar rotates into place, it pushes away a loose block that had been holding back a spring-activated lock pin. As the loose block is pushed between the root spar connectors, the lock pin thrusts through holes in the root and tip spars. To allow for proper alignment of the tip and root sections and ensure transfer of torsional loads, the aft spars were also locked together using a very similar lock pin mechanism within the wing. This securely locks the wing into flight configuration. This design was tested under full flight loading as a part of the wing. For the final flight configuration, an aerodynamic fairing (not shown) was placed over the mechanism to minimize drag.

5.3.3 TAIL

The tail was designed to minimize weight, keep the aircraft stable, and adhere to vertical spatial constraints. A balsa built-up horizontal spar with carbon spar caps wraps around the tail boom and is reinforced with plywood at the integration point. The two identical vertical stabilizers are balsa built with carbon spar caps. The vertical stabilizers are mounted at the ends of the horizontal stabilizer with interlocking ribs and plywood spar reinforcements as shown in Figure 19. The vertical spars are notched to accommodate the ends of the horizontal spar, then reinforced with the t-shaped bracket. The end horizontal rib has notches which the middle vertical ribs insert into.

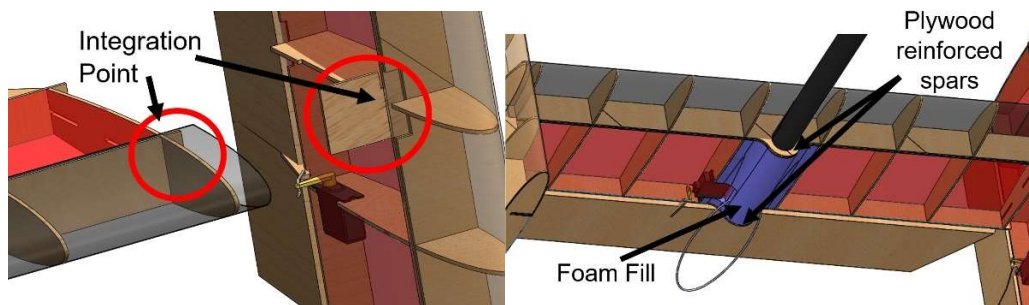


Figure 19: Integration of horizontal and vertical stabilizers (left) and of tail to tail boom (right)

The horizontal stabilizer withstands extra torsional loads with a carbon D-box, while the vertical stabilizers use balsa sheeting for minimal weight. The horizontal stabilizer transmits all tail loads to the carbon tail boom by integrating main and aft spars around the boom as shown in Figure 19.

Each spar has a plywood reinforcement around the boom. The carbon D-box wraps around the boom, and the middle section is supported with foam fill to allow for more epoxy contact area. The tail boom extends slightly behind the tail aft spar for the tail hook mount. The tail hook consists of carbon tow threaded directly through the tail boom. The load of the hook is supported by a plywood plug glued in to the end of the boom, which transfers the load directly to the fuselage. Solite is then used to cover any exposed or rough surfaces.

5.3.4 LANDING GEAR

The main gear was designed using GearSizer, an in-house software package designed by former team advisor Blaine Beron-Rawdon. A carbon wet-layup was chosen to minimize weight while maintaining durability. The book *Basics of RC Model Aircraft Design* by Andy Lennon was used to determine the locations of both the nose and rear landing gears, as well as their corresponding nose and tail angles. Their placement then gave an initial constraint of a 12 in. (30.5 cm) wheelbase to ensure the distance between the nose of the aircraft and the rear landing gear were within the 2 ft (0.6 m) requirement [17].

Finite element analysis was performed on the main gear at maximum 3g loading to simulate a hard landing, as shown in Figure 20. The composite bow gear was modeled as a single block of isotropic woven carbon fiber. The maximum deflection was 1.6 in. (4.1 cm), which was less than the 1.9 in. (4.8 cm) needed for propeller clearance.

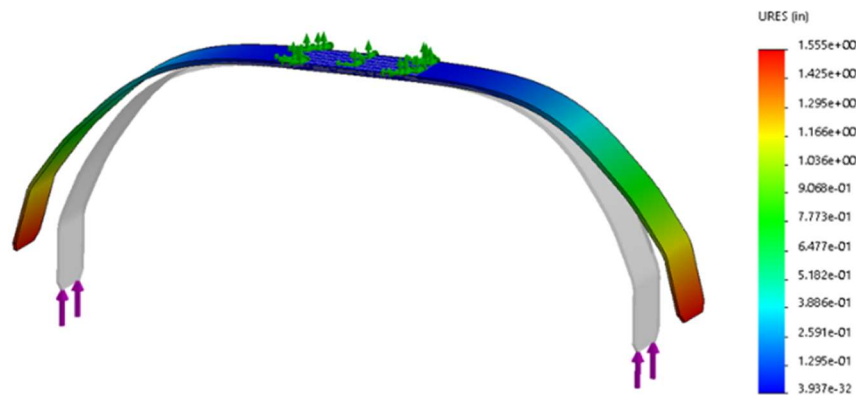


Figure 20: FEA of bow gear under maximum 3g loads, showing a deflection of 1.6 in. (3.9 cm)

5.3.5 PAYLOADS

Radome

The radome was designed to meet dimensional constraints and survive in-flight loads while minimizing drag. Various materials, shown in Figure 21, were tested out of a car at 88 ft/s (27 m/s). Only the foam and waffle-patterned plywood radomes survived. The waffle-patterned plywood was then selected for its ability to be manufactured precisely with laser cutting. It was also 0.04 lb (20 g) lighter than the foam radome.



Figure 21: Radome testing with foam, fiber glass, radial plywood, and waffle plywood (left to right)

The final design of the radome structure, shown in Figure 22, featured waffle-patterned plywood ribs with a hub in the middle that distributes load from the ribs to a 0.5 in. (1.3 cm) thick wooden dowel. Solite was used to cover the structure in a pattern of contrasting color to easily distinguish rotation during flight. The radome has a diameter of 12 in. (30.5 cm), thickness of 1 in. (2.5 cm) at the center, and dowel height of 3 in. (7.6 cm). The wetted area of the radome was minimized to reduce drag [13]. This structural design survived 8g load testing in lab as well as in a wind tunnel and in-flight. Stability analysis in Section 4.5.1 showed that the aircraft would be stable regardless of the integration location along the tail boom; thus, the radome was placed as close to the aerodynamic center as possible to reduce moments in flight.

To achieve continuous rotation during Mission 2, the team explored both active and passive rotation ideas. In the active system, the radome rod attached to a continuously rotating servo. In the passive rotation system, the radome was spun by aerodynamic forces in flight, similar to how an anemometer turns. Ultimately, the active system was chosen for its simplicity, as shown in Figure 22 since it would not compromise the structural integrity of the radome like the passive system would by replacing part of the plywood structure with a bearing, causing a discontinuity in the transfer of flight loads.

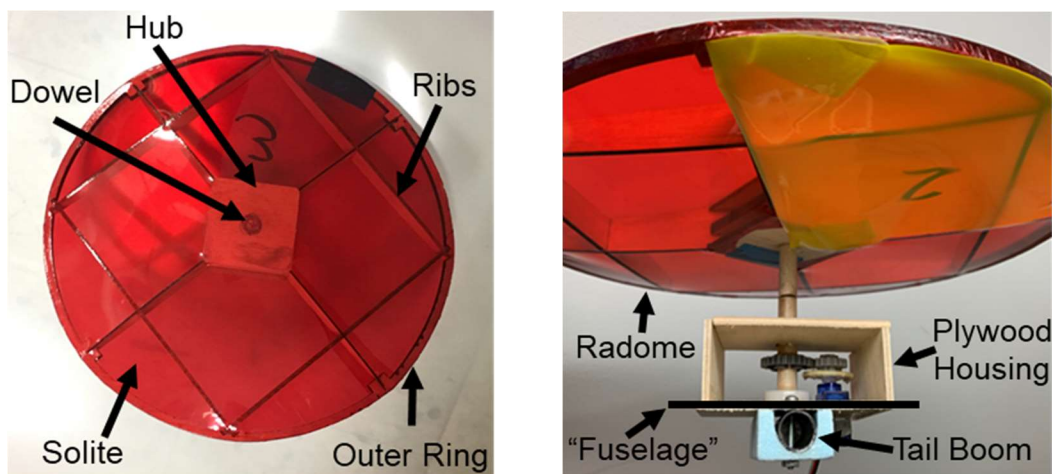


Figure 22: Radome structure (left) and full radome assembly (center)

Two ball bearings were placed on the radome shaft (both on top and bottom sides of the plywood housing structure) to allow for low-friction and axial stability. A small gear glued to a continuous servo was linked to a larger gear that integrated onto the shaft to actuate and stop the radome on command. Gears of different sizes were used to step up the torque of the servo to prevent stripping. This design is shown in Figure 23.

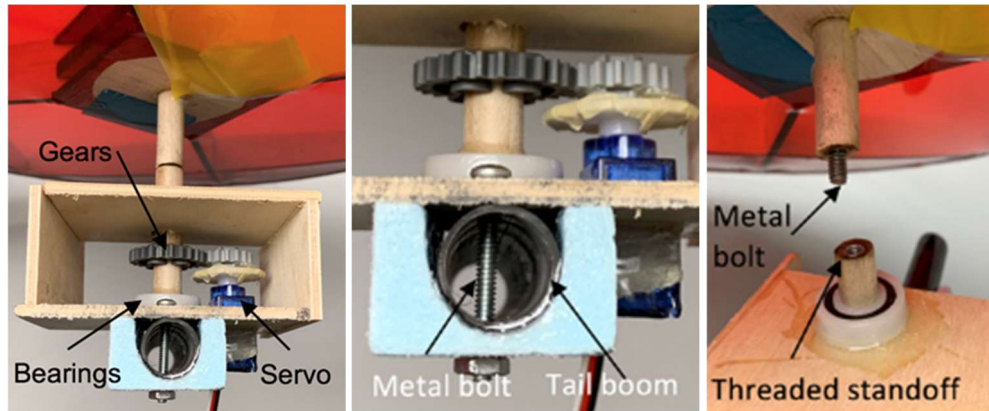


Figure 23: Rotation mechanism (left), integration to fuselage (middle), and radome removal (right)

The plywood housing structure integrates to the carbon fiber tail boom on the centerline of the plane by two metal bolts, shown in Figure 23. A portion of the radome shaft was drilled out, and a threaded standoff was inserted into one hole. A metal bolt was inserted into the other end of the shaft, which is also shown in Figure 23. For the Ground Mission, the mounting structure will already be installed, and our team member will screw the two parts of the radome rod together at their discontinuity. The metal bolt will extend about an inch into the radome rod to ensure that the radome does not separate from the plane during flight. Overall, this design reflects the team's goal of reducing $(T_{GM})_{USC}$.

Attack Stores

Attack store mechanisms were designed for quick installation and reliability so that they can successfully complete Mission 3 flight goals. Prototypes were made early in the design process as shown in Figure 24. All designs required one servo per store; designs in which stores shared a servo were not considered as the loss of a single servo in flight would result in the loss of multiple stores. Due to the importance of Mission 3, the team determined that the weight and drag saved from sharing servos did not outweigh the risk.



Figure 24: Attack store prototypes; Mylar strap, ring, and neck mechanisms (left to right)

The Mylar strap mechanism attaches stores using a zip tie and releases them using a servo. The ring mechanism holds the front and back of the stores with metal wire; a servo pulls the front ring away from the store to release it. The neck mechanism grips the store by its neck and releases stores by opening the hatch with a servo. The Mylar strap mechanism was selected for its reliability, as it stayed rigid during in-lab and in-flight testing.

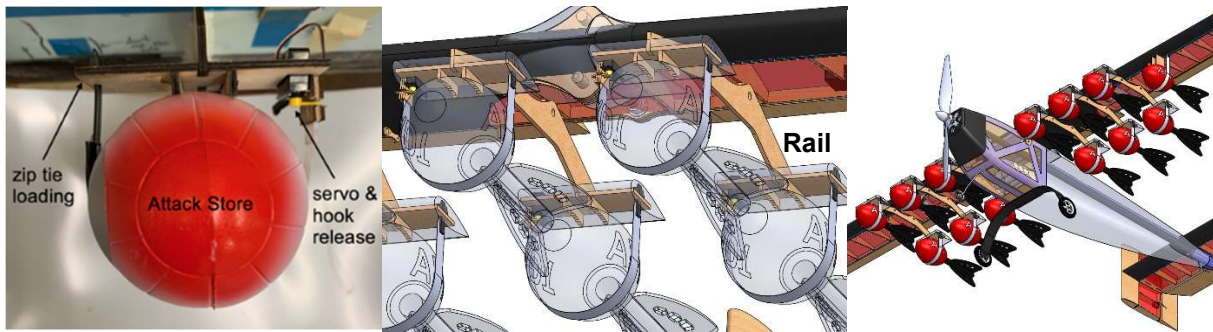


Figure 25: Integration of attack store (left), rail to wing (middle), and over store placement (right)

The final mounting configuration, shown in Figure 25, has two plywood rails that extend along the longitudinal axis of the attack store to aid in alignment during loading and to ensure payload stability during Mission 3. A servo was attached to one side of the vertical plate and sized to handle in-flight loads. Adjacent is a housing structure made from 1/16 in. (0.16 cm) plywood; a slit in the two plates aligns with the servo arm and allows for a Mylar hook to be inserted. When the servo arm sits in the housing slot, the hook locks into place. Then, once the servo is actuated, the hook unlocks and the attack store is released. Prior to deployment, a Mylar strap attached to a zip tie restrains the payload. The finger-catch mechanism for the reusable zip tie is located on the opposite side of the attack store and is where the zip tie strap integrates during loading. The Mylar strap was heat-trained to curl up into a firm loop after store deployment to reduce its drag profile. A detailed view of the store mounting and dropping mechanism is shown in Section 5.6.

The stores are strapped to horizontal plates that are mounted to a vertical rail attaching two store deployment mechanisms to a plywood wing rib. The rail is attached to tabs on the plywood rib via two metal bolts, which allow the entire fixture to be removed for Missions 1 and 2. The tabs are placed near the main spar and plywood aft spar, transferring flight loads onto the wing structure.

Calculations in Section 4.4.3 showed that stores in the propeller wash had the most drag. Since stability analysis showed that the CG shift was negligible, the stores contributing most to drag will be released first to increase flight speed since the number of laps flown for Mission 3 is the team's primary design objective. Thus, stores closest to the fuselage were dropped first. Using a microcontroller that interfaced with all 13 servos, the team pre-programmed the drop sequence and only needed to flip a single switch on the transmitter to deploy the appropriate payload. Stores will be dropped on alternating sides of the fuselage. This microcontroller has been coded and successfully tested, as shown in Figure 26.

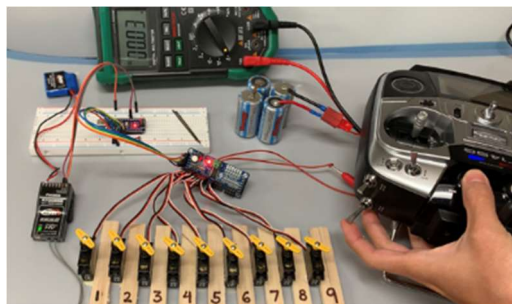


Figure 26: Microcontroller testing for independent deployment of stores

5.3.6 FUSELAGE

The fuselage was designed to transfer loads among subcomponents. It consists of a foam-fiberglass truss with a 2-layer Kevlar skin, and an integrated carbon fiber tail boom. The tail boom decreased structural weight by replacing the foam truss at the aft-end of the fuselage. Plywood bulkheads were integrated to serve as attachment points for the wing, landing gear, and motor mount. The motor mount is reinforced with carbon fiber to transfer torsional loads. The fuselage was tested in lab and flight to withstand all loads.

5.3.7 PROPULSION SYSTEM

Each propulsion component was tested to optimize the system, particularly focusing on advance ratios (J) and number of cells. A Kv below 500 was needed to meet the Mission 3 endurance and takeoff requirements to swing larger diameter propellers. Testing showed that the Neu 1415/2Y with a 4.2:1 gearbox satisfied the 10 ft (3 m) TOFL. Flight testing also confirmed that both the power and current requirements would be met for each mission's package. The components for each mission are shown in Table 16.

Table 16: Package Breakdown by Mission

	Mission 1 & 2	Mission 3
Motor/Gearbox	Neu 1415/2Y with P32 (4.2:1) Gearbox	
Propeller	APC 18x12E	APC 20x10 E
Battery	21 x Tenergy 4200mAh	23 x Elite 5000mAh
ESC	Phoenix Edge 50	
Rx	Futaba R7008SB	
Rx Pack	4 x 1/3 AAA 170mAh	
Misc.	Wiring, Solder, Connectors, Fuse	

The package for Mission 2 was optimized by using an advance ratio of 0.66 to minimize $(T_{M2})_{USC}$. For Mission 3, diameter was increased to 20 in. (50.8 cm) and pitch reduced to 10 in. (25.4 cm) to increase static thrust for takeoff. Through flight tests, the Elite 5000s allowed the plane to fly 10 minutes for Mission 3, due to their higher capacity, while the lower weight of the Tenergy 4200s allowed the plane to fly faster; thus, different batteries were used for each mission to achieve the design objectives: minimize $(T_{M2})_{USC}$ and maximize $N_{scoring laps}$. The numbers of cells were optimized in PlaneTools as seen in Figure 27.

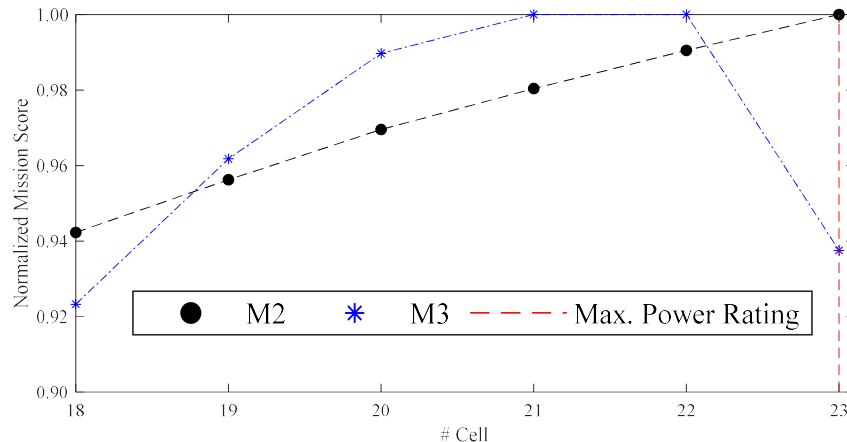


Figure 27: Cell Optimization for Mission 2 (23 cells) and Mission 3 (21 cells)

5.4 WEIGHT AND MASS BALANCE

The empty weight (*EW*) for *ExSCalibur* was 6.15 lb (2.79 kg). The flight batteries were used as a ballast to ensure the CG was within the static margin for all mission configurations. The coordinate system used to model the CG is shown below in Figure 28.

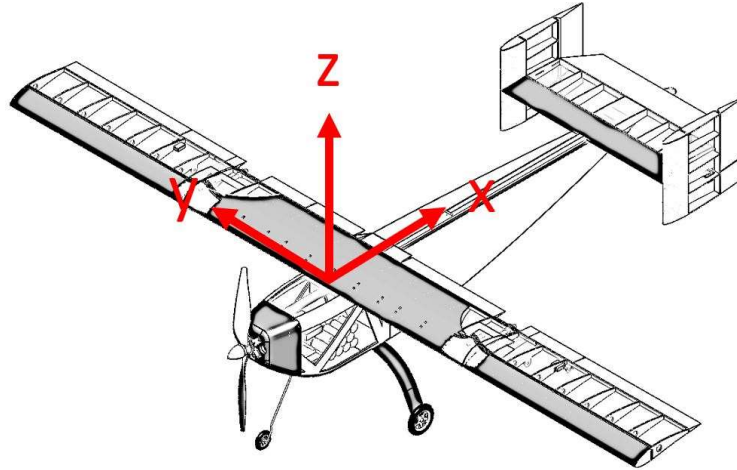


Figure 28: Aircraft coordinate system with the origin is placed at the leading edge of the wing

Table 17 shows each component's mass and CG location with respect to the coordinate system above. The Mission 3 configuration is shown with full stores and no stores (by removing the values in the attack stores row). The aircraft CG will still remain within the static margin even after the stores are dropped.

Table 17: Mass balance table for all missions

Aircraft Component	Mass		X		Y		Z	
	[lb]	[g]	[in.]	[cm]	[in.]	[cm]	[in.]	[cm]
General								
Fuselage	0.84	381	7.11	18.1	0.15	0.4	-2.60	-6.6
Wing	1.19	539	3.18	8.1	-0.04	-0.1	0.26	0.7
Motor	0.82	370	-7.46	-18.9	0.00	0.0	-1.75	-4.4
Tail	0.43	193	38.02	96.6	-0.22	-0.6	-0.54	-1.4
Landing Gear	0.30	138	3.04	7.7	-0.02	0.0	-9.58	-24.3
Mission 1								
Battery	3.39	1539	0.60	1.5	-0.03	-0.1	-5.74	-14.6
Prop	0.21	96	-10.25	-26.0	0.00	0.0	-1.75	-4.4
Mission 2								
Battery	3.39	1539	-0.52	-1.3	-0.03	-0.1	-5.74	-14.6
Prop	0.19	87	-10.25	-26.0	0.00	0.0	-1.75	-4.4
Radome	0.34	156	14.94	37.9	0.00	0.0	0.34	0.9
Mission 3								
Battery	3.21	1456	2.10	5.3	0.00	0.0	-5.74	-14.6
Prop	0.21	96	-10.31	-26.2	0.00	0.0	-1.75	-4.4
Attack Stores	1.93	876	3.88	9.9	-2.19	-5.6	-3.95	-10.0
Store Mechs	0.87	393	3.48	8.8	-1.75	-4.4	-3.28	-8.3

5.5 FLIGHT AND MISSION PERFORMANCE

The expected flight performance of the final aircraft is listed in Table 18. These figures were calculated using the PlaneTools simulation model.

Table 18: Predicted Aircraft Performance Parameters for each mission

Performance Parameters	Mission 1	Mission 2	Mission 3
C_{Lmax}	2.23	2.23	2.23
$C_{Lcruise}$	0.33	0.39	0.43
e	0.49	0.55	0.70
C_{D0}	0.08	0.09	0.13
$(L/D)_{max}$	9.70	9.68	9.69
$(L/D)_{cruise}$	4.73	3.68	4.51
Rate of Climb [ft/s]	12.6 (3.9 m/s)	12.5 (3.8 m/s)	11.1 (3.4 m/s)
W/S [lb/ft ²]	1.66 (8.1 kg/m ²)	1.69 (8.3 kg/m ²)	2.05 (10 kg/m ²)
u_{cruise} [ft/s]	70 (21 m/s)	65 (20 m/s)	62 (19 m/s)
u_{stall} [ft/s]	32 (9.8 m/s)	32 (9.8 m/s)	36 (9.4 m/s)
TOFL [ft]	7 (2.1 m)	7 (2.1 m)	10 (3.0 m)
Battery Weight [lb]	3.3 (1.5 kg)	3.3 (1.5 kg)	3.1 (1.4 kg)
Empty Weight [lb]	7.4 (3.4 kg)	7.4 (3.4 kg)	7.3 (3.3 kg)

Based upon these performance parameters, the corresponding mission results and score parameters are listed in Table 19.

Table 19 : Mission-Specific PlaneTools Scoring Predictions

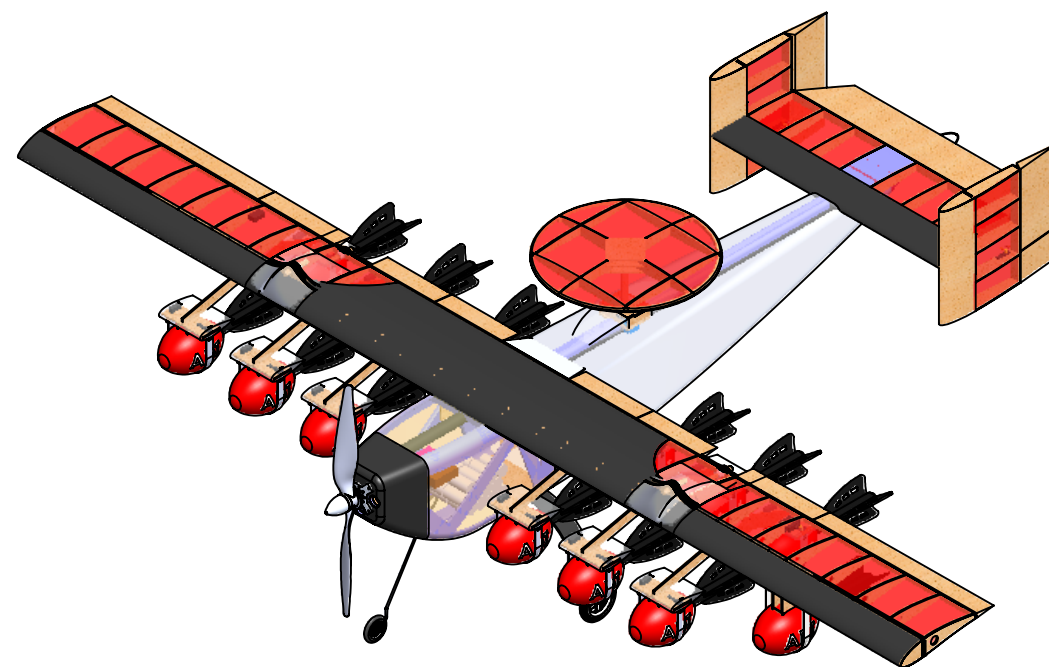
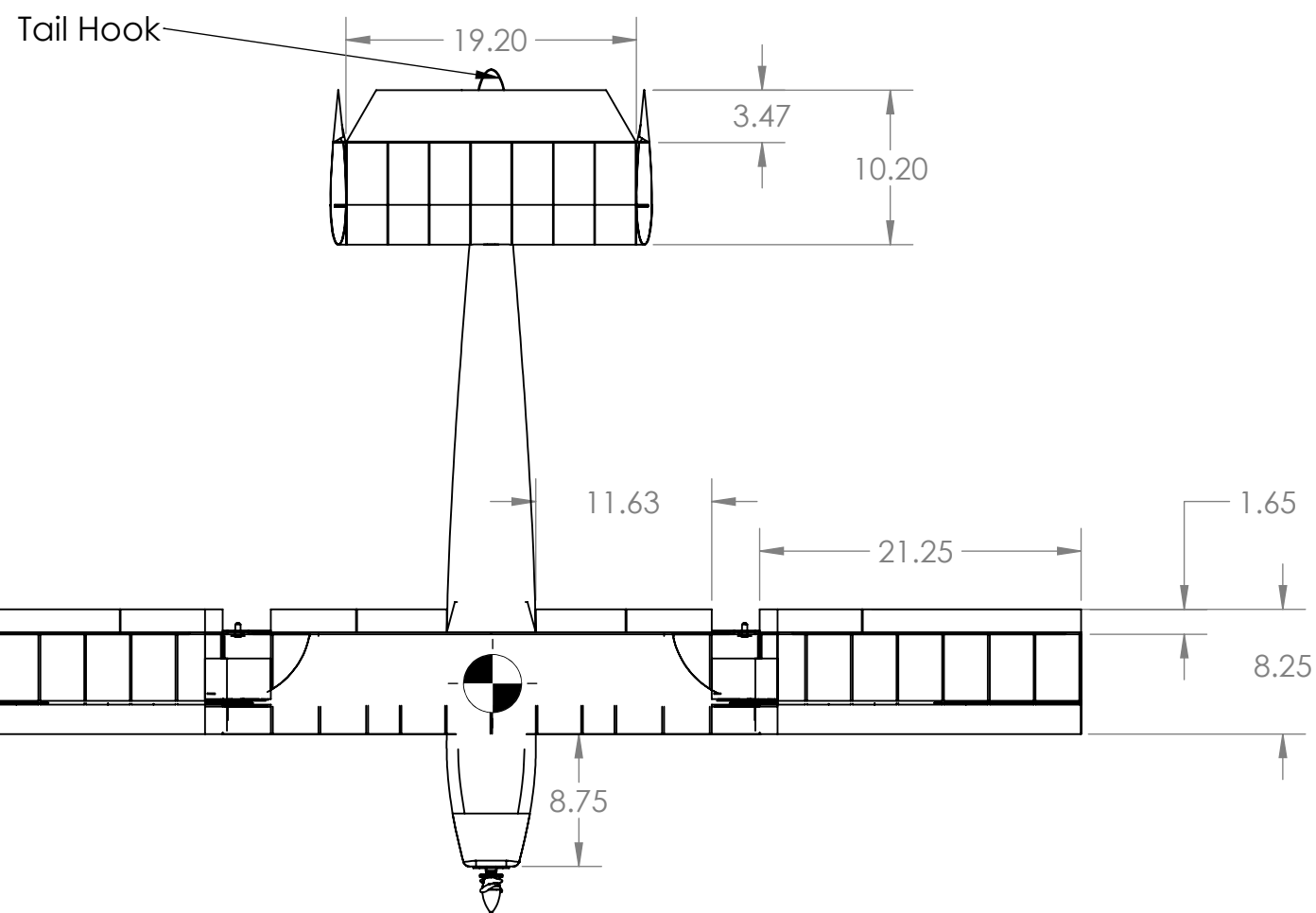
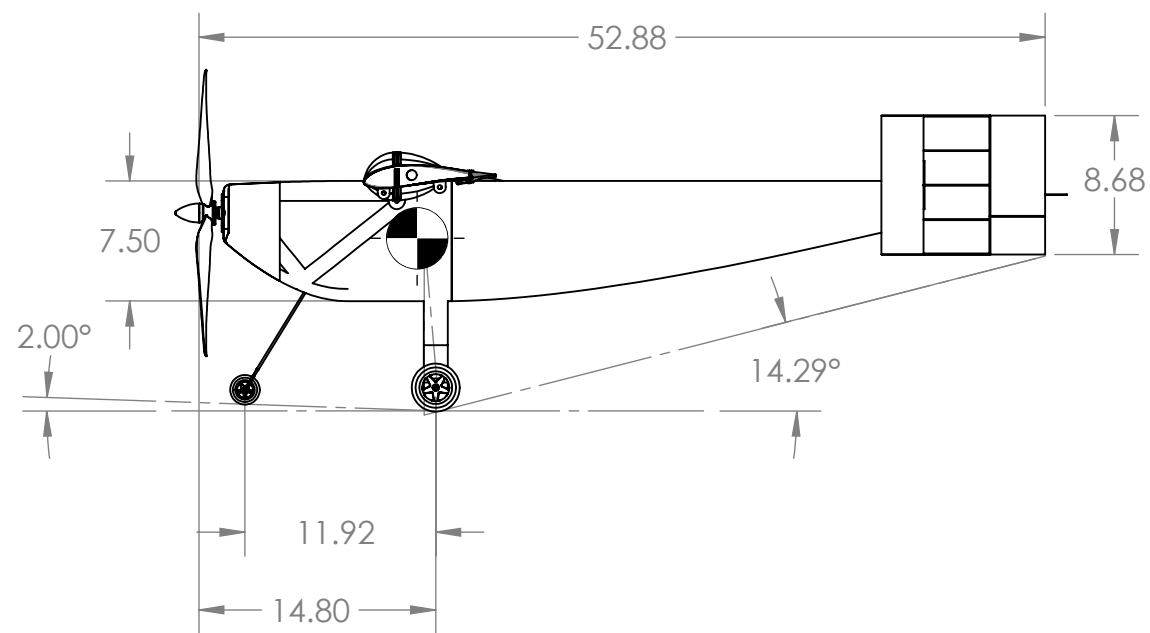
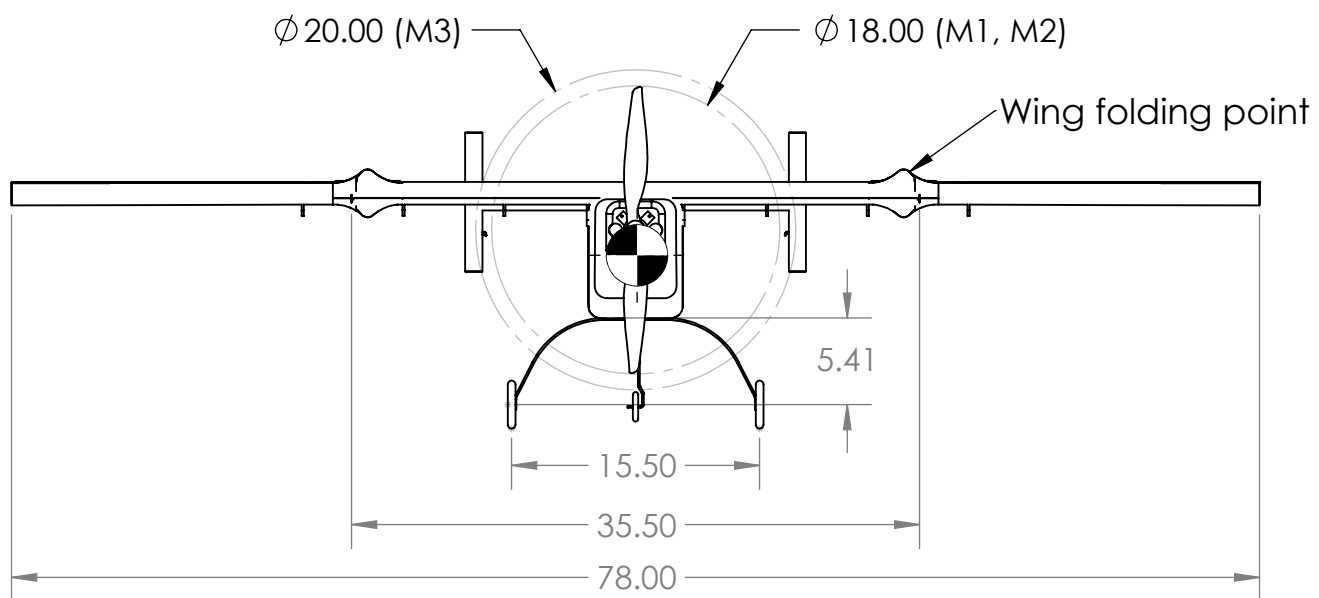
Score Parameters	Mission 1	Mission 2	Mission 3
Completion Score	1	-	2
T_{USC} [s]	-	116	-
T_{Best} [s]	-	90	-
N_{laps}	-	-	13
Mission Score	1.00	1.76	15.0
EW [lb]	7.4 (3.4 kg)	7.4 (3.4 kg)	7.3 (3.3 kg)
WS [in]	78.0 (2.0 m)		
Total Flight Score	17.76		
Ground Mission Score	0.67		
Total Score	1843		

5.6 DRAWING PACKAGE

The following drawing package includes a dimensional 3-view, structural arrangement, subassembly detail, and payload drawings. All drawings were made using SolidWorks [18].

2

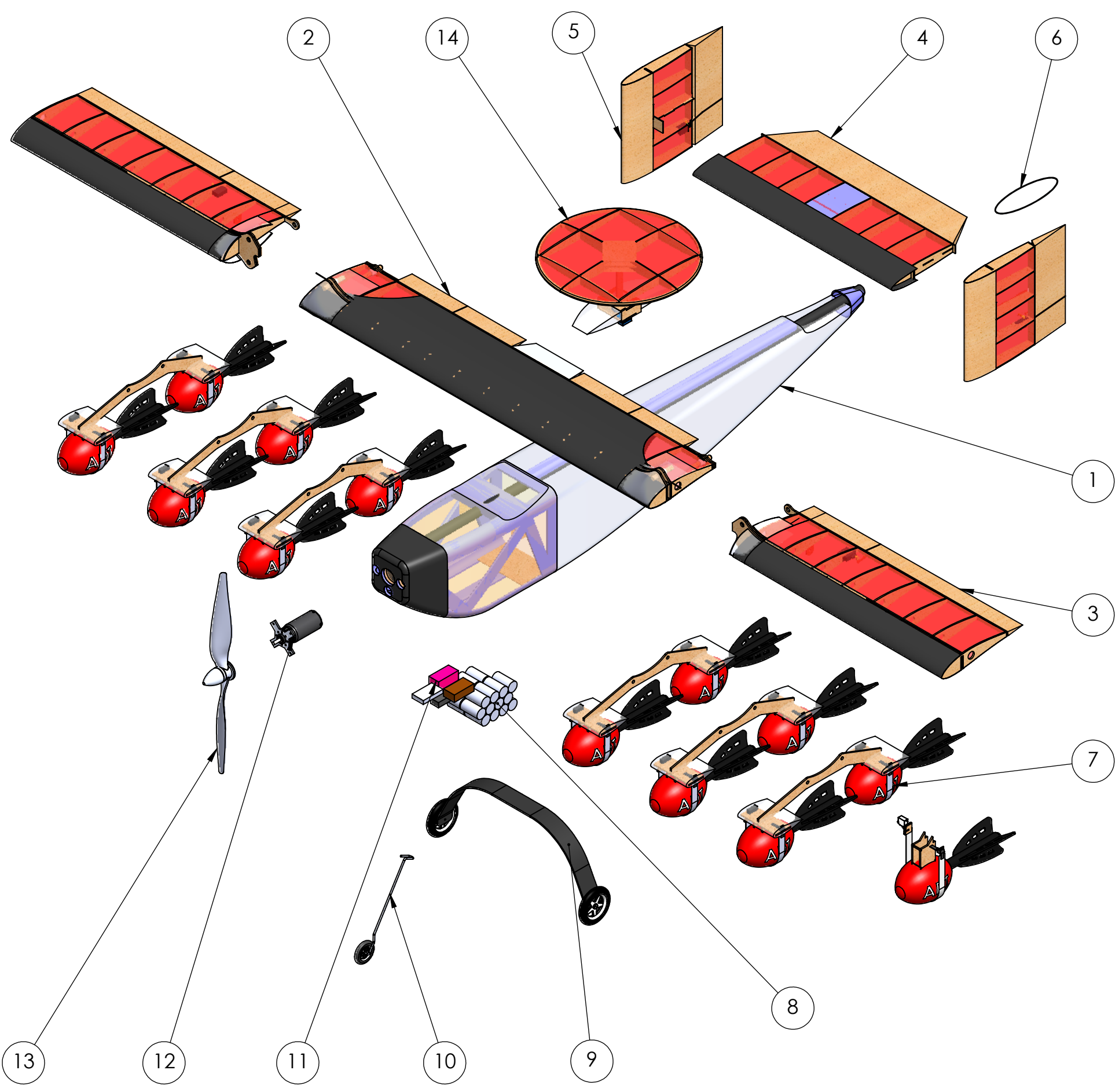
1



Radome and Attack Stores are not attached during the same flight mission

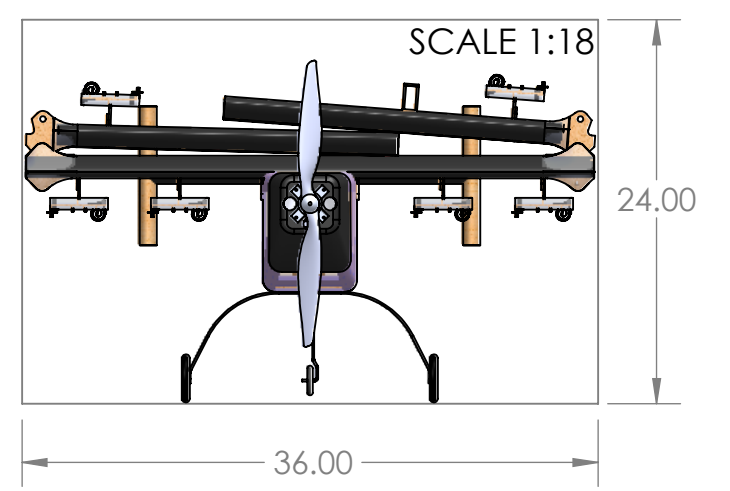
		UNLESS OTHERWISE SPECIFIED: DIMENSIONS ARE IN INCHES		SCALE 1:18	
		University of Southern California Cessna-Raytheon-AIAA Design/Build/Fly 2019			
		TITLE:			
		<h1>ExSCalibur</h1>			
		DWG NO.			B
		Aircraft 3-View			
DRAWN	LG	SCALE:1:12	Drawing Package	2/22/2019	SHEET 1 OF 4
CONSIDER					
APPVD	LS				
MFG	NR				
Q.A	ZT				

1



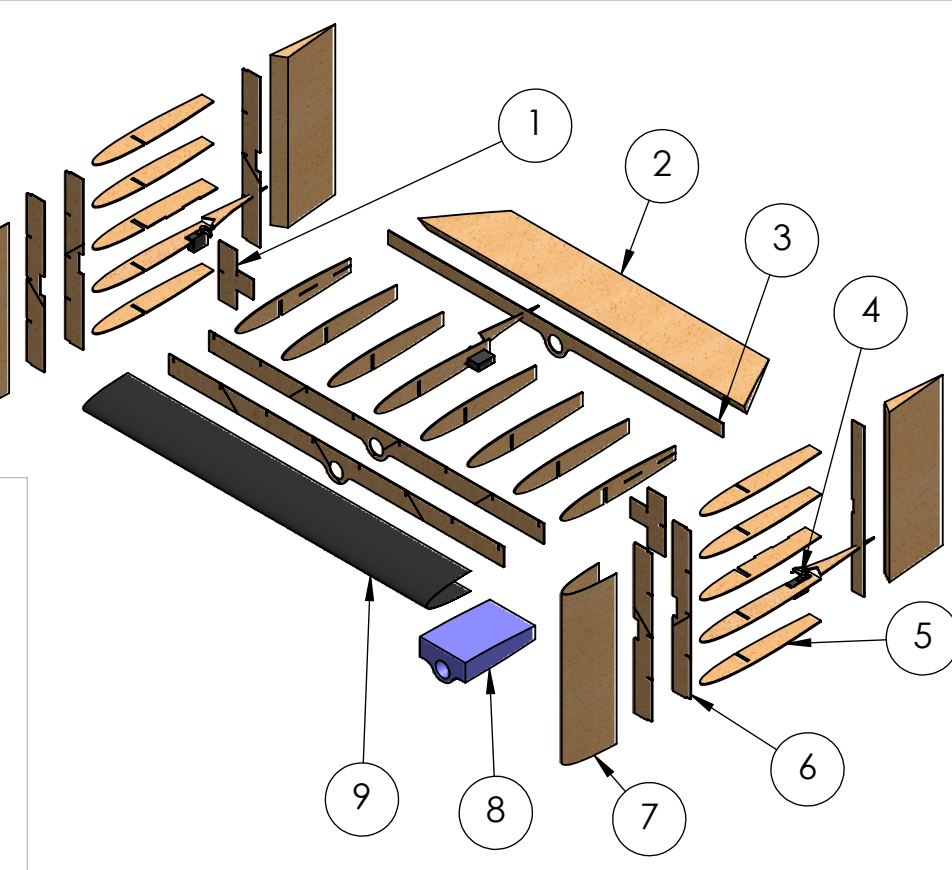
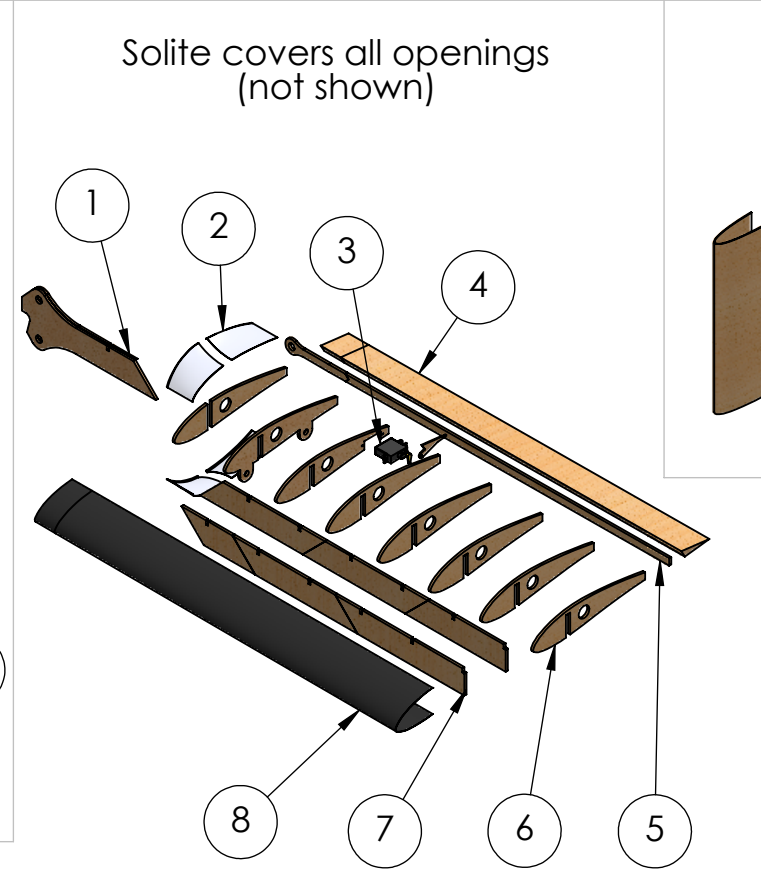
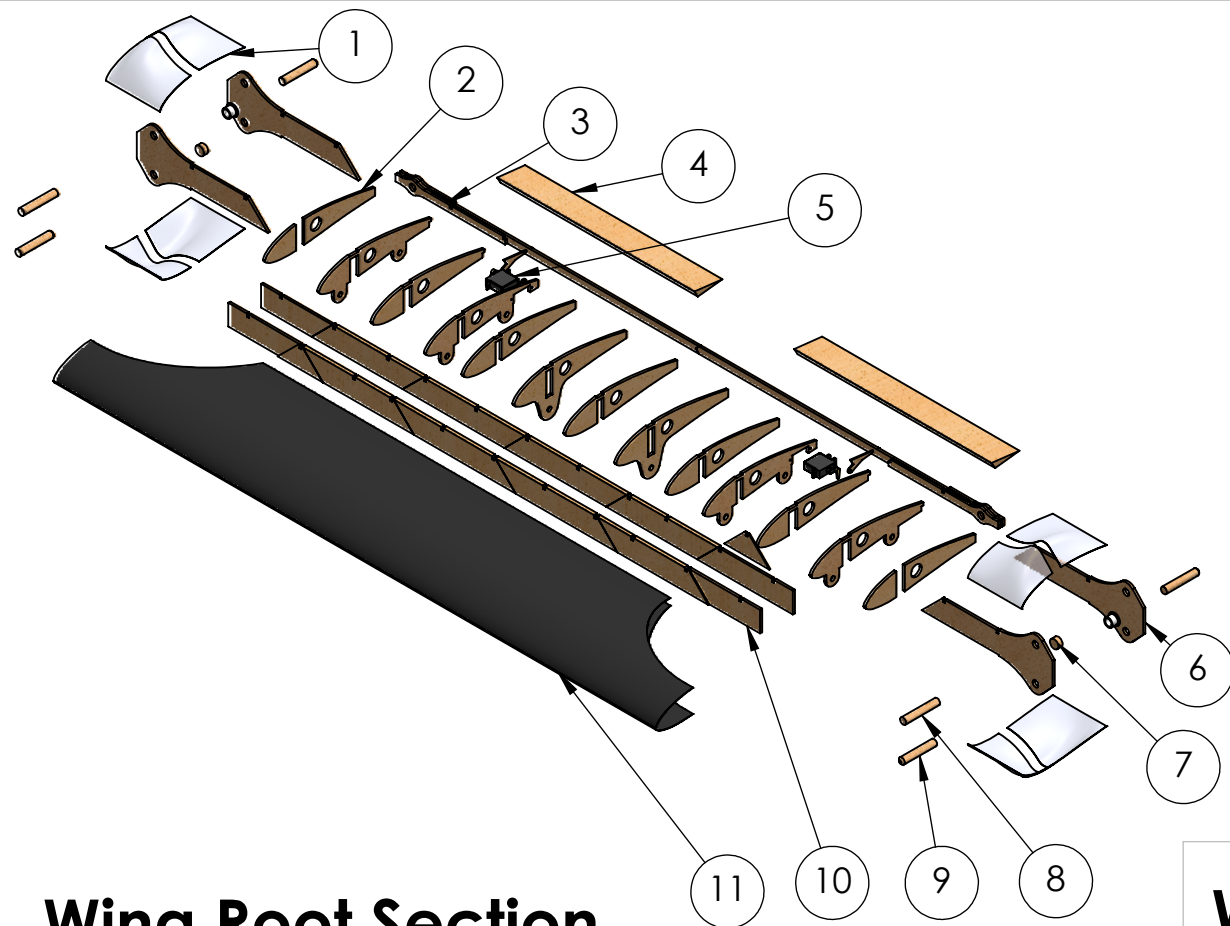
ITEM NO.	COMPONENT	DESCRIPTION	QTY
1	Fuselage	Carbon Fiber, Kevlar, Foam Stringer, Tail Boom	1
2	Wing Root Section	Plywood/Balsa Built-up, Carbon D-Box, Solite Covering	1
3	Wing Tip Section		2
4	Horizontal Stabilizer		1
5	Vertical Stabilizer	Plywood/Balsa Built-up, Balsa D-Box, Solite Covering	2
6	Tail Hook	Kevlar string	1
7	Attack Stores	Plywood, servo, Mylar, Ziptie	13
8	Battery Pack	23 x Elite 4200s / 21 x Elite 5000s	1
9	Main Landing Gear	Carbon Uni Layup, Foam/Plastic Wheel	1
10	Nose Gear	Piano Wire, Foam/Plastic Wheel	1
11	Receiver	Futaba 617FS	1
12	Motor	NEU 1415/2Y	1
13	Propeller	18x12 / 20x10	1
14	Radome	Plywood/Balsa Built up, Solite Covering	1

Stowed Configuration



Radome and Attack Stores are not attached during the same flight mission

		UNLESS OTHERWISE SPECIFIED: DIMENSIONS ARE IN INCHES		SCALE 1:12	
		University of Southern California Cessna-Raytheon-AIAA Design/Build/Fly 2019			
		TITLE: ExSCalibur			
DRAWN	LG	DWG. NO.		B	
CONSIDER		Structural Arrangement			
APPVD	LS	SCALE:1:24		Drawing Package	2/22/2019
MFG	NR				SHEET 2 OF 4
Q.A	ZT				



Wing Root Section

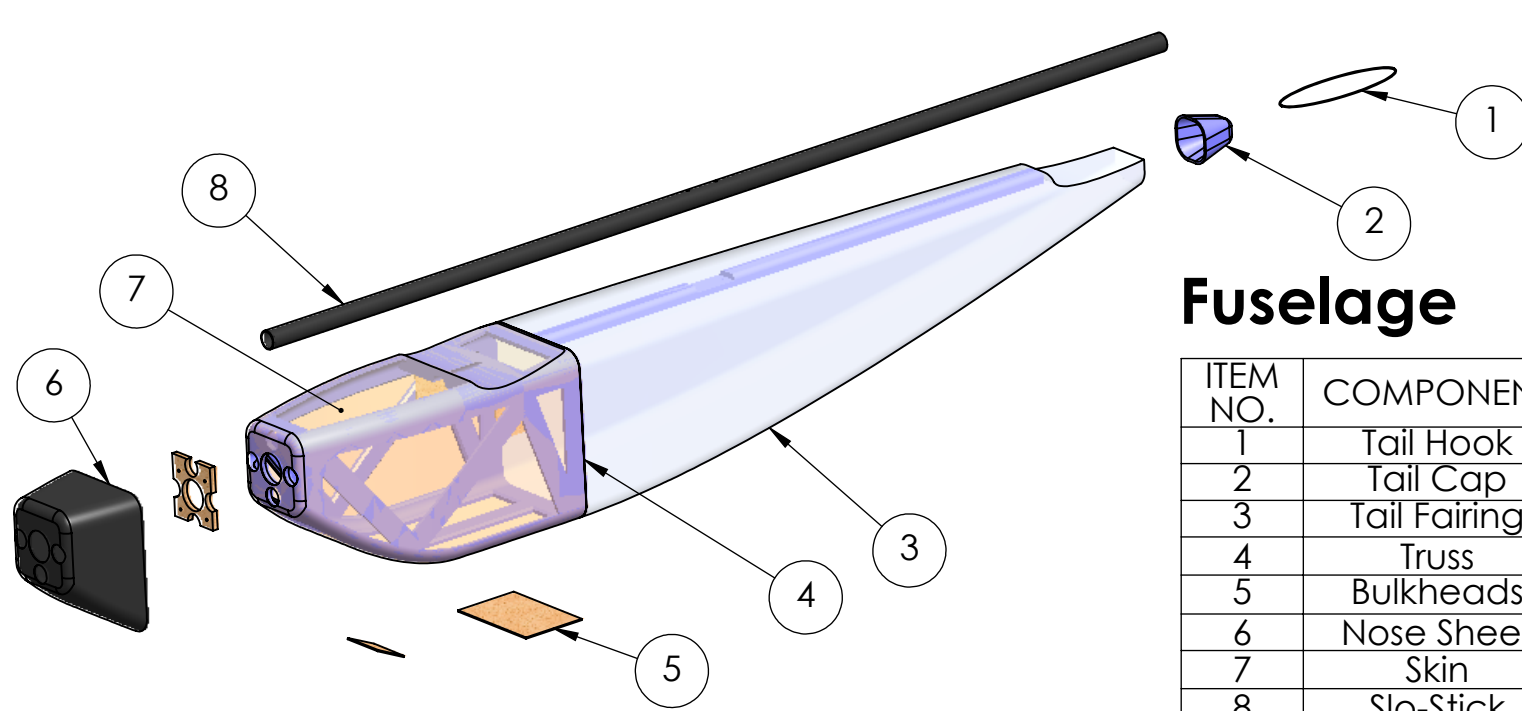
ITEM NO.	COMPONENT	MATERIAL	QTY
1	Fairing	Fiber Glass	8
2	Ribs	1/8" Plywood/Balsa	13
3	Aft Spar	1/8" Plywood/Balsa	1
4	Flap	Tapered Balsa	2
5	Servo	D60	2
6	Spar Connectors	1/8" Plywood	4
7	Pin Block	1/4" Plywood	2
8	Hinge Pin	Spruce	2
9	Lock Pin	Spruce	4
10	Front Spar	3/16" Balsa	2
11	D-Box	45° Carbon	1

Wing Tip Section

ITEM NO.	COMPONENT	MATERIAL	QTY
1	Spar Connectors	1/8" Plywood	2
2	Fairing	Fiber Glass	4
3	Servo	D60	2
4	Aileron	Tapered Balsa	2
5	Aft Spar	1/8" Plywood/Balsa	1
6	Ribs	1/8" Plywood/Balsa	8
7	Front Spar	1/8" Balsa	2
8	D-Box	45° Carbon	1

H-Tail

ITEM NO.	COMPONENT	MATERIAL	QTY
1	T-Connector	1/16" Plywood	2
2	Control Surface	Tapered Balsa	3
3	Aft Spar	1/16" Balsa	3
4	Servo	D47 & D60	3
5	Ribs	1/16" Plywood/Balsa	18
6	Front Spar	1/16" Balsa	6
7	Vertical D-Box	1/32" Balsa Sheet	2
8	Filler	Foam	1
9	Horizontal D-Box	45° Carbon	1

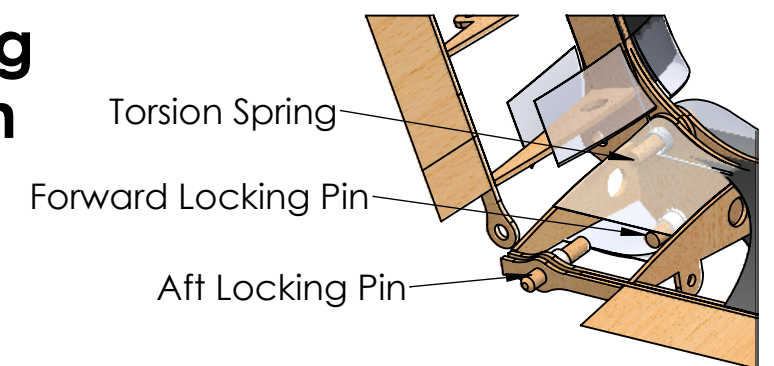


Fuselage

ITEM NO.	COMPONENT	MATERIAL	QTY
1	Tail Hook	Kevlar String	1
2	Tail Cap	Foam	1
3	Tail Fairing	Fiber Glass	1
4	Truss	Foam	1
5	Bulkheads	1/8" Plywood	5
6	Nose Sheet	45° Carbon	1
7	Skin	Kevlar	1
8	Slo-Stick	Carbon Tube	1

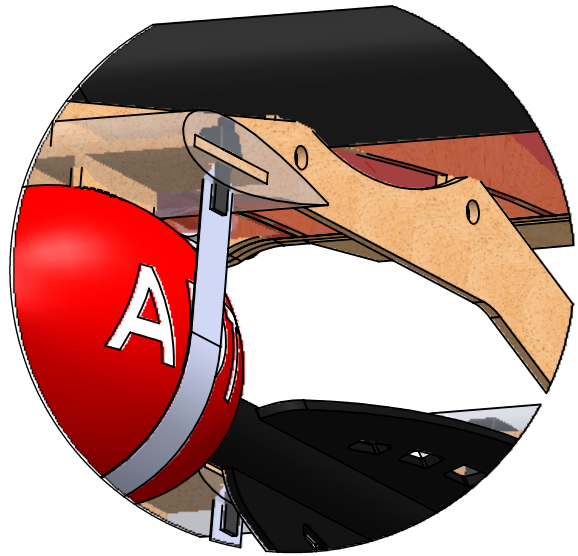
Wing Folding Mechanism

SCALE 1:6

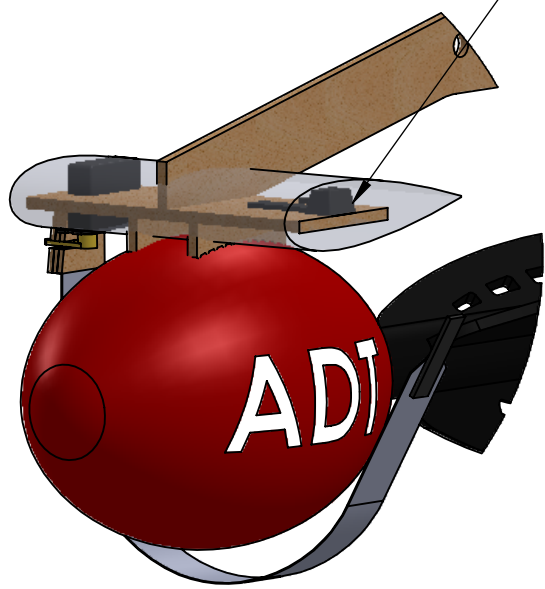


UNLESS OTHERWISE SPECIFIED: DIMENSIONS ARE IN INCHES		SCALE 1:12	
University of Southern California Cessna-Raytheon-AIAA Design/Build/Fly 2019			
TITLE:		ExSCalibur	
DRAWN	LG	DWG NO.	Subassembly Detail
CONSIDER			B
APPV'D	LS		
MFG	NR		
Q.A	ZT	SCALE:1:12	Drawing Package 2/22/2019 SHEET 3 OF 4

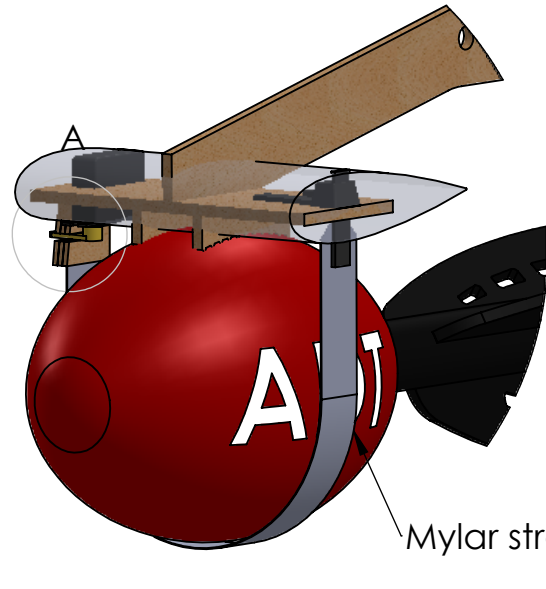
Attack Stores



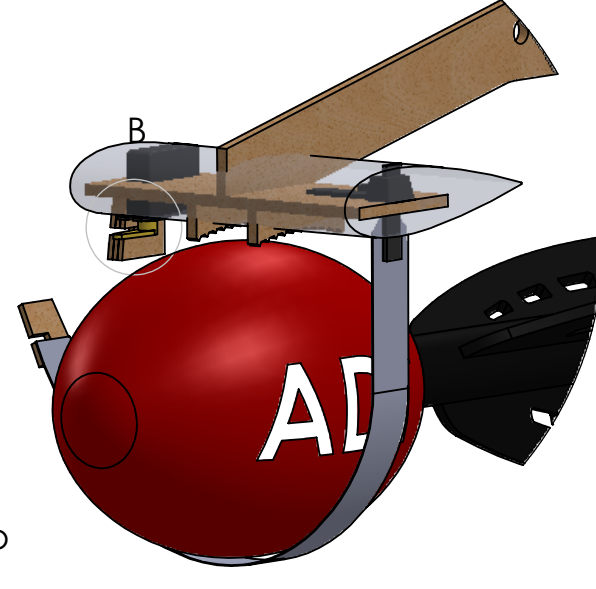
Store Structures bolt on to ribs



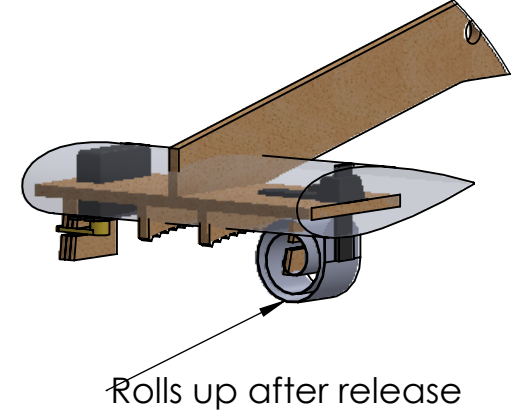
1) Fasten Stores



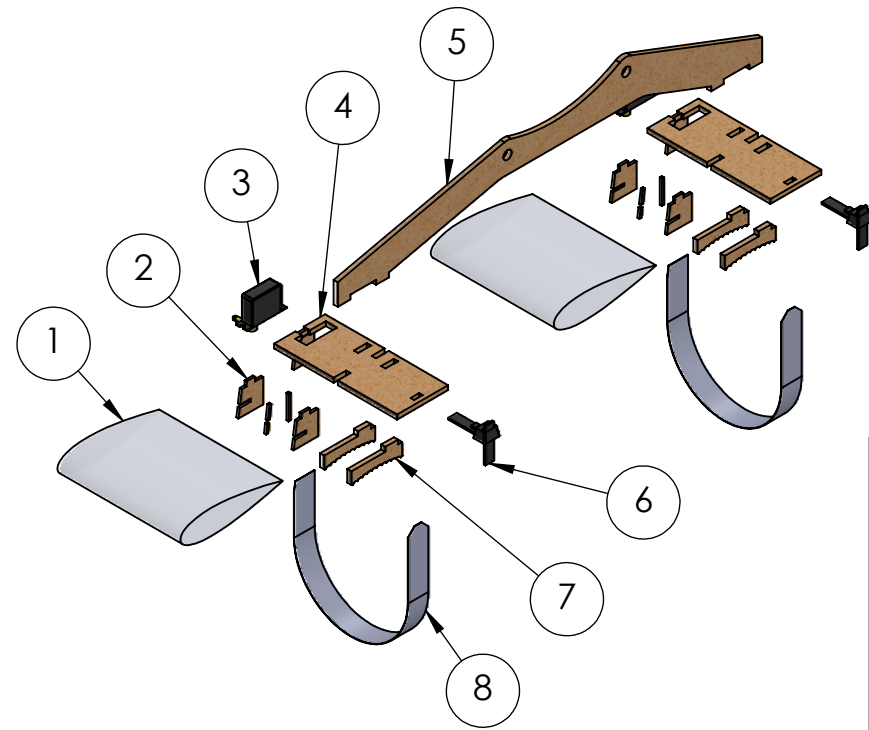
2) Hold during flight



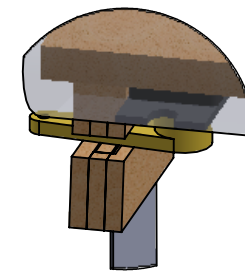
3) Release during flight



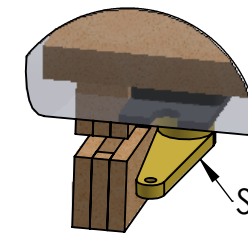
4) Minimize Drag



ITEM NO.	COMPONENT	MATERIAL	QTY
1	Fairing	Fiber Glass	2
2	Hook Plates	1/16" Plywood	4
3	Servo	D47	2
4	Bone Plate	1/8" Plywood	2
5	Rail Plate	1/8" Plywood	1
6	Ziptie	Nylon	2
7	Saddle	1/8" Plywood	4
8	Store Strap	Mylar	2



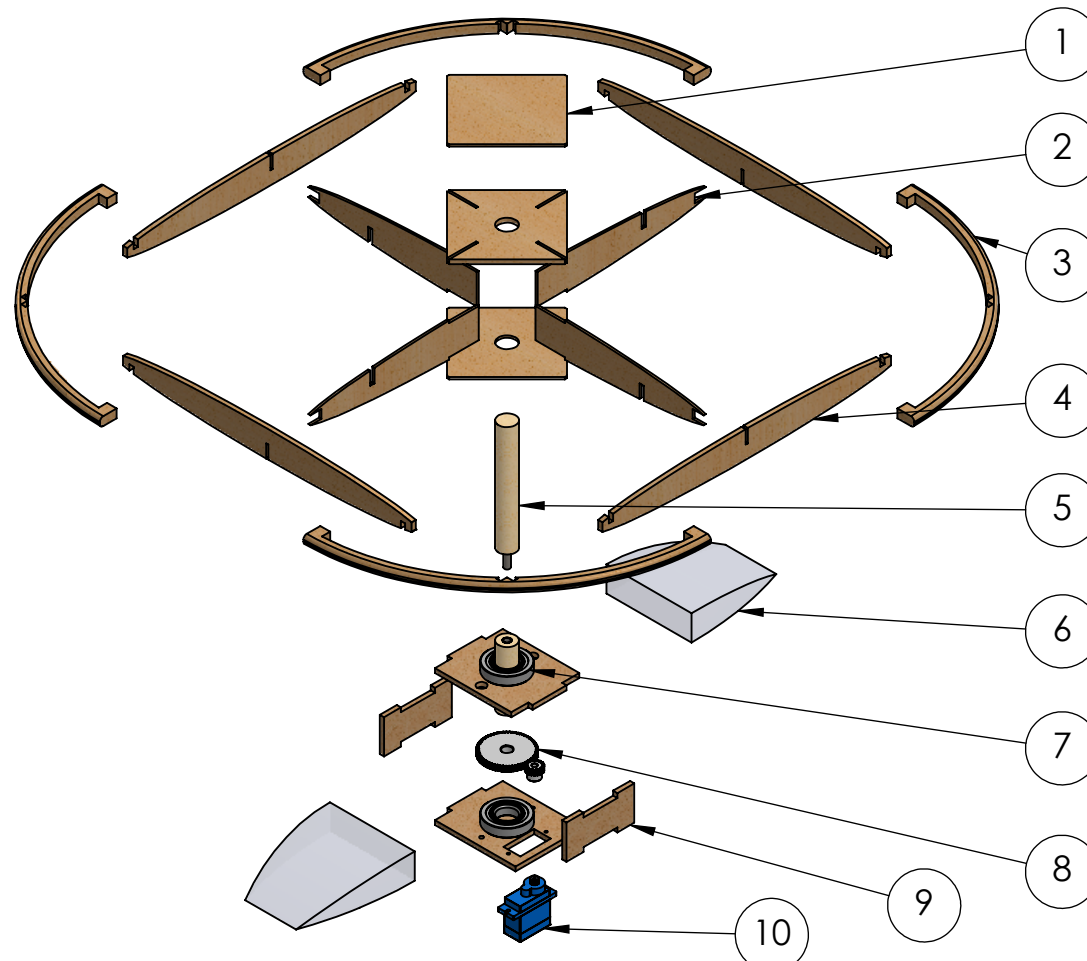
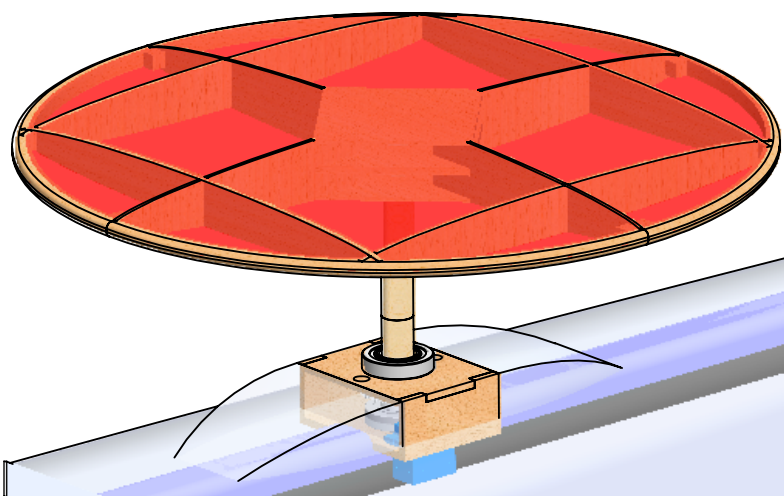
DETAIL A
SCALE 1:1



DETAIL B
SCALE 1:1

Servo actuates to release stores

Radome



ITEM NO.	COMPONENT	MATERIAL	QTY
1	Hub Plates	1/16" Plywood & 1/8" Balsa	2
2	Major Ribs	1/16" Plywood	4
3	Base Ring	1/4" Balsa	4
4	Minor Ribs	1/8" Balsa	4
5	Threaded Dowel	Spruce	2
6	Fairing	Fiber Glass	2
7	Bearing	Nylon & Glass	2
8	Gears	Nylon	2
9	Box Plates	1/8" Plywood	4
10	Servo	FS09R	1

UNLESS OTHERWISE SPECIFIED: DIMENSIONS ARE IN INCHES	
University of Southern California Cessna-Raytheon-AIAA Design/Build/Fly 2019	
TITLE: ExSCalibur	
DRAWN LG	NAME
CONSIDER	DWG. NO.
APP'VD LS	Payload Accomodations
MFG NR	B
Q.A ZT	SCALE: 1:8 Drawing Package 2/22/2019 SHEET 4 OF 4

6.0 MANUFACTURING PLAN

Numerous manufacturing processes were evaluated for each component including the wing, fuselage, tail, landing gear, wing folding mechanism, radome, and payload attachment mechanisms. The fabrication and design of each component is detailed in the following subsections.

6.1 MANUFACTURING PROCESSES INVESTIGATED

To identify the best manufacturing process for each aircraft component, benefits and drawbacks of each technique was considered.

6.1.1 FOAM

Foam is relatively cheap and can be easily shaped using a hotwire foam cutter and sanding. Although nonstructural foam elements can be lightweight, it is often heavier than balsa and composite structures. The team has extensive experience building with foam to validate the sizing of a prototype aircraft, but often shifts toward balsa or composites builds later in the design process to minimize structural weight.

6.1.2 Balsa BUILD UP

Balsa is the lowest density material used for construction of aircraft structures. Well-designed balsa structures can often be lighter than composite structures for smaller aircraft, as demonstrated by the historical success of balsa aircraft in previous AIAA DBF competitions. Balsa, however, is not as strong as composites. The accessibility of CAD and laser cutters makes balsa built up structures more precise.

6.1.3 3D PRINTING

Additive manufacturing allows for the design of complex forms that would otherwise be difficult to build. The team has access to a Markforged Mark Two 3D printer that creates high-precision (± 0.005 in.) parts reinforced with fiberglass, carbon fiber or Kevlar [14]. 3D printing can be used for rapid prototyping of complex mechanisms and reducing lead times in making molds for composites. This material, however, is heavy.

6.1.4 COMPOSITES

Composites have high semi-isotropic properties. Additionally, composites are more durable than other build methods—more likely to bend than break. The team has a strong composite build skillset and has won competitions through the innovative design of foam-reinforced Kevlar fuselages in 2014 and 2017 that were lighter than comparable balsa structures [3][20]. Building composites is expensive because of material costs and requires lead times upwards of six weeks to build molds and allow for fully cured parts.

6.2 MANUFACTURING PROCESSES SELECTED

6.2.1 WING AND TAIL STRUCTURE

The wing and tail ribs and spar shear webs were laser cut with grains aligned in the expected load directions. The shear webs were assembled with epoxy resin. The wing was divided into 3 parts by the folding mechanism, as shown in Figure 29, and manufactured separately. The folding mechanism integrated directly into the main spar on all parts. Spar caps and D-boxes were laid up and integrated separately for each section, and the final components were assembled at the folding mechanism. A solite skin was used to cover areas where the D-box did not cover the wing.

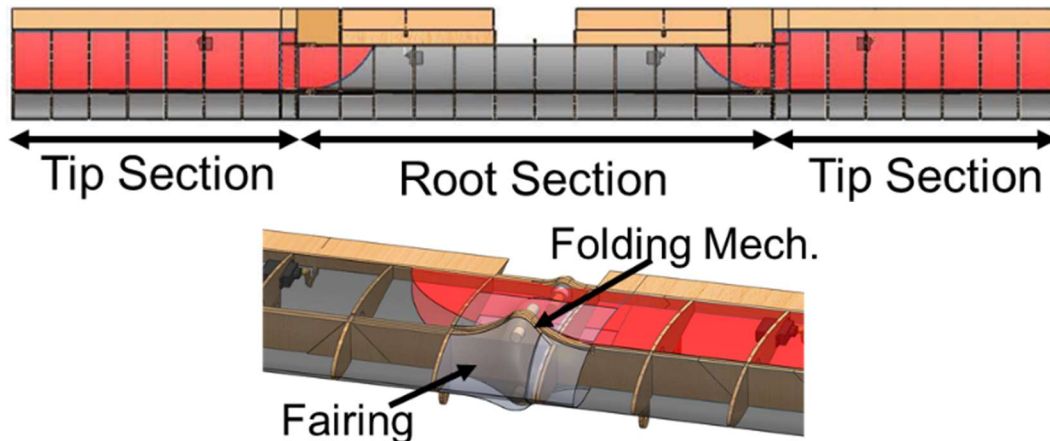


Figure 29: Full Wing Assembly (top) with integrated folding mechanism with fairing (bottom)

The tail, shown in Figure 30, was assembled by building the vertical stabilizers first in a similar fashion as the wing sections. The plywood mounting reinforcements were integrated into the verticals. Airfoil shaped notches were carved into the root-facing sides to accommodate the horizontal D-box. The horizontal skeleton was then built and the verticals were attached on each side. Once integrated, solite was applied onto the horizontal and the tail attached to the tail boom.

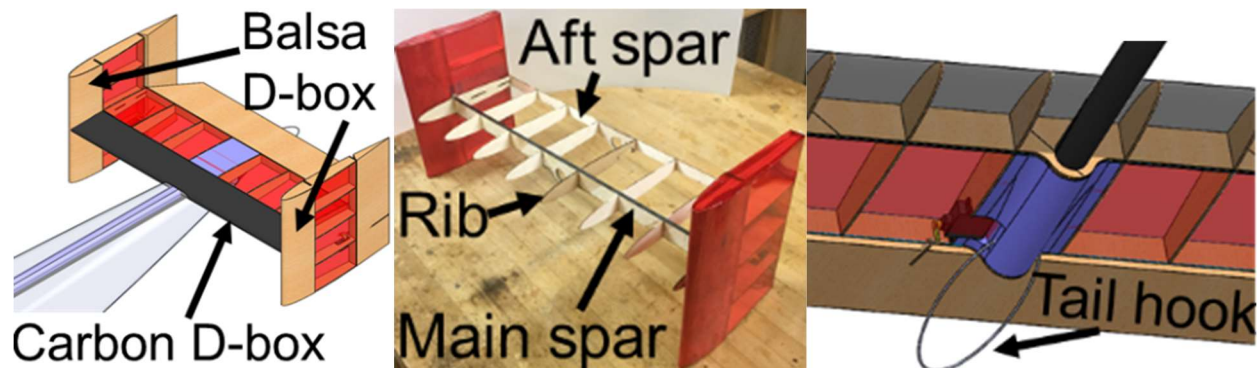


Figure 30: Full tail assembly (left), in-lab model (middle), and tail hook (right)

For the tail hook, carbon tow was threaded through a hole that was drilled through the end boom at the end. The tow was then threaded through and tied into a loop. The edges of the boom, which the tow pressed against under load, was reinforced with a thin layer of epoxy filler.

6.2.2 WING FOLDING MECHANISM

The wing folding mechanism is integrated directly into the balsa wing structure as shown in Figure 31.

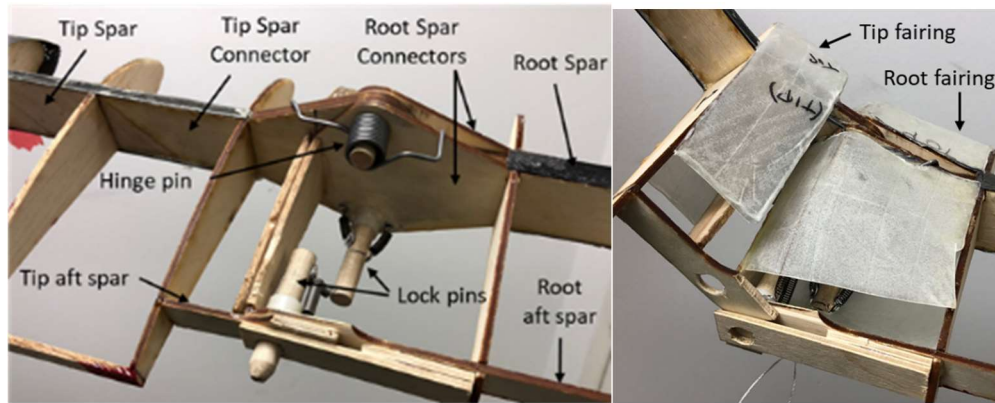


Figure 31: Wing folding mechanism integrated into the wing

In the locking mechanism, first the laser-cut 1/8" plywood root spar connectors were attached to the front and back of the 1/4" balsa spar. Then the carbon spar caps were tapered out and attached to the top and bottom of the root spar and root spar connector. The tip spar connector was adhered in-plane with the tip spar, and the spar cap was extended the same way. Linear springs were bolted to lock pins on the main and aft spar. Then, both the lock and hinge pins were inserted into holes in the spar connectors. A torsion spring was added to the hinge pin for unfolding. In flight configuration, flight loads are transferred along plywood ribs on the root and tip sections through the three pins on the main and aft spars. After the carbon D-box and solite are added (not shown), two fairings are added over the mechanism to reduce drag.

Once the wing was complete, but before adding the solite covering, a pushrod was connected to an aileron servo arm for the release mechanism. This metal pushrod and the associated plastic bushing will be positioned to hold and release the string through a hole in the wing solite.

6.2.3 FUSELAGE STRUCTURE

A foam buck was cut out with a hotwire and sanded to an aerodynamic shape. The buck was used to create a female fiberglass mold to layup the Kevlar, fiberglass, and carbon fiber skin. Plywood bulkheads were integrated into the layup. The foam truss was made of foam beams laid up with fiberglass separately, then assembled and fixed into the skin with epoxy. The tail boom was then epoxied to the fuselage body, recessed in foam truss beams. These components are shown in Figure 32.

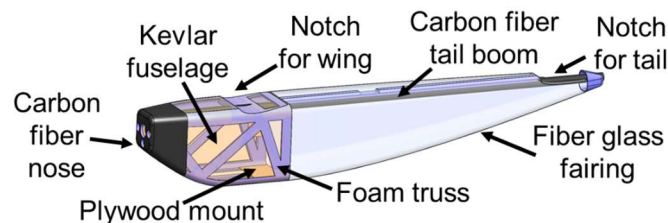


Figure 32: Assembled Fuselage



6.2.4 LANDING GEAR

The main gear was constructed with 21 plies of unidirectional carbon fiber and woven carbon, each layer differing in material and offset by 45 degrees. Slow-curing epoxy resin was used to cure the entire bow gear together for 12 hours. A hole was drilled through each strut for the placement of an axle and was secured using a hex nut. The wheel was placed upon the axle and secured using a landing gear collar.

The nose gear was constructed from 0.125 in. (0.3 cm) music wire, which was bent to shape using a wire bender. The wheel was placed upon the wire and secured with a collar.

Both the nose and main gears integrated into the plane's plywood bulkheads. The main gear was secured using two M4 nylon screws, sized to shear off in case of maximum 3g landing loads. The bolts are located 1.5 in. (3.8 cm) on each side of the centerline of the airplane. The nose gear was secured using two landing gear straps, as seen in Figure 33, which were also sized to shear at the maximum landing load.



Figure 33: Nylon bolts and straps for nose gear (left) and fully integrated nose gear (right)

6.2.5 ROTATING RADOME

The radome disk was constructed out of plywood components that were cut by a laser cutter. It was assembled using 5-minute epoxy. The radome rod is then split in half and each end is drilled into. The metal bolt and threaded standoff are then integrated into these holes with 5-minute epoxy to allow for quick radome attachment and removal during the Ground Mission. The rotation structure is assembled using plastic gears and a continuous servo, which is partially embedded into the fuselage. Two ball bearings are epoxied to the ceiling and base of the housing structure and the rod is glued to the inner rings. The entire housing structure was then attached to the carbon fiber tail boom with metal bolts and surrounded by composite fairings to reduce drag. The full design is shown in Figure 22 and 23.

6.2.6 ATTACK STORE

The tandem store mounting fixture, shown in Section 5.6, was laser-cut out of 0.125 in. (0.32 cm) thick plywood. Features on interlocking components maximized adhesion area and 8-32 metal bolts held the two rails onto plywood ribs on the wing. All components are oriented to minimize loads and drag area.

The plywood housing structure was made with a laser cutter to allow for precise manufacturing. Both the servo and zip tie mechanisms were epoxied to the tandem structure and the zip tie strap was duct taped to the Mylar. The Mylar was trained by wrapping the strap around a 0.5" wooden rod and heated for several minutes. The rails were epoxied to the ceiling of the tandem structure I-beam, which mounts to the wing.

6.3 MANUFACTURING MILESTONES

A milestone chart was produced to stay on schedule and coordinate between different sub-teams. The plan in Figure 34 only depicts aircraft prototype #5, but the same scheduling was implemented for the construction of all prototypes and the competition aircraft. Lessons learned in the development of this aircraft were incorporated into the schedule for the competition build. Build and assembly requires upwards of four weeks to produce a high-quality part. Simultaneous lab testing was conducted on the wing, tail, and fuselage, as detailed in Section 7.0 to ensure the aircraft would meet all load requirements once integrated.

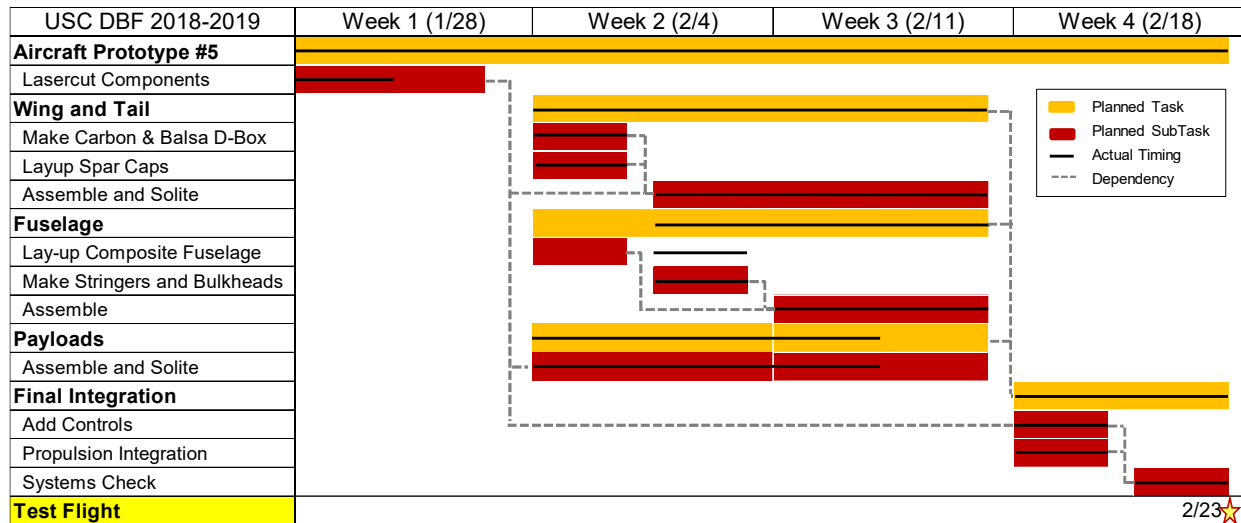


Figure 34: Aircraft manufacturing milestone chart showing planned and actual timing

7.0 TESTING PLAN

A test plan was implemented to verify propulsion, aerodynamics, structure, stability and control. Experimental data was gathered both in the laboratory and at test flights. Testing occurred during the conceptual, preliminary, and critical design phases to validate predictions and inform future design decisions. The test schedule is presented in Figure 35 and further detailed in Sections 7.1 - 7.4.

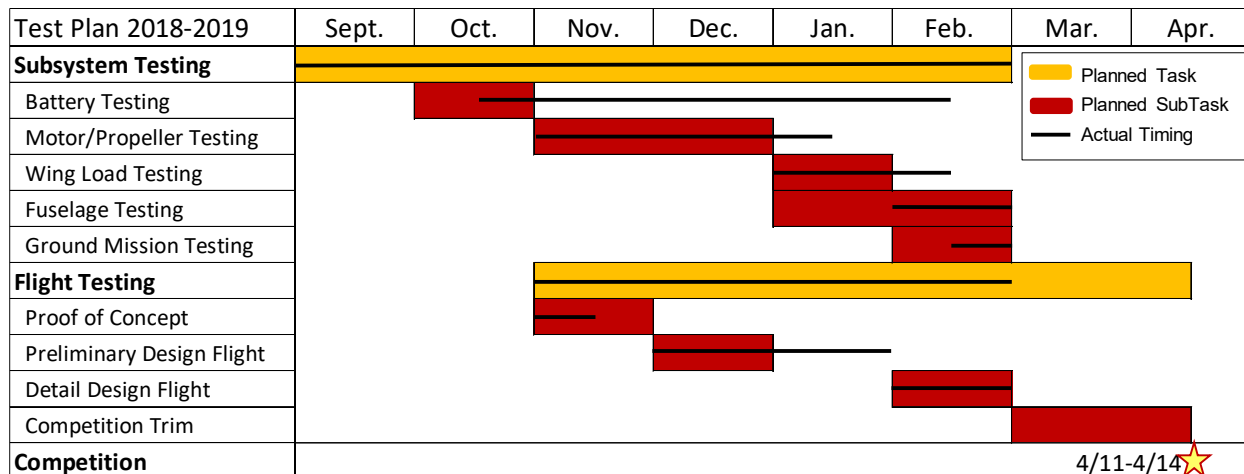


Figure 35: Testing plan for the 2018-2019 competition year



7.1 TEST OBJECTIVES

Tests for each sub-team were conducted to ensure that the designed components perform adequately to meet all competition and design requirements.

Aerodynamics

- Flight and wind tunnel tests were used to confirm AVL and XFLR predictions for lift, drag, and stability characteristics.
- Pilot feedback was used to verify that the aircraft's stability characteristics were acceptable

Propulsion

- Static and dynamic tests were used to verify the expected thrust and performance of the system
- Lab testing was conducted using a battery tester to characterize the discharge performance of assembled battery packs, further verified with flight testing

Performance

- Flight tests were conducted to validate performance predictions provided by PlaneTools including takeoff performance, cruise speed, and lap times

Payloads

- The ground crew tested that payloads could be loaded in the 5 minute window
- Payload and attachment mechanisms were tested in lab, wind tunnel, and flight to verify the mechanisms would survive flight and handling loads at all integration points
- Actuation of both radome and attack stores were tested in lab and flight

Wing

- A wingtip test was performed at maximum takeoff weight to simulate technical inspection
- Failure points and deflections predicted in SparSizer were validated through wing loading tests
- The wing folding mechanism was integrated into the wing and load testing was conducted to ensure that the mechanism could withstand flight loads and forces experienced when unfolding the wing

Fuselage

- In-lab load testing was conducted to ensure the structure could withstand maximum design loads

Landing Gear

- In-lab static load testing was conducted to validate the expected deflection, simulating a 3g landing
- Ground handling tests ensured that the aircraft would track straight for takeoff and landing

7.2 SUBSYSTEM TESTING

7.2.1 AERODYNAMIC TESTING

Slotted Flaps

A wind tunnel test matrix was developed to measure the increase in performance of a slotted flap compared to a conventional (taped) flap. The wind tunnel model consisted of a two-dimensional E560 airfoil that would be tested at a Reynolds Number (Re) of 100,000 to match takeoff conditions, as seen in Figure 36.



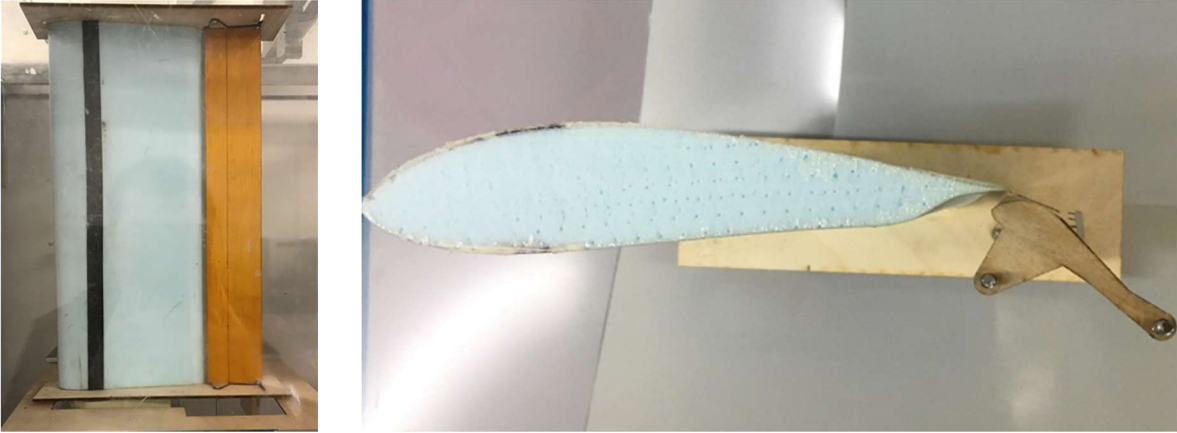


Figure 36: Wind tunnel model with endplates to negate three-dimensional effects of a wing (left) and cross section view of slotted flaps model (right)

To determine the flap deflection, δ_{flap} , that provided peak performance for the slotted flap, the two-dimensional wing was swept from $\alpha = 0^\circ$ to $\alpha = 15^\circ$, and $C_{l,max}$ was measured as a function of δ_{flap} . After the deflection at which $C_{l,max}$ is located (denoted as $\delta_{flap, C_{l,max}}$) was determined, both the slotted flap and taped flap were tested at $\delta_{flap} = \left[0, \frac{\delta_{flap, C_{l,max}}}{2}, \delta_{flap, C_{l,max}} \right]$ to determine the increase in $C_{l,max}$ due to the slotted flap. The results of this testing are shown in Section 8.1.1.

Drag of Attack Stores

To validate the drag model for the stores and radome explained in Section 4.4.2, a test was set up based on Newton's Second Law, $F = ma$. For an object in free fall, this equation can be rearranged to show that $mg - D = ma$, where $D = C_D \frac{1}{2} \rho v^2 S_{ref}$. This can once again be rearranged to show that the drag coefficient, C_D , of an object in free fall can be described by

$$C_D = \frac{2m(g - a)}{\rho v^2 S_{ref}} \quad \text{Eq. 17}$$

With Eq. 17 in mind, a single store was dropped off a building and video analysis was used to measure its acceleration, a , and velocity, v , during decent. Additionally, the mass, m , and reference area of the store, $S_{ref} = \pi * d^2 / 4$, were measured. These measurements were then applied to Eq. 17 using gravity, g , and air density, ρ , to calculate C_D of the store, shown in Section 8.1.1.

The effect on drag due to the store interactions with nearby surfaces was also researched and tested. Based off literature, it was expected that laterally spacing pairs of stores 3 inches (one diameter) from each other and placing them in tandem rather than adjacent to one another, could result in 30% and 43% reduction in drag of the pair, respectively [13]. Additionally, literature suggested that interference drag between the store and wing could cause the drag of the store to increase by a factor of four, so the vertical distance between the store and the wing should be maximized [13]. To validate these trends, a wind tunnel, shown in Figure 37, was used to measure the effect of changing lateral spacing of the stores on the wing.

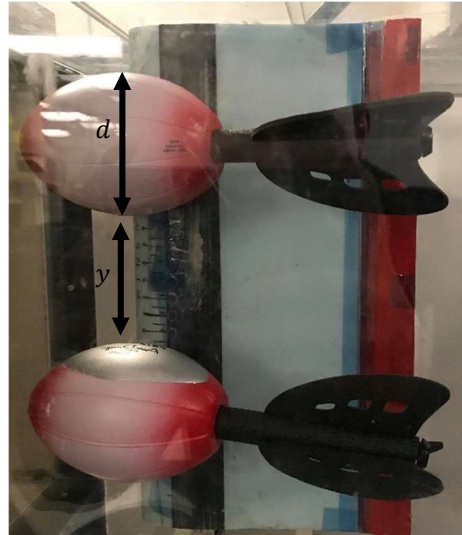


Figure 37: Wind tunnel set up, testing spacing of stores laterally

Since the lateral and vertical spacing trends were expected to be similar according to Hoerner, if the lateral trends could be validated then the expected vertical trends could be regarded as verified as well [13]. Lateral spacing, y , was measured in terms of store diameters, d , and the results are presented in Section 8.1.1.

7.2.2 PROPULSION TESTING

Propulsion testing consisted of characterizing the performance of the selected batteries as well as validating PlaneTools predictions of each propulsion package to select the highest scoring configuration. Battery testing was conducted using the West Mountain Radio Battery Tester, which draws user-specified currents and logs the voltage of the battery packs throughout the test [21]. The propulsion sub-team built, charged, and discharged various battery packs to test at the expected cruise currents. This was to ensure that the capacities of the selected batteries were sufficient for each mission's objectives. Plots of voltage versus time allowed the team to determine an expected flight time for each package and its respective mission. Testing was also conducted at 70 A to account for the higher current draw experienced at takeoff. The testing apparatus is shown in Figure 38.



Figure 38: Battery Tester (left) and lab-built mule for propulsion system testing (right)

Static motor testing was conducted using a lab-built mule, an ammeter to measure current, and a scale to measure thrust, as seen in Figure 38. The objectives of motor testing were to compare the propulsion system's performance to theoretical PlaneTools predictions.

7.2.3 STRUCTURAL TESTING

Wing

Destructive testing was performed on the wing spar to validate the spar sizing analysis. A single panel was built up and mounted to a plywood fuselage as would be in flight. The fuselage was then fixed to a table and an 8g elliptical load with a 1.5 factor of safety was hung directly from the spar with a whiffle tree as shown as shown in Figure 39.



Figure 39: Wing to fixed fuselage mount (left) and whiffle tree loading on wing (right)

Fuselage

The fuselage was tested in lab against landing, motor torque, and motor thrust loads. To test landing loads, the fuselage was dropped from a vertical distance of 12 in. (30.5 cm) to assume worst-case landing. To test motor torque loads, a bar was notched into the motor mount and the maximum torque moment of 14.4 lbf-in. (1.6 N-m) was simulated with weight hung a set distance along the bar. To test motor thrust loads, the fuselage was held in place from the tail hook and pulled on from the front with a fish scale to a maximum force of 12 lbf (53.4 N). These set-ups are shown in Figure 40 below. The fuselage passed all the load tests as further discussed in Section 8.1.3.

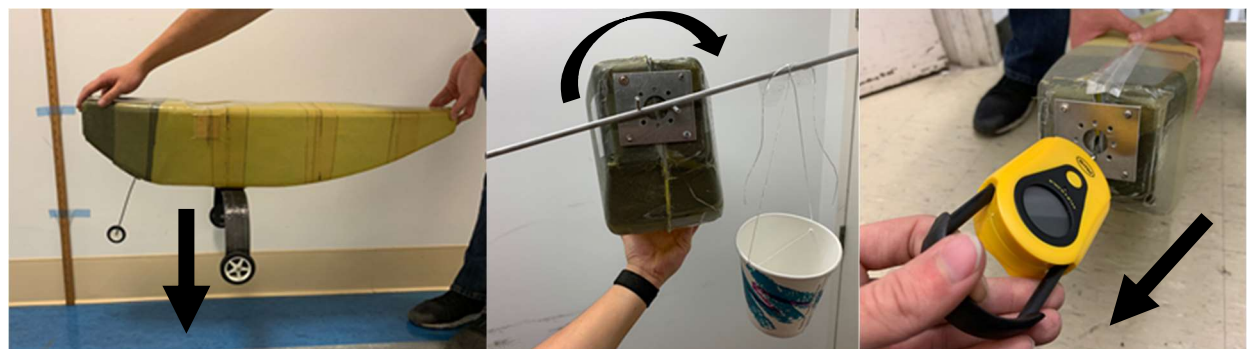


Figure 40: Load testing set up for landing (left), motor torque (middle), thrust (right) tests

7.2.4 LANDING GEAR TESTING

Rolling Friction of Ramp

To quantify the effect of the ramp on the landing gear, the coefficient of kinetic friction of the ramp was calculated. A plywood plank was laid horizontally, and a landing gear wheel was rolled along the plank, while a video camera recorded its position. Analysis was performed upon the video to determine total time and distance the wheel traveled. After modeling the wheel as a perfect cylinder and measuring the wheel's radius and mass, the coefficient of friction was determined to be approximately 0.1.

Static Test on Bow Gear

Static testing was performed on the main gear to validate the FEA analysis shown in Section 5.3.4. Determining the load at failure as well as the location and mode of failure were focus of the test. Weight was placed upon the center of the gear until the gear fractured. The bow gear was placed into rollers to allow for lateral deflection as shown in Figure 41. The allowable load was 22.4 lbf (99.6 N) and the gear failed at a load of 33 ± 3 lbf (146.9 ± 13.3 N). The gear failed as multiple layers of carbon-fiber delaminated from the structure, causing a fracture within the left strut. Since the failure load exceeded the allowable load, the test was successful and indicated that the gear sufficiently met the 3g landing load requirements.



Figure 41: Bow gear used in static testing

7.2.5 RADOME TESTING

To verify the radome's structural integrity and visible, continuous rotation in flight, the team conducted rigorous testing in lab, in a wind tunnel, and at flight tests. Load testing in lab with weights, as shown in Figure 42, was designed to simulate 8g turns to indicate that the plywood waffle structure could survive the highest predicted flight loads. Wind tunnel testing also confirmed this. The radome shaft also had weights hung from it to ensure that it would not split nor break and could continue to rotate with flight loads applied. The integration of the radome to the plane was flight tested. After flying a Mission 2 simulation, there was no indication of the radome rod separating from the tail boom. To confirm visible rotation, the team coated the structure with two contrasting solid colors for visibility; during the Mission 2 simulation, the radome was confirmed to begin visibly rotating after the first 180° turn and visibly stop rotating after the last 180° turn.

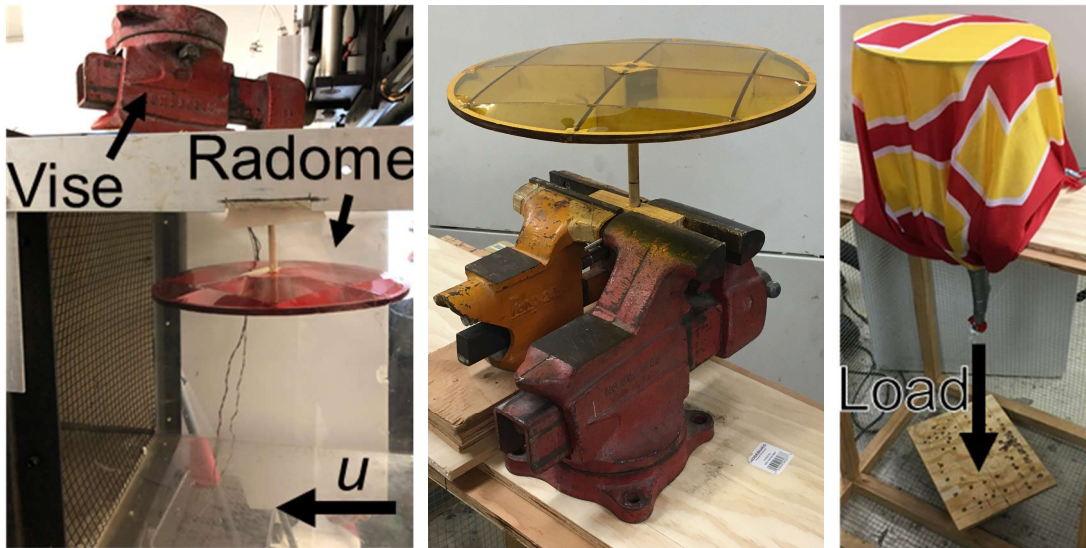


Figure 42: Wind tunnel (left) and in-lab structural test set up (middle and right) where a parachute-like testing device was used to evenly distribute load on the radome

7.2.6 ATTACK STORE TESTING

The tandem store fixture was tested under roll and drag loads as shown in Figure 43. The fixture withstood maximum drag loading and loads experienced while in an 8g turn with a safety factor of 2.6.

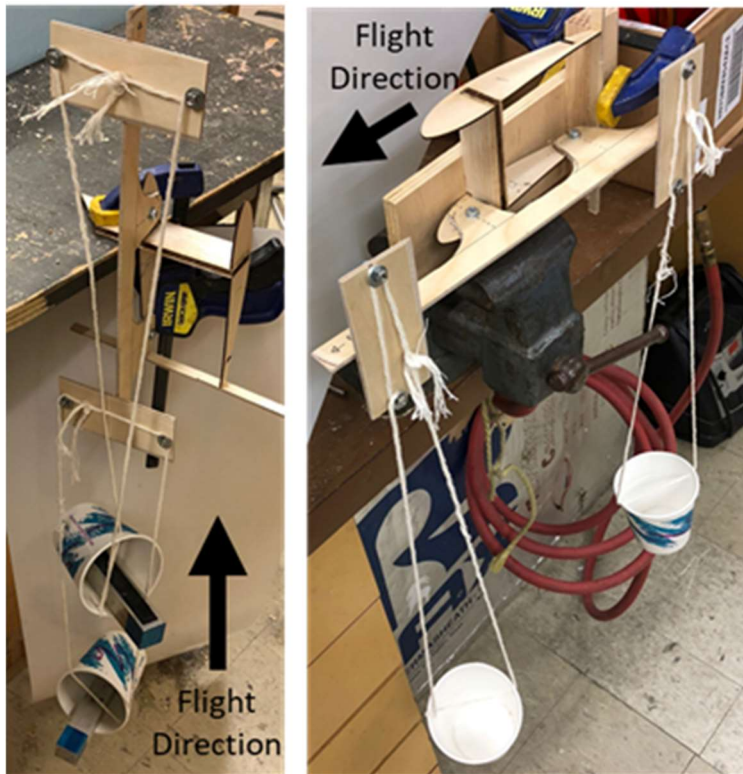


Figure 43: Tandem store fixture under turning loads (left) and drag loads (right)

The release mechanism was tested both in lab and at flight tests to confirm payload security and reliable deployment. In lab, various components of the mechanism itself were tested to ensure nothing detached during flight. The zip tie integration with the tandem structure, the servo arm, and the integration point between the Mylar strap and the plywood hook all survived load testing. The joining of the zip tie strap to Mylar was also tested and confirmed to be adequately rigidity for flight. With the attack store loaded, the servo arm was still able to actuate, both in lab and in flight. Deployment was tested and proved to be reliable at flight test using a microcontroller described in Section 5.3.5.

7.3 FLIGHT TEST SCHEDULE AND FLIGHT PLAN

Flight tests were critical to the validation of the competition aircraft. Pilot feedback allowed the team to determine aircraft stability, pilot workload, and the corresponding flight performance at different throttle settings, control inputs, and battery capacities. Propulsion data is collected through a data logging ESC that measures voltage, current, RPM, and throttle position. A custom-built sensor package records flight data that measures g-loads, rotation rates, ground speed, position, heading, and altitude. These data allow the team to compare flight data to PlaneTools predictions.

The flight test schedule and objectives are displayed in Table 20. Each flight test had explicit design objectives that were used to incrementally validate the effectiveness of all aircraft subsystems. Flight test objectives that were not met were reattempted in subsequent tests. Note that there are upcoming flight tests planned for February 24 and March 30.

Table 20: Flight Test Schedule; flight tests are conducted at the Sepulveda Basin in Van Nuys, CA

Date	Objectives
Nov. 11, 2018	<ul style="list-style-type: none"> ○ Validate TOFL ○ Determine handling/stability of preliminary design ○ Determine impact of radome on handling/stability at different positions
Dec. 09, 2018	<ul style="list-style-type: none"> ○ Compare single and dual motor configurations ○ Validate attack store drag model
Jan. 13, 2019	<ul style="list-style-type: none"> ○ Determine minimum wing area required for 10 ft TOFL ○ Optimized propulsion package (cell type: 4200mAh vs 5000mAh)
Jan. 26, 2019	<ul style="list-style-type: none"> ○ Optimized propulsion package (propeller advanced ratio and # of cells) ○ Radome structural test
Feb. 16, 2019	<ul style="list-style-type: none"> ○ Record lap times and performance data with maximum store loading ○ Radome structural test and record M2 time
Feb. 24, 2019	<ul style="list-style-type: none"> ○ Test integrated competition aircraft ○ M2 and M3 simulation with fully functional payload system
Mar. 30, 2019	<ul style="list-style-type: none"> ○ Trim competition aircraft

Each flight test was separated into specific objectives, which included the acceptance criteria to ensure all objectives were met. A sample plan from the Jan. 26, 2018 flight test is shown in Table 21.

Table 21: Jan. 26, 2019 flight test plan

Flight #	Flight Name	Objectives	Acceptance Criteria
1	Trim Flight	Trim aircraft	Aircraft trimmed for level flight
2	M1 Ramp Takeoff	Takeoff from ramp at empty weight with payload (M1)	TOFL < 10 ft (3 m), ramp takeoff successful
3	M3 Ramp Takeoff	M3 ramp takeoff with 8 stores and maximum competition weight	TOFL < 10 ft (3 m), ramp takeoff successful
4	M3 Simulation	Simulate half M3 with full laps in 5 minutes carrying 8 stores	ESC data (current/rpm), lap times, and straightaway speeds recorded
5	M3 Simulation	Repeat flight 5 but increase # of cells	ESC data (current/rpm), lap times, and straightaway speeds recorded Difference in performance evaluated.
6	M2 Simulation	Simulate full M2 with original propulsion package	ESC data (current/rpm), lap times, and straightaway speeds recorded
7	M2 Simulation	Simulate full M2 with new propulsion package	ESC data (current/rpm), lap times, and straightaway speeds recorded. Difference in performance evaluated.
8	Radome Test	Evaluate radome structure needed to survive flight loads	Radome structure surviving loads as designed

7.4 FLIGHT CHECKLISTS

The team adhered to a preflight checklist (Table 22) before each flight to ensure efficiency, proper data acquisition, and team safety. It also serves as a final flight go or no-go evaluation criterion from the pilot. The on-site inspections checklist (Table 23) was used before and after each flight to ensure aircraft and crew safety. The inspection of each category of components allows for the systematic division of duties for aircraft inspection, discrepancy noting, and maintenance if necessary.

Table 22: Pre-flight checklist

Component	Task
Fuselage (internal)	<input type="checkbox"/> Secure and connect the fully charged battery <input type="checkbox"/> Receiver has all connections plugged in and secured <input type="checkbox"/> CG aircraft <input type="checkbox"/> Attach radome mechanism (if applicable) <input type="checkbox"/> Secure and connect payload release controller (if applicable)
Fuselage (external)	<input type="checkbox"/> Close and secure all external hatches <input type="checkbox"/> Attach payload release mechanisms (if applicable)
Pilot's Checks	<input type="checkbox"/> Check all control surfaces with receiver <input type="checkbox"/> Motor run-up <input type="checkbox"/> Go/No-Go decision

Table 23: Aircraft inspection checklist

Component	Task	Discrepancies
Motor	<input type="checkbox"/> Secure motor mount and fasteners <input type="checkbox"/> Fuselage around motor mount is free of cracks or fractures <input type="checkbox"/> Motor is free of damage and debris <input type="checkbox"/> Propeller is fastened to shaft properly <input type="checkbox"/> Propeller is free of damage and balanced	
Fuselage	<input type="checkbox"/> Battery is secured to fuselage and connected properly <input type="checkbox"/> Speed controller is secure and connected <input type="checkbox"/> Receiver is secure and has all servos connected properly <input type="checkbox"/> Servo wires are all secure <input type="checkbox"/> Fuselage is secured and free of debris <input type="checkbox"/> Fuse connectors secured (internal and external) <input type="checkbox"/> Radome mechanism secured (M2) <input type="checkbox"/> Radome mechanism operational (M2)	
Wing	<input type="checkbox"/> Wings are free of tears, cracks, and fractures <input type="checkbox"/> Servo arms are secure with minimal play <input type="checkbox"/> Control surfaces are secure and free of obstructions <input type="checkbox"/> Fuselage around wing mount is free of cracks and fractures <input type="checkbox"/> Wing is securely mounted to fuselage <input type="checkbox"/> Payload release mechanisms secured and ready for loading (M3) <input type="checkbox"/> Payload release controller secured and connected (M3)	
Landing Gear	<input type="checkbox"/> Wheels spin freely and are secure <input type="checkbox"/> Torsional rigidity of gear <input type="checkbox"/> Landing gear mounted securely <input type="checkbox"/> Fuselage is free of cracks and fractures around mount	
Tail	<input type="checkbox"/> Tail hook secured properly <input type="checkbox"/> Tail boom is free of tears, cracks, and fractures <input type="checkbox"/> Servo arms are secure <input type="checkbox"/> Tail is free of tears, cracks, and fractures <input type="checkbox"/> Tail is securely mounted to tail boom	
Control Surfaces	<input type="checkbox"/> Check all control surface motion using transmitter <input type="checkbox"/> Control surfaces move freely without obstruction	

8.0 PERFORMANCE RESULTS

Predictions made during the Detail Design phase were compared to aircraft subsystem performance. Key subsystems were tested in lab and during flight tests to ensure each component performed as predicted.

8.1 DEMONSTRATED PERFORMANCE OF KEY SUBSYSTEMS

8.1.1 AERODYNAMICS

Slotted Flaps

The $C_{l,max}$ vs δ_{flap} curve that was generated through wind tunnel testing showed that the E560 airfoil gets max lifting performance at $\delta_{flap} = 20^\circ$, as seen in Figure 44. At $\delta_{flap} > 20^\circ$, drag increased without an increase in $C_{l,max}$.

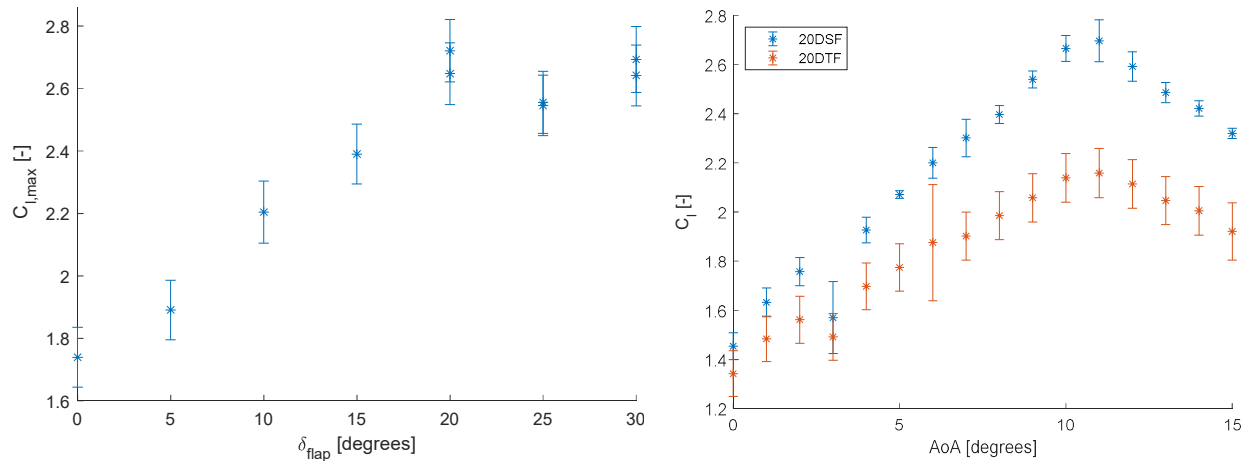


Figure 44: $C_{l,max}$ vs δ_{flap} curve (left) and taped vs. slotted flaps (right) at $\delta_{flap} = 20^\circ$ and $Re_c = 100k$

The slotted flap outperformed the taped flap at every deflection, though the largest difference was when $\delta_{flap} = 20^\circ$, as shown in Figure 44. When $\delta_{flap} = 20^\circ$, it was measured that the slotted flap and taped flap had a stall angle of attack, α_{stall} , equal to 11° but had a $C_{l,max}$ of 2.70 ± 0.09 and 2.2 ± 0.1 , respectively. The slotted flap outperformed the taped flap by 23% in terms of $C_{l,max}$ and thus can be integrated into the final aircraft to help decrease TOFL.

Drag of Attack Stores

The test setup described in Section 7.2.1 was executed for multiple trials and it was found that one store had a drag coefficient, C_D , of 0.3 ± 0.1 . This is equal to the prediction of $C_D = 0.34$ from the equations in Section 4.4.2. Once this model was validated for the store, Eq. 11-14 were applied to not only the stores but also the radome for all analysis and modeling of the aircraft’s payloads and supporting structures.

After conducting the store spacing wind tunnel test described in Section 7.2.1, lateral store spacing trends were validated. As seen in Figure 45, the total drag, D, of the system decreased as lateral spacing between the stores was increased. A nominal decrease in drag of ~10% was seen between when the stores were spaced at the minimum of 0.5 inches and at 3.0 inches.

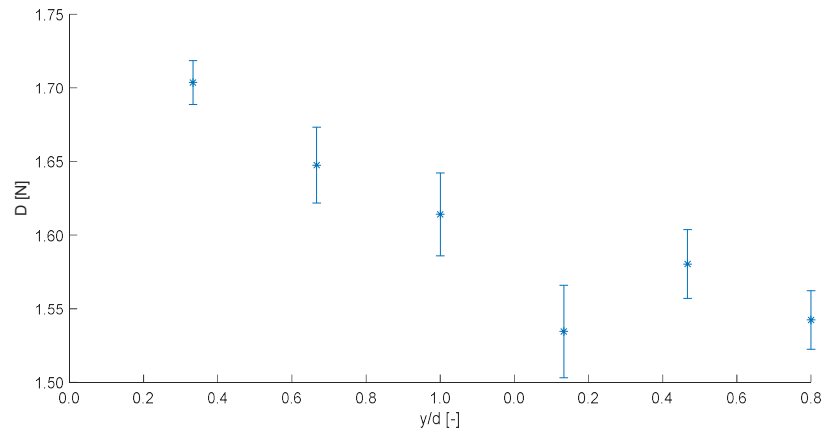


Figure 45: Drag data of system from wind tunnel while changing lateral spacing of the stores



8.1.2 PROPULSION

Motor Configurations

The team chose to explore both the single-motor tractor configuration and the dual-motor wing-mounted configuration with the initial assumption that a dual-motor configuration would increase speed. However, as seen in Table 24, there was not a significant increase in speed, and the dual-motor configuration failed to meet the TOFL requirement due to the increase in weight. Thus, the single-motor tractor configuration was chosen in order to meet the design objectives, which included taking off in 10 ft (3 m).

Table 24: Motor Configuration Comparison

Motor Configuration	TOFL [ft]	V_{cruise} [ft/s]	$\text{RPM}_{\text{cruise}}$	I_{cruise} [A]
Single	8 (2.4 m)	94 (28.7 m/s)	5300	37
Dual	33 (10.1 m)	93 (28.3 m/s)	7100	32

Battery Testing

Battery testing was conducted to characterize the performance of each battery pack to ensure the propulsion system would be capable of completing the time frame of each mission at our expected cruise currents. As specified in Section 4.3.2, the Tenergy 4200mAh cells are used on Mission 2 for a flight duration of 2 minutes while the Elite 5000mAh batteries are used for Mission 3 with a flight duration of 10 minutes. The battery discharge was performed at 25A, which was the average cruise current collected from flight test data. The results of the testing are shown in Figure 46.

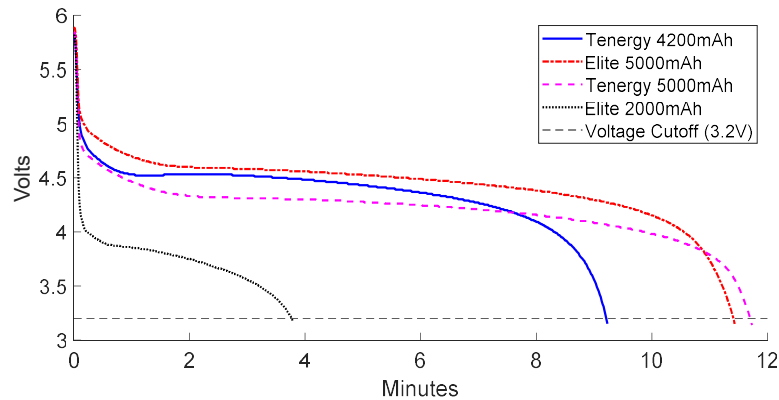


Figure 46: Battery Discharge Comparisons at 25A

Preliminary battery analysis compared the Tenergy 4200mAh, Tenergy 5000mAh, and Elite 5000mAh cells to check differences in internal resistances and nominal versus actual capacities. Each of the three types of cells were tested in packs of 4 at their respective cruise currents, with a voltage cut-off of 0.8 volts per cell to prevent damaging the packs. The Elite 5000mAh cells were lightweight and displayed the capability to successfully perform at the expected currents. The Elite cells had a higher power output than the Tenergy cells of the same capacity and were 18 g lighter per cell; thus, the team chose the Elite 5000 cells for Mission 3. However, as seen in Table 25, the Tenergy 4200 cells were chosen for Mission 2 based on flight test data that showed a faster cruise speed. The Tenergy 5000 cells were not selected due to their higher internal resistance (lowering power output) and higher weight.

Table 25: Tenergy 4200mAh and Elite 5000mAh flight test comparisons

Neu 1415/2Y	Tenergy 4200mAh (18s)	Elite 5000mAh (18s)
Propeller	20x10E	20x10E
Static Current, I_{maz} [A]	42.5	43.7
Static Thrust [lbf]	8.8	8.9
Cruise Current, I_{crz} [A]	32.0	29.4
Dynamic RPM	5130	4897
Cruise Speed [ft/s]	71 (21.6 m/s)	68 (20.7 m/s)
Battery Pack Weight [lb]	2.58 (1.17 kg)	2.65 (1.20 kg)

8.1.3 STRUCTURES

The structural tests described in Section 7.2.3 all survived the designed loads shown in Table 26. The wing failed at the root, the thrust and torque test broke the motor mount, and the landing test sheered the bolts.

Table 26: Results of structural testing on wing and fuselage

Component: Load	Designed Load	Load Tested
Wing: Single Panel Lift	28.1 lbf	29.4 ± 0.5 lbf
Fuselage: Thrust	12 lbf	24.8 ± 0.5 lbf
Fuselage: Torque	14.4 lbf-in.	22.0 ± 0.5 lbf-in.
Fuselage: Landing	22.5 lbf	35.7 ± 0.5 lbf

8.2 DEMONSTRATED FLIGHT PERFORMANCE OF COMPLETED AIRCRAFT

Several flight tests were carried out to validate predictions of aircraft performance. The goal of these flights was to evaluate the performance and capabilities of the detail design aircraft. Table 27 summarizes the flights to date as well as future flight test plans.

Table 27: Aircraft Performance evaluation from flight tests

Date	Description	Problems	Solutions
Nov. 11, 2018	- Validate TOFL and handling	- Pitch authority low - Radome broke in flight	- Move CG back for more pitch authority - Increase radome structure
Dec. 09, 2018	- Single vs Dual motor comparison	- Dual motor TOFL >> 10 ft due to reduced dynamic pressure over tail	- Increase span of horizontal stabilizer or use single motor
Jan. 13, 2019	- Determine minimum wing area	- Sluggish speeds on M2 - Radome broke in flight	- Increase propeller pitch and battery cells - Increase radome structure
Jan. 26, 2019	- Propulsion optimization	- Tail flutter at high speeds - Stores causing pitching moment	- Increase tail structure and tighter tolerances - Careful store alignment
Feb. 16, 2019	- Maximum store configuration testing	- High current	- Fly at lower throttle setting
Feb. 24, 2019	- Simulate Missions	--	--
Mar. 30, 2019	- Competition Trim	--	--

As shown in Table 27, verification of the radome structure was repeated twice (Nov. 11 and Jan. 13) due to structural failure in flight. Considerable effort was taken to redesign the radome structure and failure points to ensure that the radome was strong enough to survive flight loads, including the in-lab and wind tunnel tests described in Section 7.2.5. The team successfully completed three mission simulations at its Jan. 26th flight test and compared the collected data with predictions, as shown in Table 28.

Table 28: Comparison of predicted and flight-validated performance characteristics

Mission	Parameter	Predicted	Actual	Δ [%]
M1	V_{cruise}	69 ft/s (21 m/s)	107 ft/s (33 m/s)	55
	I_{cruise}	28 A	42 A	50
M2	V_{cruise}	65 ft/s (20 m/s)	102 ft/s (31 m/s)	57
	I_{cruise}	28 A	47 A	68
	$(T_{M2})_{USC}$	116 s	88 s	-24
M3	V_{cruise}	62 ft/s (19 m/s)	73 ft/s (22 m/s)	18
	I_{cruise}	24 A	25 A	4
	$N_{scoring\ laps}$	13	13	0
GM	$(T_{GM})_{USC}$	30 s	25 s	-17

Predicted flight speeds and cruise currents are both around 40% lower on average when compared to flight test data. The difference between cruise velocities and currents can be attributed to several factors, including high winds, turn radius, propulsion efficiency factors, and discrepancies in estimating drag for the predicted model. Especially on Missions 2 and 3, the difference can be attributed to errors in radome/store drag prediction models. These results were used to improve the fidelity of the PlaneTools model and refine theoretical predictions. The aircraft that was used to collect flight test data is shown in Figure 47. The team has completed the build for the first iteration of the competition aircraft (not shown). The aircraft will be flown at the February 23rd flight test and is expected to simulate all flight missions.



Figure 47: A successful flight test on January 26 at Sepulveda Basin, Van Nuys, CA; ramp takeoff (left) and aircraft turning (right)

9.0 BIBLIOGRAPHY

- [1] The American Institute of Aeronautics and Astronautics, "2018-19 DBF Rules," Reston, VA, 2019.
- [2] USC AeroDesign Team, "Aircraft Design Report, 2013 AIAA DBF Competition," 2013.
- [3] USC AeroDesign Team, "Aircraft Design Report, 2017 AIAA DBF Competition," 2017.
- [4] USC AeroDesign Team, "Aircraft Design Report, 2011 AIAA DBF," 2011.
- [5] USC AeroDesign Team, "Aircraft Design Report, 2018 AIAA DBF Competition," 2018.
- [6] D.P. Raymer, in *Aircraft Design: A Conceptual Approach*, Reston, Virginia, AIAA, 1999, p.78
- [7] The American Society of Mechanical Engineers, "Wing-Folding Mechanism of the Grumman Wildcat," Kalamazoo, Michigan, 2006.
- [8] "Weather Underground," [Online]. Available: <https://www.wunderground.com/>. [Accessed 22 September 2018].
- [9] A. P. P. Data. [Online]. Available: <http://www.apcprops.com>. [Accessed 25 January 2019].
- [10] Pete Carpenter, "The Watts Per Pound Rule," 2019. [Online]. Available: <https://www.rc-airplane-world.com/watts-per-pound.html>. [Accessed January 2019].
- [11] Xflr5.com. (2019). *XFLR5*. [online] Available at: <http://www.xflr5.com/xflr5.htm>
- [12] Drela, M. and Youngren, H. (2017). *AVL*. [online] Web.mit.edu. Available at: <http://web.mit.edu/drela/Public/web/avl/>
- [13] S. Hoerner, "Fluid Dynamic Drag," Bricktown, NJ, 1965.
- [14] M. Page, "Model Airplane Cook-book," 2008.
- [15] Ocw.mit.edu. (2006). *Basic Aircraft Design Rules*. [online] Available at: <https://ocw.mit.edu/courses/aeronautics-and-astronautics/16-01-unified-engineering-i-ii-iii-iv-fall-2005-spring-2006/systems-labs-06/spl8.pdf> [Accessed 21 Feb. 2019].
- [16] MIL-F-8785C, Flying Qualities of Piloted Planes, Military Specification, 1980.
- [17] A. Lennon, "Basics of R/C Model Aircraft Design," Wilton, CT, 1996.
- [18] Dassault Systems, "Solidworks," [Online. Available: <http://www.solidworks.com/>. [Accessed January 2019].
- [19] Markforged, Inc., "THE MARK TWO," 2019. [Online]. Available: <https://markforged.com/mark-two/>. [Accessed January 2019]
- [20] USC AeroDesign Team, "Aircraft Design Report, 2014 AIAA DBF Competition," 2014.
- [21] West Mountain Radio, "CBA IV – Computerized Battery Analyzer," 2019. [Online]. Available: http://www.westmountainradio.com/product_info.php?products_id=cba4. [Accessed January 2019].

Edvard Rusjan Team

University of Ljubljana, Faculty of Mechanical Engineering



Pretty Boy

AIAA Design/Build/Fly

2018-2019

Design Report



Contents

1	Executive Summary	1
1.1	Design Process	1
1.2	Key Mission Requirements and Design Features	1
1.3	System Performance Capabilities	2
2	Management Summary	3
2.1	Team Organization	3
2.2	Milestone Chart	3
3	Conceptual Design	4
3.1	Mission Requirements and Scoring	4
3.1.1	Mission 1: Delivery Mission	5
3.1.2	Mission 2: Reconnaissance Mission	5
3.1.3	Mission 3: Attack Mission	5
3.1.4	Ground Mission: Flight Deck Operations and Maintenance	6
3.1.5	Aircraft Constraints	6
3.1.6	Sensitivity Study of Design Parameters	7
3.2	Design Selection Process	8
3.2.1	Basic Aircraft Design	9
3.2.2	Fuselage Design	9
3.2.3	Attack Stores	10
3.2.4	Radome	11
3.2.5	Wing Folding	12
3.3	Final Conceptual Design	13
4	Preliminary Design	14
4.1	Design and Analysis Methodology	14
4.2	Design Trade Studies	15
4.2.1	Number of Attack Stores	15
4.2.2	Takeoff Requirements	15
4.2.3	Propulsion System	16
4.3	Mission Model	18
4.3.1	Uncertainties	18
4.4	Aircraft Lift, Drag and Stability Characteristics	19



4.4.1	Airfoil Selection	19
4.4.2	Lift And Drag Analysis	19
4.5	CFD Analysis	21
4.5.1	Airplane Fuselage Analysis	21
4.5.2	Wing Tip Analysis	23
4.6	Stability and Control	24
4.7	Estimated Mission Performance	27
5	Detail Design	28
5.1	Dimensional Parameters	28
5.2	Structural Characteristics	28
5.2.1	Fuselage	28
5.2.2	Wing Structure	29
5.3	Systems and Sub-Systems Integration	31
5.3.1	Fuselage	31
5.3.2	Wing	31
5.3.3	Wing Folding Mechanism	32
5.3.4	Rotating Radome Mechanism	33
5.3.5	Attack Store Mechanism	33
5.3.6	Tail Hook	34
5.3.7	Propulsion System	34
5.3.8	Landing Gear	35
5.3.9	Emmpenage	35
5.4	Weight and Balance	36
5.5	Flight and Mission Performance	37
5.6	Drawing Package	37
6	Manufacturing	42
6.1	Manufacturing Processes Investigated	42
6.1.1	CNC Cutting	42
6.1.2	Composite Material Construction	42
6.1.3	Foam	42
6.1.4	Purenite and MDF Molds	42
6.1.5	Balsa Build	42
6.1.6	3D Printing	43
6.2	Selection Process	43



6.3	Manufacturing of Parts	45
6.3.1	Fuselage	45
6.3.2	Wings	45
6.3.3	Bulkhead and Reinforcement Ribs	46
6.3.4	Empennage	46
6.3.5	Landing Gear	46
6.4	Manufacturing Milestones	46
7	Testing Plan	47
7.1	Schedule	47
7.2	Detailed Testing Objectives	47
7.2.1	Propulsion Testing	47
7.2.2	Aerodynamics Testing	48
7.2.3	Wing Structural Integrity Tests	49
7.3	Test Flights	49
7.4	Flight Checklist	50
8	Performance Results	52
8.1	Aerodynamics	52
8.2	Takeoff Testing	52
8.3	Test Flights	53
9	References	55



Acronyms and nomenclature

A	- Reference Area	L	- Lift
AIAA	- American Institute of Aeronautics and Astronautics	M1	- Flight Mission 1
AR	- Aspect Ratio	M2	- Flight Mission 2
AVL	- Athena Vortex Lattice	M3	- Flight Mission 3
APC	- APC Propeller Company	MAC	- Mean Aerodynamic Chord
BaS	- Barely Successful	MDF	- Medium Density Fiberboard
BLDC	- Brushless Direct Current (motor)	NiCd	- Nickel-Cadmium
C	- Coulomb	m	- Mass
CAD	- Computer Aided Design	n	- Number of Battery Cells
CFD	- Computational Fluid Dynamics	NiCd	- Nickel-Cadmium
CG	- Center of Gravity	NiMh	- Nickel-Metal Hydride
Cl	- Lift Coefficient	P	- Power
Cl_{cruise}	- Cruise Lift Coefficient	p	- Roll
Cl_{max}	- Max Lift Coefficient	q	- Pitch
C_M	- Moment Coefficient	R	- Electric Resistance
CNC	- Computer Numerical Control	r	- Yaw
Cd	- Drag Coefficient	RPM	- Revolutions Per Minute
Cd_i	- Induced Drag Coefficient	RC	- Radio Controlled
D	- Propeller Diameter	S	- Successful
DBF	- Design Build Fly	SAS	- Score Analysis Simulation
DC	- Direct Current	SD	- Secure Digital
e	- Oswald's Efficiency Factor	SST	- Shear Stress Transport
EM	- Electric Motor	TMS	- Total Mission Score
ESC	- Electronic Speed Control	t_{lap}	- Lap Time
EW	- Empty Weight	$t_{takeoff}$	- Takeoff Time
F	- Force	v	- Velocity
F_t	- Thrust at specific speed	v_{cruise}	- Cruise Speed
FEM	- Finite Element Method	v_{turn}	- Turn Speed
FoM	- Figure of Merit	α	- Angle of Attack
g	- Gravitational Acceleration	β	- Sideslip Angle
GPS	- Global Positioning System	η	- Efficiency
GM	- Ground Mission	μ	- Friction Coefficient
I	- Current	ρ	- Air Density
K_v	- Motor Velocity Constant	ω	- Angular Velocity



1. Executive Summary

This report details the design, manufacturing and testing of *Pretty Boy*, University of Ljubljana, Faculty of Mechanical Engineering's entry in the 2019 AAIA Design Build Fly (DBF) competition. The aircraft is designed to complete the following tasks: empty flight, carrying and dropping attack stores, flight with the rotating radome attached, stowed storage and remote unfolding from stowed storage configuration. At the time of writing there were 8 test flight outings with over 40 test flights.

1.1 Design Process

Pretty Boy was designed to win this competition. The aircraft capable of flying all three missions and with the ability to be stored within a 10ft by 10ft box was developed for that purpose. Detailed studies were conducted to estimate mission performance of other teams in order to evaluate the actual value of each mission for our aircraft design. The conceptual design involved a step by step procedure of component and design type evaluation. Computer tools, such as AVL, CFD and Python programming language, along with trade studies and historical data, were later used to estimate aerodynamic characteristics such as drag, lift and stability. Optimal propulsion with best power to weight ratio was determined. Preliminary design was structurally evaluated and appropriate manufacturing materials and techniques were chosen. Two prototypes and the final detailed design were created and their performance characteristics were experimentally tested.

1.2 Key Mission Requirements and Design Features

Balancing the key mission requirements was the basis for a successful design. Iterative calculations were performed by our own written optimization program; it was found that the following mission requirements and design features affect the overall score the most:

Number of Attack Stores: The number of attack stores the aircraft is capable of carrying and subsequently dropping is a significant factor in the total score. A configuration with as many stores stored below the fuselage was chosen as it minimized the total drag of each individual store. Four stores are required under the wings and any additional stores can be mounted anywhere beneath the wing or below the waterline of the aircraft.

Total Weight: Aircraft weight greatly impacts the ability of takeoff at the ramp. The team tried to minimize the weight of each separate component to ensure that a sufficient amount of batteries was available for the aircraft to fly the full duration of Mission 3.

Mission 3 Performance: Based on the performance evaluation, it was concluded that M3 score should be prioritized over others. Mission 3 will be able to provide us with the highest final score as the only limiting factor is the speed of the aircraft and the number of stores on the aircraft.



1.3 System Performance Capabilities

The maximization of the performance and, most importantly, of the final score can be summarized as follows:

- Wing span of $7.939ft$ and surface area of $11.3ft^2$.
- Top speed of $98ft/s$ and total weight of $20.21lbs$.
- Carrying up to 19 attack stores and one rotating radome.
- Average attack storage loading time of $3.5s$ and unfolding time of $2s$ from stowed configuration.
- Secure storage of attack stores and the rotating radome.
- Takeoff capability off of a $10ft$ ramp.
- Capability proven through numerous testing and two prototypes.

The final design, visible in Figure 1, is a capable single motor aircraft with folding wings; design made to achieve the optimal total mission score. The fuselage and conventional empennage are carefully sized to minimize drag and ensure stable flight, which is minimally affected by a relatively big number of attack stores. The attack stores are sufficiently secured using the optimal seat geometry and a quick release mechanism, enabling precise drop control. Aircraft landing gear consists of conventional undercarriage in the front and a tail hook. Each component was optimized in great detail in the given time frame of seven months and the team is confident that *Pretty Boy* is going to be victorious.

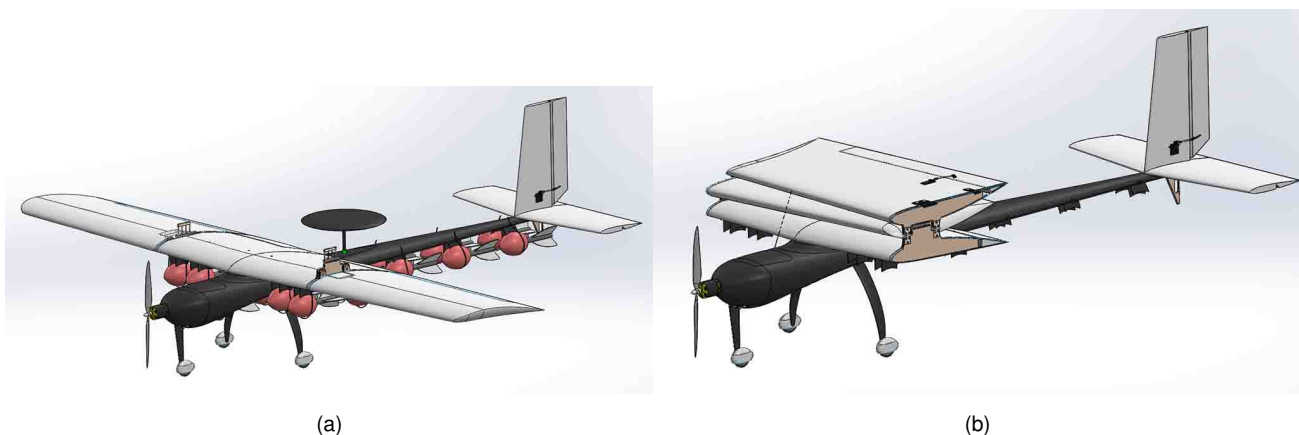


Figure 1: Final Design



2. Management Summary

The Edvard Rusjan Team consists of 19 students, 8 team members have had previous experience with designing and building an aircraft. Having an experienced team core allows passing knowledge to younger team members and laying a strong basis for later competitions.

2.1 Team Organization

The team is led by students and is organized in a hierarchical structure. Senior members, leaders of smaller teams, are responsible for process oversight and timely completion of delegated tasks. The hierarchy serves only as an outline, as team members collaborate and share knowledge in all fields of work. Many members also took part in team sections other than their main section. Each group member reported their progress to the group leader and to the project manager at weekly meetings, where the overall progress and the completion of milestones were agreed on. The team was first divided into: Manufacturing, Administration and Development. Administration was further divided into Report and Documentation & Funding, Development was divided into Propulsion, and Aerodynamics and Design teams. The management structure is shown in Figure 2.

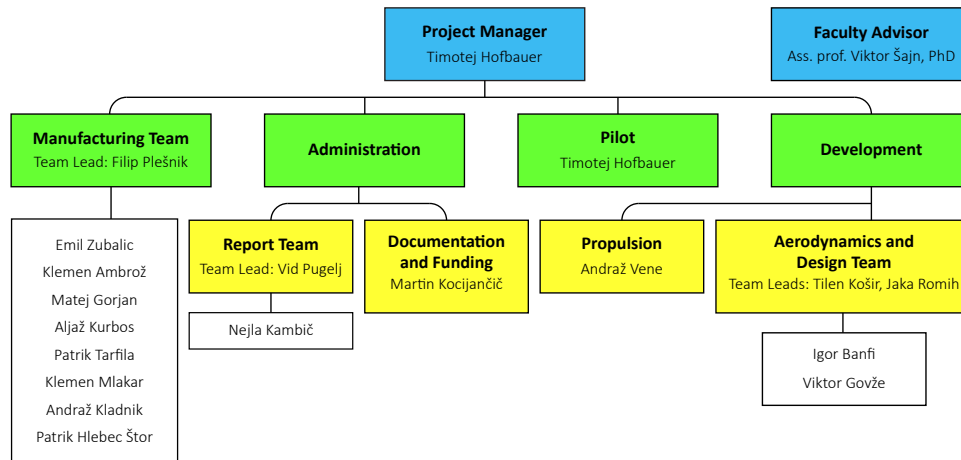


Figure 2: Edvard Rusjan Team Management Structure

2.2 Milestone Chart

A milestone chart was established during the first team meetings, its main purpose was showing important internal and competition deadlines as well as the design and manufacturing goals. The chart was supervised by the project manager and team leaders and followed closely to assure the deadlines were met. The chart is shown below in Figure 3.

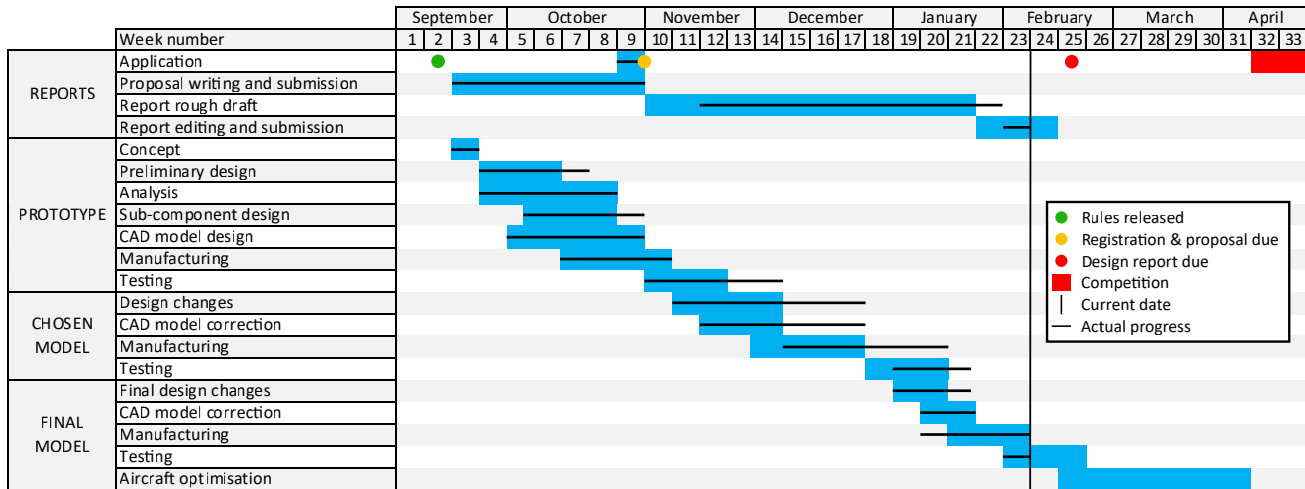


Figure 3: Edvard Rusjan Team Milestone Chart

3. Conceptual Design

In the conceptual design phase, the competition requirements [1] and scoring equations [1] were analyzed in order to set the design parameters for the aircraft. Multiple designs were evaluated in order to identify the optimal scoring configuration. The final design configuration is presented in Figure 1.

3.1 Mission Requirements and Scoring

The main objective of the 2019 AAIA Design Build Fly competition is to design a multi-purpose aircraft to support carrier operations. The rules specify a ramp takeoff and ground landing. The competition consists of three flight missions and a ground mission. The aircraft was designed for the optimal total score with the highest achievable score in each mission. The Total Score is calculated using Equation 1.

$$SCORE = WRS \cdot TMS \tag{1}$$

The Total Mission Score (TMS) is a sum of scores, obtained in Ground Mission and Missions One, Two and Three, as shown in Equation 2 below.

$$TMS = GM + M1 + M2 + M3 \tag{2}$$

Each flight mission requires a completion of a specified number of laps where each lap consists of four individual sections: a 180° turn, 1000ft straight flight with a 360° turn, another 180° turn and landing at the end of specified mission time. The lap requires both left and right turns and a successful landing within the bounds of the runway. Figure 4 shows the scheme of the official competition flight course [1].

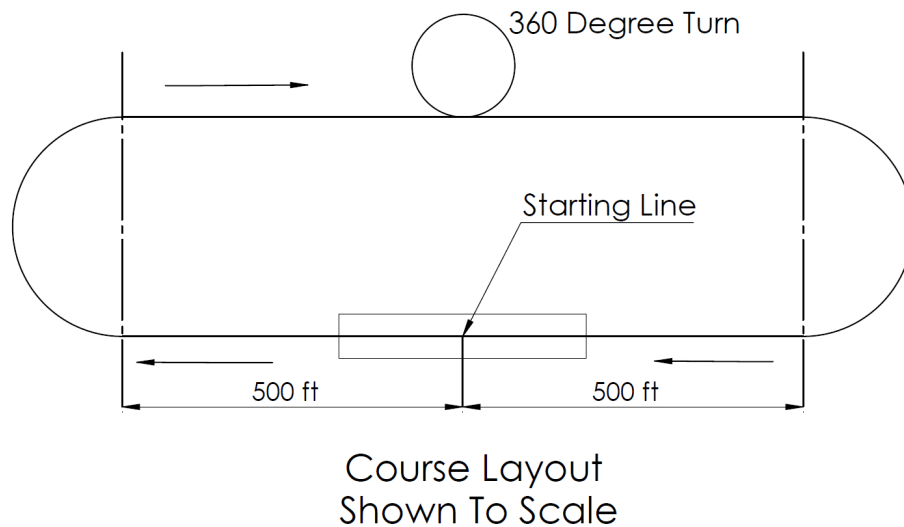


Figure 4: Official Flight Course

3.1.1 Mission 1: Delivery Mission

The aircraft must take off without any payload on a 10ft ramp at a roughly 5° angle, complete three laps, and perform a successful landing in order to receive the full score shown in Equation 3. This mission should be completed in a five minute time window.

$$M1 = 1.0 \quad (3)$$

3.1.2 Mission 2: Reconnaissance Mission

The time frame, number of laps and takeoff ramp are identical to Mission One, however a rotating radome must be installed. The radome must start rotating at the command of a line judge while the aircraft is in flight. To receive a score as described in Equation 4 a successful landing must be preformed.

$$M2 = 1 + \frac{Min_{time}}{N_{time}} \quad (4)$$

3.1.3 Mission 3: Attack Mission

Takeoff is the same as in previous missions with the added payload of attack stores, without the rotating radome. A scoring lap is one where the aircraft drops a single store on the down-wind leg of the lap. The time window for this mission is 10 minutes. The aircraft must complete a successful landing in order to get a score described by Equation 5.



$$M3 = 2 + N_{scoringlaps} \quad (5)$$

3.1.4 Ground Mission: Flight Deck Operations and Maintenance

This is a timed mission for ground demonstrations of Missions 2 and 3. The mission is broken down into 4 parts, two of which are timed. The first timed part is the remote command of the unfolding mechanism and the installing of the radome. Following is a non-timed demonstration of the radome rotation. The next part is a timed removal of the radome and an installation of 4 attack stores under the wing. The final part of the Ground Mission is not timed and consists of arming the aircraft and demonstrating the capability to remote drop the stores one by one, as well as the working of all propulsion and flight controls.

$$GM = \frac{Min_{time}}{N_{time}} \quad (6)$$

3.1.5 Aircraft Constraints

The aircraft should be designed with regard to certain basic constraints.

Design: Any design is allowed except rotary wing or aircraft lighter than air.

Propulsion: The electrical power must be provided from NiCd or NiMh batteries, no form of external takeoff system is allowed. The propeller must be a commercially available model.

Attack Stores and Radome: The aircraft must be capable of carrying at least four stores under the wings, minimum 0.5in clearance between stores and any part of the aircraft except the mounting hardware and be capable of remote detachment. The radome must be at least 12in in diameter and a minimum of 1in thick at the point of attachment, must be mounted on the aircraft centerline with a minimum of 3in clearance between any part of the radome to any other part of the aircraft. It must be capable of spinning and stopping by remote command.

Takeoff: The aircraft must be capable of taking off from a 10ft ramp at a roughly 5° angle.

Requirements for individual missions, scoring equations and guidelines were inspected and translated into design parameters crucial for each individual mission. The total score maximization was approached with the analysis of different aircraft configurations and mission scoring. Translation of mission requirements into design requirements is shown in Table 1.

Table 1: Design Parameters

Mission	Problem Statement	Key Design Parameters
Ground Mission	Fast mounting of attack stores and radome	Time
Mission 2	High aircraft speed, secured rotating radome	Power, remote rotation of radome
Mission 3	High number of scoring laps, fast individual lap, takeoff from the ramp	Number of attack store, total weight, drag and power



3.1.6 Sensitivity Study of Design Parameters

The design parameters were analyzed in a quantitative way as much as possible. To achieve that, certain relationships had to be modelled mathematically. The first crucial relationship to determine was the effect of extra load on speed, endurance and takeoff distance of the airplane. A mathematical model of each individual flight mission was created, which also included some empirical data based on previous competitions. Crucial identified design parameters were roughly evaluated.

Empty weight: Empty weight influences flight parameters (angle of attack, flight speed) and takeoff requirements. Empty weight was estimated by calculating structural weight, wing weight, empennage weight and propulsion weight. Propulsion weight was approximated by estimating weight of a battery pack and weight of EM. A quadratic equation was created to aid the comparison of weight to power for several different EM. Structural weight was roughly calculated by assessing increase in weight for each additional attack store. Wing weight was calculated by finding wing area required for the aircraft to fly. Empennage weight was estimated by calculating desired volume coefficient. Equations 7, 8, 10, 11 and 12 mathematically describe mentioned relationships.

$$W_{motor} = P_{motor}^2 \cdot k_{m1} + P_{motor} \cdot k_{m2} + k_{m3} \quad (7)$$

$$W_{battery\ pack} = \frac{E_{required}}{E_{cell}} \cdot m_{cell} \quad (8)$$

$$W_{struct} = W_{base} + N_{attack\ stores} \cdot k_{s1} \quad (9)$$

$$W_{wing} = A_{wing} \cdot \rho_{wing} \quad (10)$$

$$W_{stabilizer} = \frac{V_H A_{wing} MAC}{L_H} \cdot \rho_{stabilizer} \quad (11)$$

$$W_{rudder} = \frac{V_V A_{wing} b}{L_V} \cdot \rho_{rudder} \quad (12)$$

Attack store count: The number of attack stores is directly proportional to flight Mission 3 score, but it also increases aircraft weight due to higher required endurance and speed and the required thrust to ensure aircraft takeoff from the ramp.

Wing area: In order to reduce stall speed and consequently the required takeoff thrust, the aircraft needed to have a large wing area. Larger wing area meant larger induced drag, due to wingspan being limited, and larger weight that affected takeoff distance.

$$v_{stall} = \sqrt{\frac{m \cdot g \cdot 2}{\rho_{air} \cdot C_L A_{wing}}} \quad (13)$$

Aircraft propulsion: With every attack store the aircraft takeoff weight increased and consequently larger static thrust was required. For every additional attack store, an additional lap must be flown in M3, affecting the number



of required battery packs to successfully complete the mission. Since mission time is limited to 10 minutes, the average speed must increase as well.

Takeoff: A considerable aircraft limitation is the ability to take off from the ramp. It is primarily influenced by stall speed, static thrust and aircraft weight and drag.

3.2 Design Selection Process

In order to properly assess each configuration a Figures of Merit system was devised, based on the most important configuration factors. Each Figure of Merit (FOM) was assigned a score from 0 to 5, with 5 being the most important and 0 being a non-factor in design. Table 2 shows importance of FOM that were set.

Table 2: Figures of Merit

Factor	Importance
Simplicity	3
Weight	5
Ease of Folding	3
Speed & Drag	5
Stability	2
Takeoff/Landing	4

Simplicity: Simplicity of the airplane is one of the less important factors during the flight. However, it is significant for the ground mission, since there must be as little steps as possible to mount the attack stores and the radome to ensure a fast completion time.

Weight: The weight of the airplane was decided to be the one of the most important characteristics. It is important in M1, M2 and M3 and has a significant influence on takeoff capabilities of the airplane. Smaller weight also means that there is less induced drag in all stages of flight, as less lift is needed.

Ease of Folding: To ensure the aircraft was capable of passing the technical inspection, ease of folding for each design was taken into consideration as a complex folding mechanism is prone to failure due to multiple factors.

Speed & Drag: Speed of the airplane contributes to faster completion of missions and thus higher scoring of M2 and M3. Increasing speed produces more lift, which enables more attack stores to be carried. Less drag enables the aircraft to fly faster with less required power and enables the completion of more scoring laps.

Stability: Its importance is mediocre. An unstable plane will have trouble carrying the payload and completing missions 2 and 3, but stability can be maintained by an experienced pilot.



Takeoff/Landing: Because of the takeoff ramp limitations, takeoff was taken into special consideration. Reliable takeoff and landing greatly reduce damage risks and increase safe completion of each mission, insuring the team can take advantage of the full mission time.

3.2.1 Basic Aircraft Design

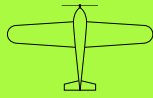
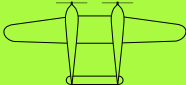

Three basic design configurations were assessed: conventional, bi-fuselage and flying wing design.

Conventional Design is easy to manufacture and has a solid all round design, although it does not excel in any specific area. It is considered to be the safest option as the team is very familiar with this shape.

Bi-Fuselage provides bigger fuselage mounting length while still having a solid carrying capacity. It requires greater attention to details in manufacturing than a conventional plane. It also provides more mounting points for dual motor design and more battery storage, compared to conventional build. However, the team does not have prior experience with bi-fuselage configuration, which provides a certain risk.

Flying Wing Design has the best aerodynamic characteristics and can enable high flying speeds. The main limitations are difficulties in manufacturing and manoeuvrability. The folding of the wings is harder to achieve. Table 3 shows the basic design assessment.

Table 3: Basic Design Configuration Assessment

Design	Weight	Conventional 	Bi-Fuselage 	Flying Wing 
Simplicity	3	2	1	0
Weight	5	2	1	1
Ease of Folding	3	2	2	0
Speed	5	1	1	2
Stability	2	2	1	0
Value	/	30	20	13

Conventional design was chosen as the most suitable configuration, since it offers simple design and payload accommodation, as well as an overall stable flight. At first sight the bi-fuselage configuration might offer better takeoff capabilities and payload accommodation, but the team was confident to come up with other ways to increase payload capacity without negatively affecting takeoff weight.


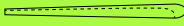

3.2.2 Fuselage Design

As the main configuration was chosen, the goal was to define some of the main aircraft parts in greater detail. In order to reduce drag of each individual attack store while maintaining structural integrity and payload capacity, the



following options were considered: round fuselage with attack stores attached without any drag reduction geometry, modified convectional fuselage design with attack stores as hidden inside as possible, and a combination of both.

Table 4: Fuselage Design Assessment



Fuselage Design	Weight	Fuselage Design 1 	Fuselage Design 2 	Fuselage Design 3 
Simplicity	3	2	1	0
Weight	5	1	1	1
Ease of Folding	3	2	2	2
Takeoff/Landing	4	1	1	2
Speed&Drag	5	0	2	1
Value	/	21	28	24

At first, Fuselage design 2 was chosen based on team predictions, but later testing showed that Fuselage Design 3 was better. Detailed testing of a different design is shown in Sections 7.2.2 and 8.1.

3.2.3 Attack Stores

Positioning: Two different configurations were taken into consideration, as shown in Table 5.

Table 5: Attack Store Position Assessment

Store Position	Weight	Position 1 	Position 2 
Ease of Folding	3	1	2
Speed&Drag	5	1	2
Value	/	8	16

Mechanism: Two different quick release mechanism were devised by the team. One more complex, seen in Figure 5, and a simpler but more crude design. They were compared using the FOM table. As seen in Table 6, the more complex design was chosen mainly due to less drag and better integration within the wing, but as seen in Section 5.3.5 the team decided to go with the simpler option in the end, due to poor 3D print quality and strength.



Table 6: Quick Release Design Assessment

Store Position	Weight	Simple	Complex
Simplicity	3	1	0
Weight	5	1	1
Speed&Drag	5	1	2
Value	/	13	15

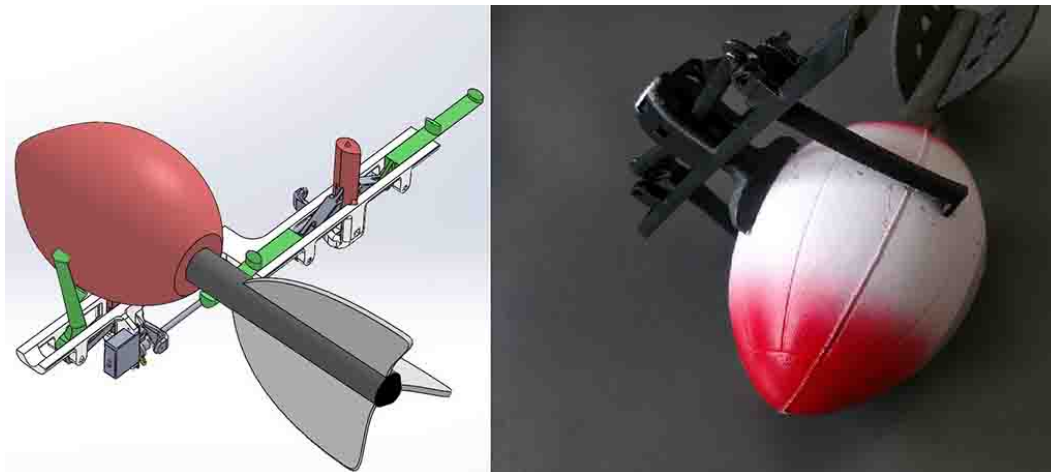


Figure 5: 3D Printed Quick Release Design

3.2.4 Radome

Positioning: The FOM were used again to compare two possible radome positions. The possible positions were either on the fuselage or on the wings, as shown in Table 7. Through test flights we determined that both positions show minimal effect on aircraft capabilities. The final position was based on the ease of manufacture.



Table 7: Radome Positioning Assessment

Fuselage Design	Weight	Fuselage	Wing
Ease of Folding	3	2	1
Speed&Drag	5	1	1
Value	/	11	8

Mounting Hardware: The goal is to make it as light as possible, with enough structural integrity and as simple to mount as possible.

3.2.5 Wing Folding

Three different folding designs were compared: rotary, folding along the fuselage and collapsing wing folding; and two folding mechanisms: layered carbon spring and torsion spring.

Rotary: This configuration consist of rotating an entire wing. Because the plane would not fit in bounding box dimensions, a fold was necessary. This demands a design of two different mechanisms; one to rotate the wing and another one to unfold it.

Wing Folding Along Fuselage: With this positioning we gain room in the bounding box, however, the center of gravity moves too far back and plane would tilt back. It is also too complicated to manufacture as it demands movement in multiple degrees of freedom.

Collapsing Wing Folding: The team decided on this option, because the wings fold onto itself. This way the center of gravity does not move, and the same sort of mechanism is used on both wings in contrast to a rotary configuration.

Table 8: Wing Folding Design Assessment

Folding Design	Weight	Rotary	Along the Fuselage	Collapsing
No. of Different Mechanism	3	1	2	2
Effect on CG	4	2	1	2
Ease of Manufacture	4	1	1	2
Value	/	15	14	22

Mechanism: Two folding mechanisms were compared and tested: **layered carbon spring** and **torsion spring**.



The torsion spring was chosen over the layered carbon spring due to easier implementation of the design. Details can be seen in Table 9.

Table 9: Wing Folding Mechanism Based on FOM

Wing Folding Mechanism Assessment	Weight	Layered Carbon Spring	Torsion Spring
Small Dimensions	4	1	2
Unfolding Speed	5	1	1
Torque	5	1	2
Value	/	14	23

3.3 Final Conceptual Design

The final configuration consists of a high wing conventional aircraft with wings that can fold and roll through a 3ft by 2ft box, with a conventionally designed tail that can carry up to 19 attack stores and a rotating radome. The aircraft has a conventional landing gear and can take off from a 10ft ramp at an angle of 5°. The final conceptual design is shown in Figure 6.

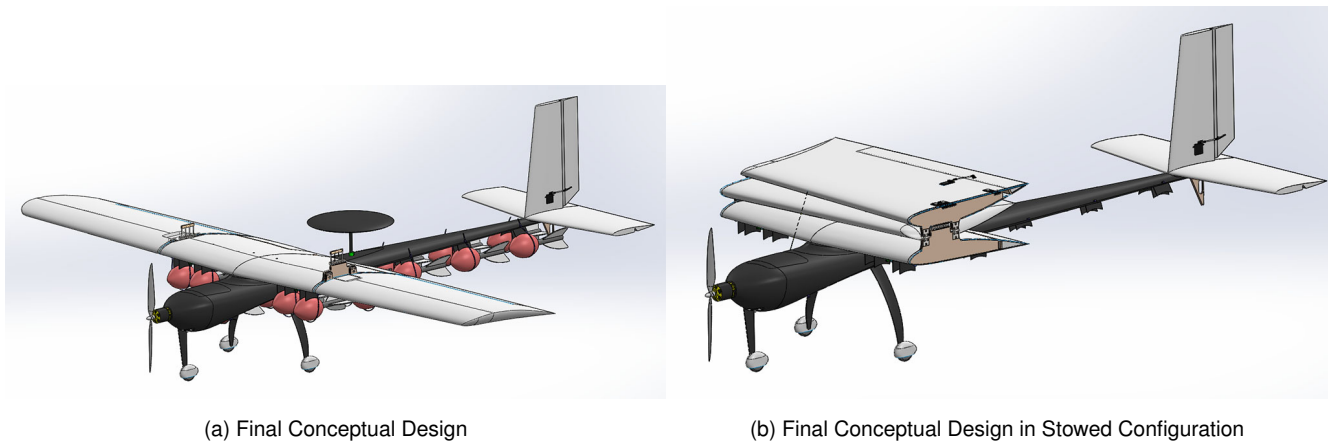


Figure 6: Final Conceptual Design

4. Preliminary Design

The objective of the preliminary design was to determine and further optimize the parameters of the conceptual design in order to maximize the final score. By taking into account the sizing/design trades, aerodynamics, and mission model, the score analysis simulation (SAS), programmed by Python computer language [2], managed to calculate the optimal aircraft parameters and estimated mission performance, visible in Table 19.

4.1 Design and Analysis Methodology

Due to its robustness and easy implementation, the iteration procedure which would yield the highest final score was used in determining the parameters of the aircraft. Over the course of the iteration, wing area, airfoils, number of attack stores and propulsion configurations (propellers, ESC, cell number, motor) were determined. The SAS scheme is shown in Figure 7.

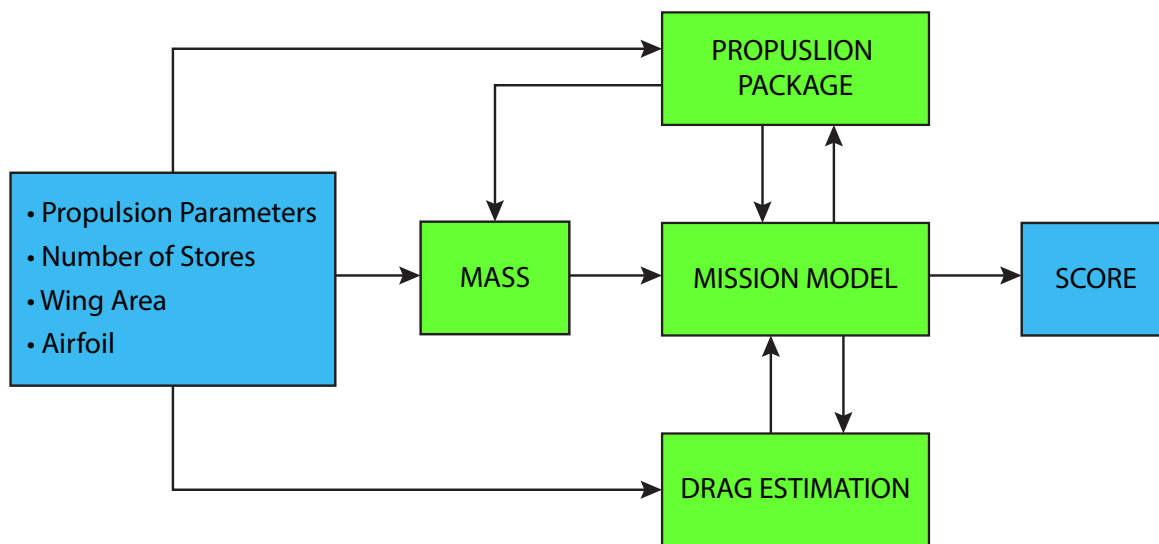


Figure 7: SAS Diagram

Since the quantity of all parameter combinations would be too demanding for our processing capabilities, the iteration procedure was carried out in stages. In the first stage only the main parameters, such as wing area and number of attack stores, were iterated. Other parameters, such as airfoils, wingspan and empennage, were kept constant at this stage. Propulsion parameters were crudely estimated by estimating efficiency. In the second stage, the priority was to determine the optimal propulsion configuration and airfoil.

The optimal aircraft configuration was found to be the one that would perform best in mission 3, since the maximum score was not limited by the success of other competitors. Therefore the success in mission 3 was prioritized.



4.2 Design Trade Studies

4.2.1 Number of Attack Stores

The number of attack stores is directly proportional to the score achieved in mission 3. With each attack store an additional lap must be flown, which in turn meant that a faster aircraft with a heavier battery pack was needed. In Figure 8 the relationship between the attack stores and weight can be seen.

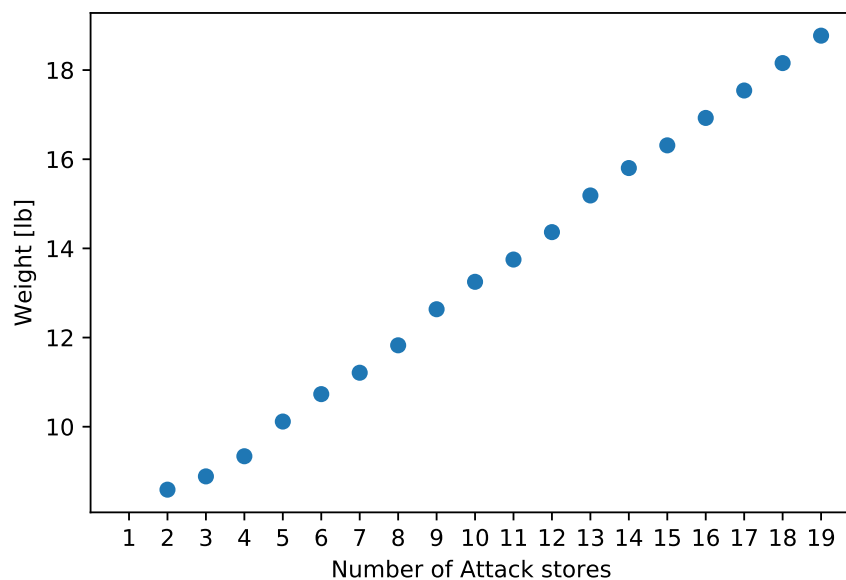


Figure 8: Relationship Between the Number of Attack Stores and Estimated Aircraft Takeoff Weight for Mission 3

4.2.2 Takeoff Requirements

The aircraft must be able to take off from a 10ft ramp, which in turn meant that it must be able to achieve stall speed determined by considering aircraft mass, $C_{l,max}$, lift increase by flaps, wing area, drag coefficient and static thrust. Stall speed was determined by Equation 13. In Figure 9 the relationship between the required takeoff force and wing area can be seen. The required thrust was determined with Equation 14 and by considering the Second Newton's law.

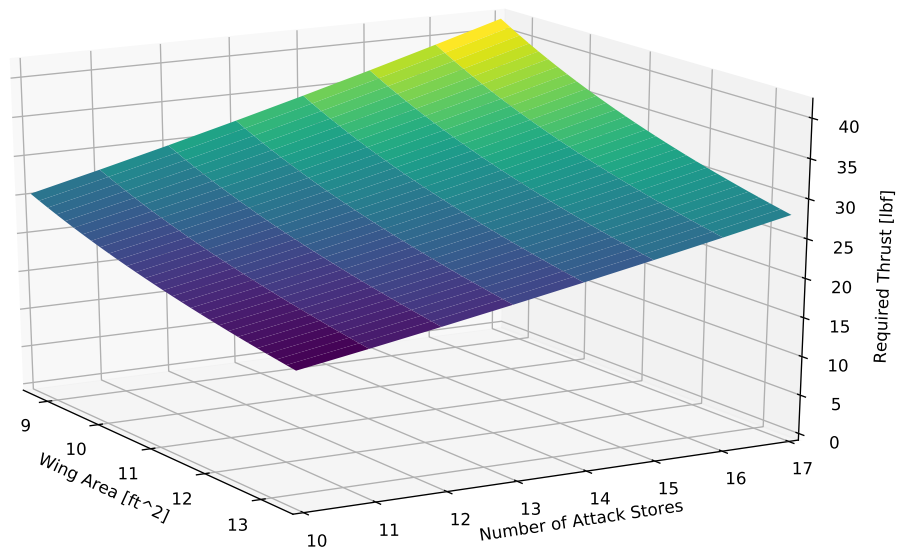


Figure 9: Relationship Between Static Thrust, Wing Area and Number of Attack Stores

4.2.3 Propulsion System

The propulsion configuration was chosen through the iteration of 102 BLDC motors, 132 propellers, 10 electronic speed controls (ESC) and 3 different types of batteries. In each iteration the of components were passed down to propulsion module, which produced the proper thrust curve for desired throttle settings. The obtained thrust curve was used as one of 4 nonlinear equations of motion of straight flight module, which is a sub module in mission module of SAS. Propulsion module scheme along with its integration to straight flight module is presented in Figure 10.

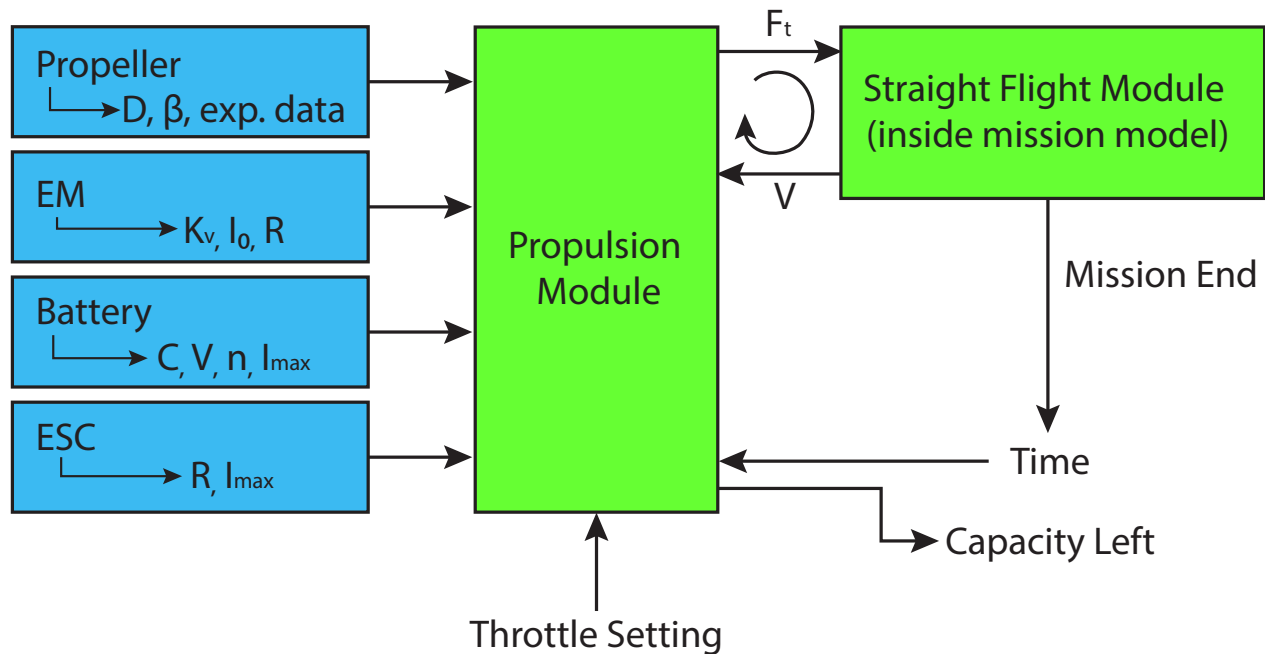


Figure 10: SAS Diagram

As mission 3 requires a 10 minute flight time at a relatively high velocity, propulsion endurance was greatly considered. SAS's flight module offered a time calculation of each lap. That, combined with velocities of each lap, enabled the propulsion module to accurately determine burned battery pack capacity.

Table 10 contains three optimal propulsion configurations. Based on the required battery capacity for a 10 minute flight and high power to weight ratio, Scorpion SII-4035-450KV with APC 16x8 propeller and batteries wired two cells in parallel and 24 pairs in series. 5000mAh Turnigy cells were chosen to be the best fit for the propulsion configuration.

Table 10: Competent Propulsion Configurations

Weight [lbs]	Motor	Power [W]	KV	Battery (series x parallel)	Propeller
7.19	Scorpion SII-4035-450KV	2960	450	5000mAh Turnigy (20x2)	APC 17x8
8.38	Scorpion SII-4035-450KV	2960	450	5000mAh Turnigy (24x2)	APC 16x8
9.62	Scorpion SII-4035-450KV	2960	450	5000mAh Turnigy (28x2)	APC 16x6



4.3 Mission Model

The missions were simulated by calculating the time needed to complete each lap. A single lap was simplified to four turns, two straight flights and one takeoff.

Takeoff was modeled by solving Equation 14 given that the speed acquired by the end of the ramp was larger than stall speed.

$$v(t) = \sqrt{\frac{2ma}{\rho AC_d}} \tanh\left(t \sqrt{\frac{a\rho C_d A}{2m}}\right) \quad (14)$$

Straight flight was modeled by solving nonlinear Equations 15 and 16.

$$m \cdot g - \frac{1}{2} \rho AC_l v^2 = 0 \quad (15)$$

$$Thrust(v) - \frac{1}{2} \rho AC_d(C_l, v)v^2 = 0 \quad (16)$$

Turning flight was simplified to take place at maximum lift the aircraft can produce. By solving Equations 17 and 18, turning speed and radius were calculated.

$$Thrust(v_{turn}) - \frac{1}{2} \rho AC_{d,max} v_{turn}^2 = 0 \quad (17)$$

$$R = \frac{2 \cdot m}{\rho \cdot A \cdot C_{l,max} \cdot \sin \alpha} \quad (18)$$

Equations 19 and 20 were later used to calculate lap times. Lap time was additionally increased by 2 seconds in order to compensate for the time needed to position the aircraft for turning maneuver.

$$t_{lap}(P, AR, m, A, C_l) = \frac{2 \cdot l}{v_0(P, m, A, AR)} + \frac{4 \cdot \pi \cdot R(P, m, n, C_{l,max}, AR)}{v} + 2 \quad (19)$$

$$t_{lap,first}(P, AR, m, A, C_l) = \frac{2 \cdot l - l_{takeoff}}{v_0(P, m, A, AR)} + \frac{4 \cdot \pi \cdot R(P, m, n, C_{l,max}, AR)}{v_{turn}} + 2 + t_{takeoff} \quad (20)$$

4.3.1 Uncertainties

Certain variables were disregarded using this model. In this mission model we assumed that the pilot has perfect skills. Further on, the model disregards the weather conditions in which the aircraft will fly. It also assumes that the aircraft will be flown at constant altitude. This assumption increases uncertainty, especially in turning maneuver where a constant altitude at $C_{L,max}$ is difficult to achieve.

The mission model also neglected other factors, such as aircraft interference drag and compressibility, as these were concluded to have minimal impact on the initial performance calculations of various aircraft configurations. In addition, the simplified model offered shorter computation time.



4.4 Aircraft Lift, Drag and Stability Characteristics

4.4.1 Airfoil Selection

Choosing the correct airfoil was crucial for a fast and stable aircraft. The airfoil was chosen primarily on $C_{l,max}$ due to takeoff requirements. The aircraft must takeoff from 10ft ramp, with velocity close to stall speed where Reynolds number is 300000. Airfoils were analyzed at Reynolds number of 200000. The three most promising airfoils were chosen using SAS, they are shown in Figure 12. Finally, ClarkY was chosen for the final aircraft, since Goe387 was considered to be too thick and Eppler420 was having questionable characteristics at a lower Reynolds number. Airfoil polars were obtained from Airfoil tools [3].

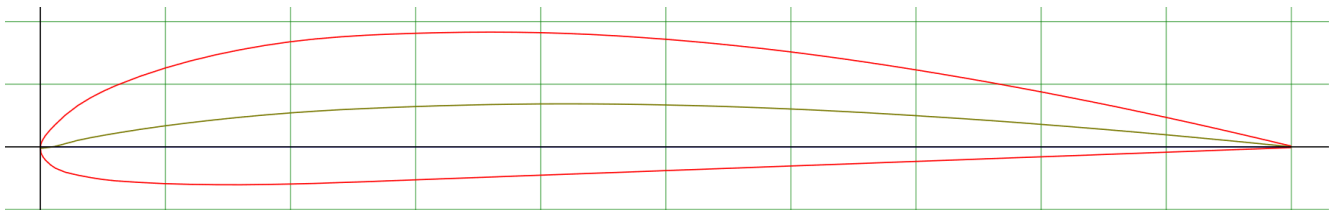


Figure 11: ClarkY Airfoil

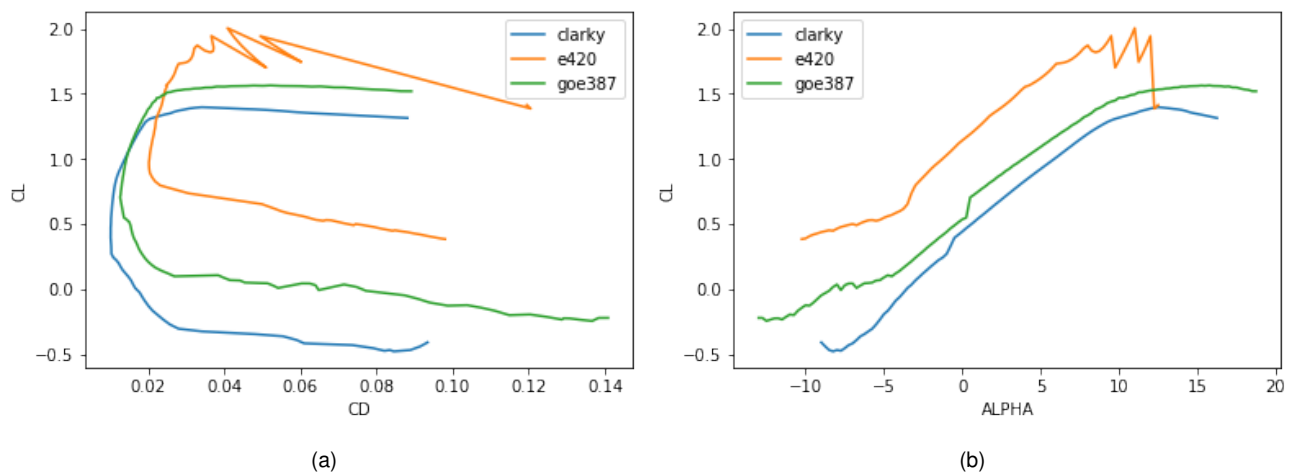


Figure 12: Airfoil Polars

4.4.2 Lift And Drag Analysis

The lift and drag analysis was carried out in 2 separate stages. During the iteration procedure the AVL analysis was too demanding, so cruise lift and drag coefficients, and max lift coefficients were calculated based on airfoil polars [3]. Drag coefficients from other components, such as the fuselage, were acquired by assuming turbulent



flow and using Schlichting's empirical equation [4] for skin friction drag. Drag from attack stores was determined experimentally as seen in Section 7.2.2. The described empirical function was properly adjusted in order to coincide with the drag coefficient values obtained from experiments. Drag contributions can be seen in Figure 13. Table 11 contains lift and drag coefficients of initial optimal aircraft design. Since our main concern was the ability of the aircraft to take off from the ramp, it was necessary to account for flaps in calculation of $C_{l,max}$ lift coefficient.

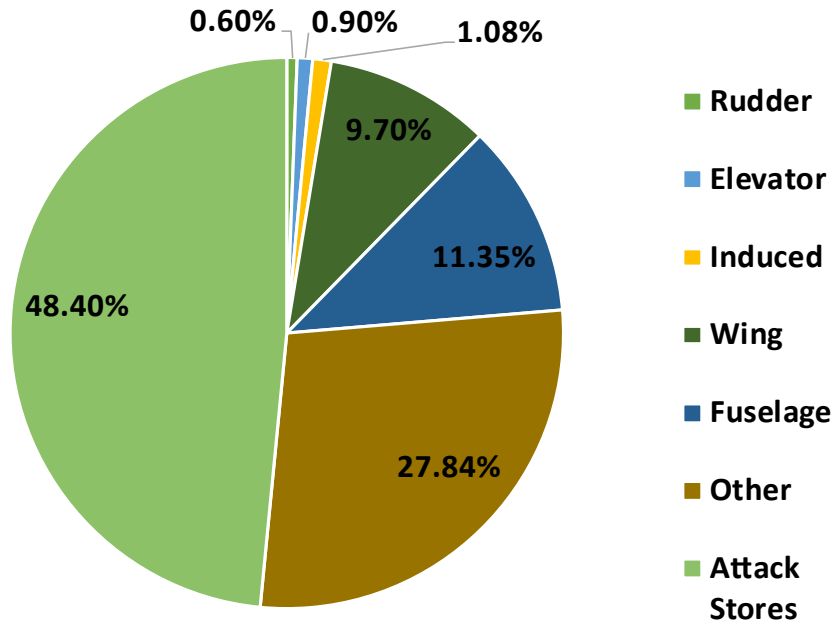


Figure 13: Drag Contributions

Due to attack stores being dropped in each lap the total drag of the aircraft was decreasing.

Table 11: Initial Lift and Drag Estimations During Iteration Process Using SAS

	$C_{l,max}$	$C_{l,avg}$	$C_{d,avg}$
Value	1.75	0.16	0.07

AVL [5] was further used to perform Trefftz plane analysis that enabled the determination of trimmed flight conditions as well as lift distribution across the wing and horizontal tail. The green curves in Figure 14 denote normalized lift distributions across the wing and tail for M3. The result applies to cruise flight at 91.68ft/s .

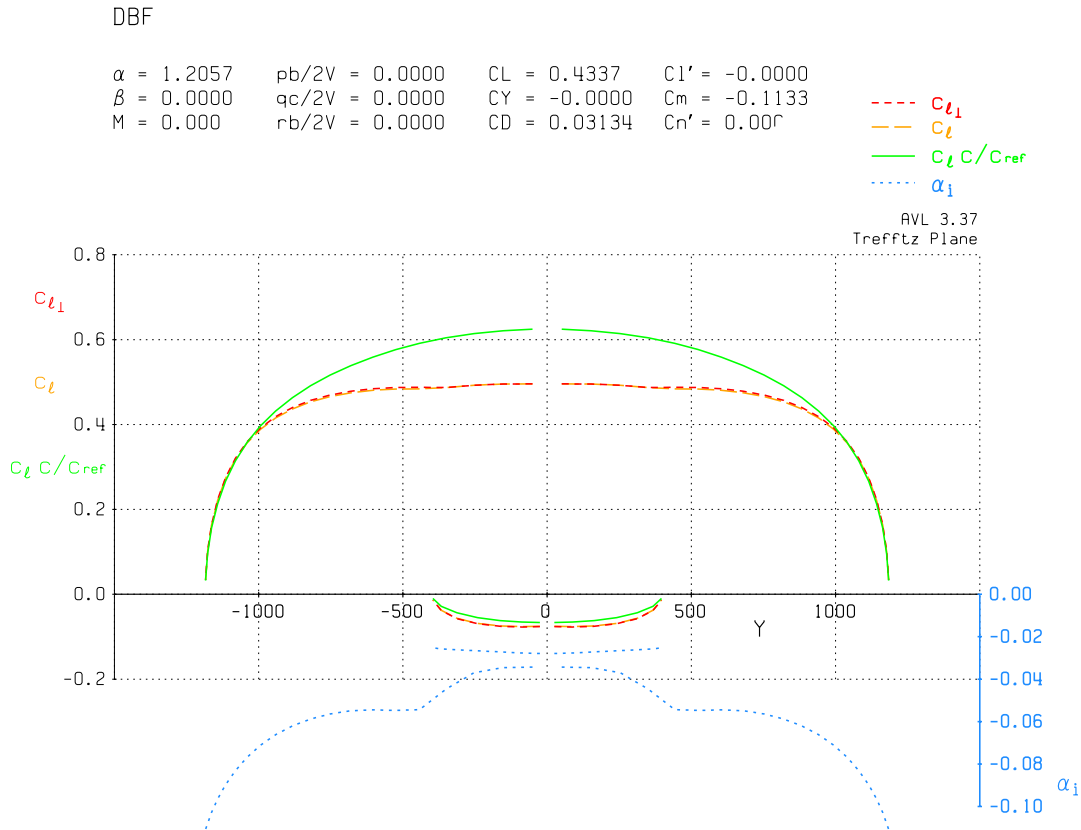


Figure 14: Lift Distribution

4.5 CFD Analysis

Several aerodynamic characteristics of the final model were determined with the use of computational fluid dynamics (CFD). The team was interested in determining the influence of the wingtip geometry on lift and drag coefficients, as well as in calculating the aforementioned aerodynamic coefficients pertaining to the airplane fuselage. In both cases, CFD simulations were done using OpenFOAM for Windows 18.02 (version 1).

4.5.1 Airplane Fuselage Analysis

The primary objective of fuselage analysis was to determine drag coefficient of the fuselage as a function of the free stream velocity. The computational mesh utilized in this simulation was based on the geometry of the bare airplane fuselage with no other aerodynamic surfaces and attack stores attached. Shown below are the simulation parameters and results for fuselage design 3, which was experimentally proven to be the most appropriate in Section 7.2.2.



We solved the momentum equations using the in-built SIMPLE algorithm (simpleFoam), and we used the $k - \omega$ SST (Shear stress transport) turbulence model as a means of equation closure. We resolved the boundary layer close to the wall with a very fine computational mesh ($y^+ < 10$). Computations were done for free stream velocities of $v_1 = 49.213\text{ft/s}$ and $v_2 = 82.020\text{ft/s}$. The reference surface area S_{ref} , defined for this calculation, is understood to be the fuselage cross section at the position of its maximum value. Additional parameters relevant to the simulation are displayed in Table 12.

Table 12: Additional Relevant Parameters for CFD Analysis

Parameter	ρ [lb/ft ³]	ν [ft ² /s]	S_{ref} [ft ²]
Value	0.07647	$16.146 \cdot 10^{-5}$	$26.996 \cdot 10^{-2}$

Lift and drag coefficients, calculated via the simulation, are displayed in Table 13.

Table 13: CFD Analysis Calculated Aerodynamic Coefficients

Parameter	Value	
v [ft/s]	49.21	82.02
C_d [/]	0.3605	0.3570
C_l [/]	-0.0427	-0.0525

A graphical representation of the calculated airflow velocity field and static pressure field acting on the airplane fuselage is shown in Figures 15 and 16:

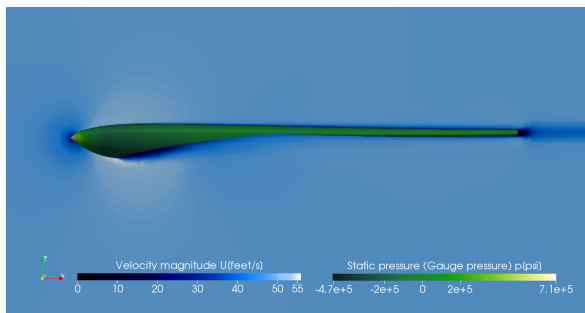


Figure 15: Airflow Velocity Field and Pressure Field for $v = 49.213\text{ft/s}$

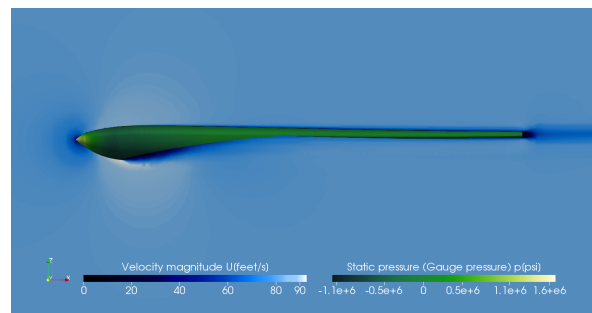


Figure 16: Airflow Velocity Field and Pressure Field for $v = 82.0209\text{ft/s}$.



4.5.2 Wing Tip Analysis

The primary objective of the wing tip analysis was to determine the wing tip lift and drag coefficients as functions of the airflow velocity and wingtip geometry, that are characterized by the characteristic wingspan distance between the upper and lower edge of the wing tip facet, which we denote as $l_{w,ch}$. Computations were made for the free stream velocity of $v = 49.213\text{ft/s}$ and characteristic lengths $l_{w,ch}$ of 0in , 2.755in , 3.937in and 5.118in . Computational meshes utilized in this simulation were based on the geometry of the outer portion of the wing measuring $l = 31.692\text{in}$ in length. The simulation settings were identical to those described in the previous section. The reference surface area S_{ref} in this case is the wing cross section normal to the lift direction. Additional parameters which are relevant to the simulation are displayed in Table 14.

Table 14: Additional Parameters

Parameter	ρ [lb/ft^3]	ν [ft^2/s]	S_{ref} [ft^2]
Value	0.07647	$16.146 \cdot 10^{-5}$	3.767

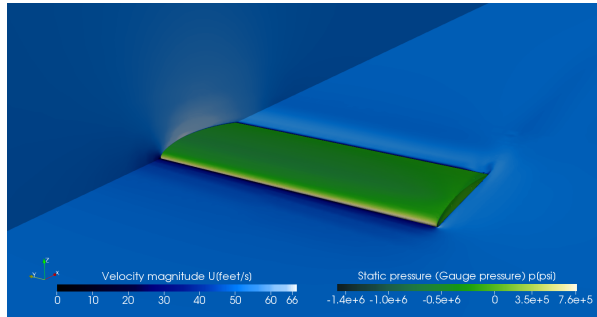
Lift and drag coefficients calculated via the simulation are displayed in Table 15.

Table 15: Calculated Lift and Drag Coefficients

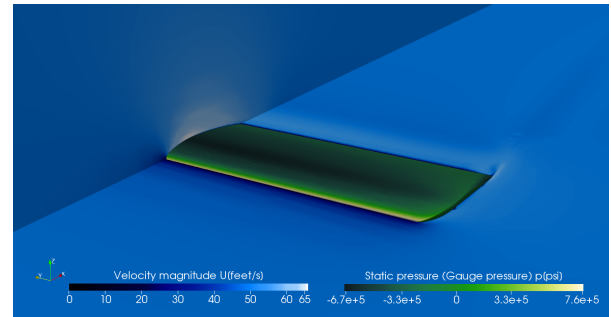
Parameter	Value			
$l_{w,ch}[\text{in}]$	0	2.755	3.937	5.118
$v[\text{ft}/\text{s}]$	49.213	49.213	49.213	49.213
C_l []	0.4338	0.4342	0.4444	0.4463
C_d []	0.0304	0.0302	0.0310	0.0312



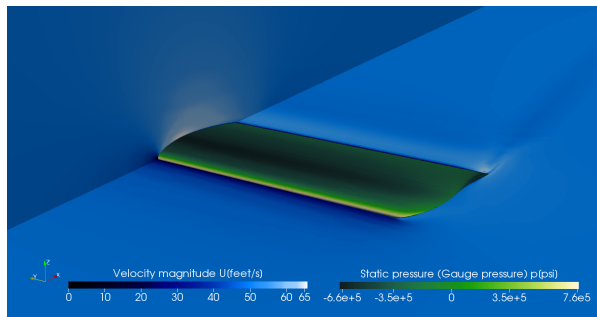
Airflow velocity field and static pressure field acting on the wing tip are graphically represented in Figure 17:



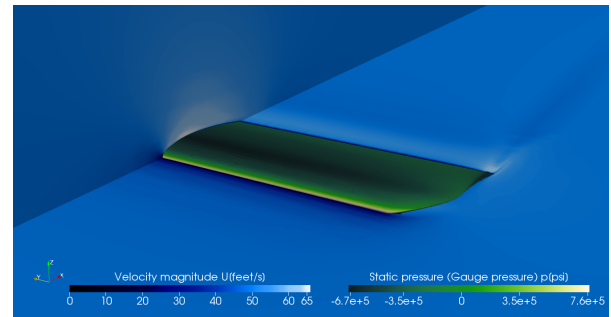
Airflow velocity field and pressure field for $l_{w,ch} = 0in$



Airflow velocity field and pressure field for $l_{w,ch} = 2.755in$



Airflow velocity field and pressure field for $l_{w,ch} = 3.937in$



Airflow velocity field and pressure field $l_{w,ch} = 5.118in$

Figure 17: Airflow velocity Field and Pressure Field for $v = 49.213ft/s$

The wing tip geometry was consequently chosen on the basis of simulation results, which suggest that there is an optimal characteristic length where the drag coefficient is minimal. It was concluded that out of the four wing tip geometries simulated, the second case ($l_{w,ch} = 2.755in.$) has the most favourable aerodynamic characteristics considering its coefficient of drag is lower than for the other three.

4.6 Stability and Control

One of the main issues was the aircraft stability. Due to a large center of gravity (CG) uncertainty a large CG envelope was required as well as a small aspect ratio. Stability derivatives were calculated via AVL and are located in Table 17 for M2 and Table 16 for M3. For both missions the derivatives were calculated at takeoff speed. The neutral point for M3 was calculated at approximately 10.6in behind the leading edge of the wing, making the aircraft longitudinally stable according to Table 23. In M2 the effect of radome must be considered. We simulated this effect by replacing it with a lifting surface with similar surface area, as seen in Figure 18.

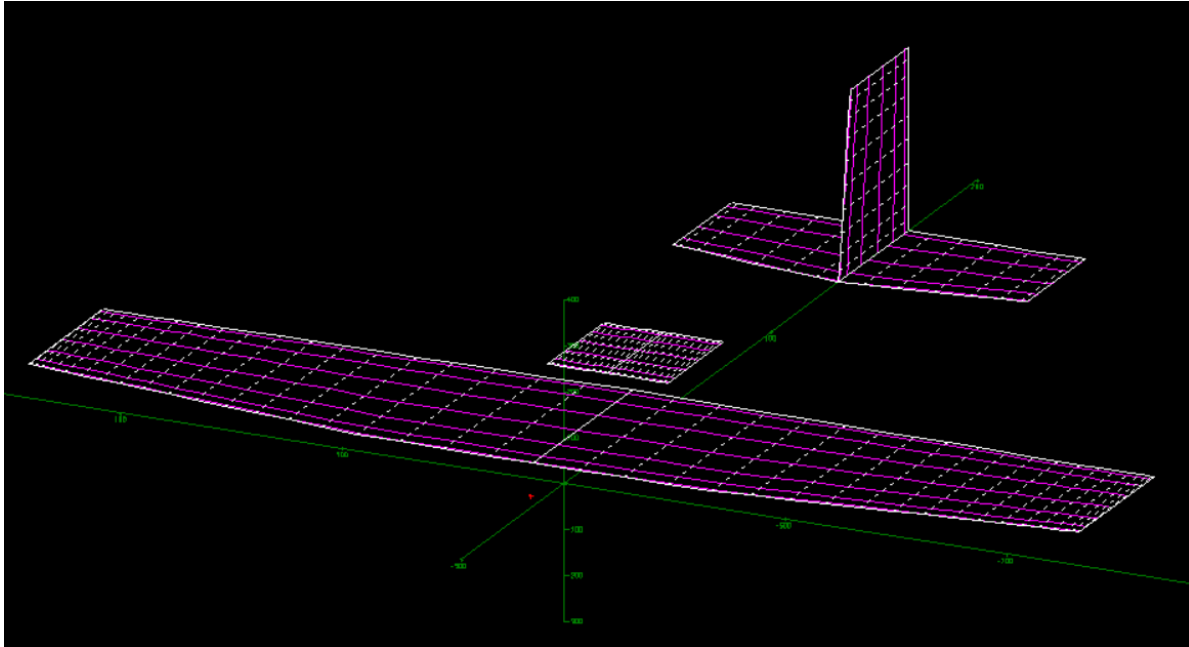


Figure 18: AVL Geometry with Radome Attached

Table 16: Static Stability at Takeoff for M3

	α	β	p'	q'	r'
C_l	-0.0	-0.087	-0.40	-0.0	0.19
C_m	-3.14	0.00	0.00	-27.67	-0.00
C_n	-0.00	0.16	-0.084	-0.0	-0.24

Table 17: Static Stability at Takeoff for M2

	α	β	p'	q'	r'
C_l	-0.0	-0.022	-0.41	-0.0	0.064
C_m	-3.327	0.00	0.00	-28.93	-0.00
C_n	-0.00	0.15	0.010	-0.0	-0.227

The AVL linearized model of nonlinear equations of motion was used for predicting the modes of dynamic stability. The calculated poles of the system matrix for an empty and a loaded aircraft are shown in Table 18. All poles of the system matrix except one, indicating spiral instability, lie in the left half of the plane (shown in Figure 19), which indicates stable modes. Even though the aircraft is considered spirally unstable, the spiral mode time constant is $T_{S,M2} = 24.4s$ and $T_{s,M3} = 27s$, which gives pilot enough time to compensate.



Table 18: Dynamic Stability of Empty and Loaded Aircraft

		Eigenvalue		Damping Ratio		Undamped Frequency [Hz]	
Longitudinal Modes		M2	M3	M2	M3	M2	M3
I	Short Period	$-17.59 \pm i15.39$	$-5.15 \pm i5.47$	0.659	0.73	23.37	7.51
II	Phugoid	$-0.061 \pm i0.45$	$-0.047 \pm i0.47$	0.991	1.00	0.45411	0.47
Lateral Modes		M2	M3	M2	M3	M2	M3
III	Dutch Roll	$-2.98 \pm i8.94$	$-1.05 \pm i3.70$	0.95	0.96	9.4236	3.85
IV	Roll	-28.501	-10.48	/	/	/	/
V	Spiral	0.041	0.037	/	/	/	/

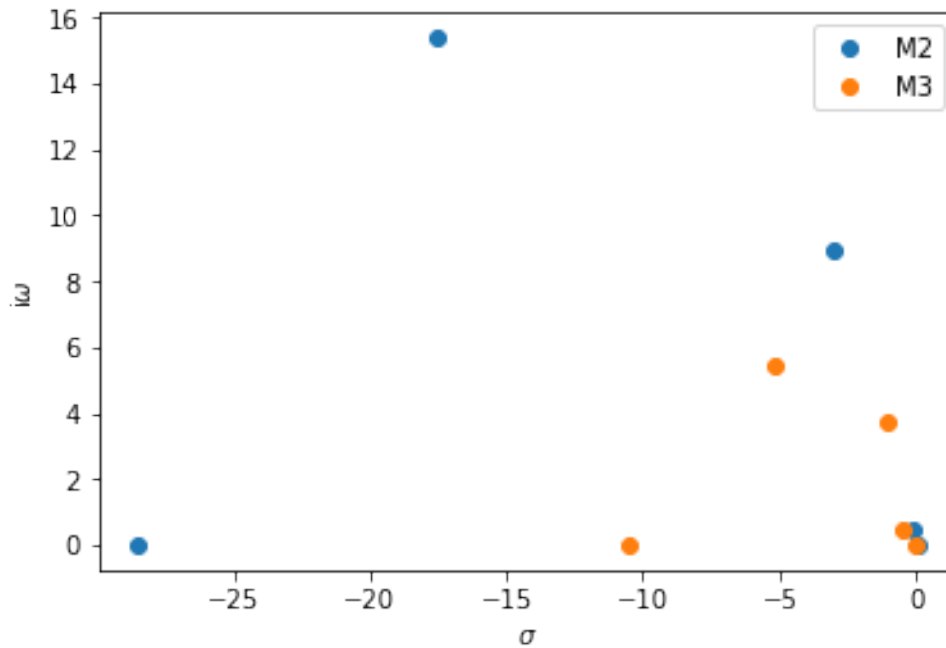


Figure 19: Eigenvalues for M2 and M3



4.7 Estimated Mission Performance

It was assumed that M1 was completed successfully, thus rewarding a score of 1. M2 and M3 scores were estimated by calculating the lap times based on the Equation 19. Mission 2 score was estimated by considering that competitors will be unable to fly much faster than 120ft/s . This value bears no influence on final design. Table 19 contains the predicted aircraft performance.

Table 19: Preliminary Design Mission Performance Characteristics

Performance Parameter	M1	M2	M3
$C_{l_{max}}$	1.15	1.15	1.15
$C_{l_{avg}}$	0.133	0.135	0.16
C_{d0}	0.054	0.065	0.07
L/D_{cruise}	2.46	2.1	2.28
Wing Loading [lbs/ft^2]	1.22	1.23	1.53
v_{avg} [ft/s]	98.1	98.0	91.68
v_{stall} [ft/s]	16.3	16.4	18.44
Aircraft weight [lbs]	14.7	14.8	18.43
Carried Payload	0	Radome	19 Attack Stores
Number of Laps	3	3	19
Mission Score	1	1.8	21



5. Detail Design

5.1 Dimensional Parameters

Table 20: Final Aircraft Dimensional Characteristics

Fuselage		Vertical Tail	
Total Length [<i>in</i>]	77.55	Airfoil	NACA 0010
Nose Length [<i>in</i>]	19.68	Span [<i>in</i>]	12.6
Tail Length [<i>in</i>]	57.87	Chord-base [<i>in</i>]	10.24
Width [<i>in</i>]	9.05	Chord-tip [<i>in</i>]	7.87
Height [<i>in</i>]	7.08	Wing Area [<i>in</i> ²]	114.1
Wing		Aspect Ratio	3.74
Airfoil	CLARK Y	Angle of Attack [°]	0
Span [<i>in</i>]	95.27	Horizontal Tail	
Chord-base [<i>in</i>]	19.68	Airfoil	NACA 0010
Chord-tip [<i>in</i>]	15.75	Span [<i>in</i>]	31.50
Wing Area [<i>in</i> ²]	1627	Chord-base [<i>in</i>]	10.24
Aspect Ratio	5.38	Chord-tip [<i>in</i>]	7.87
Angle of Attack [°]	3.5	Wing Area [<i>in</i> ²]	285.2
		Aspect Ratio	3.48
		Angle of Attack [°]	0

5.2 Structural Characteristics

5.2.1 Fuselage

A sandwich structure of composite carbon fiber and honeycomb filler was used. Based on experience from previous years and test samples the team decided on a combination of $4.7\text{oz}/\text{yard}^2$ carbon mesh and 0.12in thick honeycomb. Reinforcement ribs were added to enhance the structural integrity of the fuselage.

FEM analysis [6] was used to model the surface area of the aircraft for the duration of a turn. The complex structure of the sandwich structure was simplified to a material with comparable isotropic properties.

The most important part of the FEM analysis was to determine the distribution of internal stress as well as areas of high concentrations of internal stress. They can be seen in Figure 20. The team members were not comfortable enough with the method of simplifying to determine the absolute values. Results were later used by the manufacturing team to add additional carbon fiber mesh and roving to the areas with predicted high internal stress.

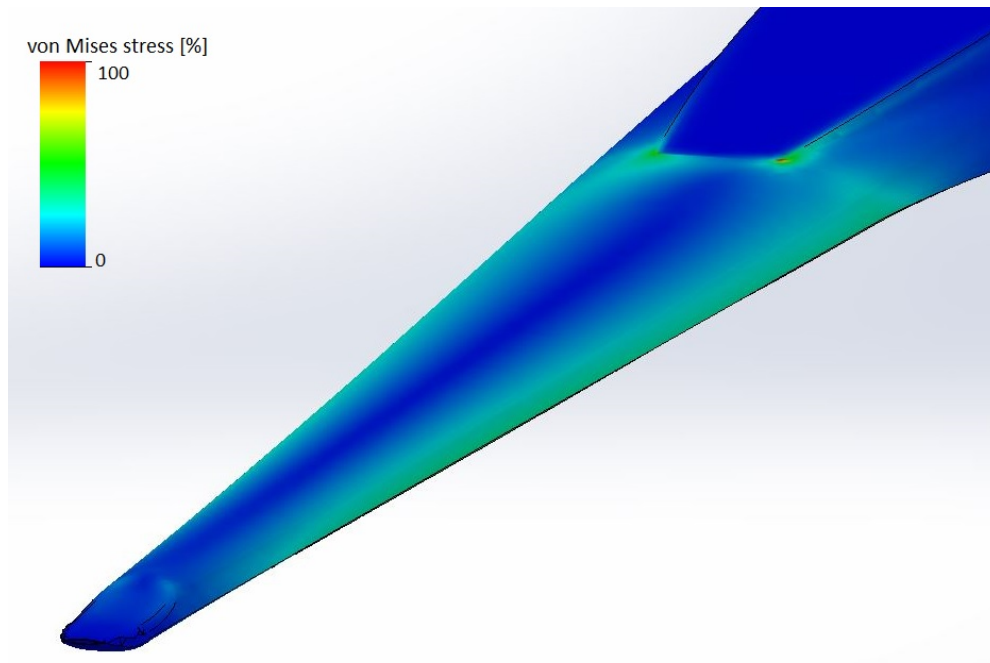


Figure 20: FEM Analysis of the Fuselage

5.2.2 Wing Structure

For the structural analysis of a wing an assumption was made that the main beam of the wings carries all bending stresses and the skin for torsional stress. The cross section of a beam is shown in Figure 21. It consists of a web made from vertically aligned balsa wood, flanges from 16k carbon roving and carbon fiber cloth at the sides. The bend moment on a wing during cornering was calculated. At that bend moment the maximal stress that occurs in beam cross section for each material was calculated. Results are shown in Figure 22. Values of used elastic modulus are shown in Table 21.

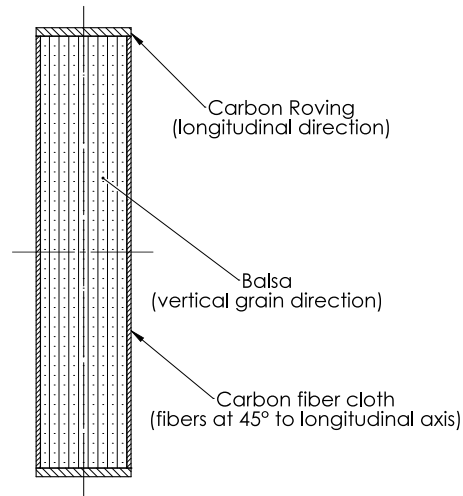


Figure 21: Main Beam Cross Section

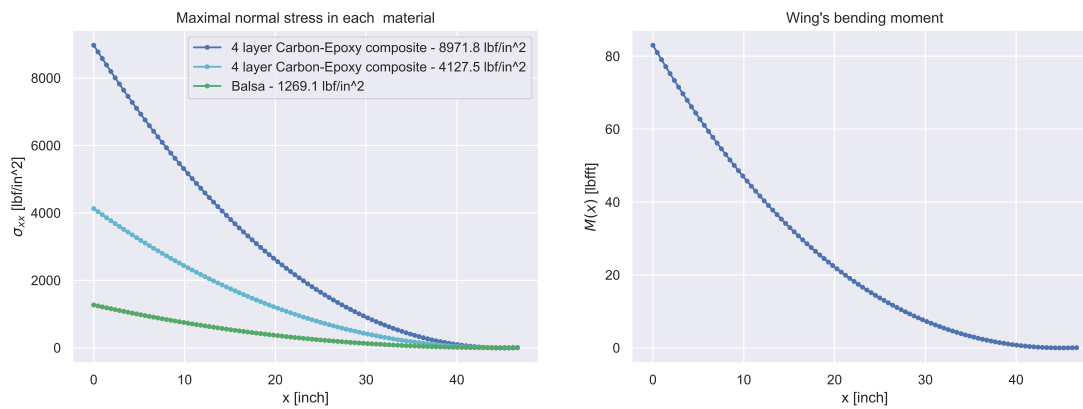


Figure 22: Normal Stress Calculations (Left) Based on Bending Moments During Turn Maneuver at 5g (right)



Table 21: Elastic Modulus Values

Material	Elastic Modulus [lbf/in^2]
Carbon Fiber Roving	3700000
Carbon Fiber Mesh	1750000
Balsa Wood	540000

Web thickness is consistent across the wingspan for ease of production. Decreasing of stress toward wing tip was taken into account by decreasing the number of carbon roving layers from 7 at wing center to 1 at the tip.

5.3 Systems and Sub-Systems Integration

5.3.1 Fuselage

The fuselage design was chosen based on testing, done in the wind tunnel, as shown in Section 7.2.2. The final design enables attack stores mounted under the fuselage to produce minimal drag force as shown in Figure 23. The front section was shaped aerodynamically to accommodate all propulsion components as well as the necessary equipment to enable RC capabilities. From the initial part the fuselage tapers towards a shape that enables the stores to have as much ground clearance as possible. Design shown in Figure 24 enables the attack stores to be as hidden from the airflow as possible, while still maintaining a high moment of inertia.

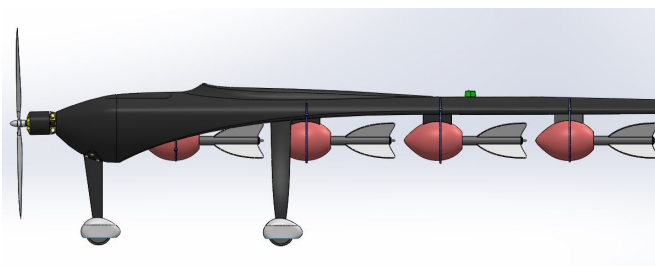


Figure 23: Fuselage Side View

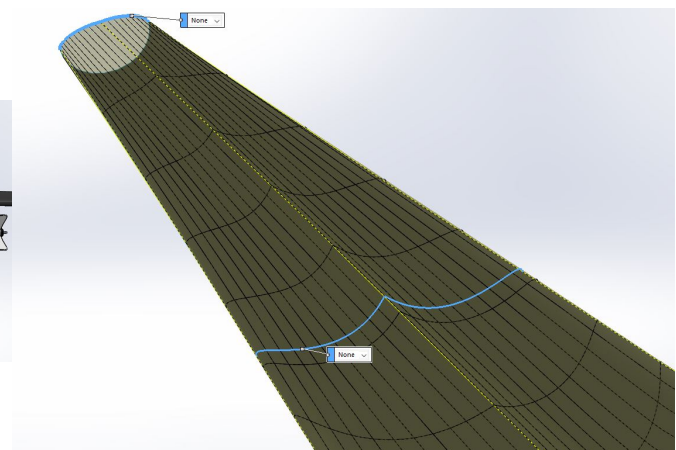


Figure 24: Fuselage Attack Storage Accommodation

5.3.2 Wing

To ensure that the wing weighs as little as possible and the shape is kept as close to the original profile and end design as possible, each section was made from a separate mold as described in Section 6.3.2. Critical points



were additionally reinforced with a carbon fiber mesh to ensure structural integrity. The team wanted to go with a full carbon fiber design due to improved mechanical characteristics but decided against it as it would be too cost prohibitive. The main structural support along the wings is provided by a vertically mounted balsa wood profile and carbon fiber mesh at the top and bottom part of the balsa wood with additional herex foam and fiberglass composite ribs for added structural rigidity. The flaps are located on the centre plane of the wing, while ailerons are mounted as close to the edge of the wings as possible. The flaps follow a classic design as it was determined that more complex designs, such as Fowler flaps, are not necessary.

5.3.3 Wing Folding Mechanism

The design shown in Figure 25 enables a maximal wingspan while still maintaining centre of gravity at the same spot as when in flight-ready configuration. This design permits the undercarriage to be as far forward as possible. The wings fold on top of the other as shown in Figure 25 to ensure the smallest possible stowed dimensions. The point of rotation of one wing is raised compared to the other, to enable aforementioned stacking. The momentum required is provided by two torsion springs on each wing, attached to reinforced surface on the wings as shown in Figure 27. Once the folding part crosses over the vertical point, the spring stops providing momentum and the force of gravity forces the wing to the final position where it is mechanically locked by three hooks on each side that hook to the underside of the wing as shown in Figure 28.

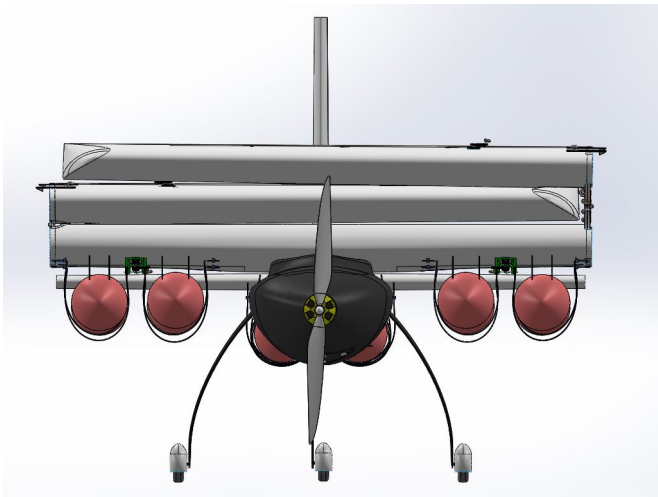


Figure 25: Stowed Configuration of the Aircraft

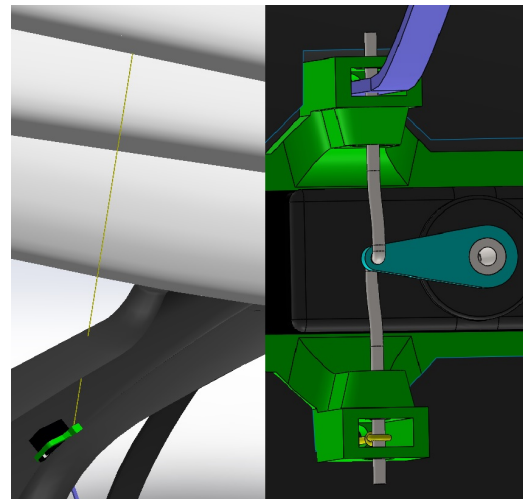


Figure 26: Wing Holding Mechanism

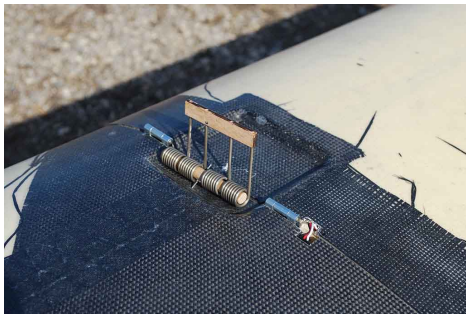


Figure 27: Actuator Torsion Springs

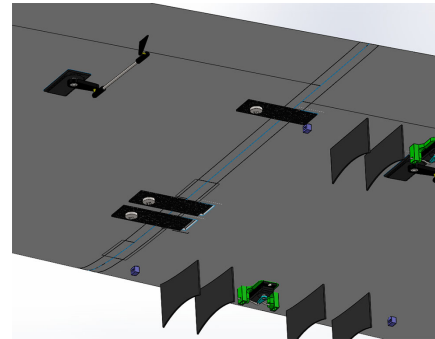


Figure 28: Wing Hooks

5.3.4 Rotating Radome Mechanism

The radome is attached behind the wing at the top of the aircraft, as shown in Figure 29, to enable the least interference in flight. It enables easy assembly during the Ground Mission and while mounting the wing to the fuselage. An electric motor is attached within the fuselage and provides continuous rotation when necessary. The attachment point of the radome is a threaded nut attached to a threaded rod as shown in Figure 30, with minimal thread engagement to ensure a fast mounting time crucial during the Ground mission. A 3D printed bushing, shaped as an aerodynamic drop, enables smooth rotation.



Figure 29: Rotating Radome Position

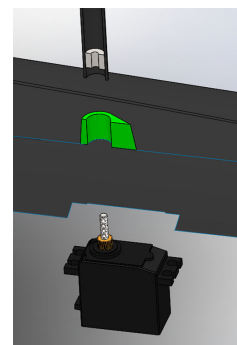


Figure 30: Rotating Radome Assembly

5.3.5 Attack Store Mechanism

Each attack store is mounted on two carbon fiber sheets that act as a part of mounting hardware. The quick release mechanism consists of plastic zip ties, attached to the wing at one end and a wire at the other. To release the store, the wire is pulled by a servomotor to disengage the wire and the attack store as shown in Figures 31 and 32. To mount each store the plastic zip ties are tightened and the attack stores are squished to the mounting sheets.

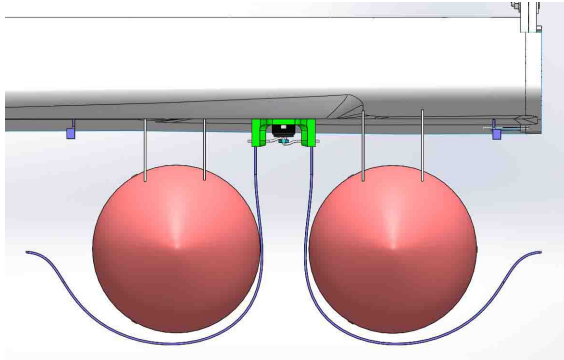


Figure 31: Attack Storage Mounting

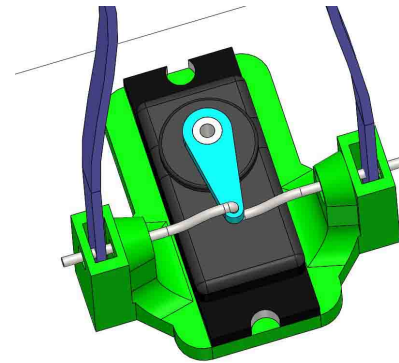


Figure 32: Attack Storage Quick Release

5.3.6 Tail Hook

It is attached to the rear part of the fuselage as shown in Figure 33. It is made from a carbon plate only so big that a team member can hold it with two fingers, and designed to act as a skid in case the rear part of the fuselage comes in contact with the ground or the ramp during takeoff or landing.

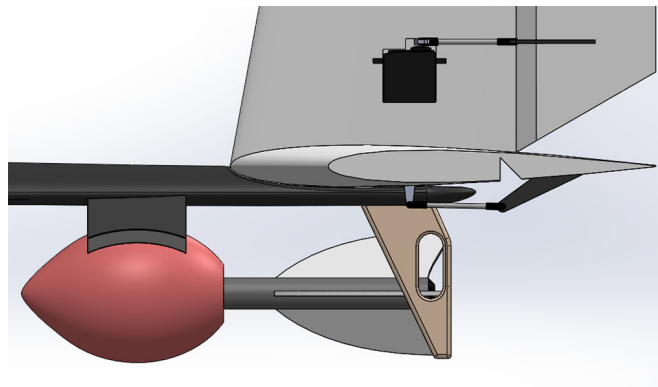


Figure 33: Tail Hook

5.3.7 Propulsion System

The motor mount consists of a carbon fiber plate attached to the front of the plane and secured with four screws directly to the main fuselage, as seen in Figure 34. A small hole is drilled to connect the appropriate cables to the ESC inside the fuselage and minimize drag across the front of the aircraft. ESC is further connected to the battery pack inside the fuselage, located right behind the motor mount to move the CG of the aircraft towards the front. Table 22 shows the final propulsion configuration.



Table 22: Final Propulsion Configuration

Weight [lbs]	Motor	Power [W]	KV	Battery (series x parallel)	Propeller
8.7	Scorpion SII-4035-450KV	2960	450	5000mAh Turnigy (24x2)	APC 16x8

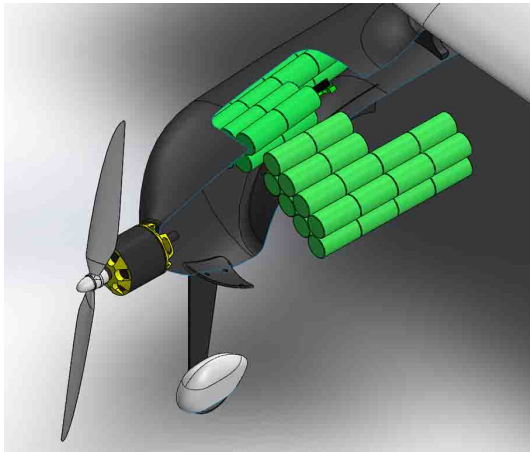


Figure 34: Propulsion Assembly

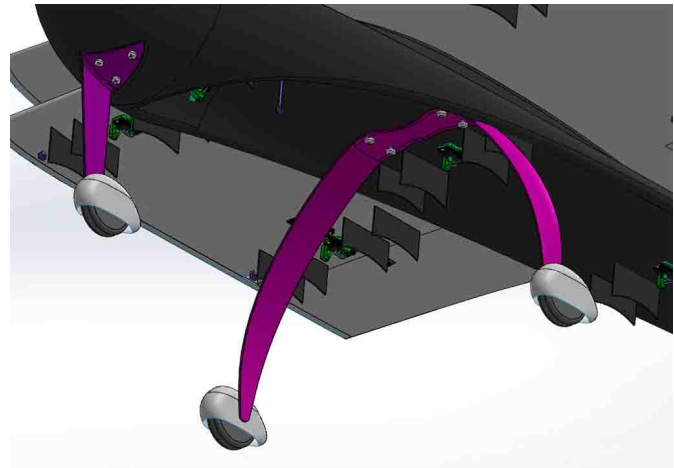


Figure 35: Landing Gear design

5.3.8 Landing Gear

The landing gear is in a tricycle configuration. It consists of one wheel at the front of the plane and a pair just behind CG, as seen in Figure 35. A tricycle design was chosen in favour of other configurations, as it enables bigger ground clearance and forward-most position of rearmost contact point with the ground. This design enables us to have the longest takeoff distance from the ramp. The landing gear was designed to prevent contact of the propeller with the ground as well as ensuring that no attack store touches the ground. In addition, the tail hook acts as a skid in case of a rough landing and has no function during takeoff.

5.3.9 Emmpenage

The empennage is made out of Styrodur core and glass fiber composite skin that provides a sturdy yet lightweight design. As with the wing it would be too cost prohibitive to have a carbon fiber composite skin, so glass fiber was used instead. It has a conventional shape with a rudder and an elevator. The conventional shape provides the best mix of landing and takeoff abilities.



5.4 Weight and Balance

The correct Center of Gravity (CG) location is crucial to achieve aircraft stability during flight. CG was determined by considering the weight of all aircraft components and their location on X, Y axes. The weight of components was estimated based on CAD model or manufacturer specifications. The CG of aircraft in flight-ready configuration was calculated to be 17.91in relative to X axis, as seen in Figure 36. Table 23 contains complete weight and balance data for all flight missions.

Table 23: Airplane Weight and Balance

Aircraft Component	Weight [lb]	X [in]	Y [in]	Aircraft Component	Weight [lb]	X [in]	Y [in]
M1				M3			
Fuselage	1.95	31.4	0	Attack Store #1	0.1375	11.2	0
Wing	4.08	19.2	0	Attack Store #2	0.1375	15.2	13.1
Tail	0.82	72.6	0	Attack Store #3	0.1375	15.2	8.6
Motor	0.96	-1.3	0	Attack Store #4	0.1375	15.2	-8.6
Propeller	0.13	-3.1	0	Attack Store #5	0.1375	15.2	-13.1
Flight Batteries	7.61	10.4	0	Attack Store #6	0.1375	22.3	2.4
Front Landing Gear	0.29	3.2	0.1	Attack Store #7	0.1375	22.3	-2.4
Rear Landing Gear	0.71	20.3	0	Attack Store #8	0.1375	25.8	13.11
Miscellaneous	1.05	20	0	Attack Store #9	0.1375	25.8	8.6
Total	17.6	17.9	0	Attack Store #10	0.1375	25.8	-8.6
M2				Attack Store #11	0.1375	25.8	-13.1
Rotating Radome	0.08	34.6	0	Attack Store #12	0.1375	33.4	2.4
Flight Batteries	7.61	10.2	0	Attack Store #13	0.1375	33.4	-2.4
Total	17.68	17.9	0	Attack Store #14	0.1375	44.3	2.4
				Attack Store #15	0.1375	44.3	-2.4
				Attack Store #16	0.1375	55.2	2.4
				Attack Store #17	0.1375	55.2	-2.4
				Attack Store #18	0.1375	66.4	2.4
				Attack Store #19	0.1375	66.4	-2.4
				Flight Batteries	7.61	8	0
				Total-start	20.21	18.9	0
				Total-finish	17.6	17.9	0

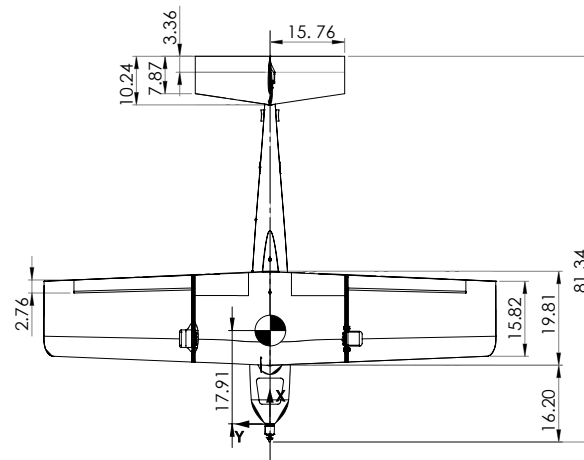


Figure 36: Airplane Centre of Gravity

5.5 Flight and Mission Performance

Flight parameters for each individual mission are gathered in Table 24.

Table 24: Performance Parameters for Final Design

Performance Parameter	M1	M2	M3
$C_{l_{max}}$	1.15	1.15	1.15
$C_{l_{avg}}$	0.133	0.135	0.16
C_{d0}	0.054	0.065	0.07
L/D_{cruise}	2.46	2.1	2.28
Wing Loading [lbs/ft^2]	1.23	1.24	1.55
v_{avg} [ft/s]	98.1	98.0	91.6
v_{stall} [ft/s]	16.5	16.5	18.5
Aircraft weight [lbs]	17.6	17.68	18.9
Carried Payload	0	Radome	19 Attack Stores
Number of Laps	3	3	19
Mission Score	1	1.8	21

5.6 Drawing Package

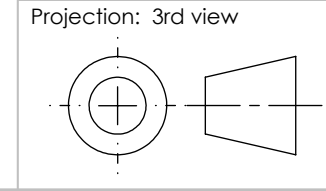
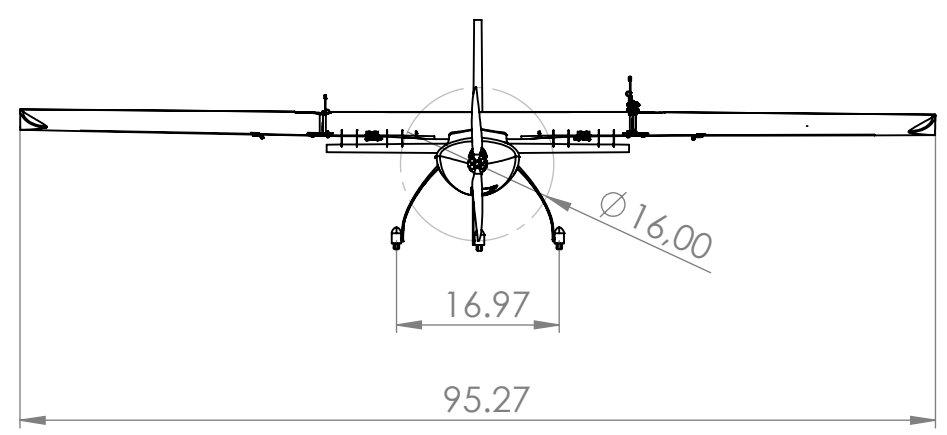
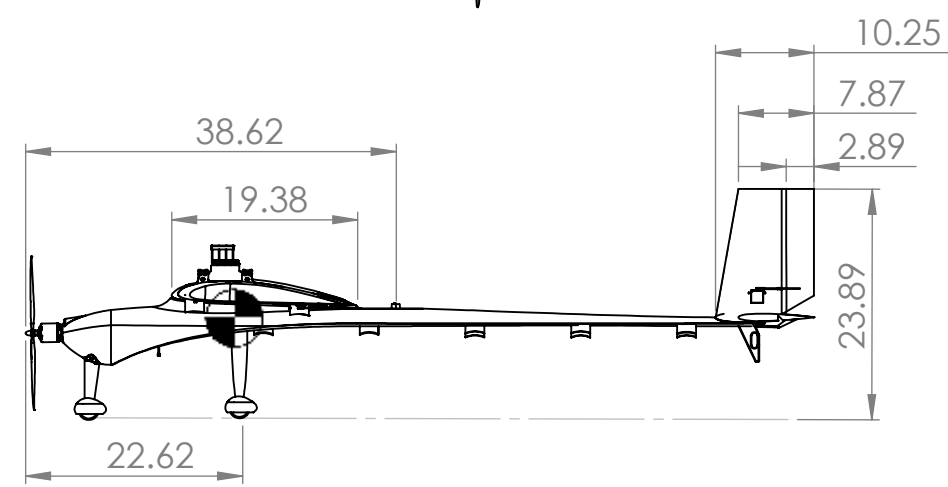
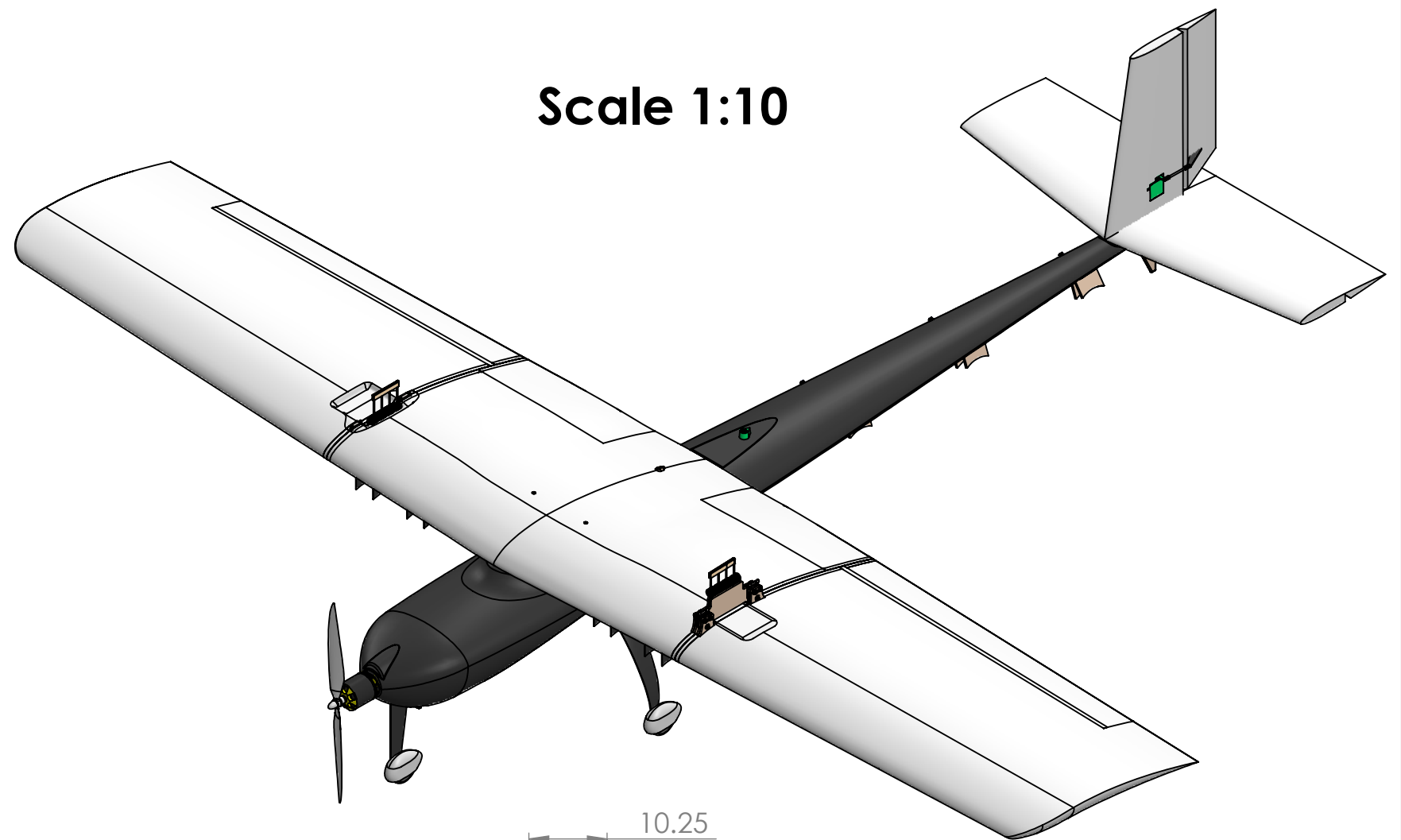
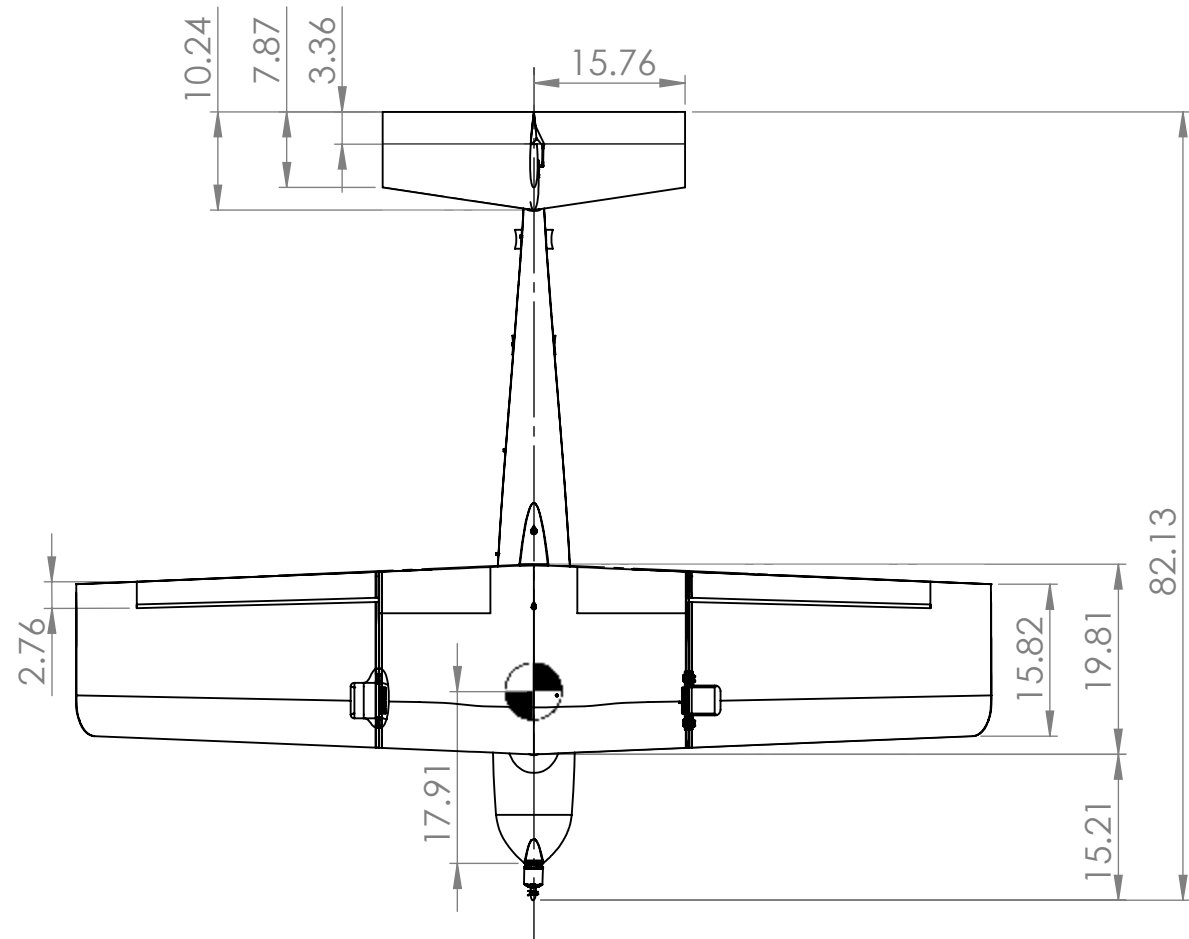
This section contains the 3-view drawing with dimensions, the structural arrangement drawing, the systems layout drawing and the payload accommodation drawing.

4

3

2

1



Comments:

Drawn by:
Klemen Mlakar

**UNIVERSITY OF LJUBLJANA,
FACULTY OF MECHANICAL
ENGINEERING**

Aircraft 3-view

TITLE:
PRETTY BOY

SIZE B	DWG. NO. DBF_2019_UL_DRW_01	REV
SCALE: 1:20 WEIGHT: 15.64 lb		SHEET 1 OF 1

All dimensions are in inches

4

3

2

1

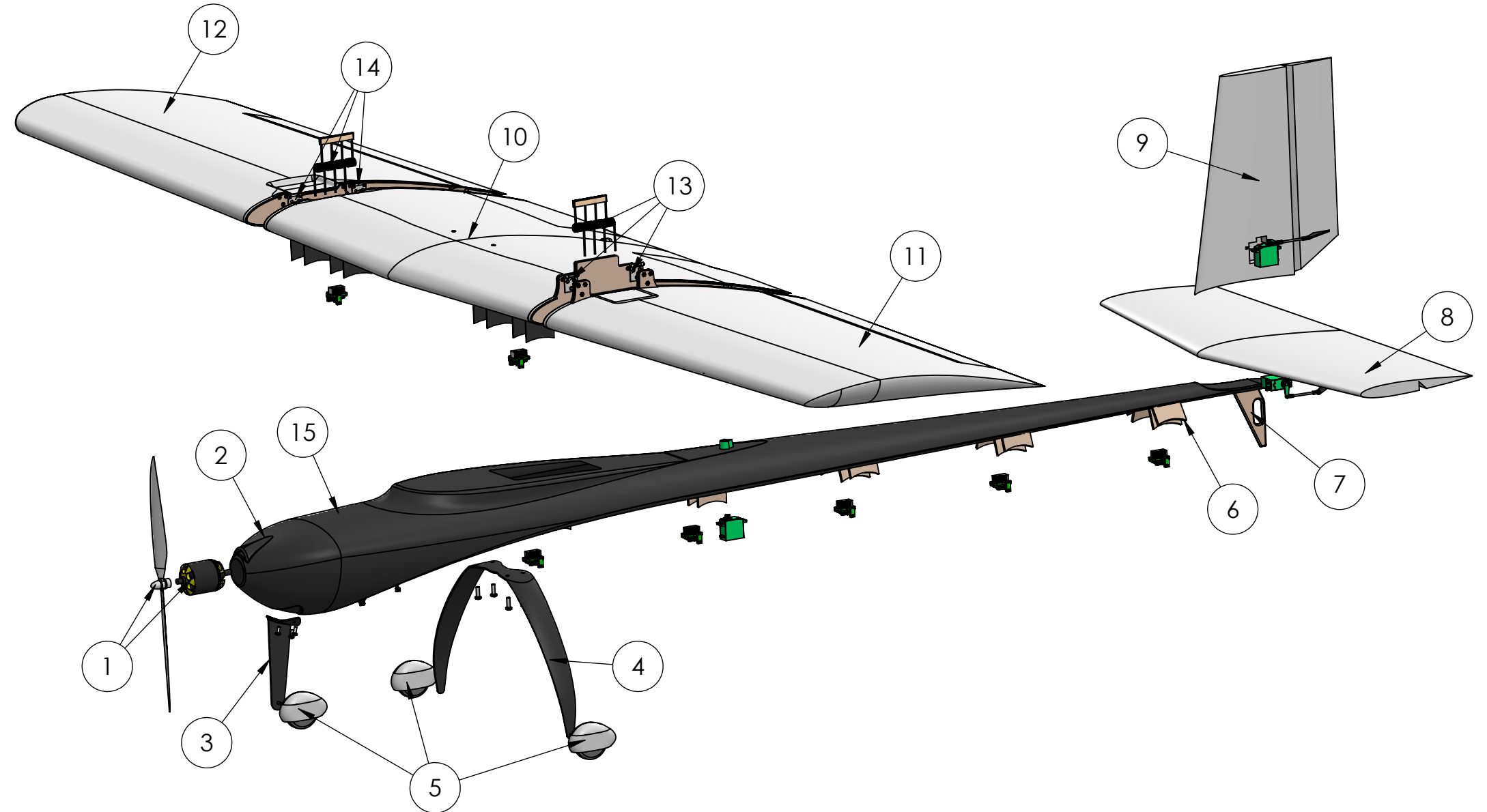
B


B

A

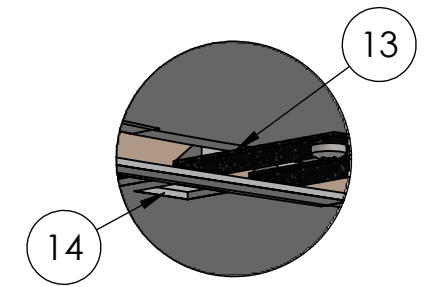
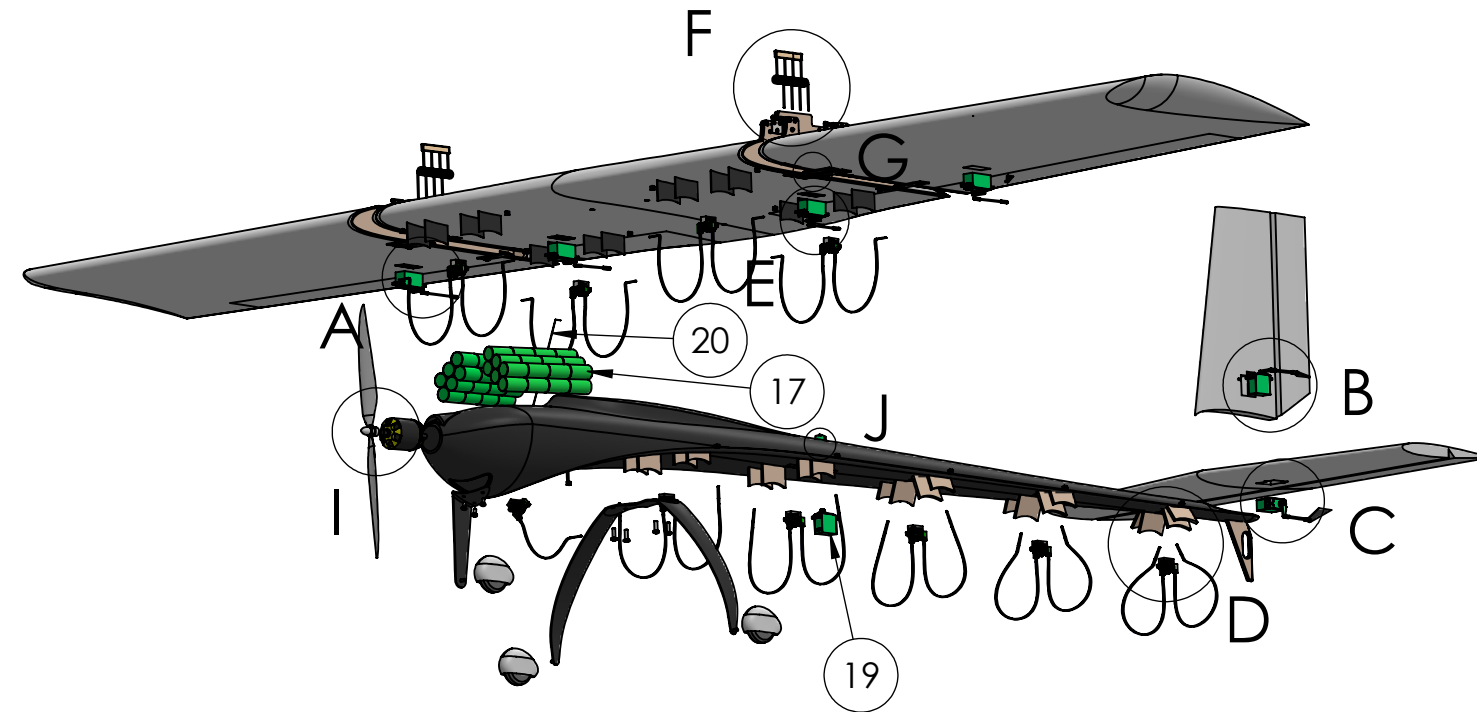
A

Item No.	Component	Description	QTY.
1	Propulsion system	16x8 propeller, 2.96 kW electric motor	1
2	Fuselage	Carbon fiber	1
3	Front wheel support	Carbon fiber	1
4	Main undercarriage	Carbon fiber	1
5	Wheel	Polymer	3
6	Attack store mount	Carbon fiber	19
7	Tail hook	Carbon fiber	1
8	Vertical stabilizer	Styrofoam & fiberglass	1
9	Rudder	Styrofoam & fiberglass	1
10	Wing-center	Airex foam & glassfiber	1
11	Wing-left	Airex foam & glassfiber	1
12	Wing-right	Airex foam & glassfiber	1
13	Folding mechanism-left	Steel, plywood	1
14	Folding mechanism-right	Steel, plywood	1
15	Electronics access hatch	Carbon fiber	1

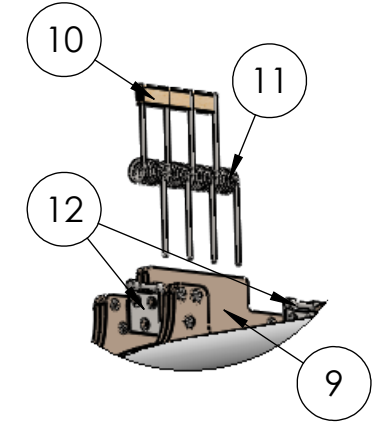


Comments:		Structural arrangement	
Drawn by: Klemen Mlakar		TITLE: PRETTY BOY	
 UNIVERSITY OF LJUBLJANA, FACULTY OF MECHANICAL ENGINEERING	SIZE B	DWG. NO. DBF_2019_UL_DRW_02	REV
	SCALE: 1:8 WEIGHT: 15.64 lb		SHEET 1 OF 1

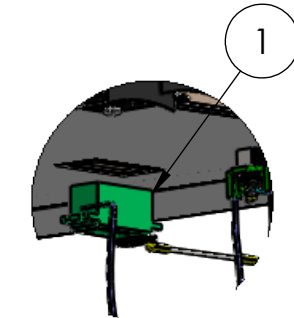
Item No.	Name	Description	QTY.
1	Servo motor 1	Aileron controll	2
2	Servo motor 2	Rudder controll	1
3	Servo motor 3	Horiz. stab. controll	1
4	Servo motor 4 holder	/	10
5	Cable tie anchor point	/	19
6	Servo motor 4	Attack store release controll	10
7	Cable tie	Attack store fastener	19
8	Servo motor 5	Flap controll	2
9	Sideplate	Wing part end	4
10	Contact plate	Distributed load transfer	2
11	Spring	Wing unfolding actuator	8
12	Hinge	Wing unfolding movement restrictor	4
13	Wing hook	Wing integrity preserver	6
14	Wing hook anchor point		6
15	Propeller	16 x 8	1
16	Scorpion SII-4035	Electric motor, propulsion, 2.96 kW	1
17	2x24 NiMH Battery cells	Battery pack	2
18	Radar attachment point	Radar support	1
19	Servo motor 6	Radar spinning	1
20	Kevlar cord	Folded wing release	1



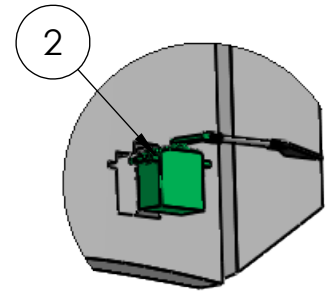
DETAIL G
SCALE 1 : 2



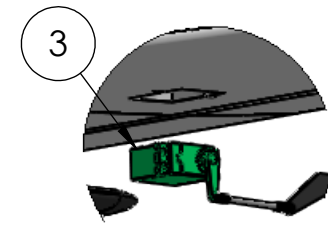
DETAIL F
SCALE 1 : 4



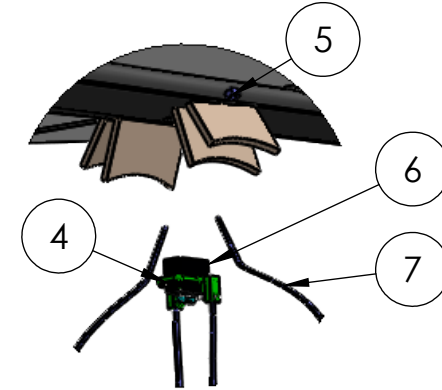
DETAIL A
SCALE 1 : 4



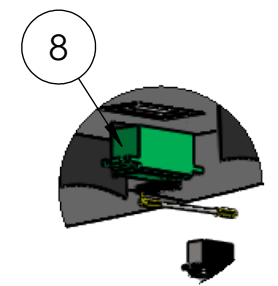
DETAIL B
SCALE 1 : 4



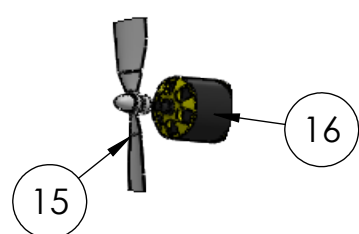
DETAIL C
SCALE 1 : 4



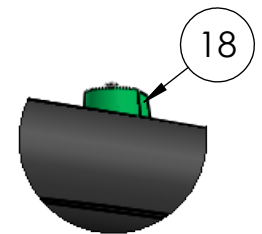
DETAIL D
SCALE 1 : 4



DETAIL E
SCALE 1 : 4



DETAIL I
SCALE 1 : 6



DETAIL J
SCALE 1 : 2



Comments:

Drawn by:
Klemen Mlakar

**UNIVERSITY OF LJUBLJANA,
FACULTY OF MECHANICAL
ENGINEERING**

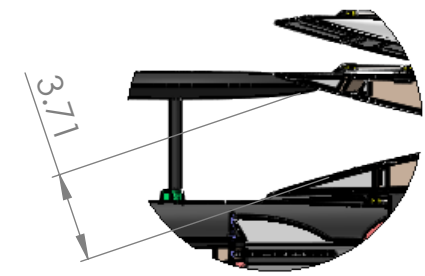
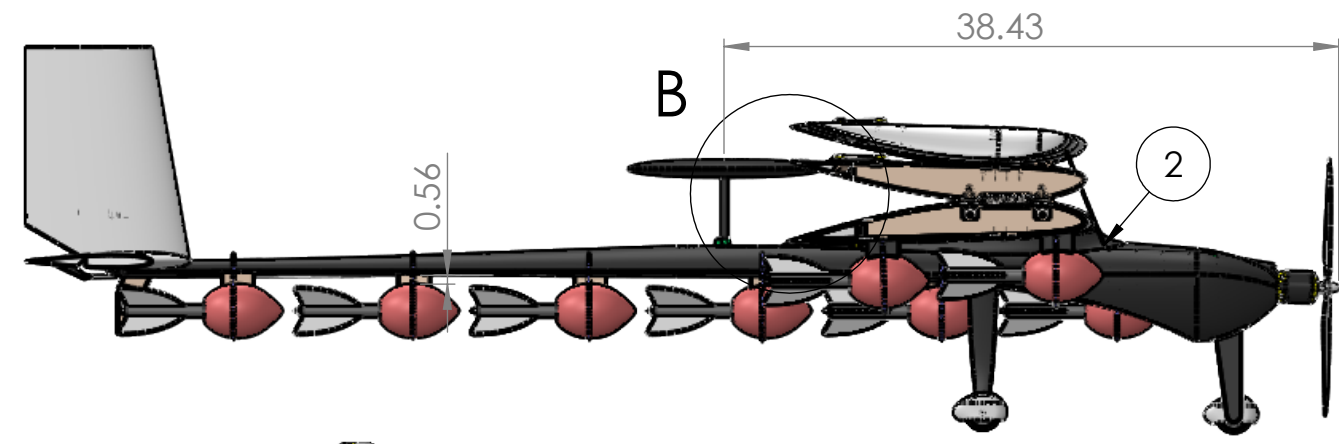
System layout		
TITLE: PRETTY BOY		
SIZE B	DWG. NO. DBF_2019_UL_DWG_03	REV
SCALE: 1:15 WEIGHT:15.64 lb SHEET 1 OF 1		

4

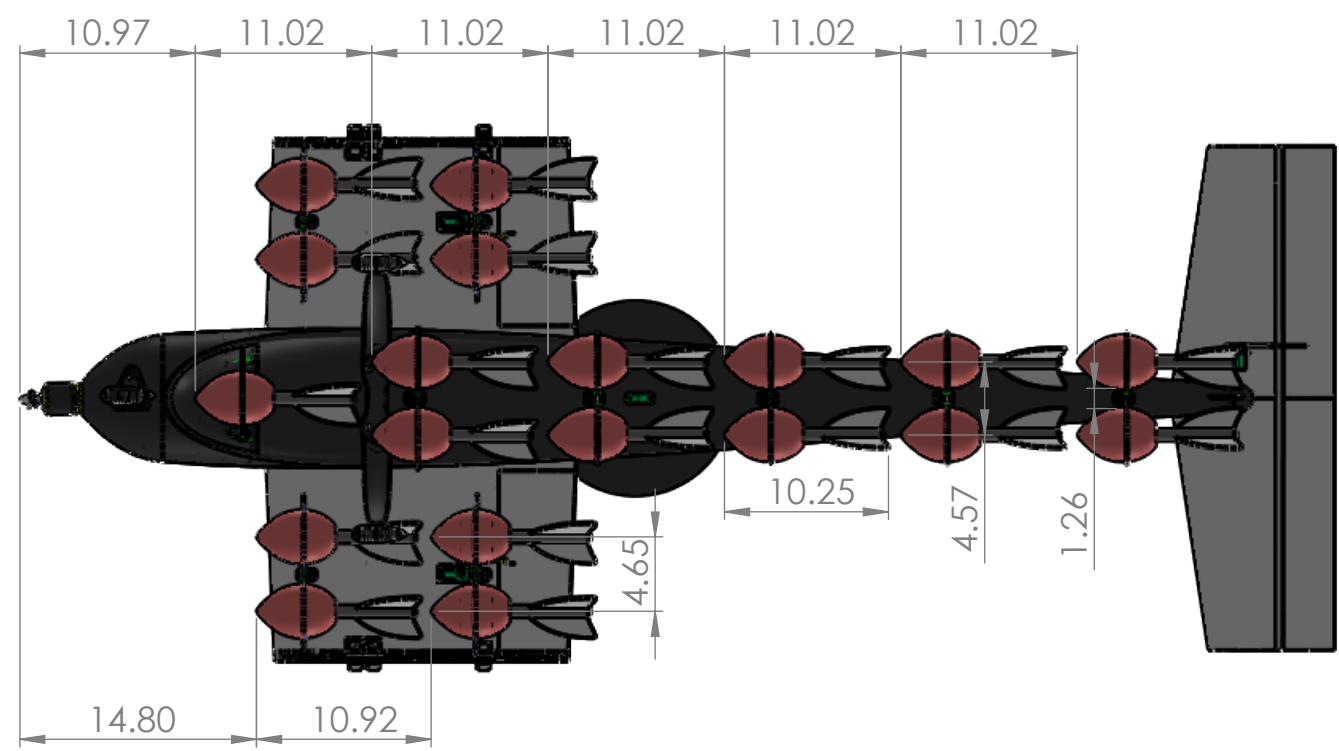
3

2

1



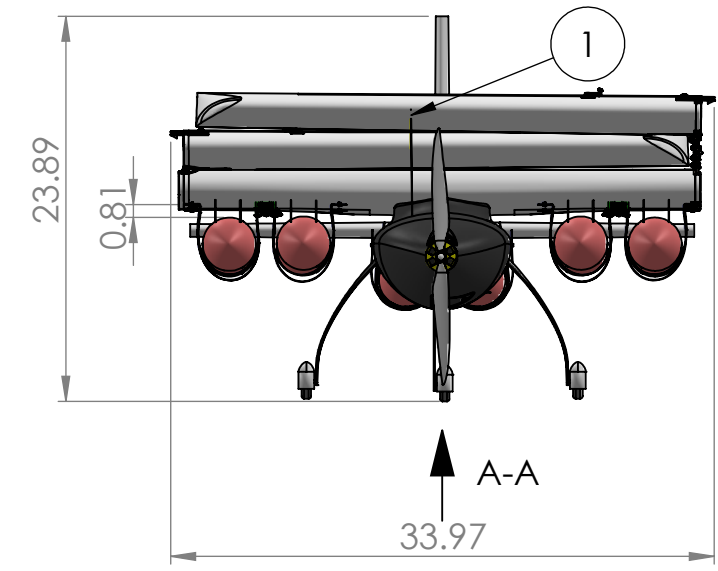
DETAIL B
SCALE 1 : 8



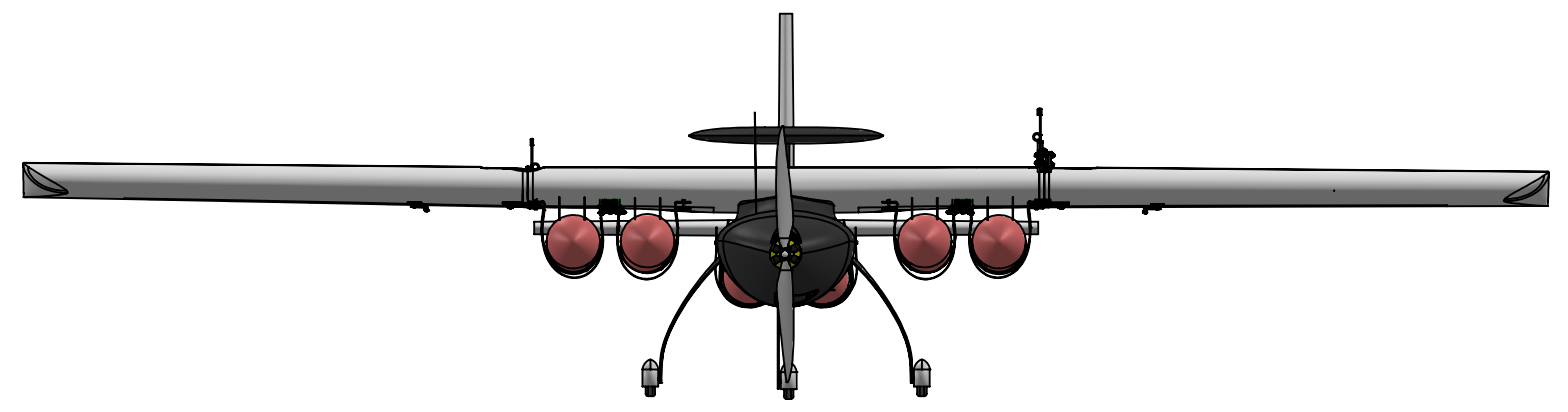
VIEW A-A
90,00°
SCALE 1 : 12

All dimensions are in inches

STORED CONFIGURATION



READY-TO-FLY CONFIGURATION



Item No.	Name	Description	QTY.
1	Kevlar cord	/	1
2	Servo motor	Ready-to-fly mode trigger	1
3	Attack store	Payload	19
4	Radar	Payload	1



Comments:

Drawn by:

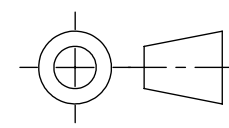
Klemen Mlakar

Payload & stored configuration

TITLE:

PRETTY BOY

Projection: 3rd view



**UNIVERSITY OF LJUBLJANA,
FACULTY OF MECHANICAL
ENGINEERING**

SIZE
B

DWG. NO.
DBF_2019_UL_DWG_04

REV

SCALE: 1:12 WEIGHT: 18.32 lb SHEET 1 OF 1

4

3

2

1

B

B

A

A



6. Manufacturing

Different manufacturing processes were considered for different constructional elements of the plane: **wings, fuselage, tail surfaces, bulkhead and reinforcement ribs, landing gear, radome and mounting mechanisms**. The most suitable process was selected for each individual element. The selection and fabrication of the components is evaluated in this section.

6.1 Manufacturing Processes Investigated

6.1.1 CNC Cutting

Useful for complex parts that require a high degree of precision. Can be used to produce a series of identical parts as well as single precise and complex parts. Simpler parts are made with less time consuming manufacturing processes that require less preparation than CNC machines do.

6.1.2 Composite Material Construction

Composites are a very attractive method of producing aircraft components. While the process is time consuming and expensive, it enables high precision and better strength to weight ratio compared to conventional manufacturing methods. They are also very durable but do not allow much deformation as fiber elongation is relatively poor and breaks instantly under high load.

6.1.3 Foam

Foam creates light structures, can be easily shaped or cut into different shapes and is one of the cheaper building techniques. It is suitable for empennage cores. Nevertheless, foam structures are still heavier and less durable than composites, making them a less attractive method for bigger structures, such as wings with a large volume.

6.1.4 Purenite and MDF Molds

Using negative molds is practical for creating different hollow parts. Purenite and especially MDF are relatively cheap materials that can be easily treated and shaped. They can be effectively used for creating different molds to shape composite structures. The making of the molds depends on CNC cutting, therefore it has similar advantages and disadvantages.

6.1.5 Balsa Build

Building with balsa wood can be more effective than other methods if designed well. A balsa structure can have a lower density than a composite structure leading to lower airplane weight and better performance of the airplane.



Parts have to be designed in a CAD program and cut precisely. High precision cuts are easiest to make with a laser cutter, meaning that a certain operator skill set and proper equipment are required for successful implementation.

6.1.6 3D Printing

The 3D printing technique can be useful for designing complex mechanisms and structures that are too time consuming or practically impossible to create with other techniques. It can be used for prototypes, molds and certain parts where strength is not the main concern, since structures made with 3D printing usually have a bad strength to weight ratio.

6.2 Selection Process

Various techniques listed in the previous section were considered. The final techniques used were selected with regard to the system of Figure of Merits (FOM) where each one is rated with an importance factor, 5 being the highest and 0 the lowest. The selection is shown in Table 25.

Table 25: Manufacturing FOM

Factor	Importance
Cost	5
Experience	2
Ease of Manufacture	3
Strength	3
Weight	2

Cost: Quality was prioritized over the airplane cost. Nevertheless, the budget was limited so the team had to resort to various makeshift equipment.

Experience: Some techniques used were selected based on team member capabilities and their familiarity with manufacturing techniques.

Ease of Manufacture: Since the parts have to be rebuilt more than once, it is important that the technique is easy to implement and can produce parts of good quality and in a satisfactory time frame.

Strength: The strength of materials and consequently the techniques used to produce the strongest structures are important for the structural integrity of the airplane and high strength to mass ratio.

Weight: Manufacturing techniques that produce the lightest possible structures were a priority, since the aircraft weight is one of the key score influencing factors regarding the ability to take off in 10ft.

The comparison of techniques and material according to the system can be seen in Tables 26 and 27 respectively. Both are rated in adequacy from 0 (lowest) to highest (2) and multiplied by the FOM importance factor.



Table 26: Manufacturing Technique Comparison

FoM	Manufacturing Technique			
	Factor Weight	CNC Cutting	3D Printing	Purenite/MDF Molds
Weight	2	2	2	2
Ease of Manufacture	3	1	0	1
Cost	5	1	1	1
Experience	2	2	1	2
Strength	3	2	1	2
Total	/	27	19	27

Table 27: Material Comparison

FoM	Manufacturing Technique			
	Factor Weight	Composites	Foam	Balsa Wood
Weight	2	2	1	1
Ease of Manufacture	3	1	1	2
Cost	5	0	2	1
Experience	2	2	0	1
Strength	3	2	1	1
Total	/	23	16	20

Based on Table 26, the manufacturing techniques were selected for various airplane parts. The most favourable methods were CNC cutting, composites and Purenite molds. The final selection is shown in Table 28.

Table 28: Manufacturing Techniques Used

Part	Manufacturing Technique
Fuselage	CNC milled Purenite molds, carbon and fiberglass composite structures, Herex foam
Wings	Carbon and fiberglass composite structures, Herex foam, CNC milled Purenite/MDF molds
Empennage	Styrofoam, Carbon and fiberglass composite structures
Ribs	Carbon and fiberglass composite structures, Herex foam
Landing Gear	CNC milled Purenite/MDF molds, composite structures
Radome	Laser cutting, composite structures
Attack Store Mechanism	3D Printing, Laser cutting, composite structures



6.3 Manufacturing of Parts

This section describes the detailed manufacturing of the main airplane parts, using techniques selected in previous chapters.

6.3.1 Fuselage

The fuselage mold is milled from two negative halves made of finely ground purenite. Each half is then coated with three layers of epoxy resin. After the epoxy has cured each half is finely sanded until the desired surface quality is achieved. Afterwards, each half is carefully coated with five layers of separating agent and covered with a layer of $0.524 \frac{\text{oz}}{\text{ft}^2}$ carbon fiber, soaked with epoxy resin, and vacuumed for about 15 minutes until epoxy is minimized. After the initial soak, $\frac{1}{16}$ in aramid honeycomb panels are inserted and vacuumed again until the epoxy thickens. The final internal layer consists of $0.262 \frac{\text{oz}}{\text{ft}^2}$ fiberglass twill. The product is then sealed and vacuumed for 24 hours. The bulkhead and reinforcement ribs are attached to one of the halves. The two halves are sealed with epoxy and a carbon sheet. Manufacturing of the fuselage is shown in Figure 37.



Figure 37: Building Composite Structure of the Fuselage Inside the Purenite Molds

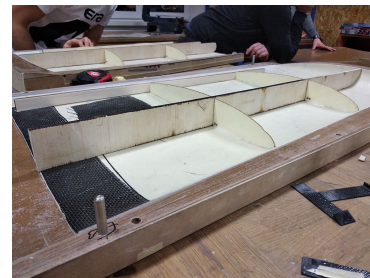


Figure 38: Manufacturing of the Airplane Wings

6.3.2 Wings

The wings are made from three separate molds that are milled from two negative halves made of finely ground purenite. Each one is coated with three layers of epoxy resin and finely sanded until it has sufficient surface quality. Each mold is then prepared in a similar fashion as the fuselage mold. Each wing mold is lined with $0.26 \frac{\text{oz}}{\text{ft}^2}$ fiberglass twill, soaked with epoxy resin, and vacuumed for about 15 minutes until epoxy is minimized. After the first vacuum treatment, herex foam panels are inserted and vacuumed again until the epoxy thickens, followed by the final internal layer of $0.196 \frac{\text{oz}}{\text{ft}^2}$ of fiberglass twill and epoxy. An additional carbon fiber mesh is added to the areas of high stress and vacuumed for 24 hours. In the next step, all of the electronic components and the reinforcement ribs are attached to one of the halves before the two halves are sealed with epoxy resin. The



process is the same for all three molds. The manufacturing of one of the wing molds is shown in Figure 38.

6.3.3 Bulkhead and Reinforcement Ribs

The bulkhead and reinforcement ribs are made with sandwich structure containing $\frac{1}{16}$ in herex foam in the middle with fiberglass layers on both outer sides. Rib placement can be seen in Figure 37.

6.3.4 Empennage

The tail surfaces are made from a Styrofoam core cut into a suitable profile. The back and the front edge are reinforced with 3k roving carbon to protect from impact. The upper and lower areas with greatest thickness are reinforced for additional bending strength. The cumulative surface is covered with one layer of $0.262 \frac{oz}{ft^2}$ fiberglass mesh to enable the tail to withstand torsion loads. Similar to the wings, the tail surfaces are also coated with epoxy resin, hardener and then vacuum tempered at $131^{\circ}F$.

6.3.5 Landing Gear

The landing gear is made in a purenite mold out of 12k carbon fiber roving and carbon fiber mesh. Carbon fiber is covered with resin, placed into the mold and vacuumed in a similar fashion to the wing and fuselage process, but without any honeycomb sandwich structure.

6.4 Manufacturing Milestones

A chart was produced so that all members could efficiently coordinate tasks and that the aircraft prototypes and final design would be built within the required deadlines, as shown in Figure 39.

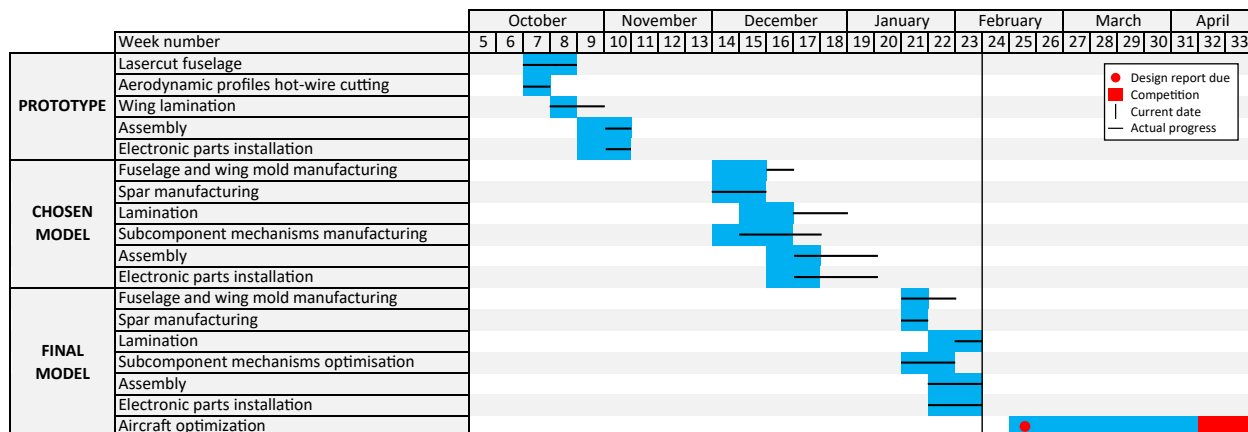


Figure 39: Manufacturing Milestones



7. Testing Plan

A number of tests of key components are necessary to compare theoretical knowledge and predictions to real life situations and to achieve the top scores. Testing enables a quick check for errors in decision making, regarding aerodynamic performance, stability, control and propulsion performance. Detailed and extensive testing objectives were proposed for that purpose.

7.1 Schedule

Testing was divided in to three categories: **subsystem testing**, **testing of prototypes with partial mechanisms**, and **final aircraft testing**. A detailed schedule, seen in Figure 40, was proposed to track errors before they negatively impacted next steps.

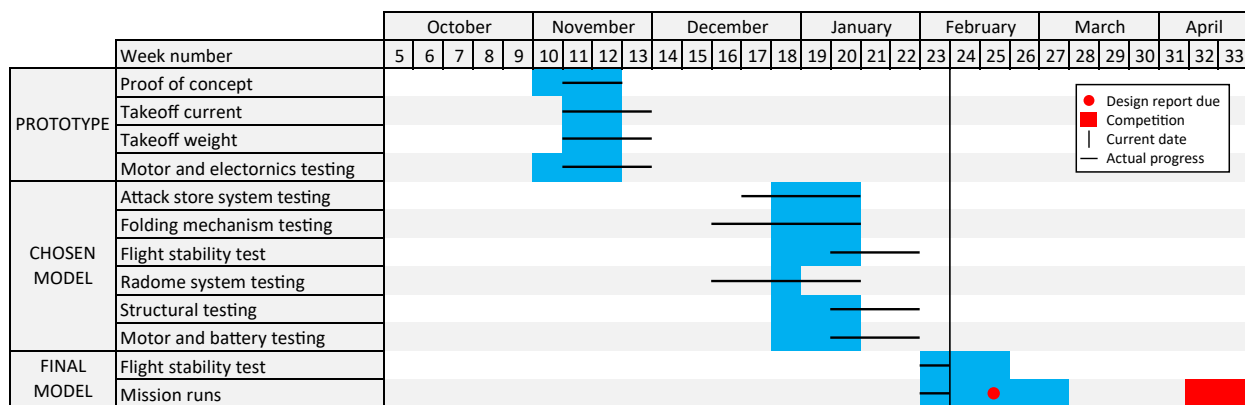


Figure 40: Edvard Rusjan Team Testing Schedule

7.2 Detailed Testing Objectives

The purpose of the initial tests was to improve the accuracy of SAS as seen in Figure 7, later tests served as a validation of proposed changes based on the initial tests. Lab tests and field tests were performed.

7.2.1 Propulsion Testing

The aim was to predict the peak current during takeoff as well as the current during flight. Testing was carried out on the first prototype as it was estimated to be the most power hungry. Peak and flight currents were measured by our on-board measuring system.



7.2.2 Aerodynamics Testing

Attack Store Aerodynamics: To determine the effects of aerodynamic drag of the attack stores attached to the wings and the fuselage we conducted a wind tunnel test. The aim was to understand the relationship that the stores have on the flight dynamics, drag and takeoff distance. Drag force was measured with a Pitot tube at various speeds. Based on the results, the drag factor was obtained and used to calculate the total drag of the aircraft.

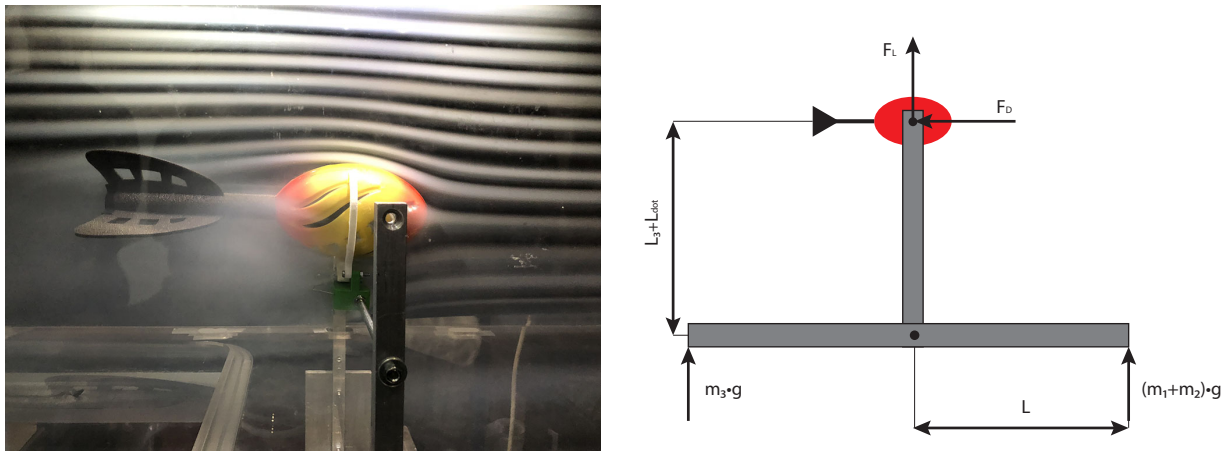


Figure 41: Attack Store During Drag Testing

The final drag was calculated based on Equation 21. Flow speed was measured with a Pitot tube. To produce only the attack store equation we super-positioned the drag of the frame and subtracted the part of the frame that was in direct contact with the flow inside the wind tunnel.

$$\sum M_{i,1} = F_i = (m_3 + m_2 + m_1) \cdot g \cdot L - F_D \cdot (L_3 + L_{dot}) \quad (21)$$

Fuselage Aerodynamics: In addition, the team tested different fuselage configurations mainly due to a high degree of drag from each individual attack store. Testing was done in a wind tunnel in a 1:4 scale to remove any negative effects the wind tunnel walls would have on the final measurements. Each variation was 3D printed and primed to have a similar surface finish to the final fuselage design. Attack stores were also printed in a similar fashion in 1:4 scale. Testing was conducted with three different fuselage designs as seen in Figure 42 with different number of attack stores as seen in Figure 45. Each fuselage was tested at different speeds in the same fashion as individual attack stores.



Fuselage Design 1



Fuselage Design 2



Fuselage Design 3

Figure 42: Different Tested Fuselage variations

7.2.3 Wing Structural Integrity Tests

Structural tests of the wings were conducted to assure the structural integrity of the aircraft during flight missions. The wingtip test was conducted before each flight attempt during flight testing to ensure the aircraft will not collapse during flight and to simulate the wingtip test performed as a part of the technical inspection. The wing was fixed at wing tips and lifted by two members of the team. If the wing did not fold or the mechanism did not partially unlock, the test was considered a success. This test also served to predict the wear and tear on the locking mechanism during the competition as it was performed before each test flight.

7.3 Test Flights

During the initial test flights the main focuses were the general conceptual design of the airplane, takeoff capabilities and flight dynamics with the attack stores and radome attached. The maximum takeoff weight and current draw were determined through these initial tests, as well as the effect of the stores on the top speed of the design and helped determine the proposed fuselage designs in Section 7.2.2. To test the maximum current draw during



Figure 43: Members of the Team During a Wingtip Test

takeoff and during flight, the aircraft was equipped with our custom made on-board measuring system, where all significant data was tracked: air speed, accelerations, GPS positioning, height, current and voltage. The main goal was to determine the required current for takeoff to design the batteries that would be able to sustain top flight speed during Mission 3 and to achieve a top score. Basic aerodynamic characteristics and propulsion system requirement calculated via SAS and AVL were validated and corrected if necessary. Final test flights were performed with the current aircraft design. The main focuses here were to compare the theoretical mission performance from SAS to the real life situation, to validate the selection of the correct propulsion system and check the overall structural integrity of the aircraft as well as its stability. All of the described flight tests and its goals were gathered in Table 29.

7.4 Flight Checklist

The team turned to the pre-flight checklist, seen in Table 30, before each flight, in order to ensure efficient test flights and proper data collection without any major interference. In addition, the pre-flight checklist will serve as the last check up before each flight mission in the upcoming DBF competition.



Table 29: Order and Goals of Performed Test Flights

Flight Test Order	Aircraft	Goal
1	Prototype 1	Propulsion Validation
		Flight Stability
2	Prototype 1	Flaps
		Attack Stores and Radome Positioning
3	Prototype 2	Attack Stores Positioning
		C_l and C_d Validation
		Propulsion Validation
4	Pretty Boy	Propulsion Validation
		Mechanisms In-flight Behaviour
5	Pretty Boy	Mission Runs

Table 30: Pre-Flight Checklist

Pre-flight Check List			
Date:		Plane:	
Time:		Prototype:	
Location:		Battery:	
Wind Speed:		Additional Info:	
Check Each Box After Inspection			
Structural Integrity			
Wing		Control Surfaces	
Receiver Battery		Attack Store Mechanisms	
Wing Folding Mechanisms		Radome Mechanism	
Avionics and Controls			
Transmitter		Controls Test	
Servo Wing		Failsafe	
Fuse			
Final Inspection			
Ground Surface Movement		Mission Restarted	
Ground Crew Clear		Pilot and Spotter Ready	



8. Performance Results

8.1 Aerodynamics

The final drag was calculated based on Equation 21. The flow speed was measured with a Pitot tube. To produce only the attack store equation, the drag of the frame was super-positioned and the part of the frame that was in direct contact with the flow inside the wind tunnel was subtracted. The measured results can be seen in Figure 44.

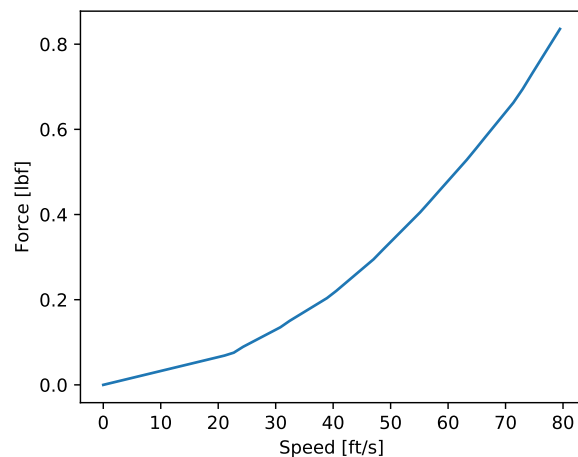


Figure 44: Attack Store Drag

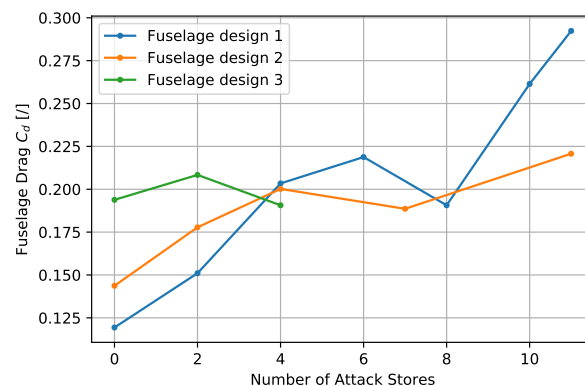


Figure 45: Number of Attack Stores in Relation to Fuselage Drag Coefficient

The drag of the different fuselage designs can be seen in Figure 45. The testing of fuselage design 2 was abandoned, as it was clear that fuselage design 3 had better drag trends.

8.2 Takeoff Testing

The takeoff current was measured as a peak current during the takeoff stage, as shown in Table 31. Measured data was used to design a battery pack capable of producing such current draw as well as capable of sustaining the heat produced during flight. The acronym *BaS* in Table 30 stands for *Barely Successful* and *S* stands for *Successful*.

Table 31: Takeoff Test Results

Test	Takeoff	v_{max} [ft/s]	l_{max} [A]	P_{max} [W]	$l_{takeoff}$ [A]	$P_{takeoff}$ [W]	Flaps [°]	Attack Stores- Wings	Attack Stores- Fuselage
1	BaS	115	105	1900	/	/	/	/	/
2	S	107	95	2083	115	2500	80-ER	2	/
3	S	112	99	2100	118	2440	/	4	/
4	S	102	100	2086	114	2500	/	6	/
5	S	105	97	1840	105	2200	/	8	/
6	S	95	95	1930	100	2000	/	8	2
7	S	88	/	/	/	/	10	8	3



Figure 46: Prototype 2 During Takeoff

8.3 Test Flights

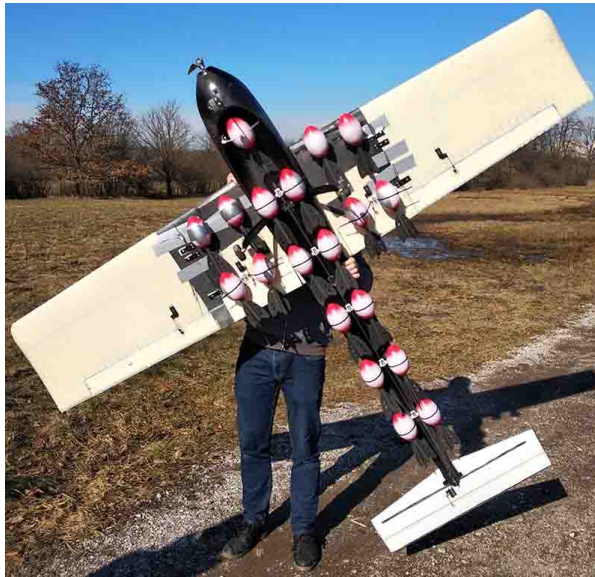
In order to understand the aircraft flight capabilities and increase pilot familiarity with the chosen design, numerous flight test were conducted with a purpose-built Arduino-based data collection system with an SD-card based storage unit on board. In this way the team gained better insights into the flight characteristics, instead of pilot feedback only. During the majority of the tests the system was mounted on the aircraft and recorded GPS data, height, velocity, accelerations, voltage and current.



Table 32: Test Flight Results

Test	v_{avg} [ft/s]	Lap distance [ft]	Average Lap Time [s]
1	91.5	2946	32.2
2	90.7	2945	32.0
3	86.9	2903	33.4
4	80.9	2936	36.3
5	80.8	2940	36.4
6	86.7	2923	33.7
7	79.3	2926	36.9
8	86.3	2978	34.5
9	85.8	2916	34.0
10	82.8	2947	35.6
11	89.6	2933	32.9
12	79.8	2944	36.9
13	79.8	2951	37.0
14	82.6	2923	35.4
15	89.2	2934	32.9
16	84.5	2925	34.6
17	86.1	2927	34.0
18	88.5	2948	33.3

The deviations of results shown in Table 32 can be attributed to several different reasons. The main reason would be human error caused by the pilot, as he had difficulties keeping constant altitude and perfectly straight flights that our mathematical model proposed. It was difficult to keep the radius constant in 360 deg and 180 deg turns, as our mathematical model assumed. Wind speed and temperature could also have a major impact on aircraft performance as aerodynamics in terms of air density [7], angles of attack and number of attack stores are changed. Another reason for the deviation are manufacturing constraints as the total drag was greater than specified in Section 4.4.2. The chosen mounting solutions differed from the one proposed in Section 3.2 which in turn increased the drag forces and power consumption, decreasing the top speed of the aircraft. The results can be improved by minor aerodynamic changes for the final aircraft design as well as with the predicted 10% lower air density in Tucson compared to the test flight area. These conditions led the team to prepare the aircraft to be mounted with 19 attack stores in M3.



Attack Store Configuration



Prototype 2 During Flight

Figure 47: Prototype 2 Design

9. References

- [1] "DBF-Rules-2019, AIAA[online],<http://www.aiaadb.org/Rules/> [retrieved 20 January 2019].
- [2] PythonCoreTeam, *Python: A dynamic open source programming*, Python Software Foundation [online], <https://www.python.org>.
- [3] "Airfoil database", Airfoil tools [online database], <http://airfoiltools.com/> [retrieved 15 October 2017].
- [4] Schlichting, H., "Turbulent boundary layers at zero pressure gradient; flat plate; rotating disk; roughness", *Boundary Layer Theory*, 7th ed., McGraw-Hill, New York, 1979, pp. 635-667.
- [5] Drela, M. and Youngren, H., *Athena Vortex Lattice [Computer software]*, <http://web.mit.edu/drela/Public/web/avl/>.
- [6] Akin, J. E., *Finite Element Analysis Concepts via SolidWorks*, World Scientific Publishing Company, 1st ed., 2010.
- [7] Anderson, Jr., J. D., "Fundamentals of Inviscid Incompressible Flow", *Fundamentals of Aerodynamics*, 5th ed., McGraw-Hill, New York, 2011, pp. 177-276.

BUZZFORMER



AIAA DESIGN/BUILD/FLY
2018-2019
DESIGN REPORT



Georgia Institute
of Technology®



TABLE OF CONTENTS

TABLE OF FIGURES	4
LIST OF TABLES	5
ACRONYMS AND NOMENCLATURE	6
1 EXECUTIVE SUMMARY	7
1.1 DESIGN PROCESS	7
1.2 KEY MISSION REQUIREMENTS AND DESIGN FEATURES	7
1.3 SYSTEM PERFORMANCE CAPABILITIES	8
2 MANAGEMENT	8
2.1 TEAM ORGANIZATION	8
2.2 MILESTONES	9
3 CONCEPTUAL DESIGN	10
3.1 RULE ANALYSIS	10
3.1.1 SCORING ANALYSIS	10
3.1.2 AIRCRAFT REQUIREMENTS FROM RULES	10
3.1.3 FLIGHT MISSIONS	11
3.2 SCORING ANALYSIS	13
3.2.1 FLIGHT MISSION ANALYSIS	13
3.2.2 TRANSLATION INTO DESIGN REQUIREMENTS	14
3.3 CONFIGURATIONS EXPLORED	15
4 PRELIMINARY DESIGN	18
4.1 DESIGN METHODOLOGY	18
4.2 DESIGN TRADES	19
4.2.1 CONSTRAINT SIZING	19
4.2.2 PROPULSION SYSTEM SELECTION	21
4.3 MISSION MODEL	21
4.3.1 DESCRIPTION AND CAPABILITIES	21
4.3.2 UNCERTAINTIES	22
4.4 AERODYNAMIC CHARACTERISTICS	22
4.4.1 AIRFOIL SELECTION	22
4.4.2 LIFTING SURFACE ANALYSIS	24
4.4.3 DRAG ANALYSIS	24
4.5 STABILITY AND CONTROL	26
4.5.1 STATIC STABILITY ANALYSIS	26
4.5.2 DYNAMIC STABILITY ANALYSIS	27
4.6 MISSION PERFORMANCE	28
5 DETAIL DESIGN	28
5.1 FINAL DESIGN – AIRCRAFT	28
5.2 STRUCTURAL CHARACTERISTICS	29
5.2.1 LAYOUT AND DESIGN	29



5.2.2	OPERATING ENVELOPE	29
5.3	SYSTEM AND SUBSYSTEM DESIGN AND IMPLEMENTATION	30
5.3.1	FUSELAGE.....	30
5.3.2	WING	31
5.3.3	MOTOR MOUNT ASSEMBLY	32
5.3.4	EMPENNAGE.....	32
5.3.5	WING LOCKING MECHANISM.....	33
5.3.6	RADOME	35
5.3.7	ATTACK STORE RELEASE MECHANISM	35
5.3.8	RECEIVER AND TRANSMITTER SELECTION.....	36
5.3.9	PROPULSION SYSTEM.....	36
5.4	WEIGHT AND BALANCE	36
5.5	PERFORMANCE	37
5.5.1	FLIGHT PERFORMANCE	37
5.5.2	MISSION PERFORMANCE.....	39
5.6	DRAWING PACKAGE.....	39
6	MANUFACTURING	44
6.1	PROCESSES INVESTIGATED.....	44
6.2	PROCESSES SELECTED	45
6.2.1	AIRFRAME STRUCTURE.....	46
6.2.2	CONTROL SURFACES AND VERTICAL TAIL	46
6.2.3	RAPID PROTOTYPING.....	46
6.3	MANUFACTURING MILESTONES	47
7	TESTING PLAN.....	47
7.1	OBJECTIVES.....	47
7.1.1	PROPULSION TESTING	48
7.1.2	STRUCTURAL TESTING.....	48
7.1.3	SUBSYSTEM TESTING	48
7.1.4	FLIGHT TESTING	49
7.2	SCHEDULE	50
7.3	CHECKLISTS.....	50
8	PERFORMANCE RESULTS.....	51
8.1	COMPONENT AND SUBSYSTEM PERFORMANCE	51
8.1.1	PROPULSION TESTS	51
8.1.2	STRUCTURE TESTS.....	52
8.1.3	SUBSYSTEM TESTS.....	53
8.2	SYSTEM PERFORMANCE	55
9	BIBLIOGRAPHY	59



TABLE OF FIGURES

Figure 1.1. Buzzformer flight test with attack stores.	8
Figure 2.1: Team organization chart.	9
Figure 2.2: Aircraft design milestone chart showing planned and actual progress.	10
Figure 3.1. Diagram depicting the Flight Mission course.	11
Figure 3.2. Combined score sensitivity.	13
Figure 3.3. Four identified design alternatives, clockwise from top right: Conventional, Twin Motor, Delta Wing, and Tandem Wing.	16
Figure 3.4. Three view and isometric view of the selected configuration.	18
Figure 4.1: The team's preliminary design methodology highlighting the multidisciplinary iterations.	19
Figure 4.2. Takeoff trajectory analysis example showing two successful takeoffs and one failed takeoff.	19
Figure 4.3: Constraint sizing and design point selection.	20
Figure 4.4. XFOIL lift and drag characteristics for several airfoils under consideration.	23
Figure 4.5. Wind tunnel test data for SD7062 compared to XFOIL at a Reynolds number of 500,000.	23
Figure 4.6: Model of the aircraft in AVL (left) and the resultant Trefftz plot at C_{Lmax} (right).	24
Figure 4.7: Drag breakdown for M1 (left), M2 (center), and M3 (right).	25
Figure 4.8: Drag polar of the aircraft for the three different missions.	26
Figure 4.9: Simulation of lap trajectories for M1 (left) and M2 (right).	28
Figure 5.1: Load paths of major forces.	29
Figure 5.2: V-n diagram showing loading as a function of velocity for all flight missions.	30
Figure 5.3. Fuselage (left) and holes for fuselage-wing interface (right).	31
Figure 5.4. Shear and bending moment distribution along the semi-span (left), deflection along the semi-span (right).	31
Figure 5.5. The inboard wing gap (left) and combined wing-fuselage (right).	32
Figure 5.6. Motor mount assembly.	32
Figure 5.7. Empennage assembly (left) and the tail hook mounted to the bottom of the center line (right).	33
Figure 5.8. Operation of the wing locking mechanism.	34
Figure 5.9. Wing hinge.	34
Figure 5.10. Locking and Radome Mechanism.	35
Figure 5.11. Single row of six attack stores mounted (left) and attack store release mechanism (right). ...	36
Figure 5.12: CG Location shift during Mission 3.	37
Figure 5.13 . Thrust available and thrust required curves for each flight mission.	38
Figure 5.14. Simulated first lap trajectory (left) and last lap trajectory (right) for M3.	39
Figure 6.1: Aircraft manufacturing milestone chart showing planned and actual timing of third prototype.	47
Figure 7.1 Aircraft testing milestone chart showing planned and actual progress.	50
Figure 7.2 Propulsion and Flight Test checklists.	51



Figure 8.1. Static thrust (left) and power draw (right) predicted by MotoCalc vs tested static thrust and power draw.....	52
Figure 8.2. Wingtip test of fully loaded aircraft.....	53
Figure 8.3. Radome function testing in wind tunnel.....	53
Figure 8.4. Radome function test in flight.....	54
Figure 8.5. Attack store release mechanism testing in wind tunnel (left) and in flight (right).....	54
Figure 8.6. Ground Mission practice.....	55
Figure 8.7. Dimension verification test using a mockup of the box.....	55
Figure 8.8. Ramp takeoff testing.....	56
Figure 8.9. Recorded flight path of a single competition lap.....	56
Figure 8.10. Simulated vs. flight test lap trajectories for M2 (left) and M3 (right).....	57
Figure 8.11. Buzzformer in Mission 3 configuration.....	58

LIST OF TABLES

Table 3.1. Flight Mission 1 scoring.....	12
Table 3.2. Flight Mission 2 scoring.....	12
Table 3.3. Flight Mission 3 scoring.....	12
Table 3.4. Ground Mission scoring.....	13
Table 3.5. Scoring targets for Buzzformer.....	14
Table 3.6. Figures of merit and their respective weights.....	15
Table 3.7. Matrix of alternatives for Buzzformer configuration selection.....	16
Table 3.8. Weighted Pugh matrix for Buzzformer configuration selection.....	17
Table 4.1. Parameters used in empty weight estimation.....	20
Table 4.2. Preliminary constraint sizing results.....	21
Table 4.3. Propulsion systems considered for MotoCalc analysis.....	21
Table 4.4. Breakdown of various sources of drag.....	25
Table 4.5. Relevant stability coefficients and derivatives for static stability.....	27
Table 4.6. Dynamic stability characteristics.....	27
Table 5.1. Final aircraft dimensions.....	28
Table 5.2. Selected propulsion and electronics components.....	36
Table 5.3. Weight and balance for Buzzformer.....	37
Table 5.4. Aircraft flight performance parameters for each mission.....	38
Table 6.1. Manufacturing FOM weighting.....	44
Table 6.2. Example manufacturing process selection.....	45
Table 8.1. Predicted vs. flight test performance results.....	57



ACRONYMS AND NOMENCLATURE

N_{laps}	– Number of Laps flown	n	– Load Factor
$S_{wet,w}$	– Wetted Area of the Wing	AR	– Aspect Ratio
g_0	– Gravitational Acceleration	Re	– Reynolds Number
t/c	– Thickness to Chord Ratio	\dot{V}	– Velocity Derivative with respect to time
AVL	– Athena Vortex-Lattice	T	– Thrust
C.G.	– Center of Gravity	m	– Mass
C_D	– Aircraft Drag Coefficient	<i>Time</i>	– Flight Time
$C_{D,0}$	– Aircraft Zero-Lift Drag Coefficient	MTOW	– Maximum Takeoff Weight
C_{fw}	– Turbulent Plate Friction Coefficient of the Wing	ρ	– Density
C_L	– Aircraft Lift Coefficient	R_{wf}	– Wing Fuselage Interference Factor
C_l	– Aircraft Rolling Moment Coefficient	$\dot{\psi}$	– Time Derivative of Heading
C_m	– Aircraft Pitching Moment Coefficient	K_1	– Drag Constant
C_n	– Aircraft Yawing Moment Coefficient	R_{LS}	– Lifting Surface Correction
ESC	– Electronic Speed Control	β	– Sideslip Angle (degrees)
EW	– Empty Weight	α	– Angle of Attack (degrees)
FOM	– Figures of Merit	W	– Weight (lb)
L'	– Airfoil Thickness Location Factor	e	– Oswald Efficiency
M1	– Mission One	S	– Reference Area (ft ²)
M2	– Mission Two	V	– Velocity(ft/s)
M3	– Mission Three	MTOW	– Maximum Takeoff Weight
NiCad	– Nickel-Cadmium	P	– Power
NiMH	– Nickel-Metal Hydride	V_{TO}	– Takeoff Speed
TMS	– Total Mission Score	\dot{x}	– Position Derivative with respect to time
T_R	– Thrust Required	D	– Drag
		η	– Efficiency



1 EXECUTIVE SUMMARY

This report details the design, testing, and manufacturing of the Georgia Institute of Technology's entry in the 2018-2019 AIAA Design/Build/Fly (DBF) competition, *Buzzformer*. This aircraft was designed to complete the four missions described by the rules: a ground flight deck operations and maintenance mission and three flight missions. The first flight is a delivery mission with no payload. The second mission is a reconnaissance mission flown with a radome attached to the aircraft. The third mission is an attack mission during which the aircraft must takeoff with and release externally attached attack stores every lap. For all flight missions, the aircraft must enter the staging area in a stowed configuration and be remotely commanded to reconfigure into the flight configuration. All takeoffs are from a ten foot ramp with the aircraft restrained by the ground crew member by a tail hook.

1.1 Design Process

The development of a light, fast aircraft that maximizes the flight score is key to the success of *Buzzformer*. Conceptual design of a competitive aircraft began with development of aircraft requirements through analysis of key mission requirements and scoring criteria. These design requirements were used to select the best aircraft configuration. During the preliminary design phase, the aircraft dimensions and propulsion system were sized using constraint analysis of critical flight phases. Weight, drag, and aerodynamic characteristics were also estimated along with stability and a model for mission performance simulation which includes a takeoff simulation and a lap trajectory estimation. The team used the preliminary design to estimate the aircraft performance and scoring potential. The detail design was eventually completed finalizing all dimensions, propulsion system components, and all subsystems including the radome mechanism, the wing locking mechanism, and the attack store release mechanisms.

1.2 Key Mission Requirements and Design Features

A thorough understanding of mission requirements and the scoring method is crucial to maximizing the flight score. Specific design requirements were identified after analysis of the competition rules which guide subsequent design of the aircraft.

Empty Weight: The aircraft empty weight including structure, propulsion system, and all subsystems has a significant effect on performance. The aircraft is designed to be as light as possible while still being able to complete all missions. This is done through selective use of materials and efficient structure design.

Takeoff: Since all flight missions must begin with taking off from the ramp, it is important that the aircraft can complete a successful takeoff for each of its three configurations. Successful short takeoffs are achieved through a combination of high thrust to weight ratio and low wing loading.

Attack Store Capacity: Mission 3 is the primary driver in overall flight score with a much larger contribution than any other mission. The aircraft must carry as many attack stores as possible with minimal additional weight and drag for the payload release mechanisms in order to maximize Mission 3 score. The team aims to carry 18 payloads for Mission 3.

Speed and Range: Completing a lap as fast as possible is important for both Mission 2 and Mission 3. Mission 2 depends directly on the completion time while Mission 3 score is maximized by completing as



many laps as possible in the prescribed time limit which involves both fast lap times as well as range. The team has determined that both high cruise speed and fast turn rates are important to achieve fast lap times. Fast cruise speeds are achieved through increasing power while minimizing drag. Fast turn rates subject the aircraft structure to a high load factor. The aircraft must also have a large enough battery to carry the required energy to maximize the number of laps flown in Mission 3.

1.3 System Performance Capabilities

The design requirements and goals to maximize the performance of the aircraft system can be summarized by the performance capabilities:

- Empty Weight of 6.38 lb
- Reliable takeoff from the ramp
- Estimated ~33 second lap time for Mission 3
- Up to 18 attack store capacity
- Wing locking by remote command
- Reliable commanded attack store release in flight
- Commanded start and stop of radome rotation in flight
- Ground Mission completion in 34 seconds



Figure 1.1. Buzzformer flight test with attack stores.

The final design is a conventional monoplane with a single motor and tricycle gear. The propulsion system is designed to have enough power to meet the ambitious takeoff and high speed cruise targets. The aircraft structure, especially the wing locking mechanism, is designed to sustain a high load factor to aggressively maneuver and reduce lap times. The team has completed numerous successful flight tests of three different prototype iterations and is continuing to improve the aircraft by reducing empty weight and drag based on pilot feedback and results from flight testing.

2 MANAGEMENT

2.1 Team Organization

A hierarchical structure was used in the completion of the Buzzformer with leadership established amongst senior members and flowing down to the junior members of the team as shown in Figure 2.1: Team organization chart.

. This large-scale project was divided up into five components: Manufacturing, Computer Aided Design (CAD) and Structure, Aerodynamics, Electrical and Propulsion, and Subsystems. During the design, construction, and testing phase, each member contributed extensively to the rapid prototyping process to construct the planes, meet deadlines, share new ideas, and write the report. Although this was the general management structure, team members moved between different areas throughout the design and manufacturing process based on need at the time and each member's previous experience.

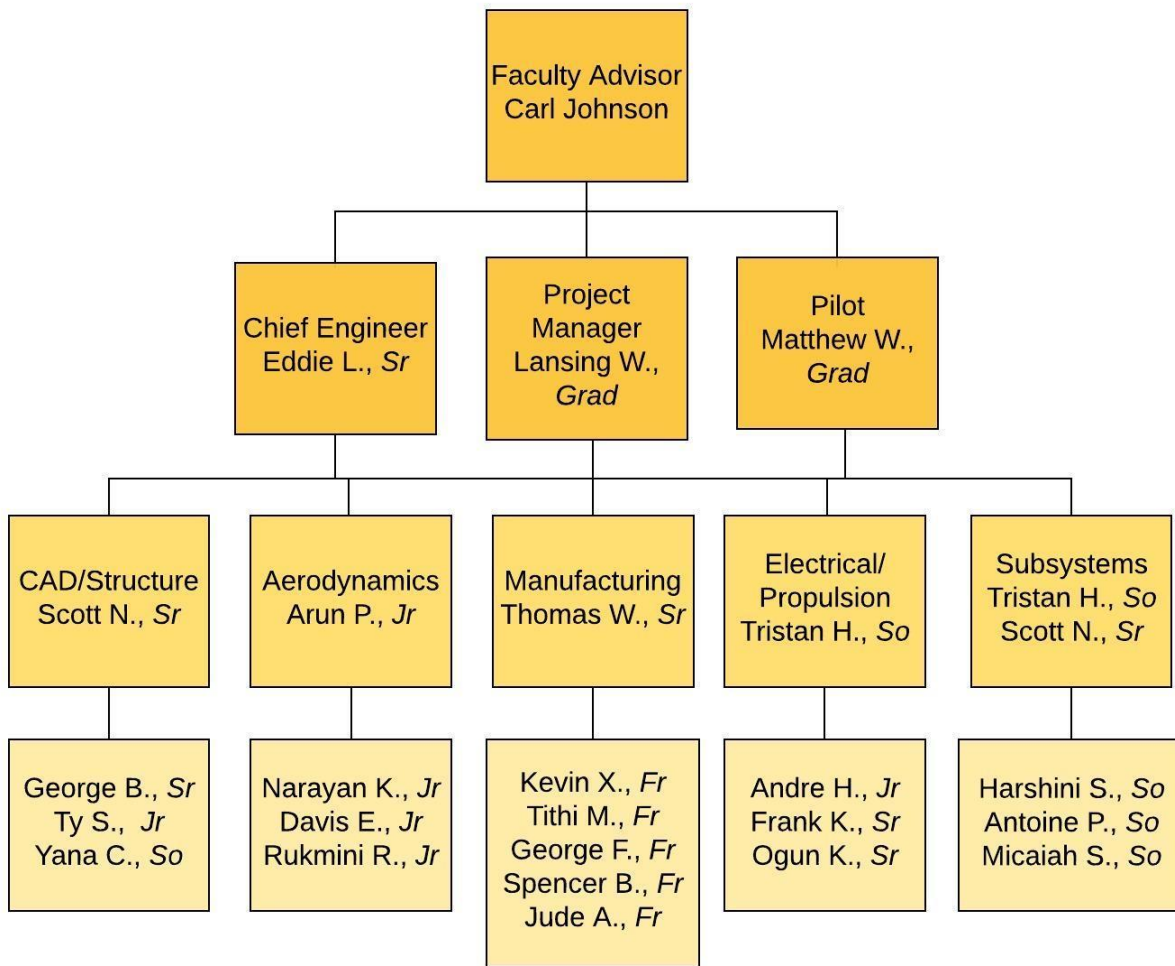


Figure 2.1: Team organization chart.

2.2 Milestones

A schedule was established at the beginning of the design process to capture major deadlines of design and manufacturing goals. Progress was monitored by the project manager to ensure all major milestones were met. The team worked throughout the entire academic year and established stringent deadlines early to ensure testing and flight experience before the competition in April. The team met frequently with the faculty advisor to discuss progress. Parallel development was a key part of the process and allowed the team to more efficiently use members to design, manufacture and test multiple systems on the aircraft at once. A Gantt chart representing important milestones is shown in Figure 2.2.

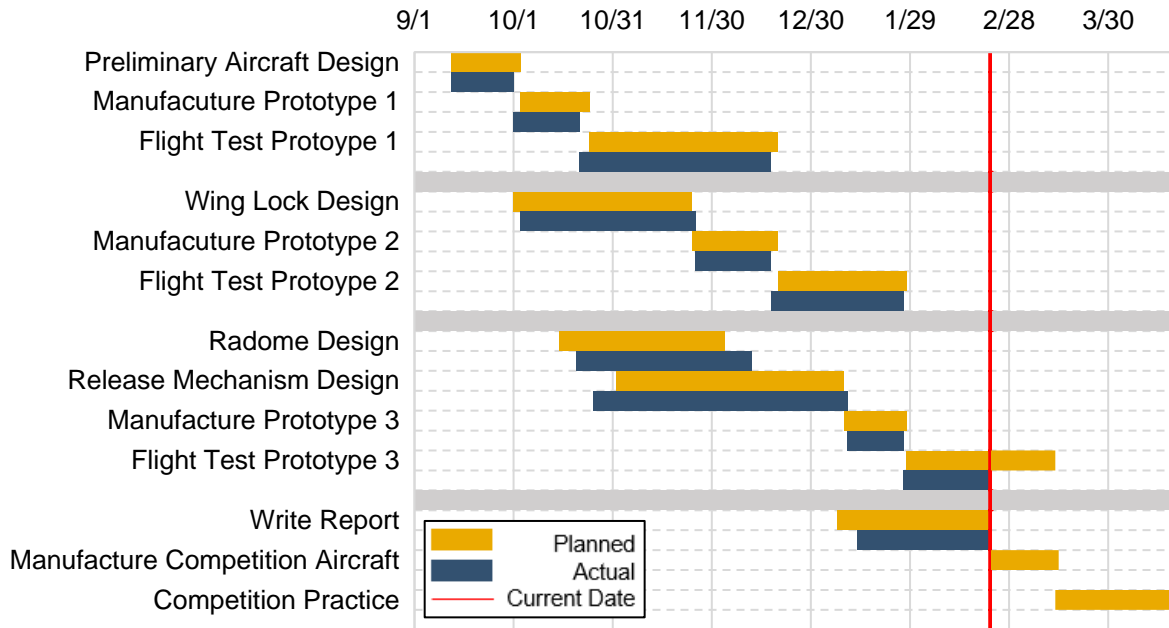


Figure 2.2: Aircraft design milestone chart showing planned and actual progress.

3 CONCEPTUAL DESIGN

In the early phase of design, the team analyzed the competition rules to identify a flight configuration that maximized potential flight score. These rules were translated into design requirements and scoring factors which in turn were translated into Figures of Merit (FOM) that were used to evaluate design choices. The FOM were applied to the design alternatives—four particularly competitive designs—to produce the chosen aircraft configuration.

3.1 Rule Analysis

3.1.1 Scoring Analysis

The AIAA Design/Build/Fly 2018-2019 competition consists of three flight missions, a ground mission, and a design report. The total score for each team is calculated as:

$$SCORE = \text{Written Report Score} \times \text{Total Mission Score}$$

Where the Total Mission Score (TMS) is:

$$TMS = \text{Mission 1 Score} + \text{Mission 2 Score} + \text{Mission 3 Score} + \text{Ground Mission Score}$$

3.1.2 Aircraft Requirements from Rules

The competition rules stipulate specific requirements on the aircraft dimensions, takeoff distance, payload, and propulsion system.

Reconfigurable Aircraft: The aircraft must have a minimum wingspan of 4 feet. It must also have a stowed configuration that rolls through a 3 foot wide and 2 foot high box without interference with the box before being remotely commanded to the flight configuration. Additionally, the nose of the aircraft and all landing gear must fit in the box within a depth of 2 feet.



Takeoff Distance: The aircraft must takeoff from a 4 foot wide and 10 foot long launch ramp at a launch angle of approximately 5 degrees, starting with the landing gear beginning wholly on the ramp.

Radome: The radome must be at least 12 inches in diameter and 1 inch thick in the center. It must be mounted on the aircraft centerline with at least 3 inches clearance between any part of the radome and any surface of the aircraft, mounting structure excepted. It must begin rotating in a manner distinguishable to the flight line judges after the first 180° turn and stop rotating in the same manner after the final 180° turn.

Attack Stores: The aircraft must carry at least four stores of which the first four must be mounted under the wings. Subsequent stores may be mounted under the wings or the fuselage. Stores are 12 inches long, 3.32 inches in maximum diameter, and 2.25 ounces in weight. There must be at least a 0.5 inch clearance between stores as well as any part of the aircraft, mounting structure excepted. All stores must be capable of individual and independent detachment.

Propulsion System: The aircraft must be propeller driven and electrically powered with commercially available components. These include the motor, propeller, speed controllers, receivers, and batteries. The battery selection is limited to NiCad or NiMH, but may be of any cell count, voltage, or capacity. There is no limit on the weight of the battery packs. The entire propulsion system must be armed by an external safety plug or fuse. The safety plug or fuse must be mounted on the exterior of the aircraft and be accessible from behind in a tractor propeller configuration.

3.1.3 Flight Missions

All flight missions begin with the aircraft in the stowed configuration before being remotely commanded to the flight configuration. A diagram and description of a single lap can be seen in Figure 3.1.

1. Takeoff from ramp
2. Climb to safe altitude
3. 180° turn 500 ft. Upwind from the Finish Line
4. 1000 ft. downwind leg
5. 360° turn during the downwind leg
6. 180° turn
7. 500 ft. Final with a successful landing

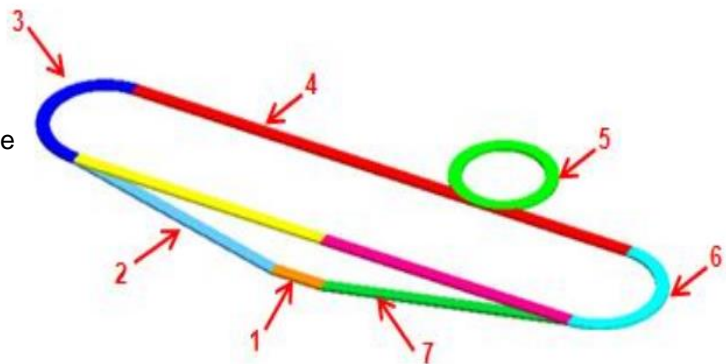


Figure 3.1. Diagram depicting the Flight Mission course.

A complete lap is defined as crossing the finish line, completing the defined pattern, and then crossing the finish line while still in the air.

Mission 1 (Delivery Mission): The aircraft, without payload, must take off from the ramp and complete three laps within a five-minute flight window. Time begins once the aircraft is released by the flight line crew



member for the first take off and ends once the aircraft passes over the finish line in the air at the end of the third lap. The scoring formula appears in Table 3.1.

Table 3.1. Flight Mission 1 scoring.

Mission	Description	Score
M1	Aircraft completes the mission with a successful landing	1.0
	Aircraft does not attempt or complete a successful flight	0.0

Mission 2 (Reconnaissance Mission): The aircraft must carry a radome, take off from the ramp, and complete three laps within a five minute flight window. The mission score is a function of the time to complete the laps, not including the landing. The scoring formula appears in Table 3.2.

Table 3.2. Flight Mission 2 scoring.

Mission	Description	Score
M2	Aircraft completes the mission with a successful landing	$1.0 + \frac{\text{Flight Time}_{\text{fastest, all teams}}}{\text{Flight Time}_{\text{Buzzformer}}}$
	Aircraft does not attempt or complete a successful flight	0.0

Mission 3 (Attack Mission): The aircraft must carry attack stores, take off from the ramp, and complete laps within a ten minute window. To count as a scoring lap, exactly one store must be dropped remotely within the downwind leg of the pattern. The landing does not have to be completed within the prescribe time limit for Mission 3. The scoring formula appears in Table 3.3.

Table 3.3. Flight Mission 3 scoring.

Mission	Description	Score
M3	Aircraft completes the mission with a successful landing	2.0 + Number of scoring laps
	Aircraft does not attempt or complete a successful flight	0.0

Ground Mission (Flight Deck Ops and Maintenance): The radome and attack stores must be installed in a timed ground mission. The time will start with the aircraft in the stowed configuration along with the uninstalled radome and four attack stores and must be remotely commanded to the flight configuration prior to installation of the radome, at which point time will stop for a demonstration of the remote activation of the rotating radome. Then, time will start again for the removal of the radome and installation of four attack stores. Time will stop once more for a demonstration of flight controls and propulsion systems prior to the aircraft being disarmed, before a final demonstration of stores being released one at a time. The scoring formula appear in Table 3.4.



Table 3.4. Ground Mission scoring.

Mission	Description	Score
GM	Aircraft completes the mission	$\frac{\text{Time}_{\text{fastest, all teams}}}{\text{Time}_{\text{Buzzformer}}}$
	Aircraft does not attempt or complete the mission	0.0

3.2 Scoring Analysis

Sensitivity analysis on the flight scoring function was performed to determine the design parameters and mission objectives that maximize the total mission score. Each mission score was analyzed individually to determine the most important design drivers. The individual analysis was then combined into an overall scoring analysis. The scoring sensitivity allowed the team to identify aircraft design requirements that would maximize the overall scoring potential of the aircraft.

3.2.1 Flight Mission Analysis

Scoring for Mission 1 is invariant because the team will always receive 1 point for a successful mission. The Ground Mission does depend on assembly time, but this does not affect conceptual design of the aircraft. Therefore, Mission 2 and Mission 3 were treated as the primary drivers of flight score.

Mission 2 score improves with *Buzzformer's* completion time, which reduces with faster flight speed. Mission 3 score is increased by completing more laps within the prescribed ten minute window, which improves with the combination of more stores dropped and more laps flown within the window. Flight speed directly improves Mission 2 score while allowing for more laps to be flown in Mission 3. As such, a combined Mission 2 and 3 analysis was performed to determine the scoring sensitivity of increasing flight speed. This analysis, shown in Figure 3.2, makes several assumptions: the aircraft flies the full ten minutes in Mission 3, laps are 2500 feet in length, and 0.3 points are earned in the Ground Mission.

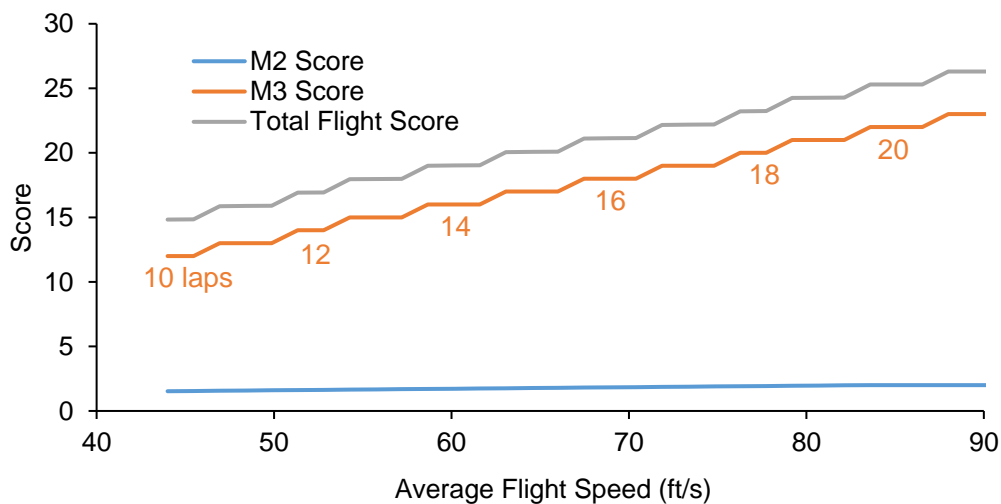


Figure 3.2. Combined score sensitivity.



Total flight score increases linearly with flight speed but in discrete steps corresponding to completion of an additional lap. Flying 10 feet per second faster improves flight score by approximately 2 points, of which 95% comes from an improvement in Mission 3 score because two more payloads are dropped. Additionally, at all speeds, approximately 85% of the total Flight Score comes from the Mission 3 score. Mission 3 is not only the largest contributor to total Flight Score, but also where most of the improvement in score can be made. As a result, Mission 3 scoring laps were treated as the primary scoring driver.

3.2.2 Translation into Design Requirements

A preliminary target of 18 scoring laps was set based on Mission 3 being the most important scoring factor. Additionally, estimates were made for *Buzzformer's* Mission 2 time and Ground Mission time to produce a baseline scoring target shown in Table 3.5.

Table 3.5. Scoring targets for Buzzformer.

Mission 2 Target Time (s)	100
Mission 3 Target Scoring Laps	18
Ground Mission Target Time (s)	50
Baseline Scoring Target	23

These targets imply the following requirements on attack store capacity and flight speed:

Attack Store Capacity: The aircraft must be able to carry 18 attack stores, of which four must mount underneath the wing. It would be simpler to carry stores with a larger wing area, although that is not necessary if payloads are mounted in a longitudinal row that is then attached to the wing. As such, this does not apply a constraint on configuration selection and so was not a driving factor in conceptual design.

Flight Speed: The aircraft must be able to fly the targeted 18 laps within a ten minute window, amounting to an average speed of 75 feet per second. To achieve this, the aircraft must have a high cruise velocity, which is primarily a function of power available and drag. Additionally, the aircraft must complete turns as fast as possible. As such, the aircraft structure and payload mounting mechanism be designed to withstand these aggressive maneuvers.

In addition, several additional requirements greatly impact configuration selection and aircraft design:

Takeoff: The takeoff roll is reduced with either increasing power to weight ratio or decreasing wing loading. The advantages of lower wing loading for takeoff trades with cruise speed because faster cruise speeds are achievable with higher wing loadings. In addition, static thrust for takeoff is maximized with a low-pitch propeller while high-speed thrust is maximized with a high-pitch propeller, a tradeoff explored further in Section 4.2.2.

Reconfigurable wing: The combination of a 4 foot minimum wingspan and a 3 foot maximum width when in the stowed configuration requires a folding, telescoping, or swinging wing. A single joint folding wing emerged as the most reasonable solution in terms of subsystem complexity and weight. For a wing



that meets the 3 foot wingspan constraint when stowed, a single folding joint on each side allows for a maximum wingspan of 6 feet in flight.

Radome: The radome must be designed to meet the rotation and visibility requirements and must not interfere with other subsystems, especially the attack store release mechanism. Placing the radome on top of the aircraft emerged as a reasonable solution.

3.3 Configurations Explored

The mission requirements and constraints translated to six figures of merit that were used to assess the design alternatives. A weight of five meant the figure of merit was the most important to consider in configuration selection, whereas a one was the least important. These figures appear in Table 3.6.

Table 3.6. Figures of merit and their respective weights.

Figure of Merit	Weight
Drag	5
Weight	4
Simplicity	3
Stability	2
Payload Integration	1
Wing Lock Complexity	1

Low drag received the maximum weight of five because it is essential to improve flight speed, which must be maximized to improve Mission 3 score. Low weight received a weight of four because it would assist in takeoff and range while not adversely affecting flight speed, unlike the alternative option of increasing wing area. Increased simplicity in design received a weight of three because it would assist in the manufacturing process. Increased stability received a weight of two because it would assist the pilot but would not directly increase flight score. Finally, payload integration and wing lock complexity both received a weight of one because both could be designed around the selected configuration with minimal impact to aircraft performance.

A matrix of alternatives was developed to identify potential configurations seen in Table 3.7. The components considered include the wing, empennage, motor, fuselage, wing reconfiguration mechanism, and payload attachment. Due to the distance limit between the rear landing gear and the nose of the aircraft, the option for a tail dragger landing gear configuration was not considered and the team only considered a conventional tricycle gear layout with wheels.



Table 3.7. Matrix of alternatives for Buzzformer configuration selection.

Component	Configuration Options				
Wing	Straight	Swept	Clipped Delta	Biplane	Tandem/Canard
Empennage	Conventional	H-Tail	T-Tail	V-Tail	Cruciform
Motor	Single Puller	Single Pusher	Twin Puller	Puller-Pusher	
Fuselage	Tubular	Dual	Blended		
Wing Locking Mechanism	Folding Wing	Swinging Wing	Telescoping Wing		
Payload Attachment	Span-wise Distributed	Double Row Pylon	Triple Row Pylon		

Four design alternatives were generated by selecting combinations of configuration options that were compatible with each other, shown in Figure 3.3. The first design is a conventional design with a single motor, straight wings, and conventional tail attached to a simple fuselage. The wings have outer sections that fold above the inboard section, and payloads attach to three pylons carried underneath the wing. The second design is a twin motor with each motor mounted onto each outboard pylon, and an H-tail. The third design is a clipped delta wing with sharp leading edges to produce vortex lift. Two vertical tails attach onto the rear of the wing planform itself without a need for tail booms. The fourth alternative is a tandem wing design with two wings and a cruciform tail attached to a simple fuselage.

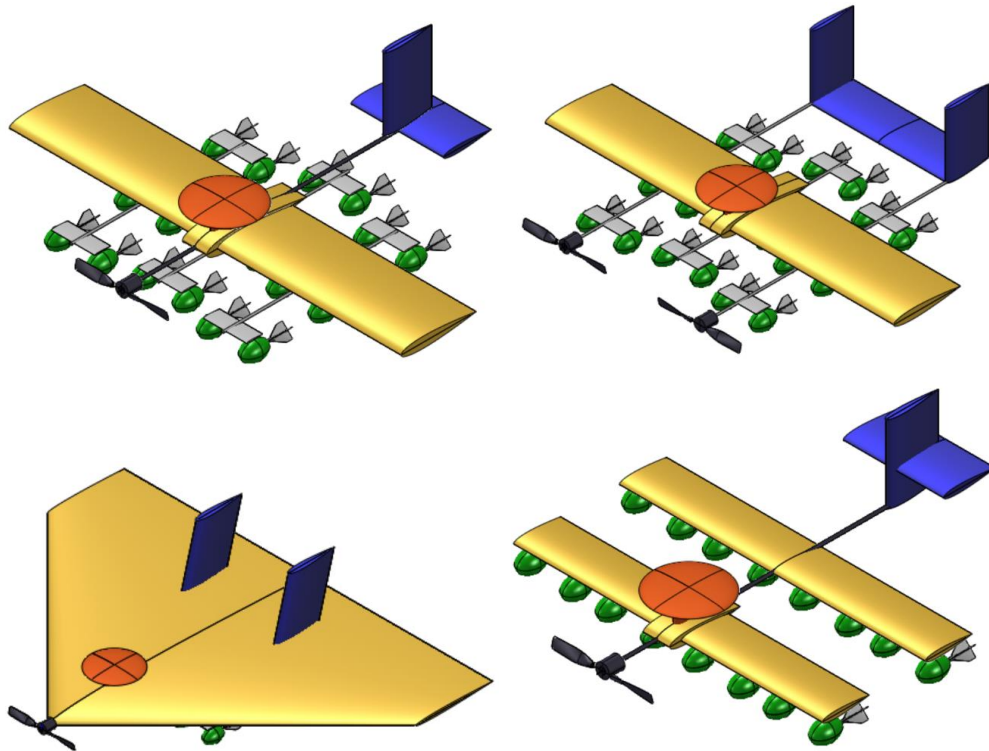


Figure 3.3. Four identified design alternatives, clockwise from top right: Conventional, Tandem Wing, Delta Wing, and Twin Motor.



The performance of each configuration with respect to the FOMs were evaluated from a scale of 1 to 3, with 3 being most effective, in the weighted Pugh Matrix shown in Table 3.8. The weighted scores were summed for each configuration to determine the best design.

The conventional single motor design featured low drag and weight with good stability due to the tail control surfaces far from the center of gravity. In addition, it would be the simplest design and one the team has experience building.

The twin motor design is slightly heavier than the conventional design, due to requiring thicker outboard rods to accommodate the load of the attack stores and the motors. Additionally, the two smaller motors required here would be slightly heavier than a single larger motor in the conventional design. Finally, mounting two motors to pylons would add complexity over the conventional design.

The clipped delta design would help in meeting the short takeoff requirement, as delta wing aircraft require very little time to trap vortices on the wing's upper surface to produce lift, and so could be relied on to take off from a ten foot ramp. Additionally, at high speed a delta wing would have the least drag of any similarly sized aircraft due to its short wingspan. While this design would be structurally more complex than a conventional design, the team has constructed and placed well with such a design in the past. However, a wing folding mechanism would be more difficult to design with wing sweep and a sharp leading edge. Moreover, the tail is closer to the center of gravity which negatively affects stability, and the payloads would not fit anywhere without affecting vortex formation and lift.

The tandem wing design allows all attack stores to mount span-wise without need of a pylon, and its stability would be similar to a conventional design. On the other hand, the extra wing area and wing-fuselage interfaces increases drag from interference and increased wetted area, as well as making manufacturing more complex. Moreover, a wing locking mechanism would be more complicated with two wings.

Table 3.8. Weighted Pugh matrix for Buzzformer configuration selection.

FOM	Weight	Conventional	Twin Motor	Clipped Delta	Tandem
Drag	2	2	3	1	2
Weight	3	3	3	1	3
Simplicity	3	2	2	1	3
Stability	3	3	1	3	3
Payload Integration	2	2	1	3	2
Wing Reconfiguration	3	3	2	1	3
TOTAL		42	39	38	22

Based on the results of the weighted Pugh matrix, the conventional design was selected as the final configuration for this year's competition aircraft. A three-view and isometric sketch of this design appears in Figure 3.4. Attack stores are carried underneath the wing and the radome above the wing.

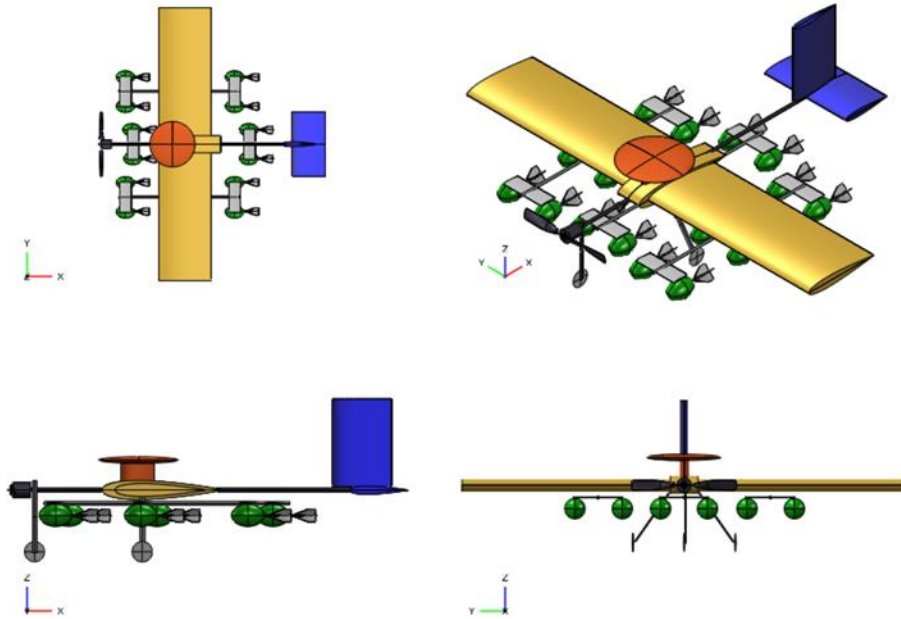


Figure 3.4. Three view and isometric view of the selected configuration.

4 PRELIMINARY DESIGN

Once the configuration was chosen during the conceptual design phase, the preliminary design phase aims to narrow the design space. Trade studies of the wing area and propulsion system were performed to identify a design point that meets the aircraft requirements identified during the preliminary design phase. Weight, drag, power, propeller performance, battery data, and aerodynamic coefficients were estimated and combined to estimate mission performance for all three flight missions.

4.1 Design Methodology

The team approached the design process with an iterative, performance-focused, multidisciplinary analysis. Power based constraint sizing was performed to select a weight-normalized design point that satisfies objectives for all three missions. From the chosen design point, the team analyzed possible propulsion systems, evaluated aerodynamic characteristics, built mission models, and compared them to estimates generated as part of the sizing process. Stability and mission performance calculations were made using these more detailed models. Georgia Tech's iterative preliminary design methodology, shown in Figure 4.1, details the process through which the design is narrowed resulting in the detailed design. An example of the iteration process is modifying the wing area at constant wing-loading if propulsion weight is lower than expected, re-evaluating stability and mission performance, or modifying the propulsion system to meet pilot requests. The design shown in this report is the final product of a more complex, iterative procedure that seeks to maximize the overall score at every stage.

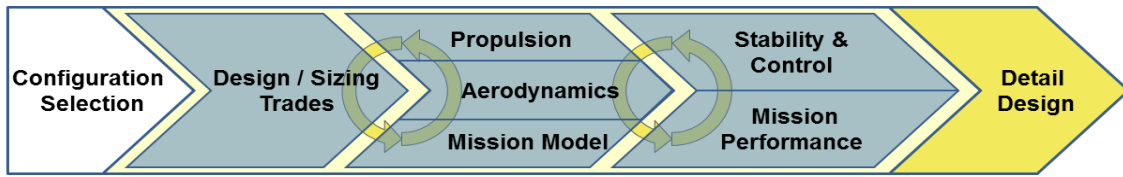


Figure 4.1: The team's preliminary design methodology highlighting the multidisciplinary iterations.

4.2 Design Trades

4.2.1 Constraint Sizing

A constraint sizing study allows the team to analyze the impact of changing wing area, weight, and power on aircraft performance. The two important constraints to consider are takeoff from the 10 foot ramp and cruise speed for maximizing the flight score for M3. The average airspeed required to complete Mission 3 based on the number of attack stores carried is calculated by determining the total distance travelled using a 2500 foot per lap estimation and dividing by the ten minutes allotted.

Takeoff analysis was performed using a physics simulation in MATLAB. Forces acting on the aircraft are calculated in the ground-fixed frame. The forces considered include lift, drag, thrust, gravity, and the ground roll friction when the aircraft is on the ramp. The summation of components of each force in the horizontal and vertical directions are used to calculate the aircraft acceleration and the result is numerically integrated over time. It is important to consider that the aircraft does not necessarily need to reach its stall speed at the end of the ramp for a successful takeoff. As the aircraft rolls off the end of the ramp, it will start accelerating towards the ground however it has vertical velocity as well as some amount of lift already. As long as the aircraft is able to accelerate to its stall speed before hitting the ground, the takeoff is successful. As a result, the simulation constrains the aircraft trajectory to the ramp geometry while it is on the ramp and allows the aircraft to freely accelerate in any direction after the end of the ramp. A takeoff attempt is considered successful when the aircraft has both positive upwards force and velocity and it does not hit the ground. An example of takeoff analysis for an aircraft with the same thrust to weight ratio and wing loading but different lift coefficients is shown in Figure 4.2.

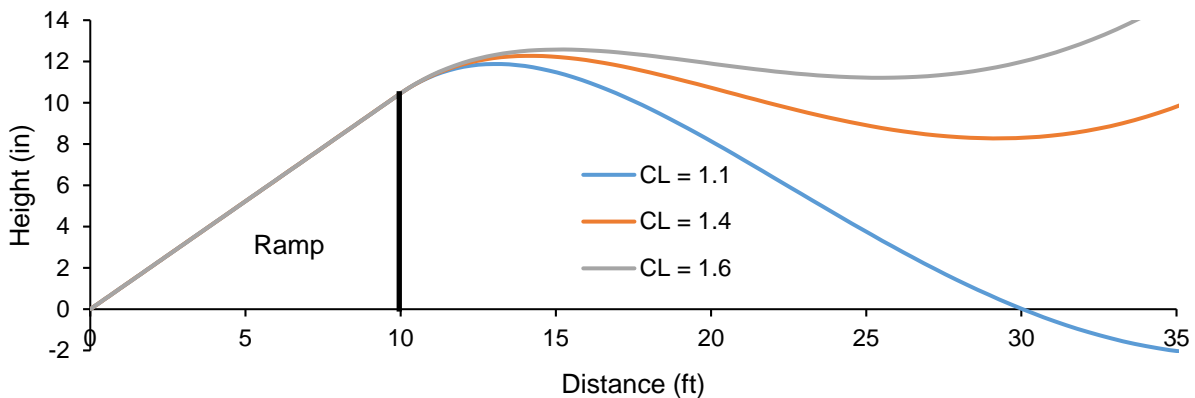


Figure 4.2. Takeoff trajectory analysis example showing two successful takeoffs and one failed takeoff.



Figure 4.3 shows the results of the constraint analysis. A design point was selected for flying 18 laps during Mission 3 and a C_L of 1.4 for the aircraft based on what is achievable from past experience. The design point was picked to have an amount of margin over the cruise power constraint and an even larger margin for the takeoff constraint since the takeoff performance is sensitive to changes in air density and wind.

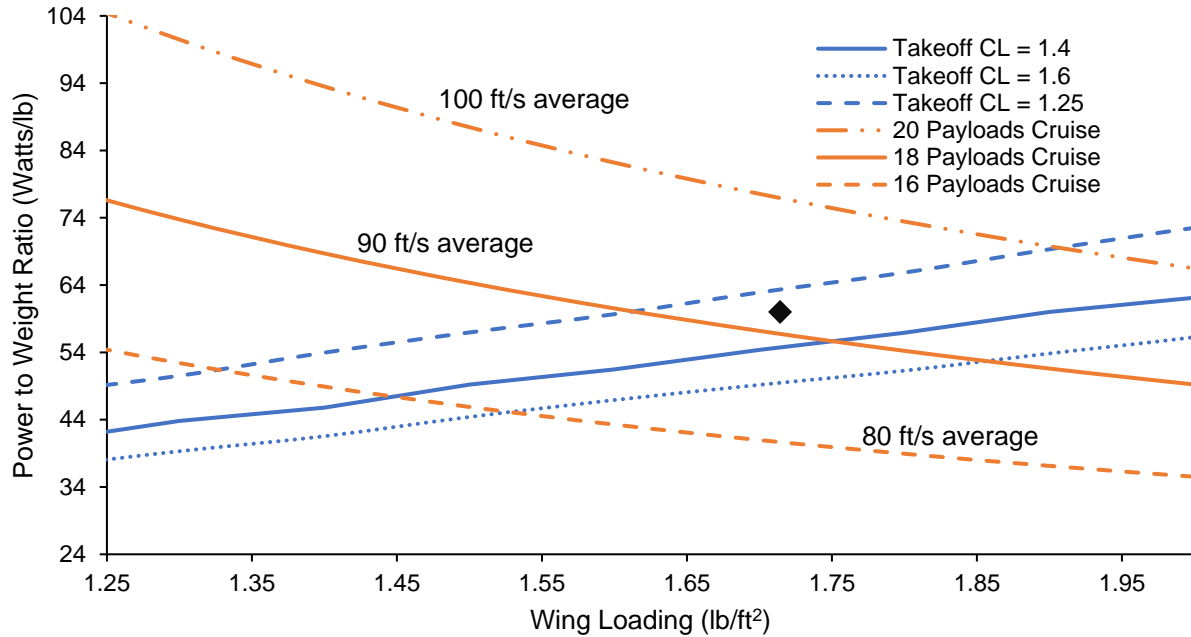


Figure 4.3: Constraint sizing and design point selection.

With the wing loading and power to weight ratio determined, the empty weight was estimated using methods adapted from Gundlach's *Designing Unmanned Aircraft Systems* [1]. Assumptions about the empty weight ratio, overall efficiency, and lift-drag ratio were made based on experience of the team's previous competition aircraft. The final design parameters are shown in Table 4.1.

$$W_{TO} = \frac{W_{Payload}}{1 - \left(\frac{W_e}{W_{TO}} + \frac{W_{batt}}{W_{TO}} \right)} \quad (4.1)$$

$$\frac{W_{batt}}{W_{TO}} = \frac{Range * Gravity}{E_{batt} \eta \frac{L}{D}} \quad (4.2)$$

Table 4.1. Parameters used in empty weight estimation.

Parameter	Value
Average Lift-Drag Ratio (L/D)	10
Empty-Takeoff Weight Ratio (W_e/W_{TO})	0.51
Battery-Takeoff Weight Ratio (W_{batt}/W_{TO})	0.25
Battery Energy Density (E_{batt})	80 Wh/kg
Overall Efficiency (η)	0.6
W_{TO} Estimate	12.0 lb



Using the results of the weight estimation, the power required and wing area were determined from the power to weight ratio and wing loading design point. The final sizing results are shown in Table 4.2.

Table 4.2: Preliminary constraint sizing results.

Parameter	Preliminary Value
Wing Loading (lb/ft ²)	1.7
Power Loading (Watt/lb)	60
Estimated Takeoff Weight (lb)	12
Wing Area (ft ²)	7
Power Required (Watts)	720

4.2.2 Propulsion System Selection

Elite 5000mAh cells were chosen to be combined into battery packs. The Elite 5000 provided the highest discharge rate and capacity out of all the cells the team was able to purchase. High discharge rate is required to provide enough power. High capacity cells are preferable as combining too many smaller cells can result in too much internal resistance.

MotoCalc, a commercially available motor analysis tool, was used to perform preliminary propulsion analysis. Using a compiled database of motors, propellers and batteries based on the size of the aircraft, MotoCalc was used to estimate the thrust produced by each system at varying airspeeds for 2,000 possible propulsion systems.

Table 4.3 shows the final motor-battery-propeller combinations and their respective produced static thrust the team considered. In the end, the Hacker A50 16s with an APC 17x10E propeller was chosen based on its balance between static thrust and thrust at speed. The validation of the chosen propulsion system with static thrust testing is described in Section 8.1.1.

Table 4.3. Propulsion systems considered for MotoCalc analysis.

Motor	Kv	Battery (cells)	Current (Amps)	Propeller	Static Thrust (lb)	Propulsion System Weight (lb)
Hacker A50 16s	365	20 (5000 mAh)	50	17x10	8.35	4.15
E-Flite Power 60	470	20 (5000 mAh)	50	16x10	6.23	4.13
Cobra 4120/22	430	20 (5000 mAh)	45	18x12	6.48	4.03

4.3 Mission Model

4.3.1 Description and Capabilities

The three missions were simulated via a set of first order differential equations (Equations 4.3-4.5) adapted from Anderson's *Fundamentals of Aerodynamics* [2] defining the position and orientation of the vehicle throughout the flight. By integrating these equations over time using a 4th Order Runge-Kutta approach in



the sequence they are flown using MATLAB, it is possible to define the position, velocity, and orientation of the vehicle over time. The thrust (T) is defined as a function of velocity, with the relationship defined by MotoCalc, the analysis tool used in the propulsion system selection. The drag (D) is represented via a parabolic drag relationship obtained from AVL and the parasitic drag modeling results. The load factor is explicitly defined for each turn segment, but if it exceeds the estimated maximum lift coefficient, it is limited to that value.

$$\dot{x} = V \quad (4.3)$$

$$\dot{V} = \frac{T-D}{m} \quad (4.4)$$

$$\dot{\psi} = \frac{g\sqrt{n^2-1}}{V} \quad (4.5)$$

4.3.2 Uncertainties

There are limitations to the approach used above. The lack of a vertical dimension in the equation means that the approach cannot model the aerodynamic effect of changing altitude. The energy required, saved, and lost by climbing and diving is also not included. The lack of any wind model discounts any additional drag due to sideslip, or the acceleration of the aircraft as due to headwinds or tailwinds. The flight path used for each lap assumes an ideal course, with the pilot achieving perfect, uninterrupted turns between each 1000 foot leg. Finally, there are additional uncertainties in the mission predictions due to modeling errors and simplifications made during the thrust and drag analysis.

4.4 Aerodynamic Characteristics

4.4.1 Airfoil Selection

Selecting an appropriate airfoil for the aircraft is important to achieve the desired aerodynamic characteristics in order to meet the design requirements. A variety of airfoils were compared based on XFOIL [3] analysis and validated using wind tunnel results from the UIUC airfoil database [4]. Several other considerations which factor into airfoil selection are discussed below.

Manufacturing: Undesirable airfoil geometry such as thin trailing edges present difficulties during manufacturing especially at a small scale. Overly complex airfoil geometries may also lead to manufacturing imperfections which will cause the aerodynamic characteristics to differ from the design.

Thickness: The airfoil selected must have enough thickness in order to accommodate internal structure and in the case of the fuselage body, the flight battery and receiver. Thin airfoils also tend to have sharp leading edges which cause abrupt stall behavior. Abrupt stall characteristics are especially deleterious on this aircraft due to the ramp takeoff; a sudden stall due to over-rotation will most likely not be recoverable right after the aircraft rolls off the ramp.



Aerodynamic Properties: The airfoil should have a high lift-drag ratio for cruising efficiently. An additional consideration that is especially important for this year's competition is the maximum lift coefficient; a higher lift coefficient reduces the power required for takeoff as seen in Figure 4.3.

Based on maximum section lift to drag ratio and the criteria described above, several airfoils from the UIUC airfoil database were considered. The lift and drag characteristics were analyzed using XFOIL and the results are shown in Figure 4.4.

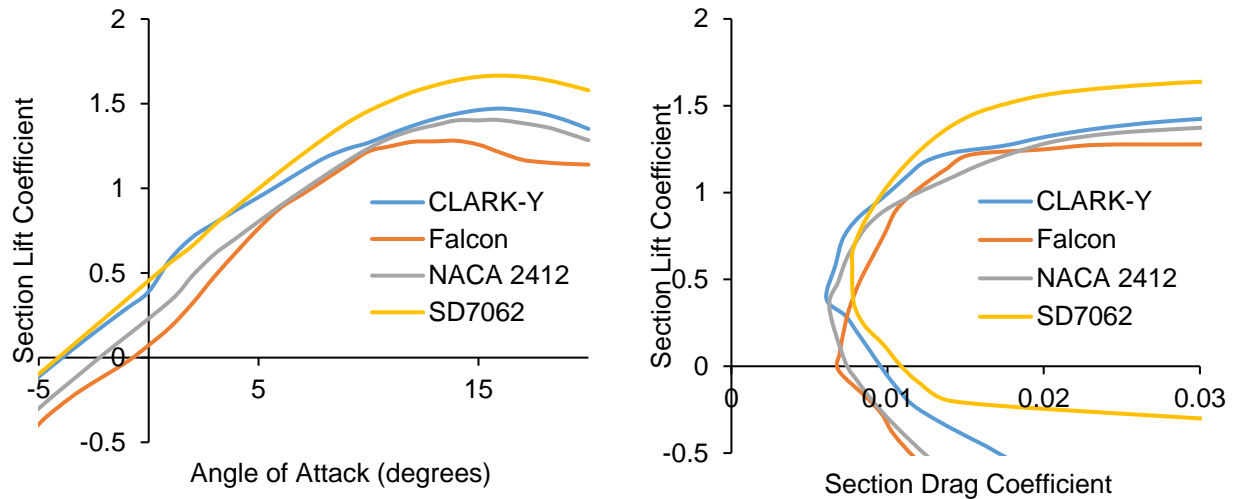


Figure 4.4. XFOIL lift and drag characteristics for several airfoils under consideration.

Examination of the drag polar shows that the SD7062 has a stable section drag coefficient over a wide range of c_l . This means that for a given range of lift coefficients, especially around 0.5, the drag coefficient remains consistently low. This is important due to the variance of c_l over the wingspan caused by downwash due to wingtip vortices. A high maximum c_l is desirable in order to meet the short takeoff constraint, however the SD7062 does not stall abruptly either. The SD7062 has a thickness to chord ratio of 14% which would accommodate a large spar which increases the geometric stiffness of the wing. The XFOIL analysis for the SD7062 airfoil was then validated using wind tunnel tests from UIUC as shown in Figure 4.5.

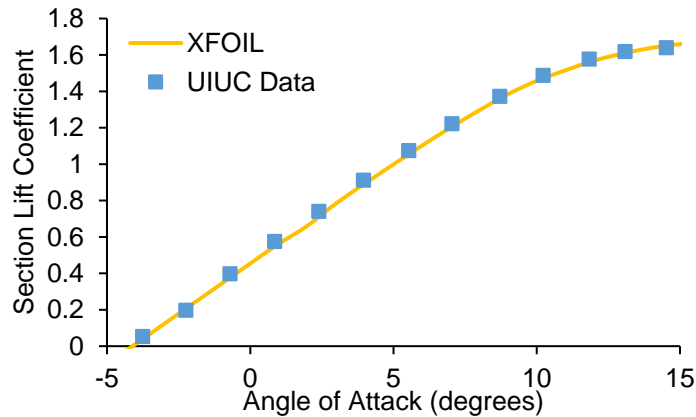


Figure 4.5. Wind tunnel test data for SD7062 compared to XFOIL at a Reynolds number of 500,000.



4.4.2 Lifting Surface Analysis

Lifting surfaces including the wing and tail were analyzed using Athena Vortex Lattice (AVL) developed by Dr. Mark Drela [5]. AVL models lifting surfaces as infinitely thin vortex sheets and calculates aerodynamic characteristics including lift and drag coefficient as well as stability derivative and trim condition analysis. The aircraft horizontal and vertical stabilizers were sized using this analysis method to achieve the required stability and controllability. The AVL analysis also considers the attack store release mechanisms with their fairings as lifting surfaces which affect the lift, drag, and stability of the aircraft. Figure 4.6 shows the lift distribution of the lifting surfaces with the angle of attack close to stall and the elevator set to maintain trim. In this condition, the elevator deflection is about 14 degrees which is well within the limits of the elevator hinge design.

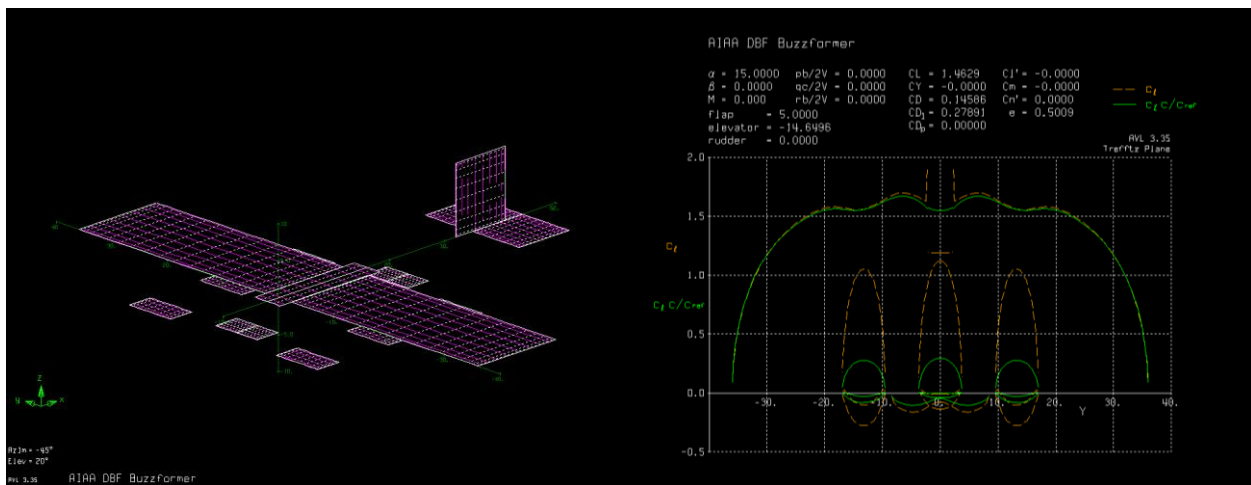


Figure 4.6: Model of the aircraft in AVL (left) and the resultant Trefftz plot at C_{Lmax} (right).

4.4.3 Drag Analysis

Preliminary parasitic drag estimates were obtained by summing each component's drag contributions, computed using the semi-empirical methods from Hoerner's *Fluid Dynamic Drag* [6], and then normalizing each component according to the wing reference area. Table 4.4 shows the contributions of the major aircraft components, with Figure 4.7 showing the same data as a percentage breakdown for each different configuration of the aircraft. The attack stores are the most significant source of drag for Mission 3 while the additional drag resulting from the radome is much smaller in comparison.



Table 4.4: Breakdown of various sources of drag.

Component	$C_{D,0}$	Mission	Total $C_{D,0}$
Wing-Fuselage	0.0208	M1	0.04
Empennage	0.0058	M2	0.043
Landing Gear	0.0054	M3	0.07
Radome	0.0029		
Attack Store Release Mechanisms	0.008		
Attack Stores	0.03		

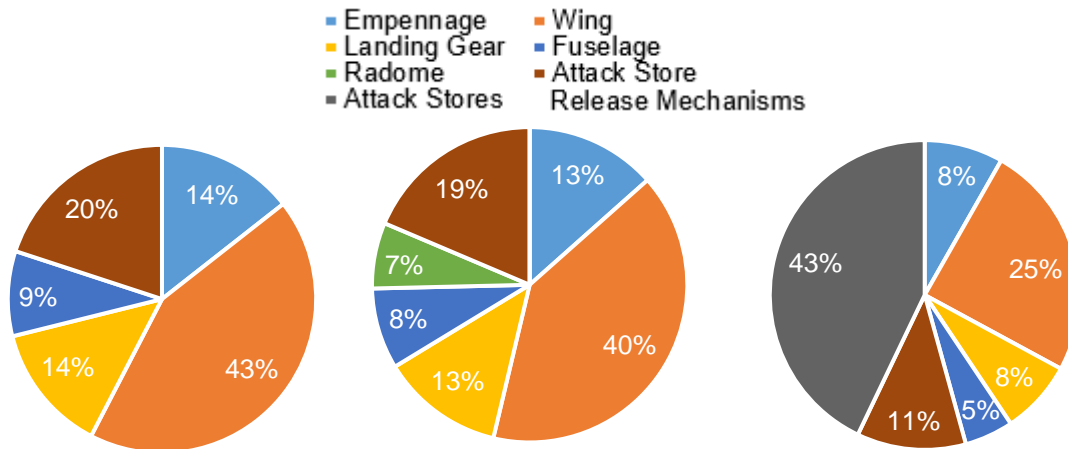


Figure 4.7: Drag breakdown for M1 (left), M2 (center), and M3 (right).

Wing: The zero lift drag coefficient of the wing was found using the semi-empirical Hoerner's method as seen in Equation 4.6:

$$C_{D,0} = R_{wf} R_{LS} C_{fw} \left(1 + L'(t/c) + 100(t/c)^4 \right) \cdot \frac{S_{wetw}}{S} \quad (4.6)$$

where R_{wf} is the wing fuselage interference factor assumed to be equal to 1.2 due to the numerous joints and interfaces between the attack store release mechanisms, fuselage, and the wing. R_{LS} is the lifting surface correction, which is a function of the sweep angle, C_{fw} is the turbulent plate friction coefficient of the wing, which is a function of Reynolds number (Re), L' is the airfoil thickness location factor, t/c is the thickness-to-chord ratio, S_{wetw} is the wetted area of the wing, and S is the wing reference area.

Empennage: The horizontal and vertical stabilizers were modeled as wings, and its drag was determined using Hoerner's method. A wing interference factor of 1.04 was used to reflect the perpendicular joint between vertical and horizontal stabilizers.

Landing Gear: The landing gear components are significant contributors to the overall drag of the aircraft. The main gear and nose gear drag contributions were calculated separately, but both were modeled as a wheel and a flat plate.



Radome: Since both the radome and its mounting hardware are airfoil shapes, they were modeled as lifting surfaces and their total drag contribution approximated using Hoerner's method for a wing.

Attack Store Release Mechanisms: Each attack store was modeled as a fuselage using Hoerner's method. The mechanisms are modeled as small wings due to the fairing around each mechanism. A wind tunnel test was used to later confirm the estimate and update it to accommodate the change in drag as payloads are released.

Combining the parasitic drag estimates with AVL for induced drag analysis, a drag polar for the entire aircraft was constructed and shown in Figure 4.8. The drag is substantially larger for Mission 3 with all attack stores. As attack stores are released, the drag will decrease with each lap.

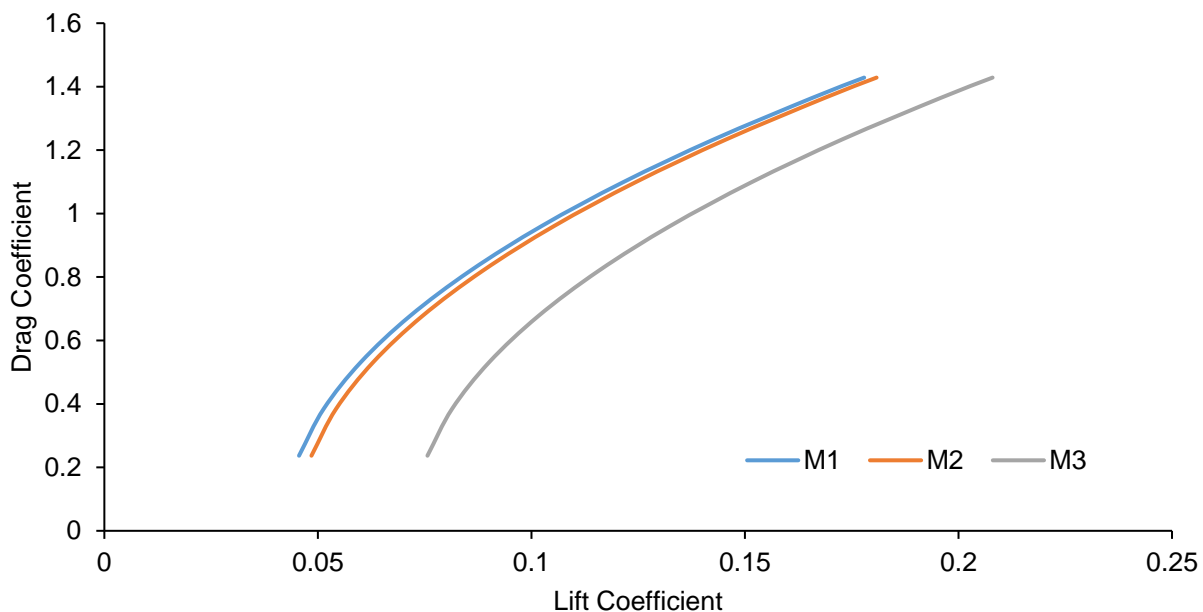


Figure 4.8: Drag polar of the aircraft for the three different missions.

4.5 Stability and Control

Static and dynamic stability were analyzed to ensure that the aircraft would be able to successfully complete the flight missions. A range of flight conditions were considered including variation in velocity, takeoff weight, climb, cruise, and turns. Only results for the critical flight condition is presented.

4.5.1 Static Stability Analysis

Static stability was evaluated using the vortex lattice method implemented in AVL. The critical flight condition is flying near C_L max right after the takeoff at the heaviest takeoff weight for Mission 3. Stability derivatives for this flight condition are presented in Table 4.5. At this condition, no extreme deflections of the elevator are required.



Table 4.5. Relevant stability coefficients and derivatives for static stability.

Parameter		Value
Inputs	W_{total} (lb)	12
	V (ft/s)	31.44
Deflections	$\delta_{elevator}$ (deg)	-14.7
	$\delta_{flaperon}$ (deg)	5
	δ_{rudder} (deg)	0
Aerodynamic Parameters	C_L	1.46
	α (deg)	15
	β (deg)	0
Stability Derivatives	$C_{l,\beta}$ (rad ⁻¹)	-0.179
	$C_{L,\alpha}$ (rad ⁻¹)	6.60
	$C_{m,\alpha}$ (rad ⁻¹)	-0.28
	$C_{n,\beta}$ (rad ⁻¹)	0.11
Damping Derivatives	$C_{l,p}$ (rad ⁻¹)	-0.345
	$C_{m,q}$ (rad ⁻¹)	-5.58
	$C_{n,r}$ (rad ⁻¹)	-0.105
Static Margin	% Chord	8

4.5.2 Dynamic Stability Analysis

Having found the trim conditions as a part of the static stability analysis as well as the stability derivatives at the trim point, the dynamic behavior of the aircraft were studied. The stability and control derivatives were obtained from the AVL, the mass properties from the CAD model, and the stability characteristics calculated from the full 12x12 6-DOF linearized differential equations found in Phillips's *Mechanics of Flight* [7]. The flight conditions used were the same as in the static stability section, listed in Table 4.5. The dynamic stability characteristics are tabulated in Table 4.6.

Table 4.6: Dynamic stability characteristics

Mode	Longitudinal Modes		Lateral Modes		
	Short Period	Phugoid	Dutch Roll	Roll	Spiral
Damping Rate (s ⁻¹)	3.464	0.021	0.93	7.51	-0.123
Time to double/half (s)	0.200	32.98	0.744	0.092	5.65
Damping Ratio (~)	0.747	0.021	0.183	-	-
Damped Natural Frequency (s ⁻¹)	3.08	0.997	4.98	-	-
Undamped Natural Frequency (s ⁻¹)	4.63	0.998	5.066	-	-

The eigenvalue and eigenvectors of the matrix revealed that the aircraft is stable in the Short Period, Dutch Roll, and Roll modes and slightly unstable in the spiral mode. The spiral mode has a double time of 5.65 seconds, consistent with competition aircraft from previous years with acceptable handling qualities.



4.6 Mission Performance

Predicting the performance of the aircraft is essential for verifying that the aircraft can complete all missions. Lap trajectories were estimated using the equations listed in Section 4.3, propulsion characteristics from MotoCalc and the aerodynamic properties found using AVL and Hoerner's method. The flight performance was calculated with a 17x10 propeller, a Hacker A-50 16s motor and a 20S 5000 mAh NiMH battery pack. There are small differences in the trajectory due to the change in gross takeoff weight and parasitic drag from the different aircraft configurations as seen in Figure 4.9.

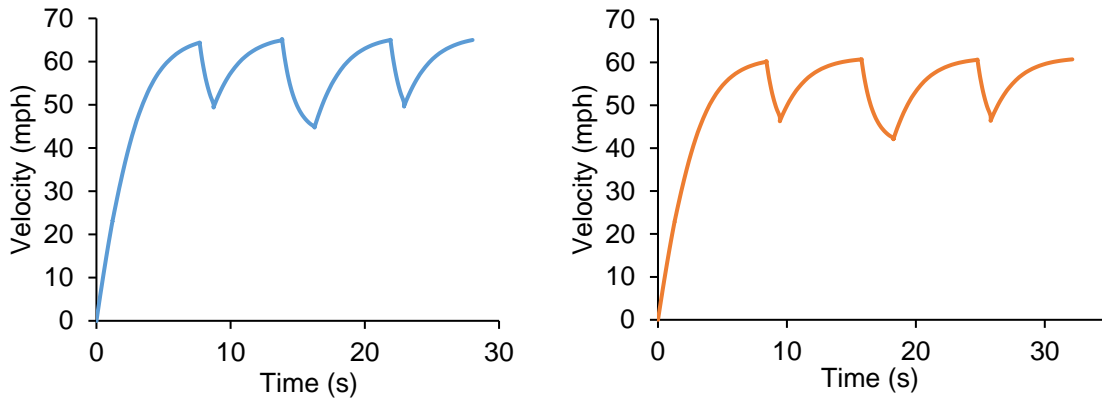


Figure 4.9: Simulation of lap trajectories for M1 (left) and M2 (right).

5 DETAIL DESIGN

5.1 Final Design – Aircraft

The final dimensional parameters are listed in Table 5.1. All wing and control surface chords were chosen to allow sufficient thickness for structure, embedded servos, and sufficient clearance off the wing locking and attack store release systems.

Table 5.1: Final aircraft dimensions.

Overall Dimensions			Vertical Tail Dimensions		
Length	59.15	in	Height	13.2	in
L.E. X-Location	17.65	in	Chord	9	in
C. G. X-Location	3.2	in	L.E. X-Location	47.65	in
Static Margin	7%	chord			
Total Wing Dimensions			Horizontal Tail Dimensions		
Span	72	in	Span	17	in
Chord	14	in	Chord	9	in
Aspect Ratio	5.14	~	L.E. X-Location	50.25	in
Area	7	ft ²			



5.2 Structural Characteristics

5.2.1 Layout and Design

The structural layout was created to ensure that all loads were accounted for and have an adequate load path to the major load-bearing components. The team divided all loads which the aircraft would experience into three categories:

Motor Loads: Includes thrust, torque, and sustained vibrations. Components should be made of harder, quasi-isotropic materials such as plywood, and all fasteners must be locked.

Aerodynamic Loads: Includes wing and control-surface lift, drag, and moment, which translate to bending, torsion, and shear. The primary aerodynamic load is bending. Components can be anisotropic for added strength in the load direction.

Ground Loads: Includes aircraft weight and landing impact. Landing gear struts should be metal, which absorbs some of the impact through bending.

The loads on the aircraft need to transfer into the major load bearing components, which includes the wing spar, center fuselage tube, and landing gear. In flight, the wing structure is designed to withstand a load up to a 9g load at maximum weight, based on the requirement of high-speed turns to complete a maximum number of laps within the time constraint of Mission 2. The aircraft structure is designed to transfer all the loads to the central structural components in the fuselage, as demonstrated in Figure 5.1.

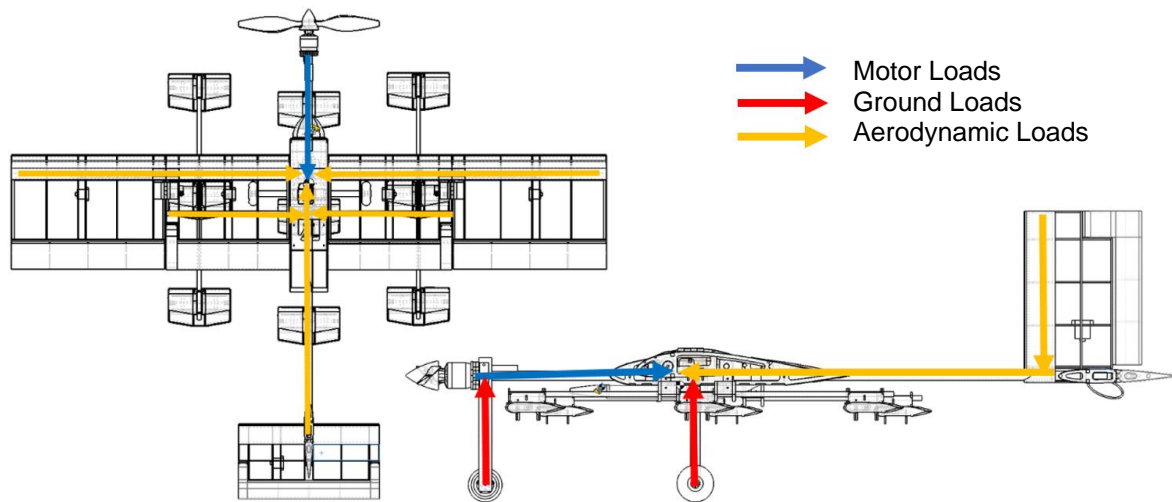


Figure 5.1: Load paths of major forces.

5.2.2 Operating Envelope

The operating limits of the aircraft are defined by the aerodynamic and structural characteristics of the aircraft. Figure 5.2 displays the limits of the aircraft in a V-n diagram. The maximum allowable load factor is limited by either exceeding the maximum C_L (which would lead to stall) or the structural limits. The aircraft is designed for a maximum load factor of 9 at the estimated gross takeoff weight of 12 pounds for Mission 3 which translates to 108 pounds total. The maximum load is derived from similar maximum load limits on



aerobatic and military aircraft. As the aircraft gross takeoff weight changes based on the configuration of each mission, the stall and maximum load factor also varies. An additional V_{NE} limit is set for the aircraft in consideration of flutter. Although the aircraft does not have enough thrust to reach V_{NE} in level cruise, it may do so in a dive.

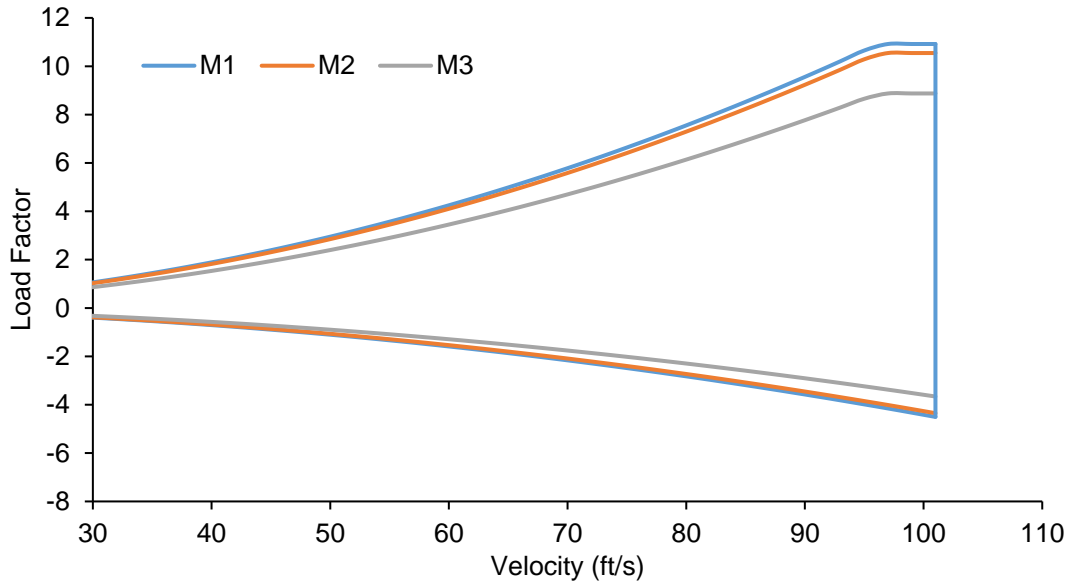


Figure 5.2: V-n diagram showing loading as a function of velocity for all flight missions.

5.3 System and Subsystem Design and Implementation

There are numerous subsystems and subassemblies that make up *Buzzformer* including the fuselage, wing, wing locking mechanism, motor mount, empennage, attack store release mechanisms, radome, and the propulsion system. The numerous subsystems must all interface seamlessly with the aircraft in each of its multiple configurations. They must not cause interference or hinder aircraft performance. Section 5.3 describes each subsystem in detail.

5.3.1 Fuselage

The main load bearing component for the fuselage is a carbon fiber tube. Loads are transferred through the plywood fuselage box into the center carbon-fiber tube. The fuselage box is designed to interface with the wing, primary structure, radome, and landing gear while minimizing weight. The fuselage was developed such that the wing spars can easily slide into the fuselage box and precisely line up the body/wing interface so they can be fastened together. This allows for the aircraft to be easily disassembled for transportation as well as support a modular construction to make production more efficient. The bottom of the fuselage has small holes to allow the batteries to be fastened to the main carbon-fiber tube with zip ties. The CAD models of the fuselage can be found in Figure 5.3.

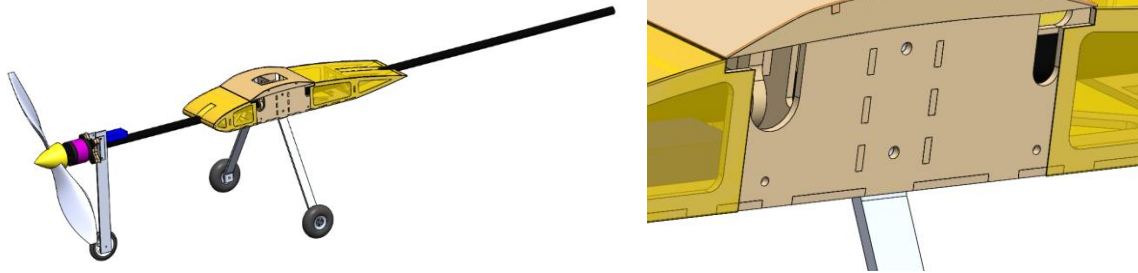


Figure 5.3. Fuselage (left) and holes for fuselage-wing interface (right).

5.3.2 Wing

The wing needed to withstand the maximum load factor of 9 specified by design. The lift distribution was obtained from AVL along the semi-span and the shear, and bending moments were calculated using Euler-Bernoulli beam bending theory. A range of commercially available carbon fiber tubes were analyzed with the results for the selected spars shown in Figure 5.4. Unidirectional carbon fiber tubes were chosen for the main spar and the smaller secondary spar in the inboard section. The main spar measures 0.75 inch inner diameter and 0.82 inch outer diameter, the aft spar measures 0.375 inch inner diameter and 0.435 inch outer diameter.

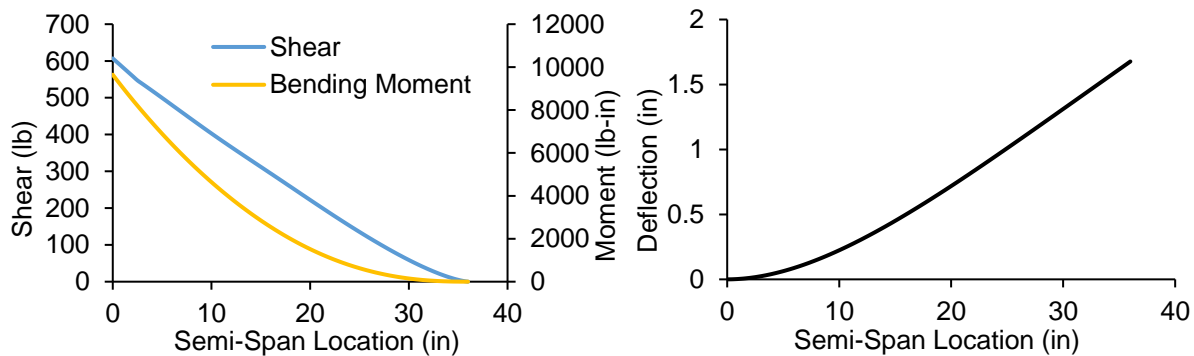


Figure 5.4. Shear and bending moment distribution along the semi-span (left), deflection along the semi-span (right).

The aircraft experiences 1.67 inches of deflection at the tip under the maximum load of 108 pounds for the 12 pound airplane at a load factor of 9. The maximum tip deflection is 4.6% of the semi-span. From the team's experience with previous competition aircraft, a tip deflection less than 10% is considered acceptable to prevent control surface binding, overstretching of the plastic covering material, and other aeroelastic problems.

The inboard wing sections follow a conventional rib and spar layout. There is a gap in the center to accommodate the fuselage box as shown in Figure 5.5. The outboard wing sections follow the same design with the omission of the aft carbon-fiber spar. The inboard and outboard wing sections are



connected using a metal hinge fastened onto a flat plate at the top surface. The plate is attached to two ribs and reinforced with carbon fiber strips, as it must transfer torsion between the outboard and inboard wing sections. The use of a metal hinge provides a solid and well constrained axis of rotation.

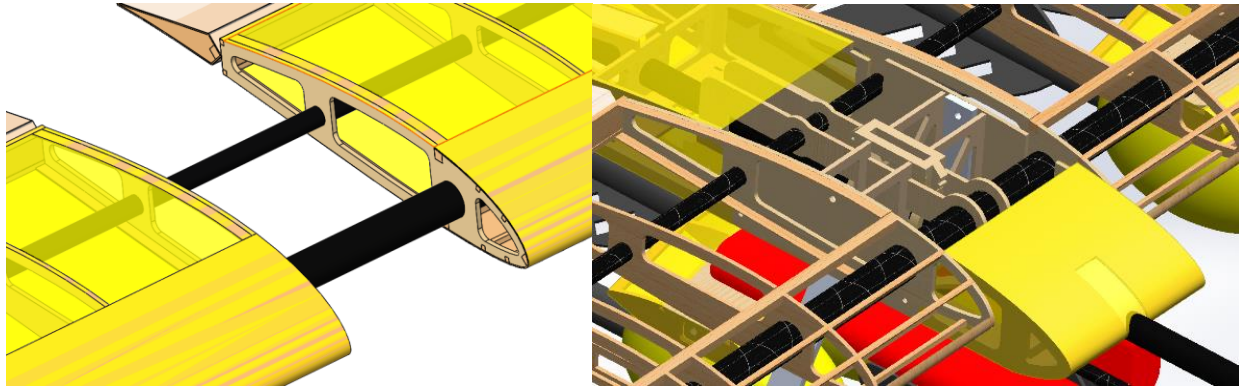


Figure 5.5. The inboard wing gap (left) and combined wing-fuselage (right).

5.3.3 Motor Mount Assembly

The motor mount is glued directly to the end of the carbon fiber rod with epoxy resin. Two pieces of 0.25 inch thick plywood are glued together as a composite firewall capable of withstanding motor thrust and torque loads. It is shaped to conform with the base of the motor mount in order to reduce flat frontal area, and therefore drag. Four holes were cut into the firewall to accommodate the fasteners used to mount the motor. The forward landing gear strut is attached to the motor mount using bolts as shown in Figure 5.6.

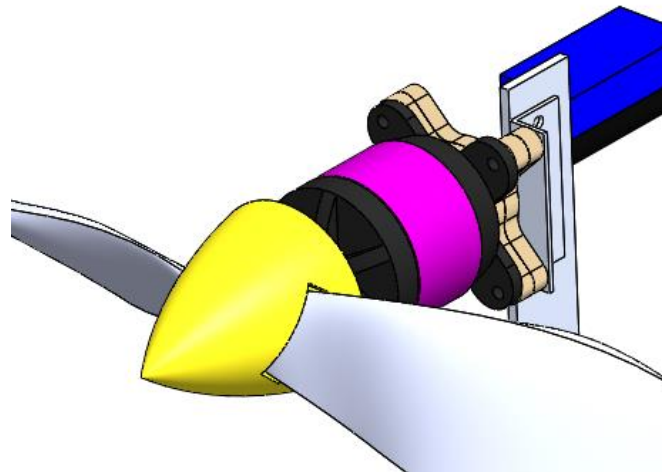


Figure 5.6. Motor mount assembly.

5.3.4 Empennage

The empennage construction uses similar materials and construction techniques as the wings, with balsa wood used for the majority of the structure, augmented by plywood members at the interface between the empennage and the carbon fuselage tube. 0.25 inch balsa wood sticks are used for spars instead of carbon fiber tubes in order to save weight. The balsa spars are reinforced with bonded carbon fiber strips along the top and bottom to increase bending stiffness. The rudder and elevator have balance tabs



because they reduce the hinge moment and reduce the tendency to flutter at high cruise speeds. Beneath the empennage is a tail hook which is used to arrest the aircraft prior to takeoff. It also serves to protect the aircraft in case a tail strike occurs. This design is shown in Figure 5.7.



Figure 5.7. Empennage assembly (left) and the tail hook mounted to the bottom of the center line (right).

5.3.5 Wing Locking Mechanism

The wing is hinged near the half span on each side to reconfigure the aircraft between the stowed configuration and flight configuration. A ferrule connects the inboard and outboard spars when the aircraft is in the flight configuration. A locking mechanism was designed that deploys the ferrule from the outboard wing section when the aircraft is in flight configuration.

The outboard wing section spar houses the ferrule when the aircraft is in the stowed configuration. While the aircraft is in the stowed configuration, the spring-loaded ferrule is restrained by a 3D printed locking tab. A slot is cut into the side of the spar to allow the locking tab to reach inside the spar. A compressed spring and guide rod are used to push the ferrule into the inboard wing when changing to the flight configuration. As the outboard wing section rotates to the flight position, a carbon fiber pin attached to the inboard wing section pushes on the locking tab, releasing the spring-loaded ferrule. The locking mechanism in various stages of activation is shown Figure 5.8. In the flight configuration, the ferrules transfer the shear and bending loads between the outboard and inboard spars. The torsional loads are transferred to the inboard wing section via the metal hinges.

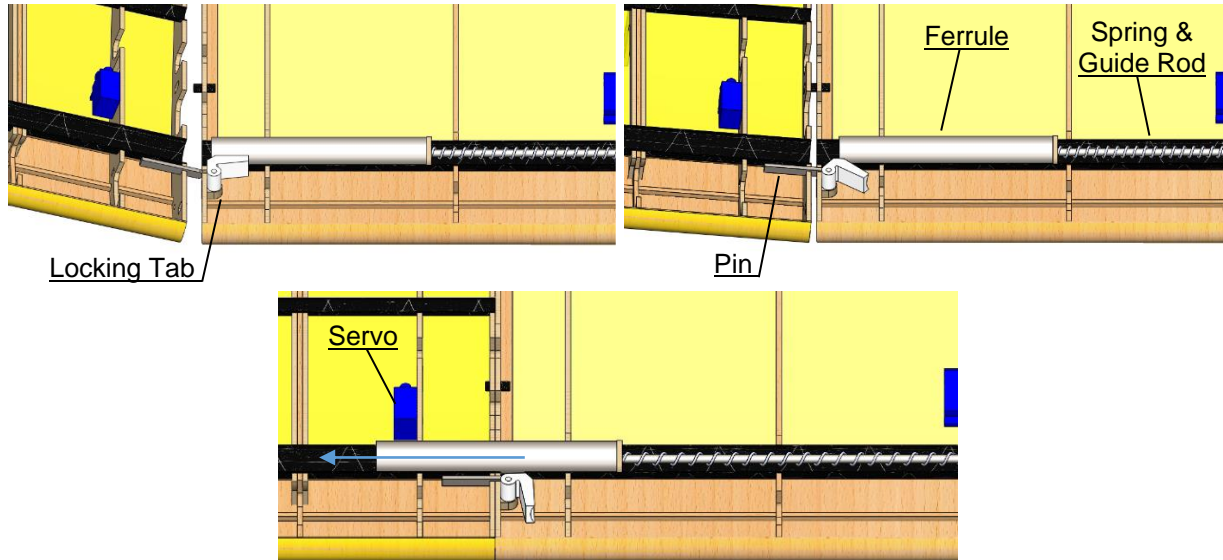


Figure 5.8. Operation of the wing locking mechanism.

In order to release the wing locking mechanism when the aircraft is in the flight configuration, the ferrule is pulled back using string attached to the guide rod which can be done by reaching inside the outboard spar from the wingtip. With the ferrule pulled back, the outboard wings can be manually rotated upwards to reset the aircraft back to the stowed position.

The outboard wing sections sit on top of the inboard wing while the aircraft is in the stowed position as shown in Figure 5.9. A small carbon fiber rod embedded in the innermost rib on the outboard section is attached to a continuous rotation servo in the inboard wing section via a length of Kevlar string. When the pilot commands the aircraft to reconfigure from the stowed position to the flight configuration, the continuous rotation servo winds the Kevlar string onto its spool which pulls the outboard wing section down, engaging the locking mechanism.



Figure 5.9. Wing hinge.



5.3.6 Radome

The radome mechanism was designed for rapid attachment and removal. A plywood locking mechanism was designed using a set of pins and an elastic band which interfaces with a plywood mast. The pins and elastic band automatically lock when the mast is inserted. The mast is removed manually by removing the pins and lifting the mast. The mast is surrounded by a series of balsa and plywood NACA 0030 airfoils in a rib and spar configuration which act as a fairing. Attached to the mast is a carbon fiber shaft which attaches directly to the radome, located above the mast. The shaft is rotated by a set of 0.75 inch plywood gears connected to a continuous rotation servo contained within the fairing. A servo was used instead of a motor because of its internal gearing system and ease of integration with the receiver. The radome has a diameter of 12 inches and is tapered to reduce drag. The radome is constructed out of insulation foam and manufactured using a CNC mill. The radome is colored orange and black in alternating radial quadrants for increased visibility based on tests conducted at a height of 50 yards. The locking mechanism and radome mechanism are shown in Figure 5.10.

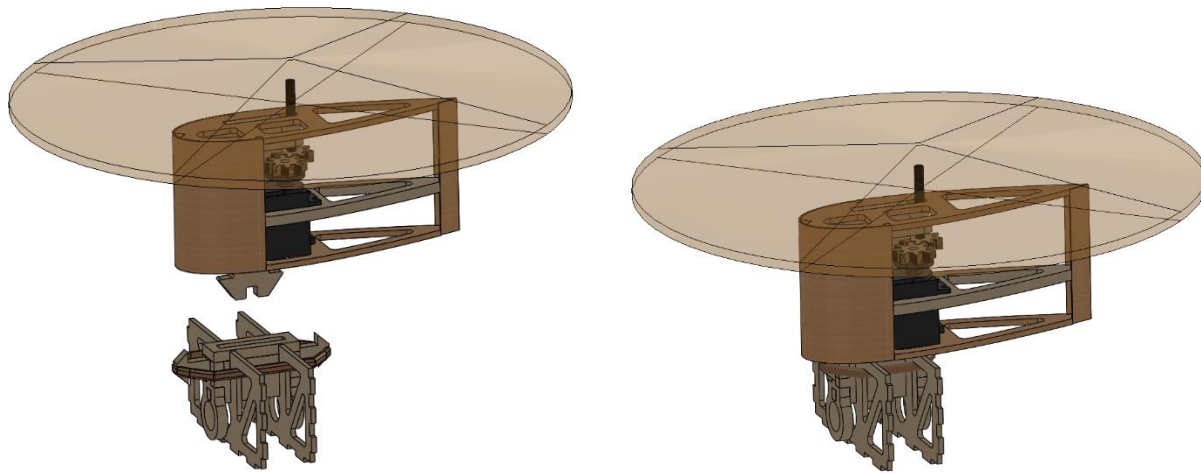


Figure 5.10. Locking and Radome Mechanism.

5.3.7 Attack Store Release Mechanism

Each attack store release mechanism holds two attack stores, each of which is retained with an elastic band. Each elastic band is permanently fixed in the center and stretched across the attack store to a release pin held between two supports. The release pin is attached to a length of braided Kevlar which is tied to a servo arm. At the command of the ground crew, the servo is rotated, pulling out the release pin and releasing the attack store. A row of attack store release mechanisms is attached to a carbon fiber tube, which is then mounted onto a hardpoint located under the wing. This allows for high-density payload storage while minimizing drag and ensuring that at least four attack stores are under the wing. Each mechanism also has a fairing to further reduce drag as seen in Figure 5.11.

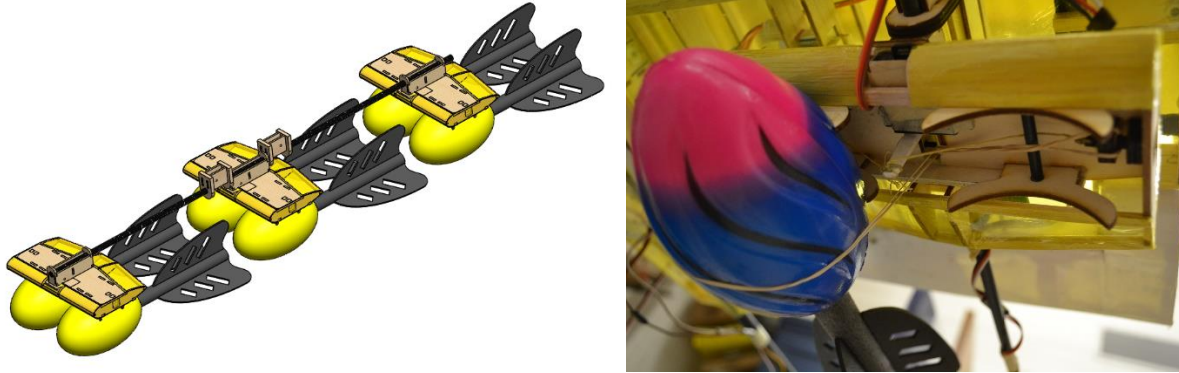


Figure 5.11. Single row of six attack stores mounted (left) and attack store release mechanism (right).

The mechanisms are also designed for quick loading. Prior to the Ground Mission, the elastic bands and release pins are installed in the supports which arms the mechanisms. To load the mechanisms, the elastic bands are stretched and the attack stores are placed within the payload cradle.

5.3.8 Receiver and Transmitter Selection

Due to the high number of actuators, it was necessary for attack store release to be commanded from an independent transmitter and receiver. The team selected the Futaba R6008HS for both the aircraft control receiver and the attack store release mechanism. *Buzzformer* uses two Futaba T14SG 2.4 GHz radio transmitters to communicate with the receivers.

5.3.9 Propulsion System

Two 10 cell Elite 5000 mAH NiMH battery packs were selected to provide the power and minimize weight. A variety of motors and propeller combinations were analyzed using the MotoCalc program with this battery choice, as described in Section 4.2.2. The Hacker A50 tested with varying propeller sizes, as described in Section 7.2. The APC 17x10 propeller was chosen for its combination between thrust at cruise and the static thrust it provides for takeoff. The final selected propulsion system is listed in Table 5.2.

Table 5.2: Selected propulsion and electronics components.

Components	Description
Motor	Hacker A-50 16S
Battery	20 x Elite 5000 mAh
Speed Controller	Castle Phoenix Edge Lite HV 60
Propeller	APC 17x10

5.4 Weight and Balance

A correct center of gravity (C.G.) location is critical for longitudinal control and stability. All C.G. analysis was performed in Solidworks using models of each component with proper weights and densities. Component weights were first estimated using the CAD model and then confirmed with the physical vehicle. Table 5.3 contains the results for all three missions for the aircraft. The x-axis was measured positive aft of the nose of the aircraft. The battery must move significantly in order to control the C.G.



Table 5.3. Weight and balance for Buzzformer.

Component	Weight (lb)	C.G. Loc. (inch x-axis)
Fuselage	0.7	22.3
Wing	1.53	22.4
Motor Assembly	1.10	3.5
Outboard Attack Store Release Mechanism Rows	1.12	22.5
Center Attack Store Release Mechanism Row	0.57	24.7
Empennage	0.23	53.8
Onboard Electronics	0.283	17.8
Main Gear	0.66	22.3
Nose Gear	0.19	6.2
Aircraft Totals	6.38	19.8

Component	Weight (lb)	CG Loc. (inch x-axis)
Mission 1		
Battery	3.51	23.3
Aircraft Totals	9.89	21.1
Mission 2		
Battery	3.51	23.1
Radome Assembly	0.35	23.2
Aircraft Totals	10.24	21.1
Mission 3 - Full Load		
Battery	3.51	21.6
12 Outboard Attack Stores	1.52	23.0
6 Center Attack Stores	0.76	25.2
Aircraft Totals	12.17	21.1
Mission 3 - Zero Attack Stores		
Battery	3.51	21.6
Aircraft Totals	9.89	20.4

Between the start of Mission 3 and the end, the C.G. moves forward 0.7 inches due to releasing the attack stores. Drastic changes to the C.G. during Mission 3 are avoided by dropping the attack stores in a symmetric manner back to front and left to right. This process is repeated for each inner pair of rows. Figure 5.12 shows the change in C.G. between the start and end of Mission 3.

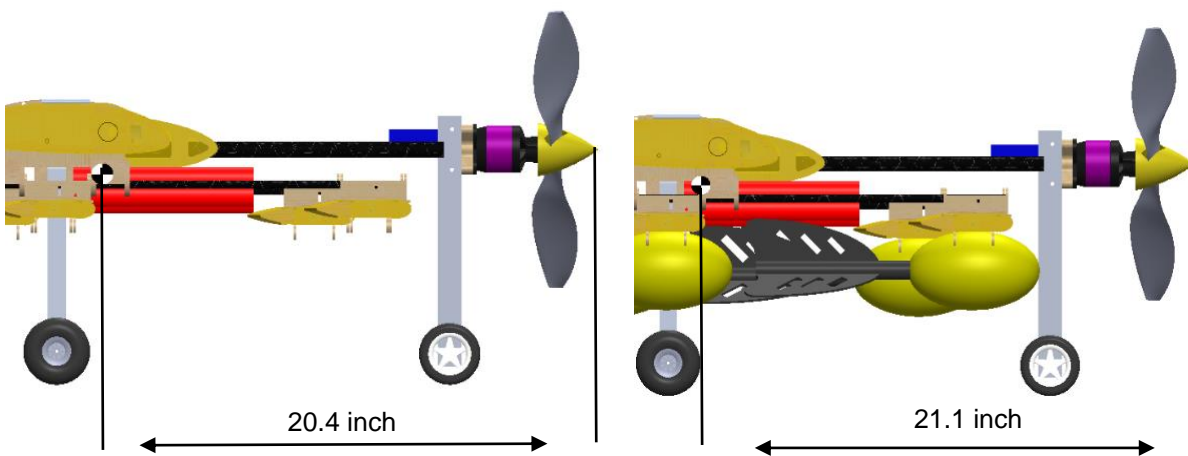


Figure 5.12: CG Location shift during Mission 3.

5.5 Performance

5.5.1 Flight Performance

The important flight performance characteristics are cruise velocity and turn performance. The weight and drag of the aircraft vary between all three missions which affects flight performance. Point performance



parameters for all three missions are shown in Table 5.4. The wing loading and stall speed are calculated at a load factor of one for the gross takeoff weight of each mission using an estimation of C_{Lmax} from AVL modeling and section lift data. The load factor for each mission was calculated by dividing the maximum design load of 108 pounds by the gross takeoff weight for each mission. The maximum load factor is intended to be a maximum while measured loads from flight tests are lower. The turn radius is calculated using the maximum allowable load factor in a level turn.

Table 5.4. Aircraft flight performance parameters for each mission.

	Mission 1	Mission 2	Mission 3
Weight (lb)	9.89	10.24	12.17
C_{D0}	0.04	0.043	0.070
W/S (lb/ft²)	1.39	1.54	1.72
V_{Stall} (ft/s)	30.2	31.7	33.5
V_{max} (ft/s)	92.4	92	91
Max Load Factor	11.08	10.02	8.97
Turn Radius (ft)	135.7	150.2	167.8
Time for 360 (s)	5.01	5.22	5.70

From MotoCalc, the thrust available with respect to velocity was used to compute the maximum cruise speed. The lift and drag was computed using AVL and matched with the thrust available to determine the maximum cruise speed. Figure 5.13 shows the thrust required curves for each mission configuration as well as the thrust available curves for the two propellers considered for the propulsion system. The 17x10 propeller was chosen due to its higher static thrust for takeoff.

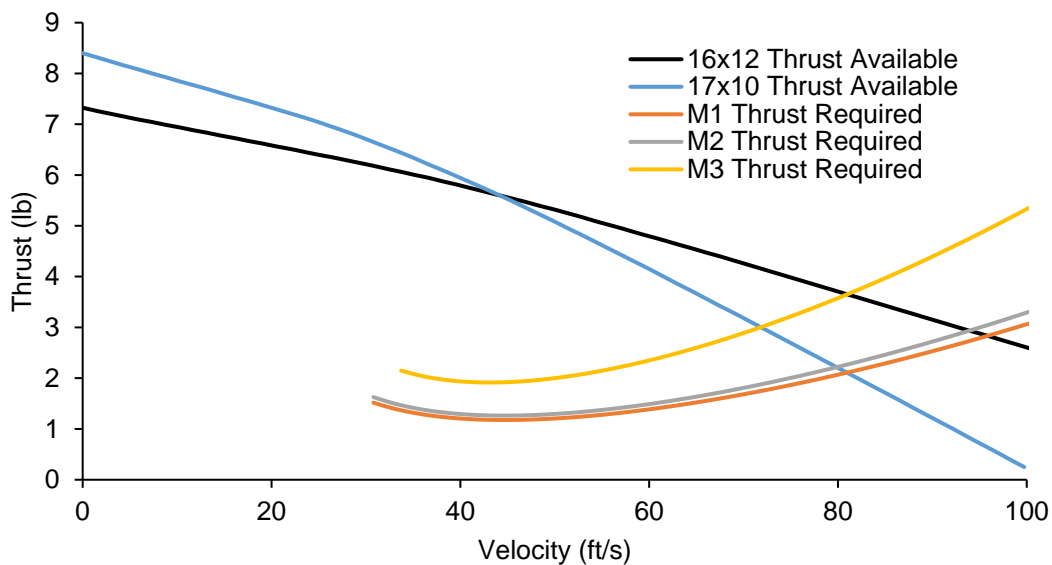


Figure 5.13 . Thrust available and thrust required curves for each flight mission.



5.5.2 Mission Performance

The mission model described in Section 4.3 was used to estimate the overall mission performance of the aircraft. The computed lap times represent an estimate that combines aerodynamics from AVL, power and current characteristics from wind tunnel testing, and the physics of the mission model. Figure 5.14 shows the first and last laps trajectories of Mission 3. The first lap is slower due to the aircraft taking off, but as attack stores are dropped, the aircraft also becomes lighter and drag decreases, causing the subsequent lap times to decrease with each attack store dropped. The first lap of Mission 3 is 33.7 seconds while the last lap is 27.5 seconds

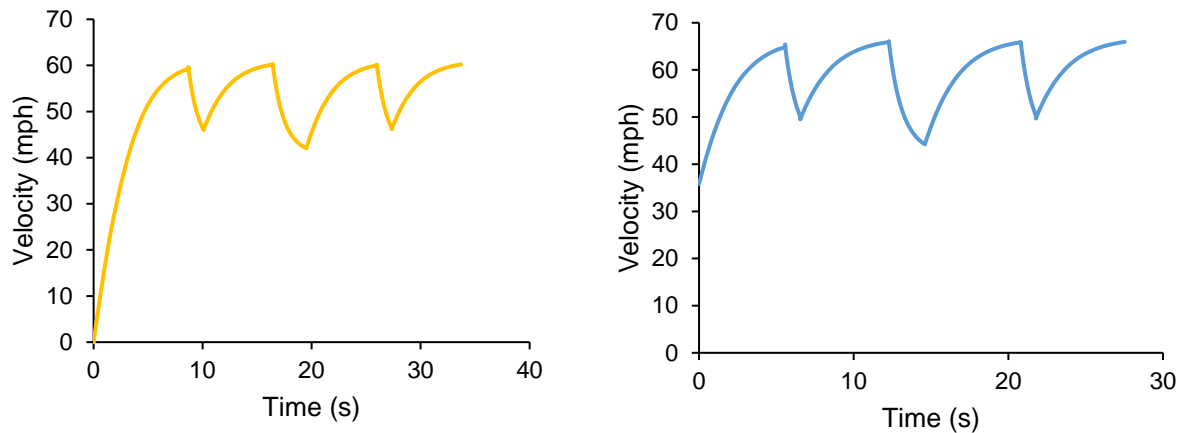


Figure 5.14. Simulated first lap trajectory (left) and last lap trajectory (right) for M3.

5.6 Drawing Package

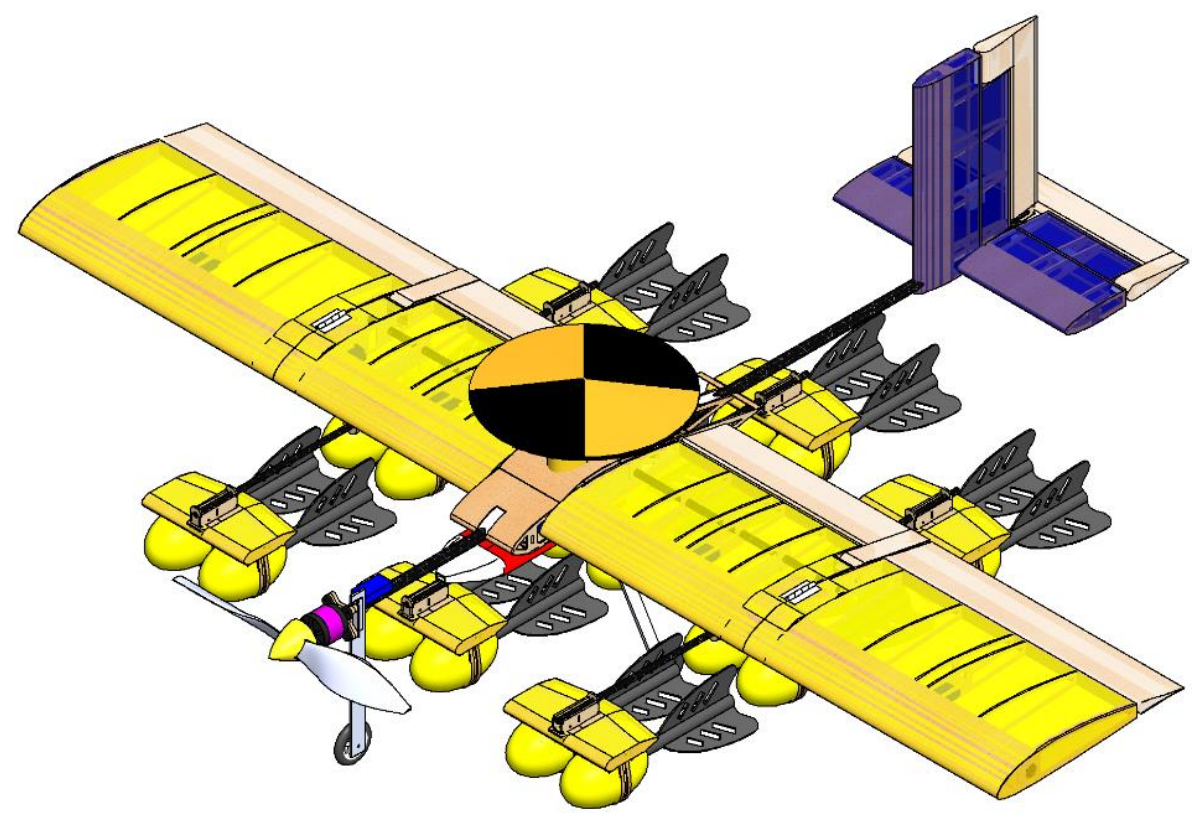
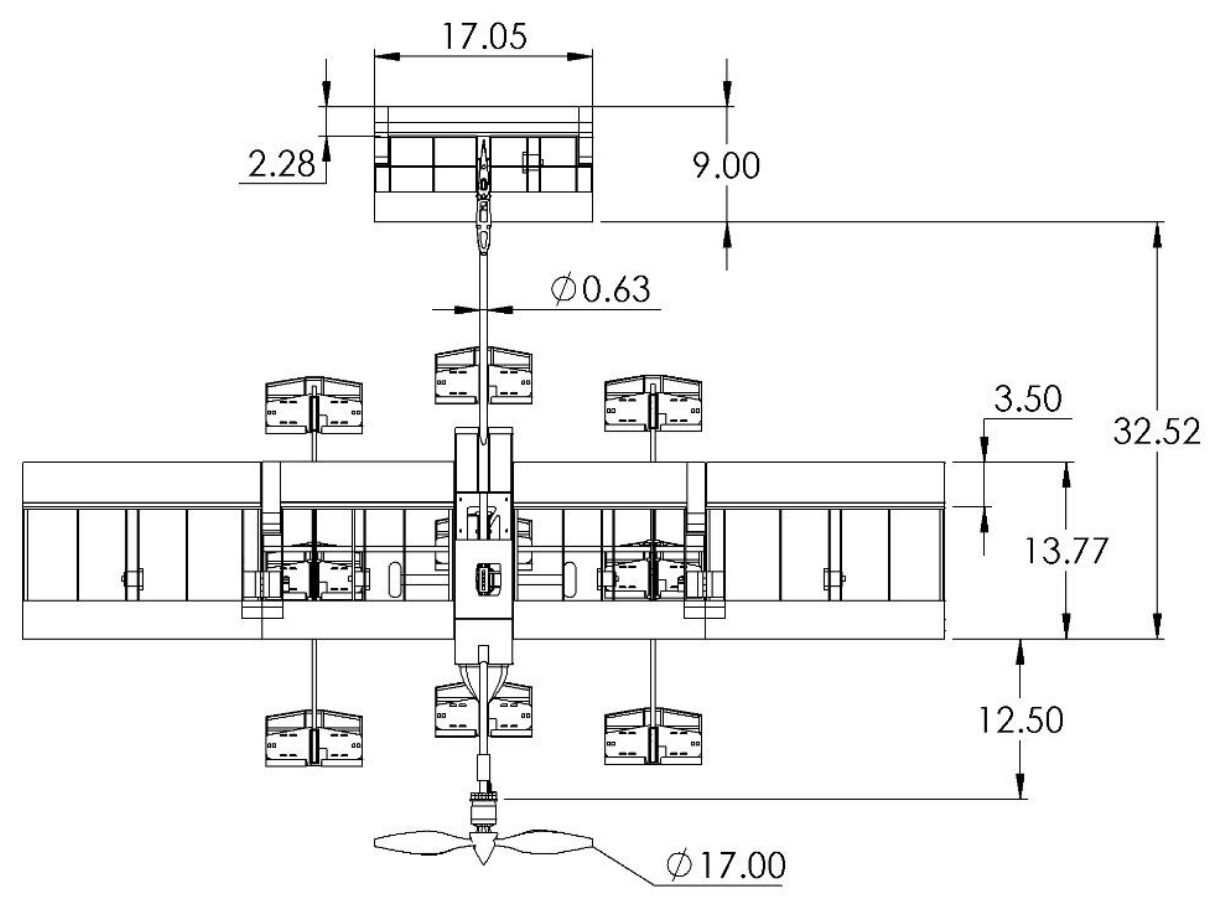
The following four pages illustrate the detailed CAD of the *Buzzformer* system. The first sheet contains the three-view diagram with relevant dimensions. The second sheet contains the structural arrangement of all major components. The third sheet shows the system layout of electronics and mechanisms. The fourth sheet displays the payload accommodations.

4

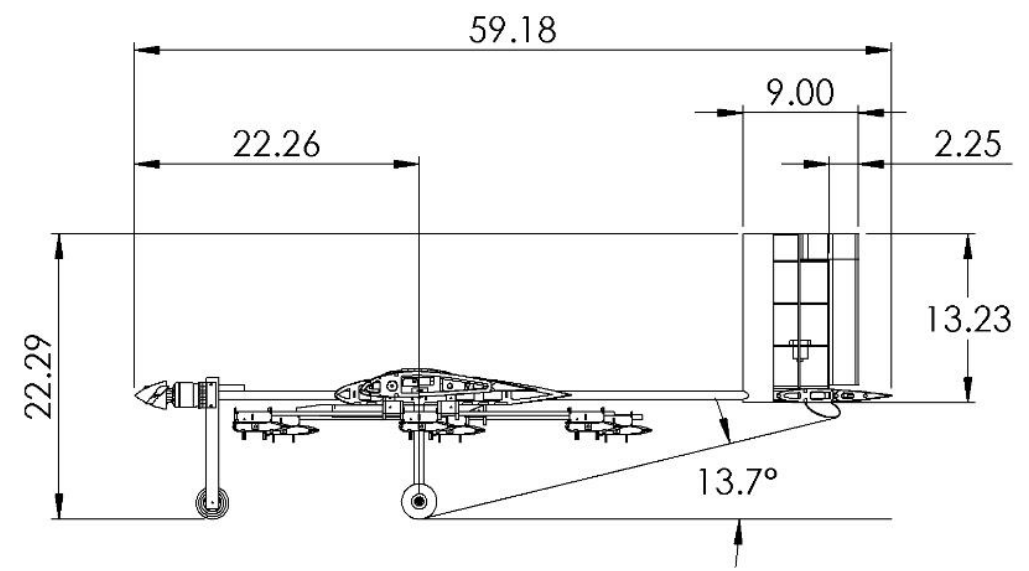
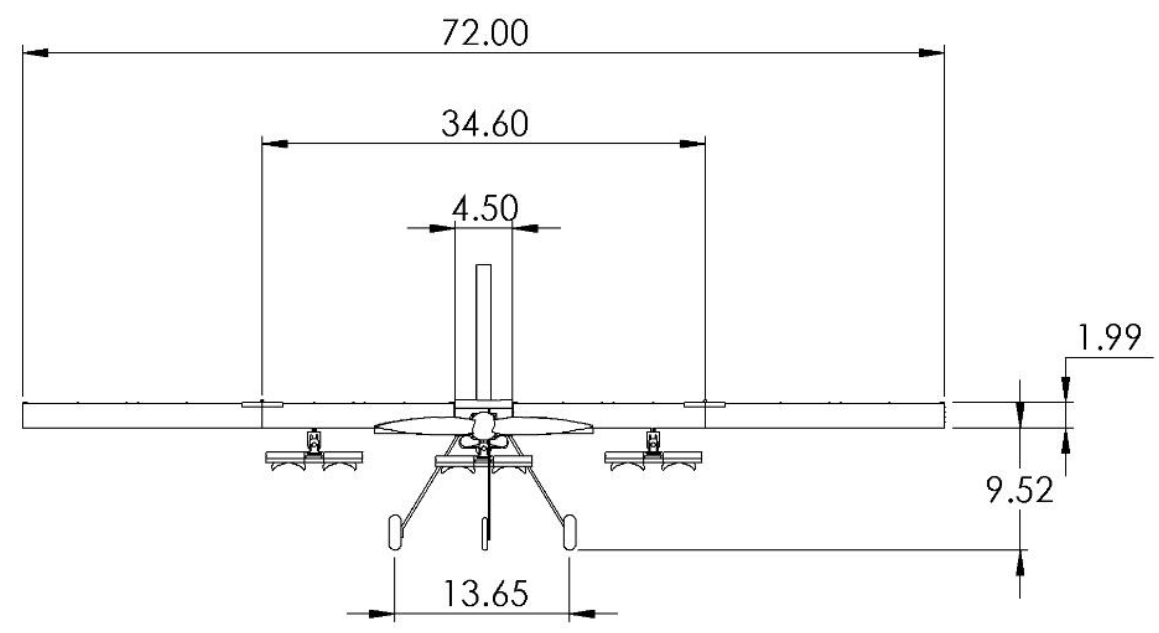
3

2

1



ISO SCALE 1:10



B

B

A

A

4

3

2

1

2/22/2019	Georgia Institute of Technology	
Drawn by: Scott Nealon	Buzzformer	
Checked by: George P. Burdell	Size B	Aircraft Three-view with Dimensions
Scale 1:15	All Dimensions in Inches	Sheet 1 of 4

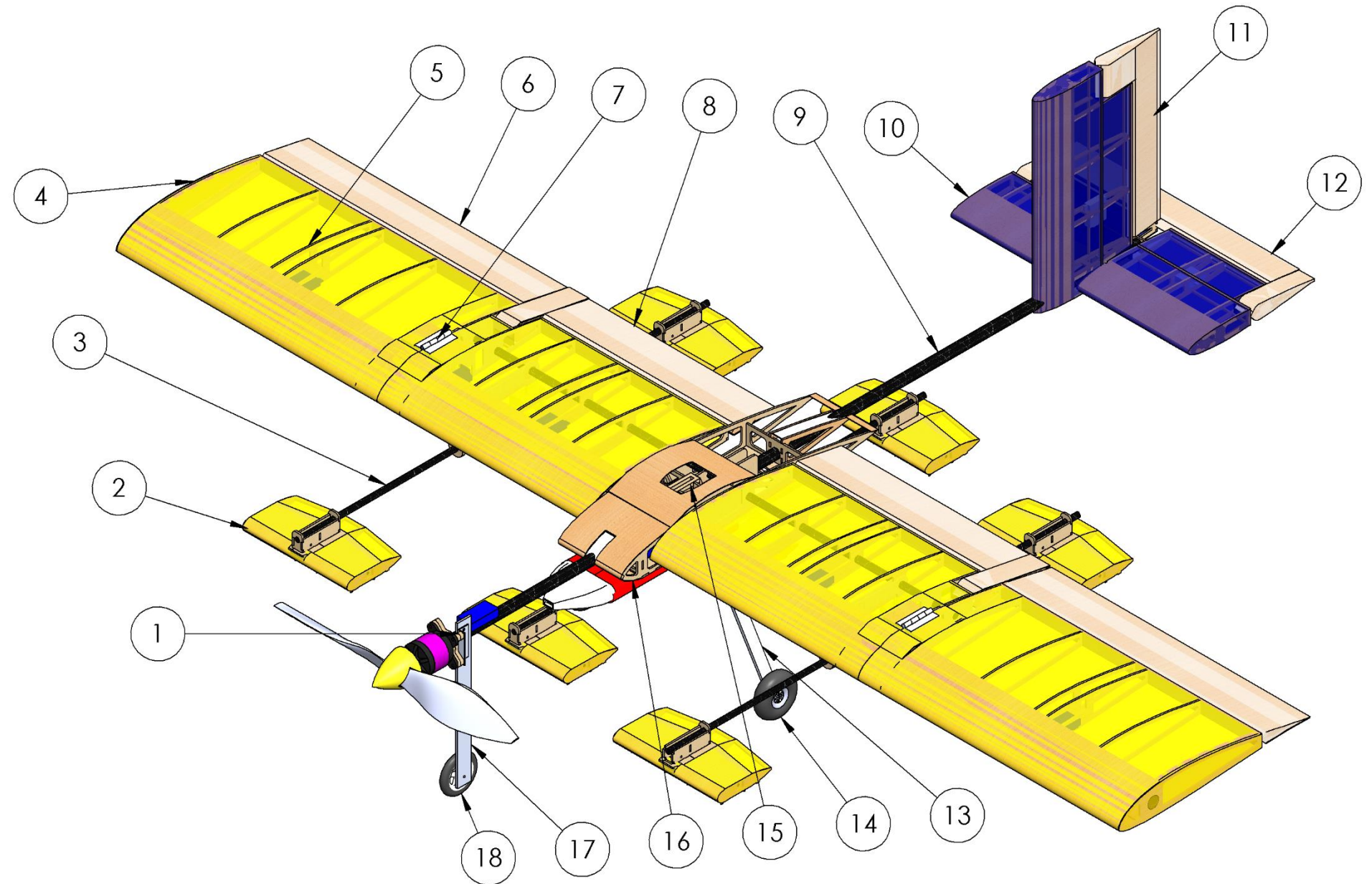
4

3

2

1

PARTS LIST			
ITEM	QTY.	ITEM NAME	MATERIAL
1	2	Motor Mount	Plywood
2	9	Attack Store Release Mechanism	Balsa and Plywood
3	3	Attack Store Boom	Carbon Fiber
4	26	Wing Rib	Balsa and Plywood
5	2	Outboard Wing	Balsa
6	2	Aileron	Balsa
7	2	Wing Hinge	Brass
8	2	Flaperon	Balsa
9	1	Boom	Carbon Fiber
10	1	Empennage	Balsa
11	1	Rudder	Balsa
12	1	Elevator	Balsa
13	2	Rear Landing Gear	Aluminum
14	2	Rear Wheel	Rubber
15	1	Radome Locking Mechanism	Plywood
16	1	Fuselage	Plywood
17	1	Front Landing Gear	Aluminum
18	1	Front Wheel	Rubber



2/22/2019

Georgia Institute of Technology

Drawn by: Scott Nealon

Buzzformer

Checked by: George P. Burdell

Size
B

Aircraft Structural Arrangement

Scale 1:7

All Dimensions in Inches

Sheet 2 of 4

4

3

2

1

B

A

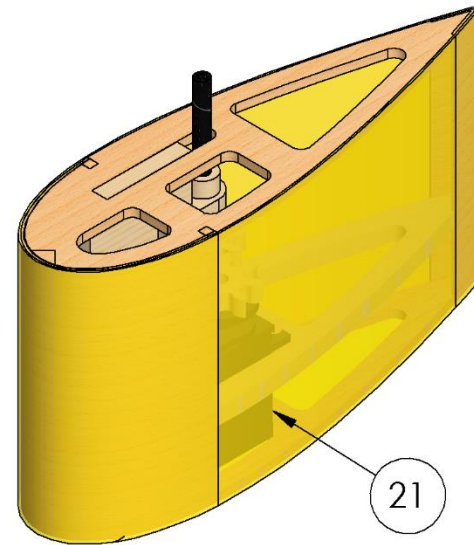
4

3

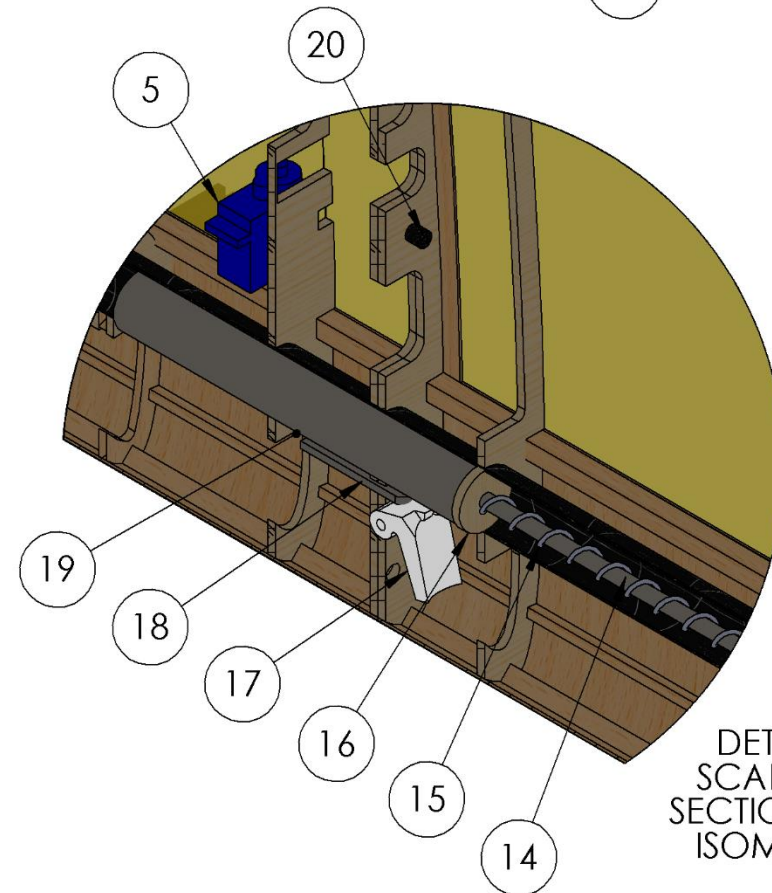
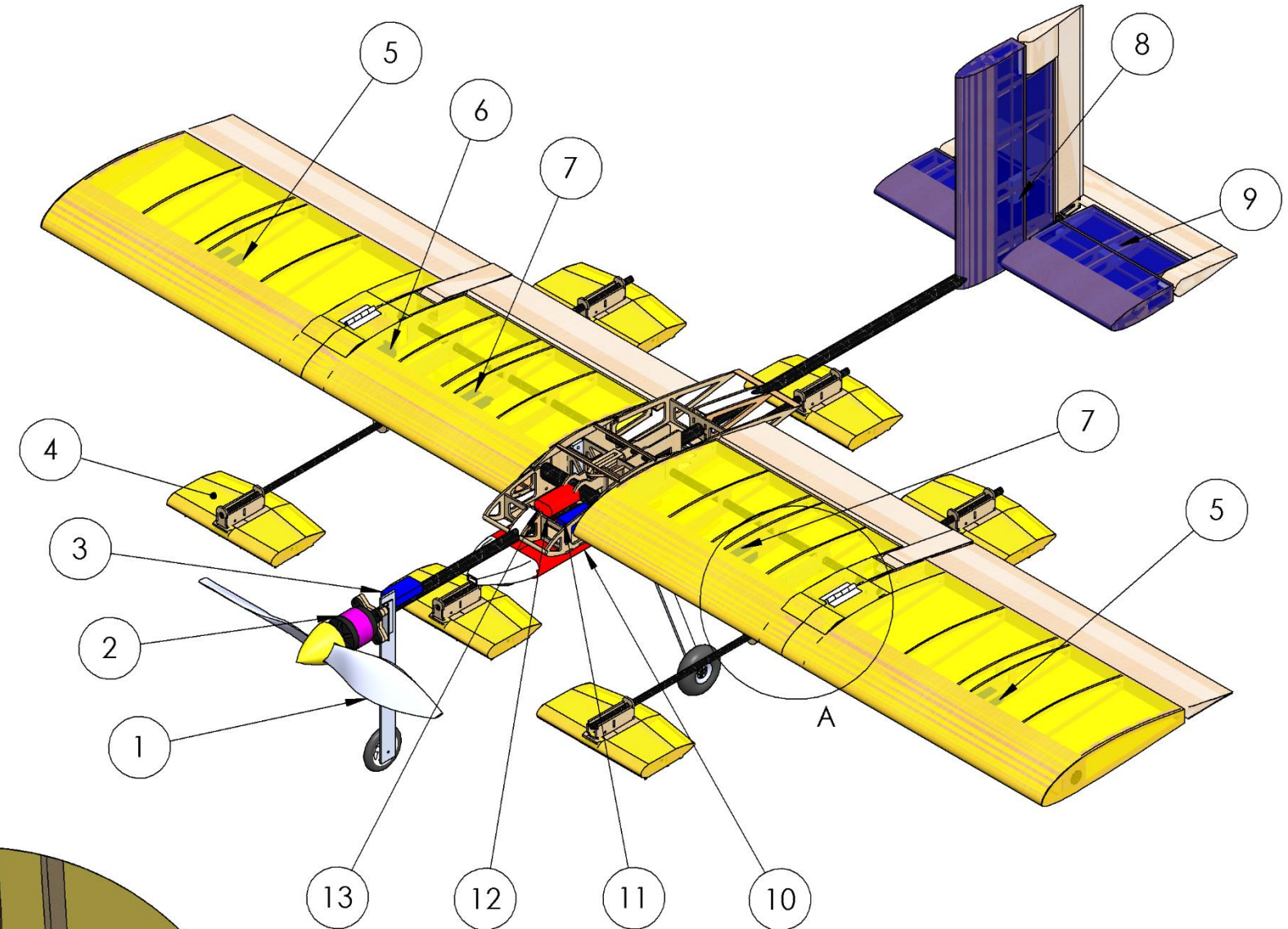
2

1

SYSTEMS LIST			
ITEM	QTY.	ITEM NAME	DESCRIPTION
1	1	Propeller	APC 17 x 10 E
2	1	Motor	Hacker A50-16S
3	1	Speed Controller	Castle Phoenix Edge Lite HV60
4	9	Attack Store Servo	Corona CS-239 MG
5	2	Aileron Servo	TGY-712G
6	2	Wing Hinge Servo	FEETECH FS90R
7	2	Flaperon Servo	TGY-712G
8	1	Rudder Servo	TGY-380 MAX
9	1	Elevator Servo	TGY-712G
10	2	Battery	10 Cell NiMH
11	1	Main Receiver	Futaba R7008SB
12	1	Receiver Battery	4 Cell NiMH
13	1	Attack Store Receiver	Futaba R7008SB
14	2	Guide Rod	Carbon Fiber
15	2	Lock Spring	Spring Steel
16	4	Ferrule Plate	Plywood
17	2	Lock Tab	Nylon
18	2	Lock Pin	Carbon Fiber
19	2	Ferrule	Carbon Fiber
20	2	Shear Pin	Carbon Fiber
21	1	Radome Continuous Servo	FEETECH FS5106R



RADOME SCALE 1:2

DETAIL A
SCALE 1 : 2
SECTION VIEW
ISOMETRIC

2/22/2019	Georgia Institute of Technology	
Drawn by: Scott Nealon	Buzzformer	
Checked by: George P. Burdell	Size B	Aircraft Systems Layout
Scale 1:8	All Dimensions in Inches	Sheet 3 of 4

4

3

2

1

4

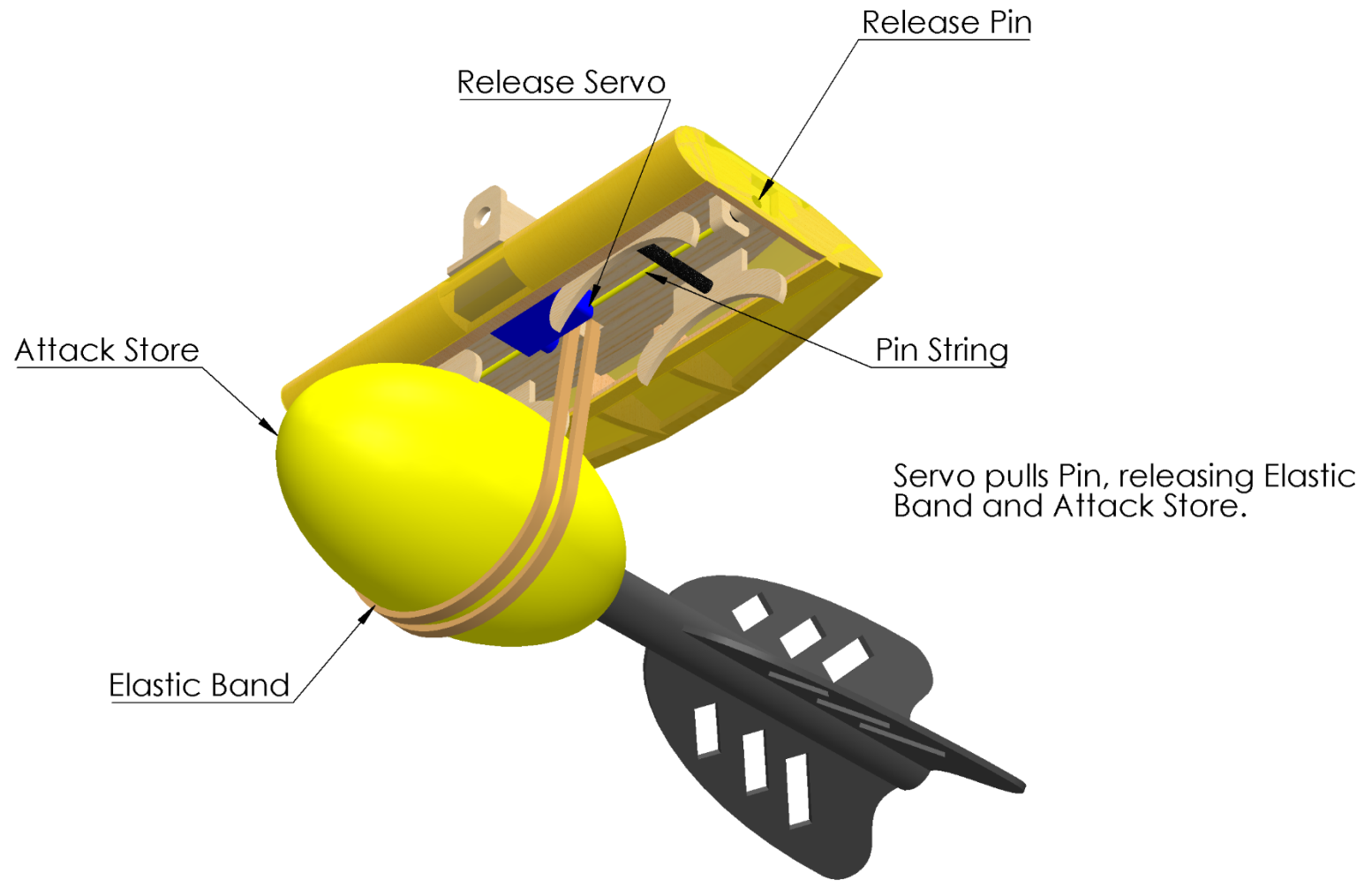
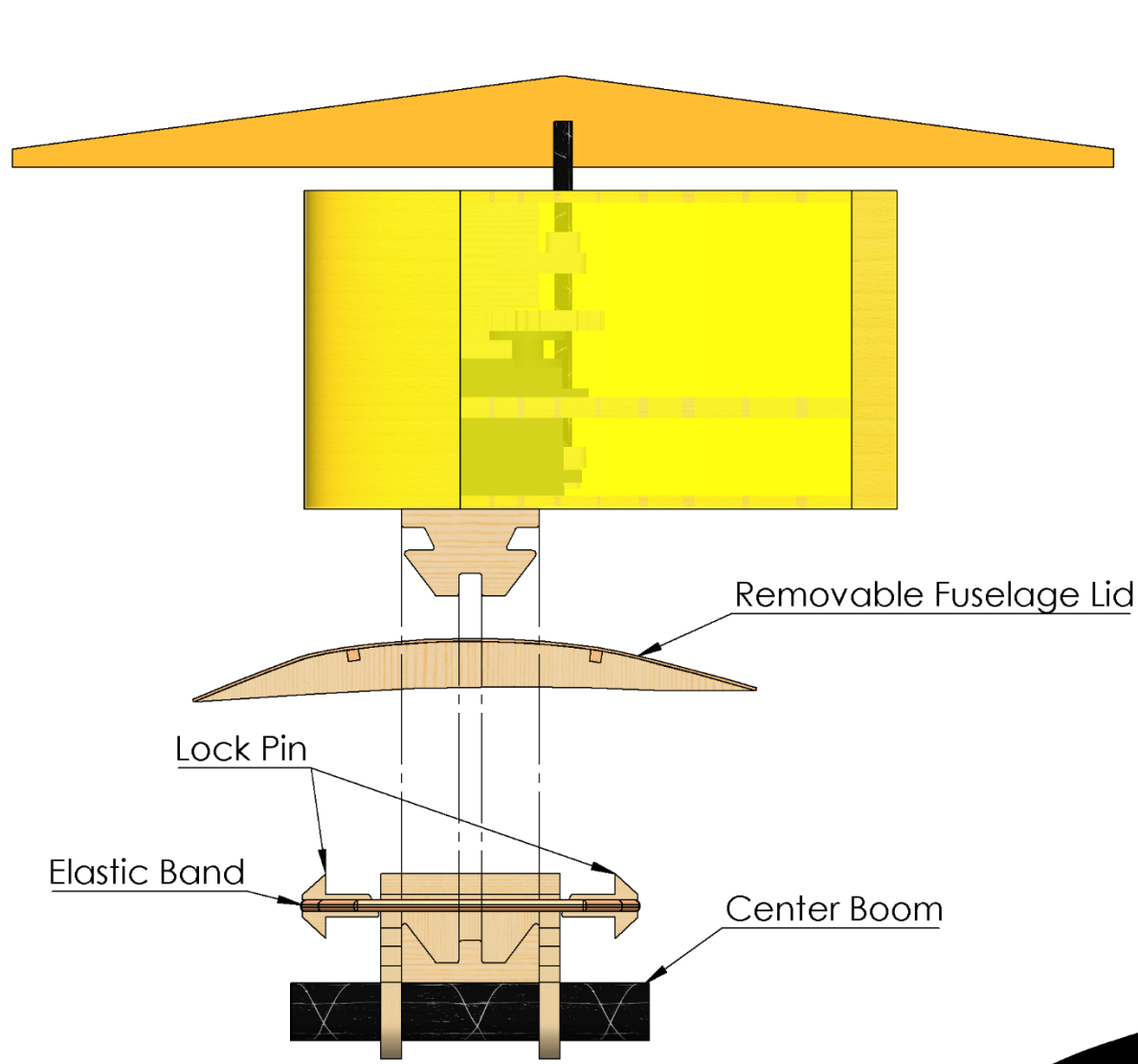
3

2

1

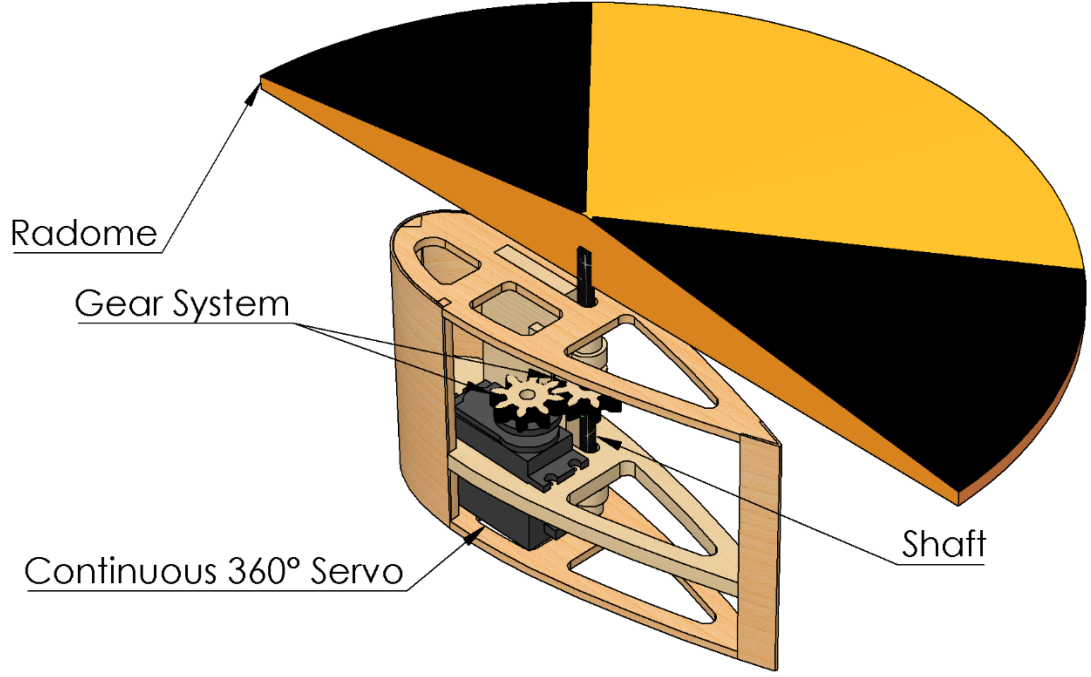
B

B



A

A



2/22/2019	Georgia Institute of Technology		
Drawn by: Scott Nealon	Buzzformer		
Checked by: George P. Burdell	Size B	Aircraft Payload Accommodation	
Scale 1:2	All Dimensions in Inches	Sheet 4 of 4	

4

3

2

1



6 MANUFACTURING

The team considered various manufacturing processes and materials to construct the aircraft. The manufacturing process selected represented the best combination of weight, ease of repair, speed of manufacturing, team experience with the process, and cost.

6.1 Processes Investigated

The team had a wealth of experience using the built-up balsa wood manufacturing technique. However, there were other viable manufacturing processes that could be superior. The most important factors that played a role in the decision of which manufacturing process to use were ranked using Figures of Merit, detailed below and summarized in Table 6.1.

Weight: As with conceptual design, weight was still the most important factor for any design decision and was assigned a FOM of 5.

Ease of Repair: Minor damage is an inevitable part of the testing process so the ability to quickly repair an aircraft must be accounted for and was assigned a FOM of 2.

Ease of Manufacture: The ability to quickly produce aircraft to specification is critical for rapid prototyping to meet important deadlines. It is directly related to Ease of Manufacture and was therefore assigned a FOM of 3.

Experience: The team's knowledge was given some weighting because it relates to the ability of team members to produce quality results, as well as to refine existing techniques. However, since the team is always willing to learn new techniques, experience was only assigned a FOM of 2.

Cost: Keeping in mind that the team had limited resources, cost was added as a FOM. However, since the team emphasizes winning above all, cost was assigned a FOM of 1.

Table 6.1. Manufacturing FOM weighting.

Figure of Merit	0	1	2	3	4	5
Weight						5
Ease of Manufacture				3		
Ease of Repair			2			
Experience			2			
Cost		1				

Based on these Figures of Merit, a number of manufacturing processes and materials common to remote control aircraft construction were investigated. The possible processes that could be used to manufacture the airframe have been detailed below.

Built-up Balsa: Pieces made of competition grade balsa wood are laser cut from CAD models and glued together using cyanoacrylate (CA) adhesive to form the airframe and the tail surfaces of the aircraft.



Carbon Fiber and plywood are used in key areas when required. The aircraft components are then covered with Monokote heat shrink film.

Fiber Reinforced Plastic (FRP): Foam molds are created based on the outer-mold line of the aircraft. A fiberglass-epoxy layup or carbon fiber-epoxy layup is then made within a vacuum bag, and the system sealed for 24 hours to allow for a full cure. The molds are then removed and the reinforced plastic acts as the primary structure.

3D Printed ABS: CAD models are printed using professional grade 3D printers. Print time increases proportionally with the volume of the aircraft.

Foam Core Composite: Large blocks of foam are cut with a hot-wire or CNC router to form the basic shape of the aircraft. Structural reinforcements are locally added if needed, and the entire foam-core is coated in fiberglass or carbon fiber, adding strength as a monocoque.

The processes were evaluated against each other by assigning each one a FOM score, with a score of five indicating a superior choice, three an average choice, and one equaling an inferior choice. All methods were assumed to result in an aircraft designed for an identical load. The results of the comparison are summarized in Table 6.2

Table 6.2. Example manufacturing process selection.

FOM	Value	Manufacturing Process			
		Built-up Balsa	Fiberglass	3D Printing	Foam Core Composites
Weight	5	5	4	2	3
Ease of Manufacture	3	3	2	4	3
Reparability	2	3	4	1	1
Experience	2	5	2	4	3
Cost	1	5	3	2	3
Total	13	55	41	34	35

Based on the Figures of Merit, built-up balsa was considered the best method for the major airframe and empennage structure. However, the team determined that different elements of the design could use different manufacturing processes, such as 3D Printing or Foam Core Composites, to create an aircraft that emphasized the priorities listed in Table 6.1.

6.2 Processes Selected

The team used the above comparison to optimize the built-up balsa and ply technique to achieve the most competitive aircraft by prioritizing speed and weight without sacrificing structural integrity. Of the many ways



to apply built-up balsa and ply, the team chose specific techniques and materials that would minimize the aircraft structural weight without compromising its strength. These strategies are as follows.

Selective Material Use: Since wood can vary significantly in density and strength, the team sorted its entire stock of balsa and ply by weight. The lightest pieces were selected for construction and were cut using the team's laser cutter, with the lightest of the cut parts reserved for the final competition aircraft.

Local Reinforcements: Due to the very low density of balsa used, several inherently problematic locations could potentially fracture during normal operations. Rather than compensate by over-building the entire aircraft, these locations were reinforced with composite or additional balsa, increasing strength with minimal penalty in weight.

Lightening Holes: An efficient structural design eliminated significant loading from most structural members. Lightening holes were integrated into the airframe to reduce weight without reducing the overall stiffness and strength of the aircraft.

Covering: The aircraft was coated with a heat shrink adhesive infused plastic covering material called Monokote.

6.2.1 Airframe Structure

The airframe was constructed using the balsa build-up method to minimize weight. Jigsaw-like parts were laser cut, fit together, and bonded with cyanoacrylate (CA). The center fuselage was made using plywood as it was determined that using balsa for this part would compromise the structural integrity of the plane. Additional balsa sheeting and sticks were cut and bonded on to reinforce and complete the structure.

6.2.2 Control Surfaces and Vertical Tail

The control surfaces and vertical tail were constructed using the balsa build up method to minimize weight. Ribs and spars were laser cut with fitting slots. Balsa sheeting around the entire control surface provided a lightweight way to add stiffness.

6.2.3 Rapid Prototyping

Due to the delicateness of materials used and the fact that each flight test would push the plane to its limits, it was determined that it would be more beneficial to continuously manufacture prototypes rather than attempting to test and constantly repair a single aircraft. Manufacturing techniques were refined, and the team quickly became more efficient in manufacturing the aircraft, with members specializing in different tasks to create an "assembly-line" like structure. This allowed for multiple aircraft modifications to be tested individually in a short period of time. This method of rapid prototyping also extended to subsystems, such as the wing-lock mechanism and the attack store release mechanism. Each iteration of the plane had a new iteration of these mechanisms for concurrent testing and development of not only the basic airframe, but the important subsystems. After design considerations were finalized, a rate of production of one aircraft every 1 to 2 weeks was achieved. Expensive parts such as servos, motors, and landing gear were salvaged from previous prototypes for use in the next iteration.



6.3 Manufacturing Milestones

A production schedule containing manufacturing milestones was established prior to initial prototype manufacturing to ensure a logical, consistent order was followed during construction. Progress was recorded and monitored by the manufacturing lead to ensure all major milestones were met. The Gantt chart that represents this is shown in Figure 6.1, capturing the planned and actual timing of manufacturing steps. While most of the time required for different processes remained the same, some parts, such as the construction of the body, took longer due to the integration of a locking mechanism within the wing sections. The team constructed many prototypes, so Figure 6.1 describes the typical manufacturing timeline for a single aircraft.

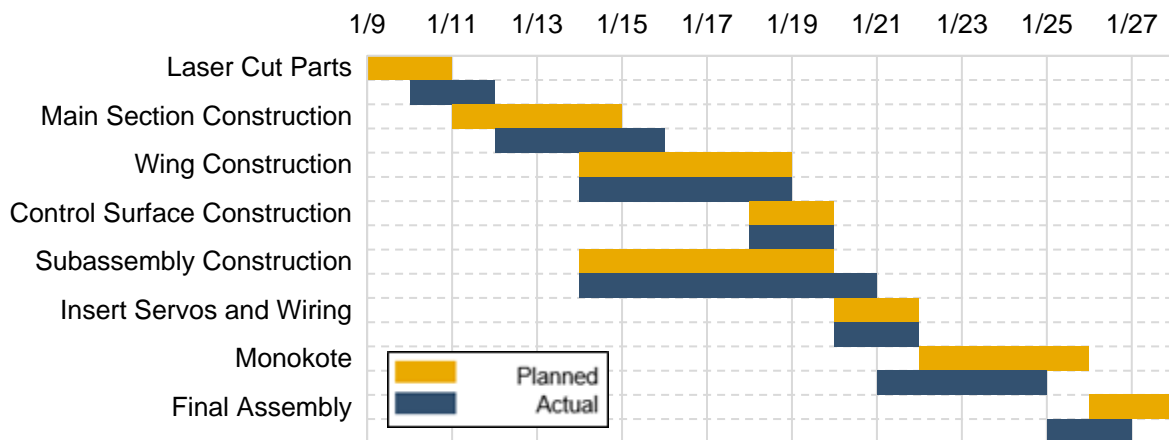


Figure 6.1: Aircraft manufacturing milestone chart showing planned and actual timing of third prototype.

7 TESTING PLAN

A plan for an extensive testing campaign to validate the aircraft and its components was created to ensure functionality and minimize risks of malfunction during flight tests and competition. Testing culminates in test flying a full round of competition flights on the final competition airframe.

7.1 Objectives

The testing was broken up into four main categories: propulsion, structures, subsystems and flight performance. Propulsion testing was done to verify the performance of the combination of motors, propellers and batteries chosen in Section 4.2.2. The objective of the structural testing was to ensure the airframe and wing-locking mechanism's ability to withstand shear, bending and torsion loads in flight. Subsystem testing, which included the wing-locking mechanism, radome mechanism, and attack store release mechanism, required the most time and a variety of testing procedures to prove readiness for flight. Finally, flight performance was tested to ensure integration of all systems and provide verification of performance models.



7.1.1 Propulsion Testing

The motors and propellers tested were based on MotoCalc predictions as expressed in Section 4.2.2. Thrust versus velocity for vehicle performance and power draw for motor performance for each motor-propeller-battery combination were determined using measurements of thrust, torque, RPM, voltage, and current draw. Using data obtained from testing, the team was able to compare the static thrust of the motors to the MotoCalc predictions to gather a better estimate of actual performance. This information allowed the team to select the best propulsion system to achieve the best score possible.

A rig that included a scale to measure thrust as well as an electric motor measurement system was constructed for static testing. The team used the rig to perform static thrust tests and used the data to compare it with MotoCalc predictions. The electric motor parameters were monitored with an EagleTree system that records the RPM, voltage, and current draw of the motor. Custom written software was used to collect the torque and thrust values as well as to remotely control the motor for 30-second intervals with 10-second full thrust intervals and 10-second acceleration and deceleration intervals.

7.1.2 Structural Testing

The wing locking mechanism must be able to sustain a substantial load factor. A test section of the wing was constructed with the wing locking mechanism for independent testing. Using the lift distribution from the vortex lattice analysis, the team found the shear, bending and torsion loads that the locking mechanism needed to withstand. The mechanism was tested to the design load. After multiple tests, the wing-locking mechanism was integrated into the aircraft for flight testing to ensure it could handle those loads in flight.

Additionally, a wing tip test was done to simulate the loading the wings would experience in flight by loading the maximum number of attack stores and lifting at the wing tips. The wing tip test simulates a maneuver resulting in a root bending moment of 2.5g. The test also helped to determine the structural integrity of the wing locking mechanism to ensure that it would not fracture when subjected to these loads.

7.1.3 Subsystem Testing

Wing Locking Actuation: The wing locking mechanism was tested to ensure reliability of the self-locking operation. The wing locking mechanism was prepared in the stowed configuration and remotely converted into the flight configuration.

Radome Mechanism: The radome mechanism underwent a three-phase testing process comprised of ground testing, wind tunnel testing, and flight testing. The radome mechanism was tested using a servo tester to determine the viability of the gearing system. Once verified, the radome mechanism was advanced to testing in a wind tunnel to simulate airflow reaching speeds comparable to those it would experience in flight. Finally, the radome mechanism was incorporated onto the full aircraft to validate whether it could function in actual flight conditions.



Attack Store Release Mechanism: The attack store release mechanism underwent a similar three-phase testing process to the radome mechanism. The attack store release mechanism was tested using a servo tester to verify the elastic band released attack store properly. Then, a row of attack store release mechanisms was tested in a wind tunnel to verify structural integrity at flight speed and to measure produced drag in a variety of configurations to help reduce drag in future iterations. To measure drag, the attack store release mechanisms were suspended from the roof of the wind tunnel. After passing the ground and wind tunnel tests, the attack store release mechanisms were attached to the wing and flown as part of a flight test to ensure it could perform under similar circumstances to competition.

7.1.4 Flight Testing

Flight testing was the culminating point of the iterative design and manufacturing process. It allows the team to compare the estimated aircraft performance against the performance of the prototype. The results can then be used to evaluate the feasibility of the performance targets and identify areas for improvement. Each subsystem was tested thoroughly before being put on the plane, and then the aircraft and subsystems were tested together to make sure every component worked well together. Based on performance, improved designs were suggested, and the process continued until the final iteration.

The team takes a conservative approach to flight testing to avoid damaging or crashing the prototype aircraft during flight testing. The first prototype aircraft was flown without any payloads or subsystems attached and takeoff is not done from the ramp. The aim of the first flight is to verify the function of the propulsion system and aircraft controls, as well as to determine the trim of the aircraft. Once the first flight is completed, subsequent iterations with subsystems can be performed. Ramp takeoff testing similarly began with an empty aircraft without payloads or subsystems. Weight was gradually added to the aircraft to minimize the risk of exceeding the aircraft performance limits. Testing and practicing of Mission 3 begins with minimal payloads loaded onto the aircraft and with each subsequent flight, more payloads are added and the aircraft is flown more aggressively. This gradual envelope expansion minimizes the risk of overloading the aircraft and prematurely depleting the batteries in flight.

Intermediate iterations are currently being used as testing platforms, with changes being implemented based on feedback from assembly teams and the pilot. This form of testing is low risk because the team does not need this version of the aircraft anymore, so preliminary tests can be done to see if the change being made is worth being added to the final aircraft.

The current iteration of *Buzzformer* is being used to verify the required battery size to complete M3. Experience and data gained from all iterations will be used to generate a final design that will go to



competition. The final iteration will fly simulations of the flight missions to verify and validate the aircraft's capabilities as well as train the pilot for competition.

7.2 Schedule

A testing schedule was established mirroring the aircraft design milestone to monitor the success of the propulsion, structure, and subsystem designs. Progress was monitored by the project manager to ensure all tests were conducted in a timely manner. A Gantt chart representing important testing milestones is shown in Figure 7.1.

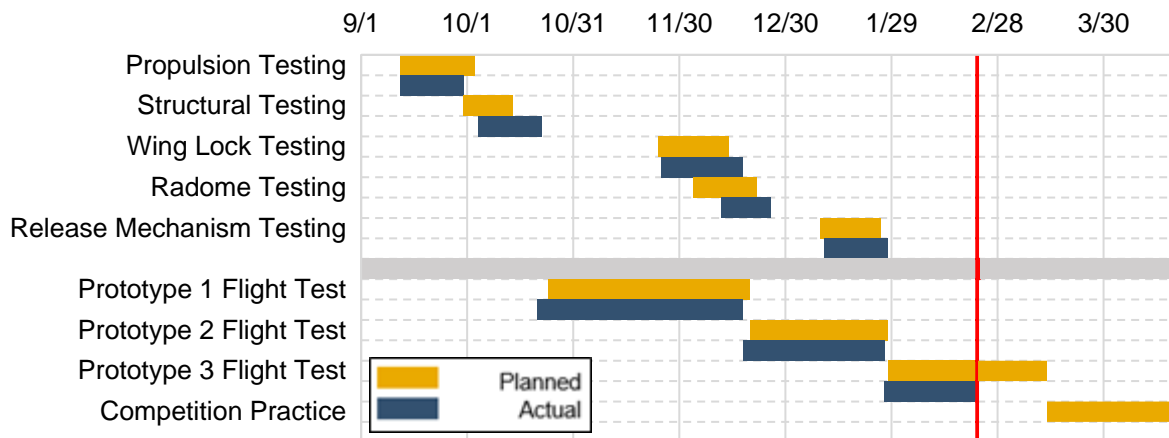


Figure 7.1 Aircraft testing milestone chart showing planned and actual progress.

7.3 Checklists

Various tests have specific procedures which must be followed accurately to produce the desired objectives and ensure safety. This section lists the checklists utilized by *Buzzformer* while conducting tests that required a significant number of steps, such as propulsion and flight testing.

The propulsion test checklist was created to ensure safety while dealing with propellers and electrical equipment and in flight as well as to make sure the test is not wasted due to some mistake in preparation. This checklist was used in the testing of all motor, battery, and propeller combinations.

The flight test checklist was created with the important goal of preventing any system from malfunctioning, which could lead to the in flight failure of aircraft and subsystems; its thorough execution is paramount to the team's success, and it will be used at the DBF event as well. The final checklists are shown in Figure 7.2.



Propulsion Test Checklist	
Before Test	
Propeller.....	Secure
Motor Mount.....	Secure
Connections.....	Secure
Batteries.....	Peaked
Throttle.....	Down
Data System.....	On
Custom Code.....	Running
Testing Rig.....	All Clear
During Test	
Aircraft.....	Restrained
Throttle.....	Full
Current and Voltage.....	Checking
After Test	
Throttle.....	Idle
Battery.....	Disconnected

Flight Test Checklist	
Before Flight	
Propeller.....	Secure
Fasteners.....	Tightened
Connections.....	Secure
Primary Battery.....	Secure/Charged
Control Surfaces.....	Free/Correct
Receiver Pack.....	Plugged In
Receiver Battery.....	Secure/Charged
Radome.....	Secure
Attack Stores.....	Secure
Runway.....	All Clear
After Test	
Throttle.....	Idle
Battery.....	Disconnected

Figure 7.2 Propulsion and Flight Test checklists.

8 PERFORMANCE RESULTS

8.1 Component and Subsystem Performance

8.1.1 Propulsion Tests

Static thrust testing was performed to better measure the available thrust for short takeoff and determine the propeller size that provides the optimal balance of static thrust and high-power draw in this situation. The combination of a Hacker A50 motor and a 20-cell 5000 mAH NiMH battery pack was chosen as the propulsion system using MotoCalc with the method described in Section 4.2.2. This data was verified against data gathered from static test stand testing. Figure 8.1 gives the comparison between the static thrust and power draw data with the chosen propeller system and varying propeller sizes from these tests and the corresponding predicted values from MotoCalc.

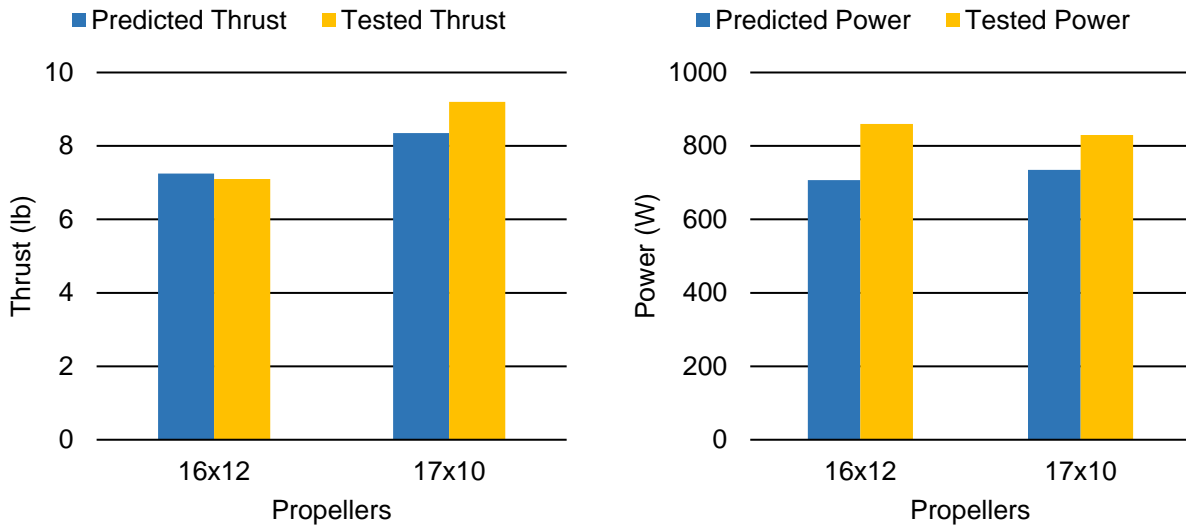


Figure 8.1. Static thrust (left) and power draw (right) predicted by MotoCalc vs tested static thrust and power draw.

Figure 8.1 shows that the static thrust values predicted by MotoCalc are largely validated by the test stand data. In the case of the 17x10 propeller, the combination produced more thrust than was predicted by MotoCalc. A discrepancy exists where the 16x12 propeller's tested power is higher than the predicted power draw. The results indicate the model is reasonably accurate however, it still does not account for various factors such as manufacturing tolerances for the various components and prop blockage caused by the stand.

8.1.2 Structure Tests

A test section of the wing locking mechanism was subjected to the shear and bending loads at its span location on the wing by hanging weights on the main spar once the mechanism was locked together. The section was loaded for 5 seconds and inspected visually for damage. This process was repeated several times to ensure the locking mechanism would survive cyclic loading.

Once the performance of the test section was deemed acceptable, the wing-locking mechanism was incorporated into a prototype aircraft and flown during flight tests. An inertial measurement unit (IMU) was attached to the aircraft to measure the load factor. The test pilot flew the aircraft in laps and increased the bank angle gradually with each test lap. Once the aircraft landed, the IMU data was collected to ensure the maximum achievable load was reached and is still less than the maximum allowable load, and the aircraft structure was once again visually inspected for damage. During flight testing, the maximum instantaneous load factor was measured to be 7.6, well below the designed maximum allowable load factor of 9.



The full-size airplane was subjected to the required wingtip test specified in the rules as a part of the technical inspection process. The wingtip test was conducted for the heaviest aircraft configuration for Mission 3. The successful wingtip test is shown in Figure 8.2.



Figure 8.2. Wingtip test of fully loaded aircraft.

8.1.3 Subsystem Tests

Wing locking Mechanism: The wing lock mechanism was successfully able to remotely convert between stowed configuration and flight configuration. This was demonstrated through a subsequent wingtip test.

Radome Mechanism: The radome mechanism's gearing system was validated during the ground test. During the wind tunnel test, the radome mechanism was successfully able to rotate at various angles of attack between -20° and 20° . This is shown in Figure 8.3. During the flight test, the radome mechanism was successfully able to start and stop rotations on command throughout the flight, including during tight turns. This is shown in Figure 8.4.



Figure 8.3. Radome function testing in wind tunnel.

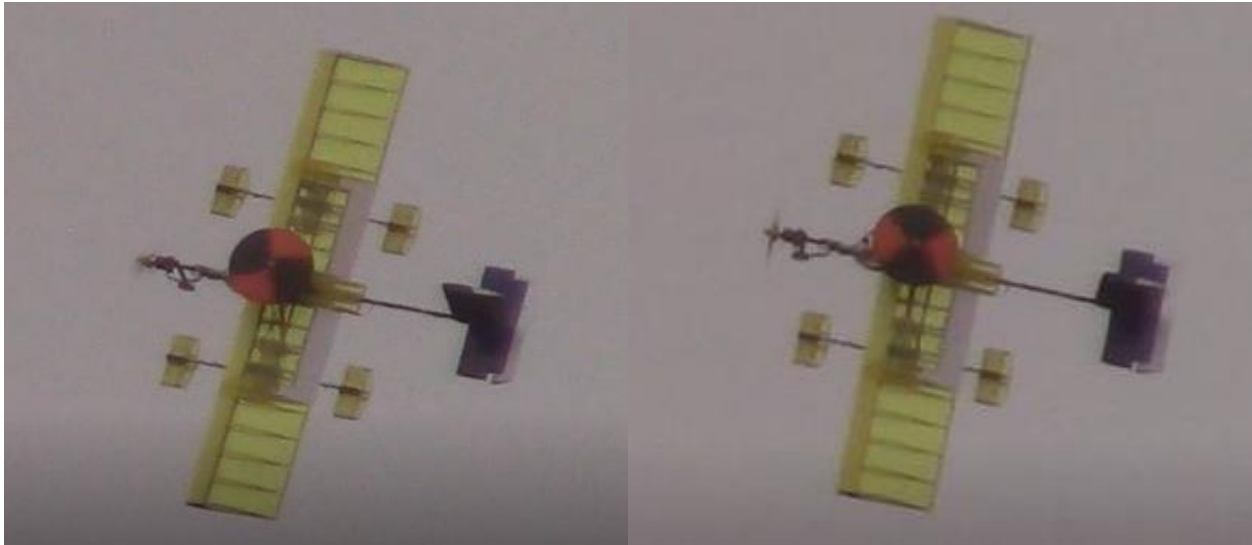


Figure 8.4. Radome function test in flight.

Attack Store Release Mechanism: The attack store release mechanism was successful in dropping attack stores during the ground test. In the wind tunnel test, the increase in drag between the test without the attack stores and with the attack stores was found to be 3 ounces at 37 miles per hour. Using the density of air in the wind tunnel, the ΔC_D caused by a single attack store was found to be 0.0013 resulting in a ΔC_D of 0.0234 between M1 and M3. This is slightly less than the predicted ΔC_D of 0.03 from Table 4.4, potentially due to the tandem arrangement reducing the total front cross sectional area of the attack stores. The attack store drop mechanism was integrated into the full aircraft and was able to successfully deploy the attack stores on command. The tests are shown in Figure 8.5.

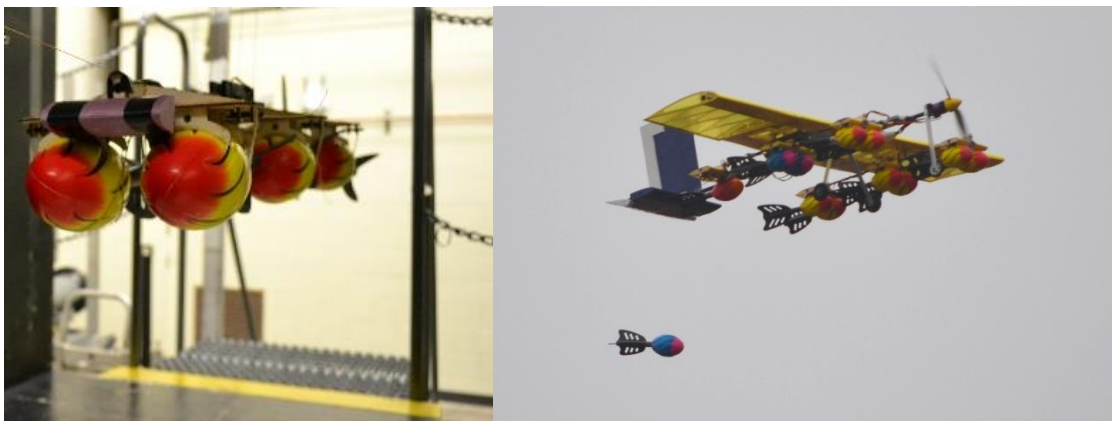


Figure 8.5. Attack store release mechanism testing in wind tunnel (left) and in flight (right).



8.2 System Performance

A practice Ground Mission was performed according to the rules and is shown in Figure 8.6. The time required to complete the Ground Mission was 34 seconds which is already significantly faster than the target. The team believes with further improvements to the aircraft and more practice, the Ground Mission time could be improved.



Figure 8.6. Ground Mission practice.

The dimensions of the aircraft were verified on the prototype aircraft. A mockup of a box with the same height and width was constructed from wooden sticks. The prototype aircraft was rolled through the mockup to verify that the dimensions comply with the aircraft requirements. The height, width, and maximum distance between the nose and rear landing gear were demonstrated to be within the limits. A picture of this test is shown in Figure 8.7



Figure 8.7. Dimension verification test using a mockup of the box.



Takeoff tests were completed as a part of flight testing. The aircraft was able to takeoff reliably from the ramp without headwind. More takeoff tests are planned for the future with the inclusion of subsystems and additional weight. A picture of ramp takeoff testing is shown in Figure 8.8.



Figure 8.8. Ramp takeoff testing.

The team equipped the aircraft with a data collection system that could capture GPS data in order to compare the actual trajectory to the estimated mission trajectory outlined in Section 4.6. Competition length laps were flown with team members signaling turns visually in accordance with competition rules. Figure 8.10 shows a simulated aircraft trajectory for a single lap compared to the recorded aircraft trajectory for M2 and M3 and Figure 8.9 shows the recorded flight path of a single lap.

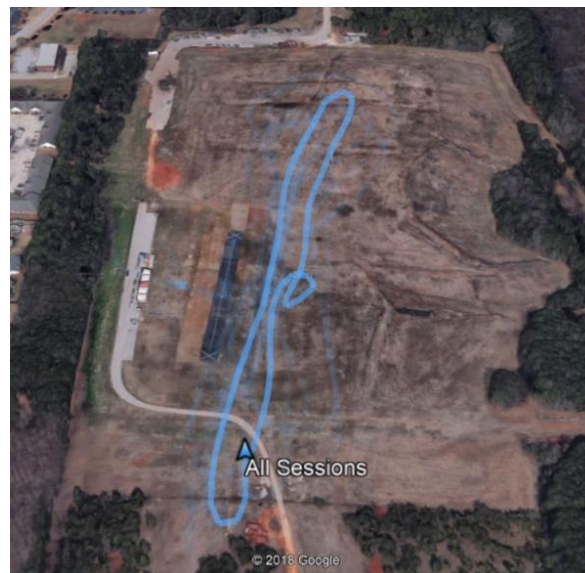


Figure 8.9. Recorded flight path of a single competition lap.

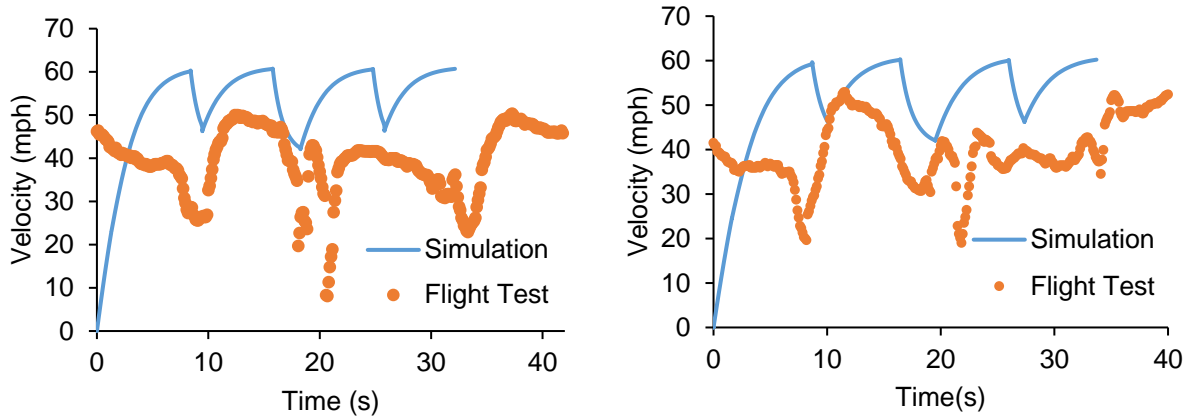


Figure 8.10. Simulated vs. flight test lap trajectories for M2 (left) and M3 (right).

Table 8.1 shows the aggregated system performance from various flight tests of the current iteration. The results indicate the performance predictions were realistic. The team hopes to improve system performance with further improvements of the aircraft such as weight and drag reduction and increasing pilot familiarity to exceed the current performance.

Table 8.1. Predicted vs. flight test performance results.

	1 st Lap Time (s)		Time for 360 (s)		Laps Flown		Max. Speed (mph)	
	Pred.	Act.	Pred.	Act.	Pred.	Act.	Pred.	Act.
M1	28.2	40.4	7.4	10.3	-	-	65.2	50.4
M2	32.1	43.8			-	-	60.7	50.3
M3	33.7	43.6			18	12	60.3	52.9

The difference between the predicted performance and the actual performance can be attributed to a combination of factors. The weather conditions on the day of the flight test were poor. The cold temperature impeded the performance of the NiMh battery packs. There was also a significant crosswind measuring up to 10 miles per hour. One very important aspect is pilot behavior. The simulations were made with the assumption of no delay between the end of one maneuver and the beginning of the next. In addition, miscellaneous delays such as recognizing the visual signal to turn are not captured in the simulation either. The rest of the discrepancies can be attributed to inaccuracies in aircraft thrust and drag estimation which affect performance.

Since Mission 3 is the most important flight mission according to the analysis in Section 3, more emphasis is placed on Mission 3 flight testing. Flight testing of the attack store mechanisms have demonstrated the ability to reliably drop attack stores on command and prevent inadvertent attack store releases. In order to



reduce the risk of losing prototype aircraft, the team did not immediately attempt Mission 3 with all 18 attack stores attached. Mission 3 testing is currently ongoing with more attack stores being added once reliable takeoff and completion of Mission 3 inside the allotted ten minute window has been demonstrated.

While pilot familiarization and experience can help improve the flight score, the team is also committed to continually making improvements to the aircraft especially to weight and drag reduction which have major effects on flight and mission performance. The team has completed 15 flights of prototype aircraft with increasing number of developed subsystems as of the time of report. The current prototype is shown in Figure 8.11. The team is awaiting more testing opportunities before the competition to make further improvements on the aircraft and meet the target mission performance. The concept of a single-engine mono-wing conventional aircraft proved to be capable of meeting the aircraft requirements and completing all missions. The team is confident that the overall configuration for *Buzzformer* has the best scoring potential and is well positioned to compete and succeed in Tucson.



Figure 8.11. *Buzzformer* in Mission 3 configuration.



9 BIBLIOGRAPHY

- [1] Gundlach, J., *Designing Unmanned Aircraft Systems: A Comprehensive Approach*, 2nd ed., American Institute of Aeronautics & Astronautics, 2012.
- [2] Anderson, J. D., *Fundamentals of Aerodynamics*, 4th ed., McGraw Hill, 2004.
- [3] Drela, M., and Youngren, H., "XFOIL", *Massachusetts Institute of Technology* [online], 2013, <https://web.mit.edu/drela/Public/web/xfoil/> [retrieved 21 February 2018]
- [4] Lyon, C.A., Broeren, A.P., Giuere, P., Gopalarathnam, A., and Selig, M.s., "Summary of Low-Speed Airfoil Data Vol. 3", December 1997.
- [5] Drela, M., and Youngren, H., "AVL Overview", *Massachusetts Institute of Technology* [online], 2008, <http://web.mit.edu/drela/Public/web/avl/>. [retrieved 21 February 2018],
- [6] Hoerner, S. F., *Fluid Dynamic Drag*, 2nd ed., Published by author, 1992.
- [7] Phillips, W. F., *Mechanics of Flight*, 1st ed., Wiley, Hoboken, NJ, 2004.



joanneum
AERONAUTICS

2018-2019
Aircraft Design Report

FH JOANNEUM
University of Applied Sciences

Graz
Austria

Contents

1	Executive Summary	3
1.1	Description of Selected Design	3
1.2	Key Mission Requirements	3
1.3	Performance of the System	4
2	Management Summary	5
2.1	Team Organization	5
2.2	Milestone Chart	6
3	Conceptual Design	6
3.1	Mission Requirements	7
3.2	Translation of the Mission Requirements into Design Requirements	12
3.3	Configurations Considered	13
3.4	Concept Weighting and Selection Process	13
3.5	Final Conceptual Design Configuration	17
4	Preliminary Design	17
4.1	Design Methodology	17
4.2	Design Trades	18
4.3	Mission Model	20
4.4	Aerodynamics	22
4.5	Stability and Control	27
4.6	Estimated Aircraft Performance	30
5	Detail Design	31
5.1	Dimensional Parameters	31
5.2	Structural Characteristics	32
5.3	Systems and Sub-Systems Selection, Integration and Architecture	35
5.4	Weight and Balance	39
5.5	Flight Performance	40
5.6	Mission Performance	41
5.7	Drawing Package	41
6	Manufacturing Plan and Processes	46
6.1	Manufacturing Processes Investigated	46
6.2	Manufacturing Processes Selected	47
6.3	Manufacturing Milestone Plan	49
7	Testing Plan	49
7.1	Objectives and Schedule	49
7.2	Ground Test	50
7.3	Flight Test	52
7.4	Checklists	53
8	Performance Results	55
8.1	Performance of Key Subsystems	55
8.2	System Performance	57
8.3	Differences to Predictions and Improvements	58
	Bibliography	59

1 Executive Summary

This report describes the design, production and testing processes adopted by the FH JOANNEUM, University of Applied Sciences, Graz, Austria to compete in the 2018/19 Design, Build and Fly contest (DBF) by the American Institute of Aeronautics and Astronautics (AIAA). The objective was to design a multi-purpose aircraft to support carrier operations. The aircraft must have foldable surfaces such that it will fit inside a box of 3x2x2 ft. This box represents the elevators on an aircraft carrier. Additionally, the aircraft needs to be able to take off from a 10-foot-long ramp and must carry payload in form of a radome and a minimum of four ejectable dart rockets. To ensure a successful takeoff from the ramp, the aircraft must be restrained by a crew member with a tail hook during power up.

1.1 Description of Selected Design

After analyzing the scoring criteria, the team decided to develop a light and fast aircraft, while maximizing the payload to maximize the flight score. The first step in the design process was the conversion of the mission and scoring criteria into a list of design metrics. These metrics were used to decide on the conceptual design of the aircraft. During the preliminary design phase, the aircraft was further defined by evaluating different wing and control surface configurations, motors and propellers. A monoplane configuration was identified as the most promising option because it allows for the attachment of a large number of attack stores and offers more options for a folding system solution. Its design simplicity allowed the team to devote energy to design a reliable and light-weight folding mechanism and a mechanism for ejecting the attack stores. After the calculation of the aerodynamic characteristics and a simulation of the estimated mission performance, FH JOANNEUM's aircraft *Bobby* went into the detailed design phase for finalizing the dimensions, the propulsion unit and the integration of all components.

1.2 Key Mission Requirements

Scoring sensitivity analysis was done for each mission to determine which scoring parameters have the highest effect on the overall score. The team identified four key mission requirements that most affect the design: payload requirement, folding surfaces, takeoff scenario and the flight time.

Two of the three flight missions require the aircraft to carry payload. Mission 2 (M2) requires a rotating radome that must be mounted on the centerline of the fuselage and Mission 3 (M3) requires a number of attack stores to be carried externally. The number of attack stores carried has a significant impact on the total mission score and defines the number of laps that have to be flown. Since the number of attack stores has such a great impact on the overall score, concessions to the aircraft's speed and weight were accepted, and the aircraft was designed to carry fourteen attack stores. The mounting mechanism for both kinds of payload needs to be easily accessible, since this has an influence on the ground mission score.

The requirement of foldable surfaces results from the fact that the minimum wingspan of four feet is longer than the available width of the box in which the aircraft must fit. Furthermore, the aircraft must transition from the stowed configuration to flight configuration remotely and mechanically lock prior to each mission. This needs to be taken into consideration when designing the wings and the fuselage.

The takeoff scenario stipulates that the aircraft is required to take off from a 10-foot-long ramp with a gradient of 5 degrees. To meet the takeoff requirement, a balance must be achieved between the wing area, propulsive power and weight. This was accomplished by building a light-weight structure in combination with a large wing area and a strong propulsion system.

Finally, flight time was identified as the fourth key mission requirement. M2 requires the aircraft not only to carry the payload but also to finish the laps in a certain amount of time. This time limit is not directly set by the rules but by the other teams, since the score is derived from the relation of the fastest time to the team's time. Therefore, a powerful propulsion system was chosen in order to maintain a continuous near full-throttle flight.

1.3 Performance of the System

FH JOANNEUM's contest aircraft (Figure 1) is the result of the design parameters created to maximize scoring. The aircraft was designed to minimize weight and payload loading time as well as performing well under the given takeoff constraints whilst maximizing speed and payload capabilities. *Bobby* will take off at 33 ft/s before climbing to cruise altitude and velocity. *Bobby* will complete M2 in 105 s and will be able to carry 14 dart rockets for M3. The aircraft will be able to transition from the stowed configuration to the flight configuration in 10 s. The wingspan in flight configuration is 6.88 ft and the maximum takeoff weight yields to 16.99 lbs.



Figure 1: *Bobby* in flight

2 Management Summary

The *joanneum Aeronautics* team from the FH JOANNEUM, University of Applied Sciences consisted of 29 students: 19 students of the master’s program and 10 undergraduates. The team is entirely student-led but receives guidance and suggestions from faculty members at weekly meetings and design reviews. All team members have experience in different fields such as engineering, building and flying model aircraft and management.

2.1 Team Organization

The hierarchical structure of the *joanneum Aeronautics* team establishes leadership and responsibility among the master’s students, where undergraduate students assume less responsibility. This hierarchy only served as an outline, as all team members worked closely together to meet deadlines, share ideas and learn from each other. During the design phase, tasks were divided into three main branches: management, technical documentation and engineering. The Contest Manager and Chief Engineer divide tasks such that the chief engineer supervises design, build and test efforts while the Contest Manager sets major milestones and obtains funding and manages team logistics. In addition, a student is solely responsible for documenting all important steps in the design process and writing all required documents. Figure 2 shows the different positions and roles of each team member.

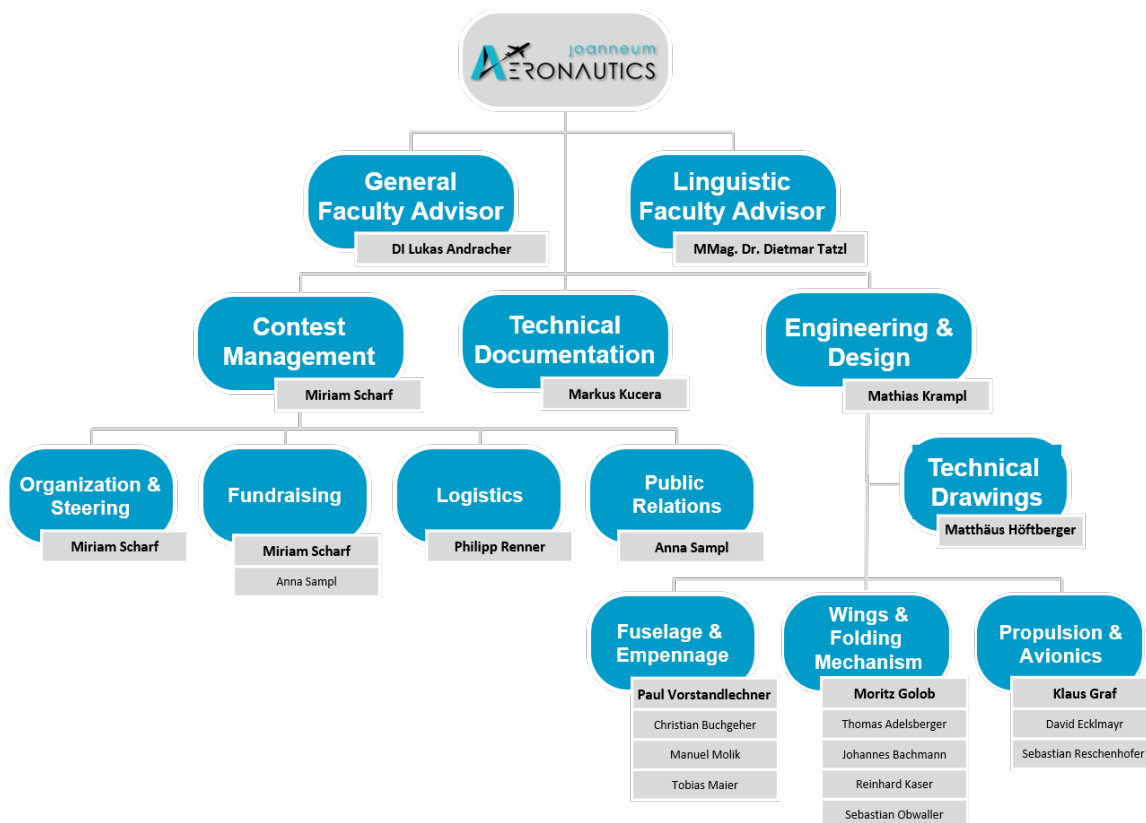


Figure 2: The *joanneum Aeronautics* team structure for the 2018/19 DBF contest

2.2 Milestone Chart

A milestone chart was established at the beginning of the design process to mark major deadlines, design objectives and manufacturing goals. Progress was monitored by the team leaders throughout the entire process, while the team members of all branches met weekly to discuss the work completed. The milestone chart is shown in Figure 3, capturing the planned and actual timing as well as major milestones.

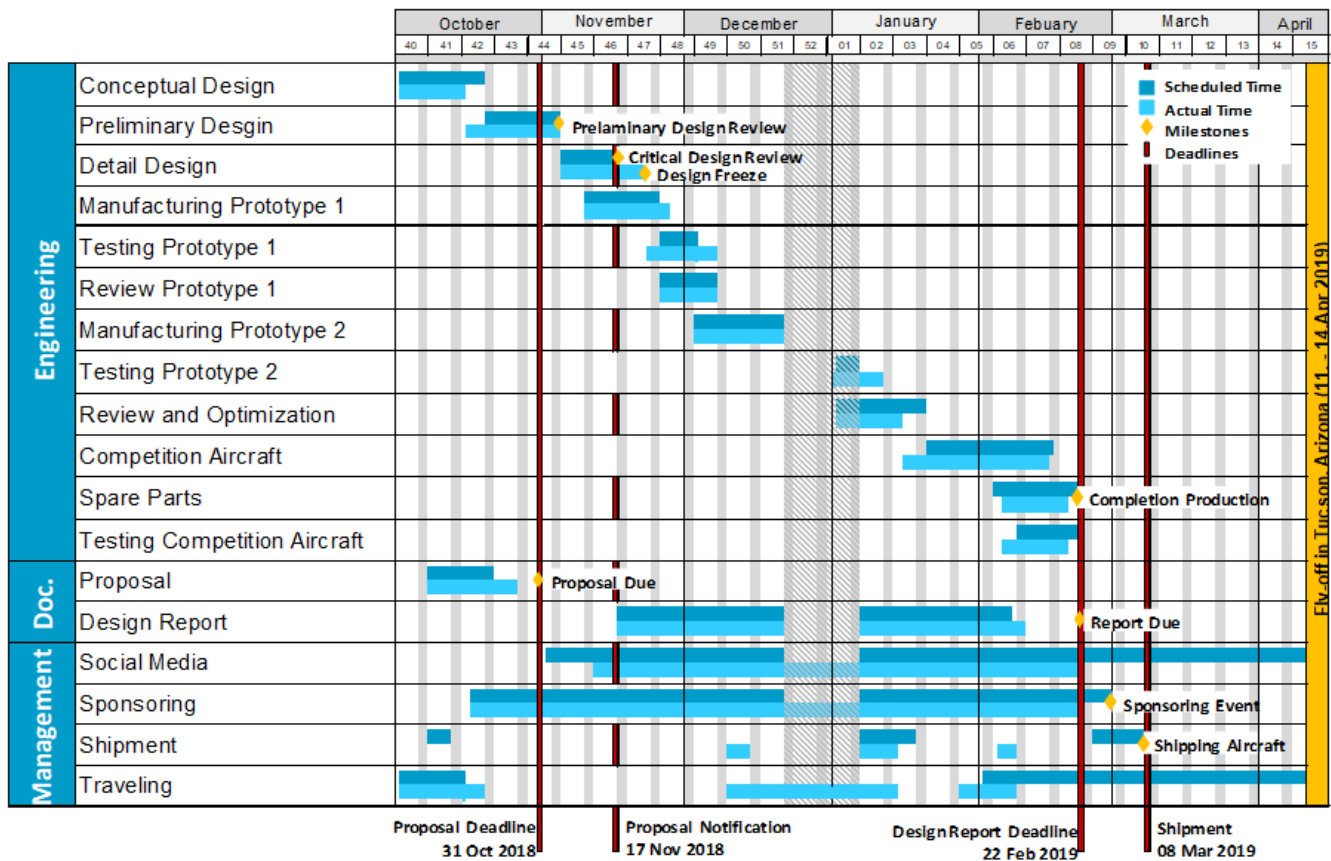


Figure 3: joanneum Aeronautics Gantt chart of the preparation phase for DBF 2019

3 Conceptual Design

The conceptual design phase was primarily used to analyze the mission requirements and translate them into design parameters and outline a feasible configuration that has the greatest potential to maximize the final score. Additionally, a quantitative scoring analysis was performed in order to identify the scoring drives. The scoring analysis and mission requirements were translated into Figures of Merit (FOMs), a metric to weigh different solutions against each other to find the most promising aircraft configuration. The FOM were applied to a design space consisting of various possible configurations and yielded a conceptual design. The resulting configuration is a

conventional airplane with a tricycle landing gear, high-wing design and a single engine. The conceptual solution for the folding surfaces is to horizontally sweep the wings backwards.

3.1 Mission Requirements

3.1.1 Mission and Score Summary

The AIAA Design/Build/Fly competition 2019 scoring consists of one ground mission three flight missions and a design report. The overall score for each team is calculated as shown in Equation 3.1.

$$SCORE = Written\ Report\ Score * Total\ Mission\ Score \quad (3.1)$$

The Total Mission Score will be computed from the Flight Missions and Ground Missions Score using Equation 3.2.

$$Total\ Mission\ Score = M1 + M2 + M3 + GM \quad (3.2)$$

The ground mission (GM) can be attempted at any time, whereas the flight missions have to be flown in order. The GM score is dependent on the loading time. For a short loading time, the aircraft must have an easily accessible and fast locking mechanism for securing the payload of M2 and M3. The loading time is measured for two turns. First the payload for M2 needs to be attached and then, in the second run, the payload for M2 will be removed and the minimum payload for M3 will be attached. The sum of these two runs is the loading time. The final GM score is the ratio between the fastest time among all teams and the loading time of the team, as shown in Equation 3.3.

$$GM = \frac{Fastest\ Time}{Time} \quad (3.3)$$

All three flight missions are flown along the same pattern. Figure 4 shows the competition track, which consists of two 1000 ft straights and one 360-degree turn. A successful lap is defined as beginning and ending at the start/finish line while the aircraft is still airborne. The required number of laps is dependent on the mission. The maximum takeoff distance is limited to a ramp with the length of 10 ft and a launch angle of approximately 5 degrees. To successfully finish each mission, a landing on the paved runway without significant damages is required.

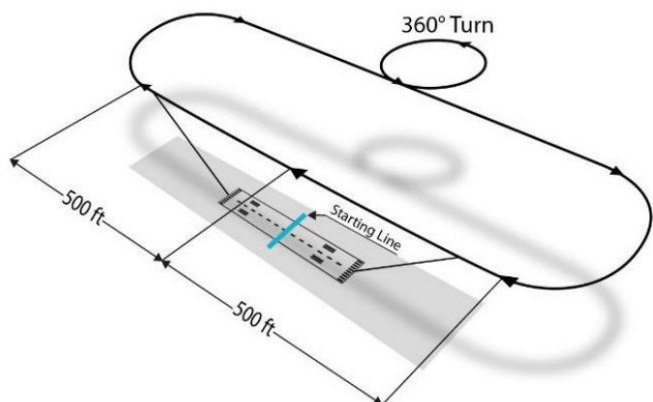


Figure 4: AIAA competition Flight Course

The starting procedure for all three flight missions is as follows: The aircraft enters the staging area in the stowed configuration and must be remotely controlled to the flight configuration with a following wing tip locking test. The

required payload needs to be secured during the staging time of five minutes. Takeoff is from the launch ramp, whereby a ground crew member manually restrains the aircraft during power up and releases it at the pilot's command.

Mission 1 - Delivery Mission: For Mission 1 (M1) no payload is required. The aircraft must complete three laps within a flight window of 5 minutes. A successful completion of this mission is rewarded with 1.0 points (Equation 3.4).

$$M1 = 1.0 \text{ for successful mission} \quad (3.4)$$

Mission 2 - Reconnaissance Mission: The required payload for Mission 2 (M2) is the radome with the dimensions stated in Table 1. The radome shall only rotate after the completion of the first 180-degree turn until the completion of the final 180-degree turn. The aircraft must complete 3 laps within five minutes. As Equation 3.5 states, the score for this mission is computed as the ratio of the fastest time of all teams to the team's total time for three laps plus 1.

$$M2 = 1 + \frac{\textit{Fastest Time Flown}}{\textit{Flown Time}} \quad (3.5)$$

Table 1: Payload composition for Mission 2

Payload	Sizing		
	Diameter	Thickness	Weight
Radome	12.00 in	1.00 in	8.48 oz

Mission 3 - Attack Mission: The required payload for Mission 3 (M3) consists of a number of team selected, but at least 4, dart rockets (Figure 5). Each dart rocket has a length of about 10 in, maximum diameter of around 3 in and weighs about 3 oz. On the down wind leg of the pattern, a single store must be dropped, by remote command. A scoring lap is a drop of a single store on the down wind leg. If more than one store is dropped, the lap does not count as a scoring lap. There will be a ten-minute time window for this mission. Equation 3.6 shows that the resulting score for this mission is the sum of 2 plus the number of scoring laps.

$$M3 = 2 + \textit{number of scoring laps} \quad (3.6)$$



Figure 5: Dart rockets as payload for Mission 3

3.1.2 Aircraft Constraints

In addition to the flight missions, the aircraft must meet the following constraints:

Takeoff

- Takeoff from 10-by-4 ft launch ramp which has an inclination of approximately 5 degrees.
- Aircraft must not touch the ground beyond the high side of the ramp.
- Aircraft must be restrained during power up by one team member

Configuration Conversion

- The aircraft must be radio-commanded from the stowed configuration into the flight configuration.
- All folded surfaces must be moved electrically and must be locked mechanically in flight configuration.
- Folded surfaces or other components must not temporarily separate from the aircraft.

Propulsion System

- The aircraft must be propeller driven and electrically powered.
- Batteries must be Nickel-Cadmium (NiCd) or Nickel-Metal Hydride (NiMH).

Payload

- The radome must be mounted horizontally on the aircraft centerline and must be able to rotate.
- There must be a minimum clearance of 3 inches between the radome and any surface of the aircraft.
- The aircraft must be able to carry a minimum of four dart rockets under the wings.
- There must be a minimum clearance of 0.5 inches between the darts and any part of the aircraft.

Sizing

- The aircraft must have a minimum wingspan of four feet.
- It must have foldable surfaces, so that it can roll through a box that is 3 feet wide and 2 feet high.
- The nose of the aircraft and all landing gear must fit within the box within a depth of 2 feet.

3.1.3 Flight Score Sensitivity Analysis

A sensitivity study is a tool to compare different solutions with variables such as weight, speed, time or battery capacity. A sensitivity study on the flight score drivers was performed to gain an understanding of the influence of each flight mission. With the formulas introduced in Section 3.1.1 and an assumption of 60 s for the best M2 time, an initial score analysis was performed. As it can be seen in Figure 6, the number of scoring laps for Mission 3 has the biggest impact on the overall flight mission score. Since the total mission score changes only slightly with the M2 time, it is not justifiable to optimize the design for the second mission. It was, therefore, decided to maximize the number of dart rockets.

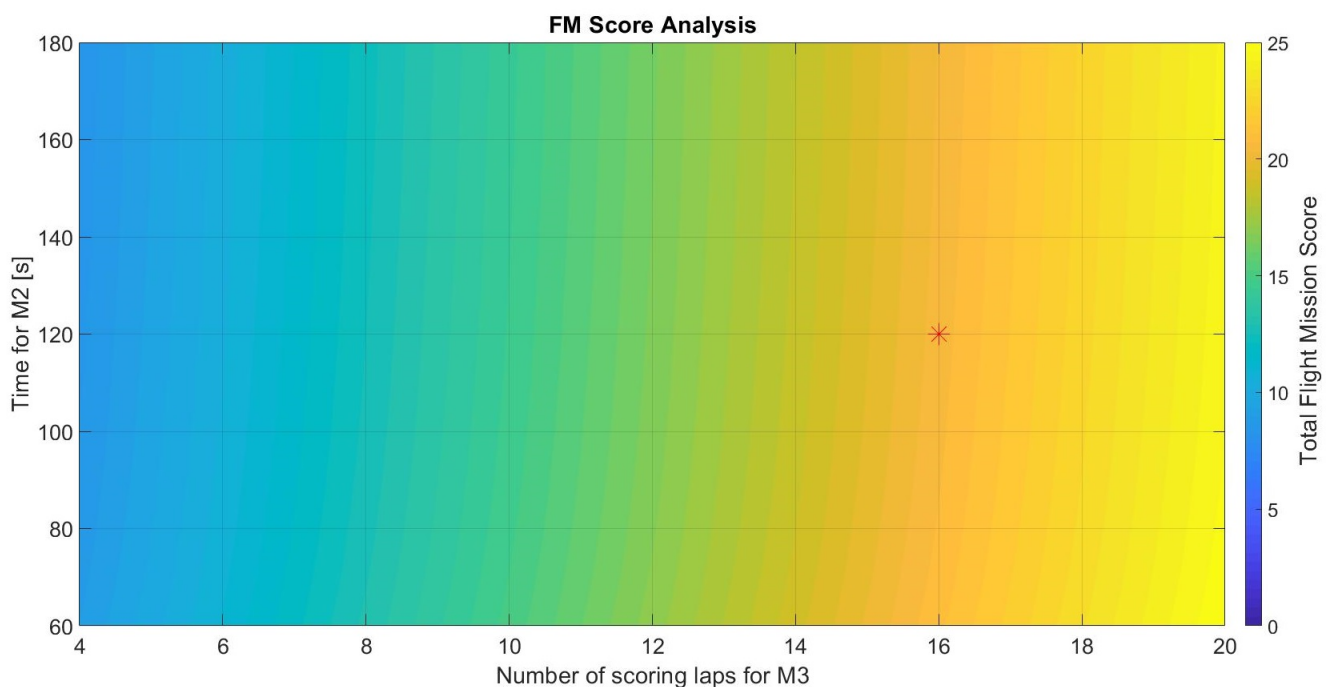


Figure 6: Flight Score Analysis per Mission. The team's chosen conceptual design point is noted by the red star.

Since the sizing or weight of the aircraft has no direct impact on the score, it is theoretically the best solution to take so many dart rockets until the legal weight of the aircraft is reached. However, this would lead to an aircraft size that requires a very complicated folding mechanism and would be difficult to fly.

Therefore, the team has tried to find a meaningful limit for the aircraft design and has decided on the advice of the pilot for a maximum wing cube loading (WCL). In general, the WCL is used to group aircraft by similar flight characteristics. To meet the takeoff requirement and potentially high speeds, depending on the number of darts, it was decided to design the aircraft for a WCL of around 12. This resembles sport scale aircraft [1].

The WCL is calculated as shown in Equation (3.7)

$$WCL = \frac{m_{aircraft(oz)}}{(Wing\ Area(ft^2))^{1.5}} \quad (3.7)$$

To perform this calculation, some estimates were made based on the aircraft from jA team 2015 [2] (jA15), which had about the same WCL. For the wing area were 7,5 ft^2 assumed and for the aircraft weight without the dart rockets 13.22 lbs. Rearranging Equation 3.7 yields the available mass for the dart rockets of 2.27 lbs which is equivalent to 16 dart rockets and a complete aircraft mass of 15.49 lbs.

The approximate time for the second mission was 120 s, which is slightly faster than the 2015 team's but realistic, as the aircraft have a similar WCL.

It should be noted that the calculation performed for the WCL is based on rough estimations. Therefore, the results were used to realistically assess the scoring space and guide the team's design.

3.1.4 Ground Score Sensitivity Analysis

The ground mission score is only dependent on the loading time of both types of payload and the time the aircraft needs to convert from the stowed condition to the flight configuration. Since the number of dart rockets that need to be loaded is fixed to four for all teams, the overall number of attack stores carried by the aircraft has no influence on the GM score.

In order to achieve a good result for the ground mission the folding mechanism needs to be able to move the folded surfaces as fast as possible, since the ground crew cannot proceed with the attaching of the radome as long as the flight configuration is not reached.

For the loading time, the crew member has to attach the radome first, run back to the start line, and after a demonstration of its rotation capabilities, run back to the aircraft, detach the radome again and mount four attack stores. The loading time also includes the time that the crew member needs to shuttle back and forth to the aircraft. The loading time and dart rocket capacity for M3 are the top priorities for the team because they constitute a high portion of the total score. The flight performance for M1 and M2 are lower priorities, but are still critical to fielding a winning design.

3.2 Translation of the Mission Requirements into Design Requirements

The scoring analysis revealed that the overall flight score is driven principally by the M3 scoring laps. However, since all mission score is multiplied by the report score, design parameter have been set to perform well on all missions. The analyses conducted yielded qualitative design criteria (Table 2) that were used to compare different aircraft configurations.

As the payload for M3 needs to be transported under the wings, a sufficient wing sizing is required as well as a powerful propulsion system to be able to takeoff with the additional weight. Since the weight of the radome is roughly the same as one dart rocket, it is expected that if the aircraft performs well in M3 it will do the same for M2. As per Mission 2 and Mission 3, the aircraft top speed has a significant impact on the mission score. Mission 2 score is dependent on the time the aircraft needs to finish 3 laps, whereby Mission 3 score is dependent on the number of scoring laps. Since the desired number of laps for M3 is almost 5 times higher than the required number of laps for M2, it can be assumed that the propulsion system, when designed for M3, also performs well in M2. For the Ground Mission the time the aircraft needs to convert from the stowed condition to the flight configuration and the time to load both kinds of payload are of big importance. In order to minimize the unfolding time, the goal is to build a fast mechanism that reliably unfolds and locks the wings. Besides human factors, the payload loading time is dependent on the simplicity of the design. To minimize the loading time, the target should be to design an easy and fast to use mechanism.

Table 2: Translation of mission requirements into design requirements

Requirement	Objective	Design Parameter
Payload	Sufficient wing area and wing thickness and powerful propulsion system to maximize the number of scoring laps	<i>number of scoring laps</i>
Loading Time	High accessibility and fast to use attachment mechanism to minimize the team's loading time	$\frac{\text{Fastest Time}}{\text{Time}}$
High Top Speed	Powerful propulsion system and drag reduction so that the aircraft can maximize the number of scoring laps and minimize the time for M2	$\frac{\text{Fastest Time Flown}}{\text{Flown Time}}$; <i>number of scoring laps</i>
Unfolding Time	Build a fast folding mechanism to minimize the GM time	$\frac{\text{Fastest Time}}{\text{Time}}$
Takeoff	The aircraft needs to be restrained during power up by a tail hook	<i>Tail hook of sufficient strength</i>

3.3 Configurations Considered

After determining the design requirements, the next step in the design process was the definition of a design space that includes all possible aircraft concepts. Even though the aircraft is required to have folding surfaces, the configuration alternatives are not significantly narrowed down. The potential configurations for each component are listed in Table 3.

Table 3: Matrix of alternatives

Component	Alternatives		
Wing Layout	Blended Wing-Body	Biplane	Conventional
Wing Positioning	Low	Mid	High
Empennage Type	V-Tail	Conventional	H-Tail
Empennage Attachment	One Boom	Two Booms	On Fuselage
Number of Engines	1	2	
Engine Location	Pusher	Tractor	Both
Landing Gear	Taildragger	Tricycle	

3.4 Concept Weighting and Selection Process

In order to reach a well-founded analytical decision on which configuration to use, figure of merit (FOM) analyses were conducted for the aircraft, wing, and empennage configurations. Table 4 shows the weighted characteristics for the conceptual design. The values of importance, scaling from non-relevant (0) to most important (5), are derived from the design requirements and the score sensitivity analysis respectively. To reduce the design space from the alternatives presented, aircraft components were measured against each other with the relevant FOM. Each component was given a rating, which was then multiplied by the FOM value. The component with the highest score was then selected for the further design.

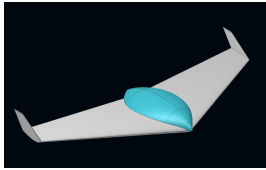
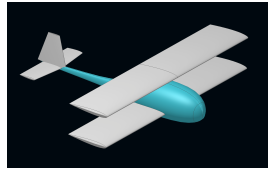
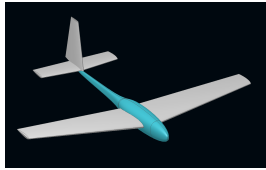
Table 4: Figures of merit

Figure of Merit	0	1	2	3	4	5
Weight						5
Payload capacity						5
Payload accessibility					4	
Simplicity of design				3		
Foldability			2			

3.4.1 Aircraft Configuration

The team considered three basic configurations: a blended wing-body, a biplane and a conventional monoplane design as shown in Table 5. The conventional monoplane configuration offers the highest payload capacity, especially for the third mission. Because of the wing placement, it also scored well on the payload accessibility. Additionally, the structural arrangement of the monoplane configuration can be designed and changed quickly and was therefore chosen for this year's aircraft.

Table 5: Figure of merit analysis for the aircraft configuration

		Aircraft Configuration		
				
FOM	Value	Blended Wing-Body	Biplane	Conventional
Weight	4	3	4	3
Payload capacity	5	4	2	5
Payload accessibility	2	2	1	5
Simplicity of design	3	3	2	3
Foldability	5	3	3	4
Result		62	54	72

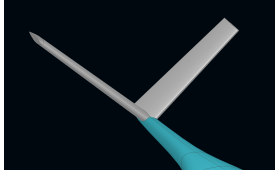
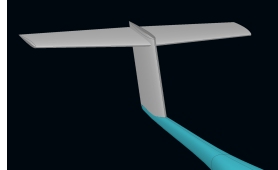
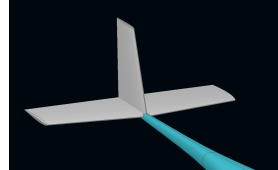
3.4.2 Landing Gear Configuration

The two possible landing gear configurations are a tail-dragger and a tricycle configuration. With respect to the requirement that the aircraft must fit within a box within a depth of a minimum of two feet and all landing gear, the tail-dragger was quickly discarded, since it would have made the design much more complicated.

3.4.3 Tail Configuration

The tail configuration was also subject to figure of merit analyses (Table 6). The empennage might be a constraint to the folding surfaces so it was included within the analysis. Since the empennage might be a constraint to the folding surfaces it was taken into the analysis. Since the conventional configuration is simple and can be built with light-weight methods, it was chosen for the aircraft.

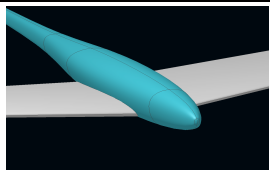
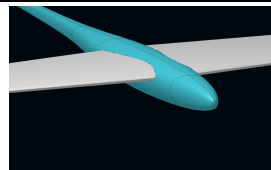
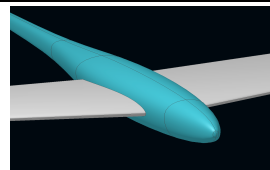
Table 6: Figure of merit analysis for the tailplane configuration

		Tail Configuration		
				
FOM	Value	V-Tail	T-Tail	Conventional
Weight	4	3	4	4
Simplicity of design	3	2	3	4
Foldability	2	3	3	2
Result		24	31	32

3.4.4 Wing Placement

Three possible wing placements were taken into consideration: a low-wing, a mid-wing and a high-wing configuration (Table 7). All three designs are very similar in structural efficiency, payload capacity and accessibility. The deciding factor is the foldability. Since a location for the folding mechanism is needed, the high-wing configuration offered the best solution.

Table 7: Figure of merit analysis for the wing configuration

		Wing Configuration		
				
FOM	Value	Low-Wing	High-Wing	Mid-Wing
Weight	4	3	3	3
Payload capacity	5	3	3	3
Payload accessibility	2	3	4	3
Simplicity of design	3	3	4	3
Foldability	5	4	4	4
Result		62	67	62

3.4.5 Payload Configuration

The payload attachment is critical for a reduction in loading time. The radome needs to be mounted horizontally on the centerline of the fuselage, which means the only reasonable location was on top of the fuselage. Since at least four dart rockets need to be mounted under the wings and dropped during flight, the team decided to place all dart rockets under the wings. Another possible location would have been underneath the fuselage but this would have resulted in difficulties with positioning the ejection mechanism.

3.4.6 Propulsion Placement

The only reasonable choice for the placement of the propulsion system was a tractor motor, since a pusher configuration could potentially interfere with the Mission 3 payload drop. Furthermore, since the aircraft needs to be held back by one team member during the power up, a pusher configuration represents a safety hazard and would raise the complexity of the aircraft to an unnecessary level.

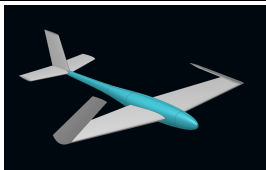
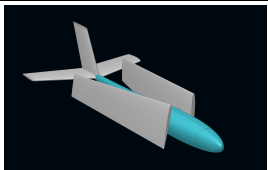
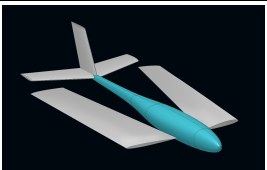
3.4.7 Folding Mechanism

The team investigated three different possibilities for the folding mechanism. For the "Upward" folding mechanism, the team would have built a fixed wingspan close to the box width and then folded the wingtips upward. This mechanism would have been the lightest because of its simplicity, but because of a weak spot, created by the hinge, on an outer position of the wing, this mechanism would have limited the payload capacity significantly.

Compared to the "Upward" folding mechanism the "Sweep" mechanism has a higher payload capacity but limits the wing in its sizing because of the sizing of the box, and it may interfere with the empennage. It is relatively easy to build, since both wings can be rotated using only one servo motor and a hinge on the trailing edge near the fuselage. This mechanism seemed to be the most promising and was therefore chosen for the aircraft.

The "Double Rotation" would have included a rotation around the y-axis and the z-axis of the aircraft. This would have been the most complex mechanism of all three, since it relies on two rotations, and, therefore, more parts would have been needed to build it. This would have increased the weight of the the whole system.

Table 8: Figure of merit analysis for the folding mechanism

		Folding Mechanism		
				
FOM	Value	Upward	Double Rotation	Sweep
Weight	4	5	3	4
Payload capacity	5	2	5	5
Payload accessibility	2	0	0	0
Simplicity of design	3	4	2	3
Foldability	5	4	4	5
Result		62	63	75

3.5 Final Conceptual Design Configuration

The final configuration is a high-wing conventional aircraft with a conventional empennage. It offers minimum loading time while allowing a high mission speed and high payload count. To transition from the stowed configuration to the flight configuration, the wings rotate by almost 90 degrees around the vertical aircraft axis and is locked by two spring-loaded bolts. The aircraft a tricycle landing gear and a tractor propulsion systems. The final conceptual configuration is designed to carry 16 dart rockets.

Using the assumed best capabilities of the other aircraft in the competition, this aircraft would be capable of achieving the mission scores tabulated in Table 9.

Table 9: Predicted Flight Scores

Aircraft	M1	M2	M3
<i>Bobby</i>	1.0	120 s	16 Darts
Assumed Best	1.0	90 s	18 Darts
Score	1.0	1.75	16

4 Preliminary Design

The preliminary design built upon the concept chosen in the preceding chapter. Based on the estimations made during the conceptual phase, an iterative design process led to the preliminary design. Frequent flight testing enabled the *joanneum Aeronautics* (jA) team to adjust calculations and gain data points to match theoretical calculations with real-world performance. The preliminary design provided a foundation for the detailed design as well as the final manufacturing plan.

4.1 Design Methodology

The chosen design method was a flight test-based process with multiple optimization iterations. This allowed the team to incorporate the experience gained with the construction and flight testing of the prototypes into the next iteration cycle. A rough estimate of the empty weight and the wingspan of the aircraft for a fixed number of attack stores was taken as a basis for designing the wing and the aerodynamics of the aircraft. This led to the selection of an appropriate propulsion system. The fuselage had to match the aerodynamic and propulsion system parameters and was therefore designed next. The design verification process, in which every team member was involved, analyzed the preliminary design and suggested improvements for the next iteration in order to maximize the final score. As far as possible, the theoretical performance estimates were examined with flight testing of prototypes leading to a refined design for the next iteration. The design process, detailed in Figure 7, was in line with the dynamic approach the *jA team* adopted across all branches and enabled efficient time management.

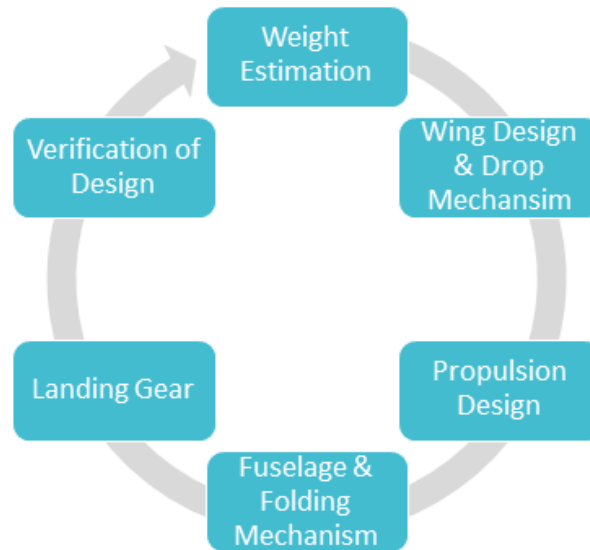


Figure 7: Iteration process overview

4.2 Design Trades

During every iteration of the design process, sizing trades were performed. On the one hand, the goal was to reach a high scoring number and, on the other hand to build a well flying aircraft. To reduce the risk of a structural failure during the contest, the robustness of the airplane was favored over the weight.

4.2.1 Folding Mechanism

The initial approach to folding the wings was to rotate them around the z-axis via a hinge on the trailing edge. However, the team had underestimated the resulting torsion moment on the hinge caused by the weight of the wing. To compensate for this load, a very strong and heavy structure would have been needed and this would have raised the aircraft weight. For this reason, this folding mechanism was discarded, and the second-best scoring mechanism was chosen. For this mechanism, some extra space and reinforcements in the fuselage are required but the resulting weight is still lower than the resulting weight from the first mechanism. This is why the team decided to move on with this new folding mechanism. Moreover, due to contact of the drop mechanism with the fuselage, the two innermost dart rockets had to be removed, reducing the amount of carried dart rockets to 14. This measure does not affect the desired WCL since the reduced weight because of the removed dart rockets has been transferred to a more complex and heavier folding mechanism. Figures 8 and 9 show the aircraft with the new folding mechanism in the stowed and flight configuration.



Figure 8: Aircraft in flight configuration



Figure 9: Aircraft in stowed configuration

4.2.2 Wing Shape

The most critical phase during the flight is the takeoff phase. The basis for the design of the wing shape was to achieve the desired WCL as well as generate sufficient lift. Equation 4.1 shows the parameters lift is dependent on.

$$F_{Lift} = \frac{1}{2} * \rho * C_L * v^2 * S_{ref} \quad (4.1)$$

The terms marked in red are the only ones that can be changed in this equation by changing the wing shape. In order to raise F_{Lift} , both the lift coefficient (C_L) and the wing area (S_{ref}) need to be as high as possible.

The highest possible wing reference area, with respect to the sizing constraints caused by the box, can be achieved with a rectangular wing. A known disadvantage of this wing design is the induced drag caused by a low aspect ratio. But since sufficient lift is such an important factor, this downside was compensated for with enough thrust.

The lift coefficient is mainly dependent on the chamber of selected airfoil. Since the takeoff from a ramp requires much lift, it was decided to use high-lift devices to increase the chamber of the wing. For the high-lift devices conventional flaps on the trailing edge were chosen. Furthermore, it was decided to use endplates on the wings which also increase the C_L .

4.2.3 Propulsion

Preliminary sizing for the propulsion system was focused on providing the necessary power for takeoff. Mission 3 was the limiting case for sizing due to the increased payload weight. Along with completing the takeoff, the propulsion system must also produce enough power to satisfy the corresponding number of laps for M3.

NiMH battery chemistry offers more energy density than NiCD batteries, so NiMH cells were chosen for the

aircraft's propulsion system. For preliminary sizing, battery packs with 6 Sub-C cells each were chosen for their promising performance based on eCalc [3] calculations. From prior propulsion analysis [4], a well-sized propulsion package can achieve a maximum of about 85% efficiency from the power supplied by the battery pack.

As takeoff performance was shown to be the primary to mission performance, a target power loading of 150 W/lb, which is comparable to aerobatics performance [5], was determined to satisfy the takeoff requirement. Thus, by sizing for 14 dart rockets, a minimum power of 2323.5 W was calculated (Equation 4.2).

$$15,49 \text{ lbs} * \frac{150 \text{ W}}{1 \text{ lb}} = 2323.5 \text{ W} \quad (4.2)$$

With the estimated efficiency of 85%, the required power was calculated using Equation 4.3.

$$P_{\text{Battery}} = \frac{2446.5 \text{ W}}{0.85} = 2733.53 \text{ W} \quad (4.3)$$

Based on that power calculation a motor and propeller database was created, to find a appropriate combination that fulfills the power requirement but also generates enough thrust.

The Hacker A50-12L Turnado V3 motor was chosen as it fulfilled the power requirement from Equation 4.2. Furthermore, this motor achieved the best score on eCalc, which was also used to select the preliminary propeller that would provide enough thrust. Additionally, it was decided that only one motor shall be used since it is more efficient than two smaller ones with the same power. Moreover, one motor reduces the weight on the wings which is beneficial for the folding mechanism.

For the preliminary battery pack 36 Sub-C cells combined in packs of six were chosen. They have a nominal voltage of 7.2 V per pack and a nominal capacity of 3000 mAh. This propulsion package provides about 20 lbs of thrust based on eCalc calculations and was therefore purchased for further testing.

The preliminary propulsion package is shown in Table 10.

Table 10: Preliminary propulsion package

Motor	Battery Pack	Propeller
Hacker A50-12L Turnado V3	36 x Sub-C cells (1.2 V)	Aeronaut CamCarbon 18x11

4.3 Mission Model

In order to simulate the missions and the respective performance of the aircraft, a tabular mission model was developed. This mission model was used to calculate estimated mission scores for M2 and M3. During the design verification process, the calculated aerodynamic and propulsion-based parameters were taken in order to conduct this analysis and optimize the final design.

4.3.1 Description and Capabilities

Modeling the flight missions to be performed by the competition aircraft, the different phases can be considered as singular stages:

- **Ground-based takeoff:** Ground-based takeoff was assumed to be performed at maximum throttle setting using high-lift devices. Testing was performed to determine the launch speed of 42 ft/s.
- **Initial Climb:** The aircraft was assumed to climb to 65 ft above ground level with a static rate of climb.
- **Cruise:** This phase of flight was assumed to be a level, constant-speed flight without any maneuvering apart from compensating for gusts. For each mission, the optimum cruise thrust setting was selected in order not to exceed the nominal battery capacity.
- **Level turns:** coordinated level turn with constant speed and radius was assumed for both types of turning maneuvers (two 180° turns and one 360° turn). The load factor on the aircraft structure was calculated based on predicted turn radius.

4.3.2 Uncertainties

The uncertainties described in this chapter (Table 11), are mainly due to different geographic location and climate between contest location and the design, manufacturing and test location. These differences influence several aspects of the performance, such as battery pack endurance and maximum power from the propulsion system, which cannot be verified before the contest and thus remain uncertain.

Table 11: Comparison of the design, manufacturing and test location and the contest location

Uncertainties	Europe - Austria - Styria	North America - USA, Arizona - Tucson
Season of the Year	Winter	Spring
Temperature [°F]	37.4	80
Wind [ft/s]	5	12
Gusts	No Wind Gusts	Regular Wind Gusts
Terrain	Alps: Mountains & Hills	Desert: Hills
Elevation [ft]	1564	2389

The parameters which significantly influence the performance of the design are the temperature, elevation and wind. Due to the higher temperature and elevation, a lower density can be expected, which decreases the propeller efficiency. At the same rotations per minute (rpm), the propulsion system will provide lower thrust in Arizona. To compensate for this effect the pilot will have to increase the thrust setting and will draw more current. This will decrease the flight endurance and affect the number of attack stores that can be dropped and is decreasing the

score of Mission 3. On the other hand, the temperature would increase the efficiency of the battery pack, but this uncertainty can be eliminated when using warm battery packs. Wind is for aircraft of this weight category a not a big issue, although upwind is, on one hand beneficial for takeoff, but if it is too strong it is disadvantageous for lap times. The sandy terrain is a potential problem for the propulsion system, but it is expected that these problems would just have a significant impact in a long term use and no influence on the design during the contest.

4.4 Aerodynamics

The aerodynamic configuration was designed and analyzed using XFOIL [6], MATLAB® [7] and CFD-software. XFOIL is a program for the design and analysis of subsonic airfoils and it was used to analyze the performance of the airfoil and high-lift devices as well as to compute the static and dynamic stability derivatives. CFD software was used to get an understanding of endplates and identify regions that might promote flow separation.

4.4.1 Airfoil Selection

The main requirement of the wing is to be suitable for the different flight envelopes. This does not only mean to lift the airplane, but also to have as little drag as possible for high speeds in Mission 2, sufficient lift to carry the payload during Mission 2 and 3 and an efficient wing to drop as many attack stores as possible in Mission 3. Using XFOIL and the experience gathered from previous DBF competitions, numerous airfoils were analyzed for takeoff and cruise conditions at a Reynolds number of 500,000. Table 12 states the design and aerodynamic parameters of the most promising airfoils: HQ3.0/12, E221, MH114 and the NACA2412.

The airfoils were not only filtered based on their aerodynamic coefficients but also on their geometry and predicted manufacturing effort.

Table 12: Airfoil Comparison

Parameter	HQ 3.0/12	NACA 2412	E221	MH114
Max. Thickness [%]	12	12	9.4	13
Max. Thickness at Chord Length [%]	35	30	28.1	28.1
Max. Chamber [%]	3	2	1.6	6.40
Max Chamber at Chord Length [%]	50	40	32.6	50
Max. Lift Coefficient [-]	1.43	1.4	1.14	1.8
Min. Drag Coefficient [-]	0.0072	0.0063	0.006	0.0083
Crit. Angle of Attack [deg]	17.75	19	16.5	19.25
Lift Slope [deg ⁻¹]	0.1055	0.1134	0.1096	0.0972
Max. Lift/Drag [-]	109.4	87.3	86.7	131.2
AoA at Max. Lift/Drag [deg]	4.5	5	5.5	3.5
Zero Lift Angle [deg]	-3.8	-2.3	-1	-10.25

Manufacturability and geometry: Complex geometries may have excellent aerodynamic characteristics but can be extremely difficult to manufacture. Especially high curvatures and sharp trailing edges are difficult to manufacture and can cause imperfections in the surfaces of the airfoil. These imperfections can have unpleasant impacts on the airfoil performance.

Another requirement is the thickness of the wing. Since some payload needs to be mounted underneath the wings, the wings need a sufficient thickness for mounts. Afterwards, the filtered airfoils were further analyzed based on their maximum lift coefficients and lift-to-drag ratio (Figures 10 to 13) . The corresponding curves were calculated with XFOIL and plotted with MATLAB®.

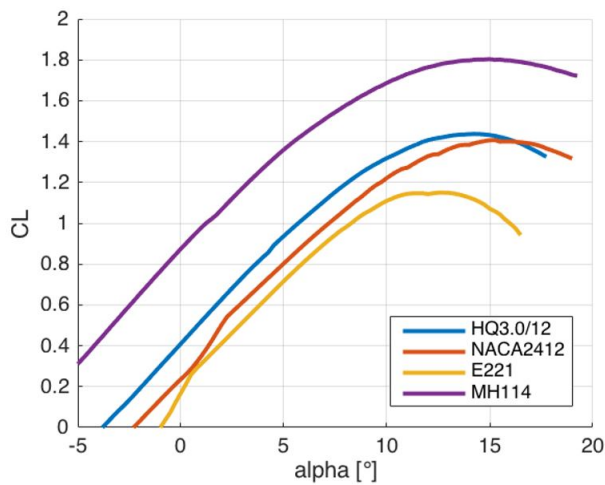


Figure 10: Lift Coefficient over the AoA

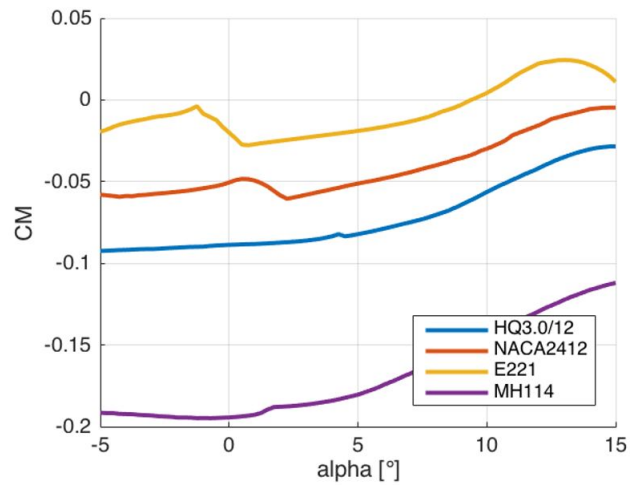


Figure 11: Moment Coefficient over the AoA

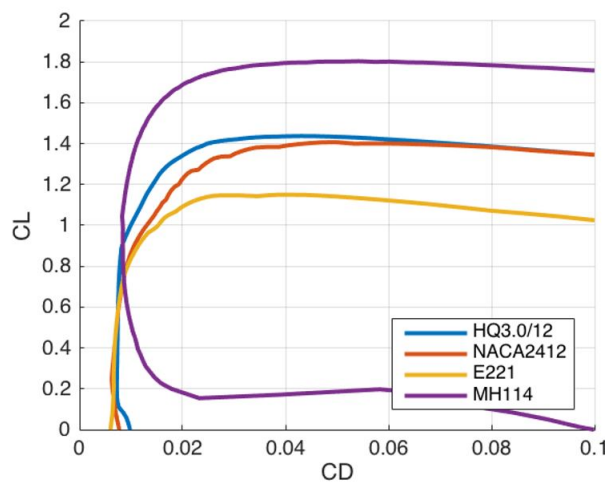


Figure 12: Lift Coefficient over Drag Coefficient

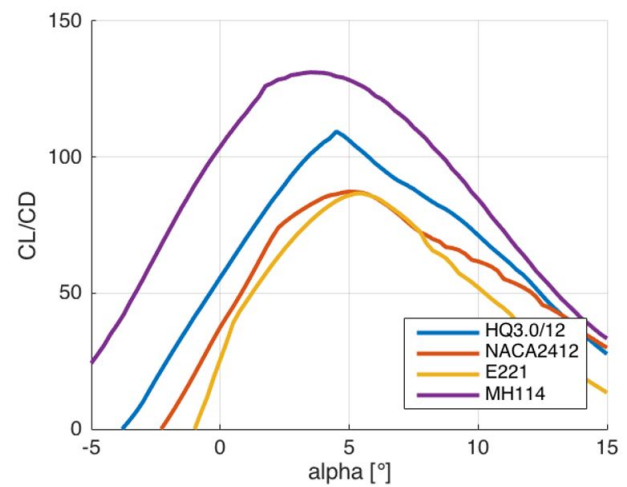


Figure 13: Lift over Drag over AoA

The four graphs in Figures 10 - 13 imply that the MH114 is the best airfoil for the aircraft, but its geometry is very complex and difficult to build. In comparison to the NACA and Eppler airfoil, the HQ3.0/12 provides a high C_{lmax} value which is beneficial for a short takeoff. Furthermore, the drag coefficient stays low for a wide range of lift

coefficients. Another advantage of the HQ airfoil over the MH114 is that the value of C_m stays low and more or less constant for low angle of attack (AoA). As Figure 13 shows the L/D ratio of the HQ3.0/12 is consistently better than the others, which is especially beneficial for Mission 3. Therefore it was chosen to be used for this competition. The geometry of the airfoil can be seen in Figure 14.

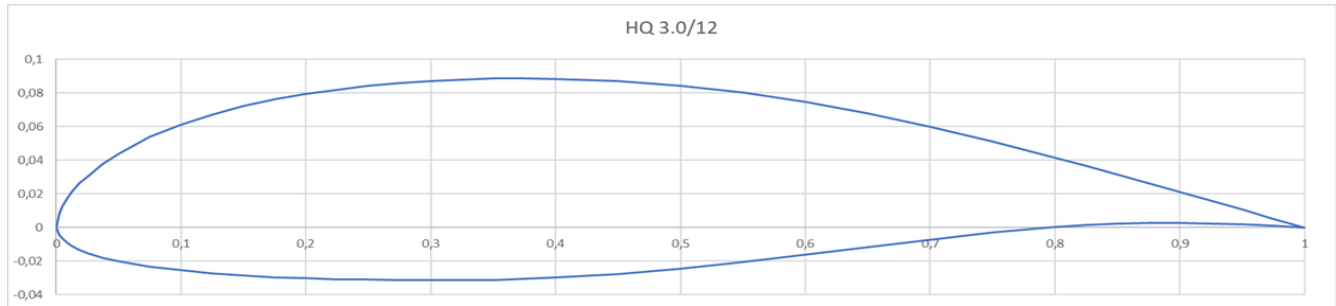


Figure 14: Shape of the HQ3.0/12

4.4.2 High-Lift Devices

As already mentioned, the team decided to use flaps to increase the generated lift. The span of the flaps is 50% of half the wingspan and the chord is 22% of the wing chord. These sizing parameters are based on a general rule of thumb for radio controlled aircraft [8]. The maximum deflection of the flaps is 30° and results in a 30% higher lift coefficient at a lower AoA compared to a wing without flaps. These flaps are only going to be used during the start since this is the phase where the most lift is needed. Figure 15 shows the different C_l over α values for no flaps (blue line) and fully deflected flaps (red line) at a Reynolds number of 320,000.

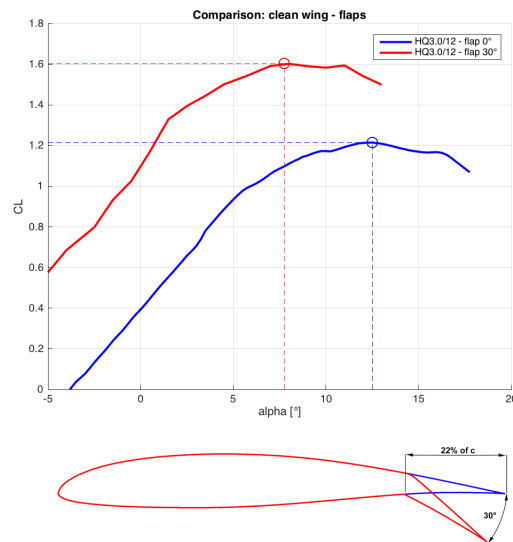


Figure 15: Change of C_l with the usage of flaps ($C_{l,max}$ is marked)

4.4.3 Endplates

In an effort to maximize the lift, a study was performed to analyze the aerodynamic effect of endplates on wings at cruise speed. By adding endplates, the aspect ratio of the wing increases, and the net lift increases and the induced drag decreases [9]. The endplates were sized using Equation 4.4, which provides a relation for the effective aspect ratio (AR_{eff}) achieved when endplates of a specific height to wingspan ratio (h/b) are used [10]. This relation is

generally valid for values $h/b \leq 0.4$.

$$\frac{AR_{eff}}{AR} = 1 + 1.9 * \frac{h}{b} \tag{4.4}$$

The final sizing of the endplates was a trade-off with the box-width and the width of the aircraft in the stowed configuration. Solving the equation $h/b = 0.4$, with a wingspan of 7 ft, for h yields a height for the endplate of 2.8 ft. Since this height would cause interference with the box, the height was reduced to 0.49 ft. The effectiveness of the endplates was validated with a CFD-simulation (Figure 16) with a slightly increased drag and increased lift as it can be seen in Table 13.

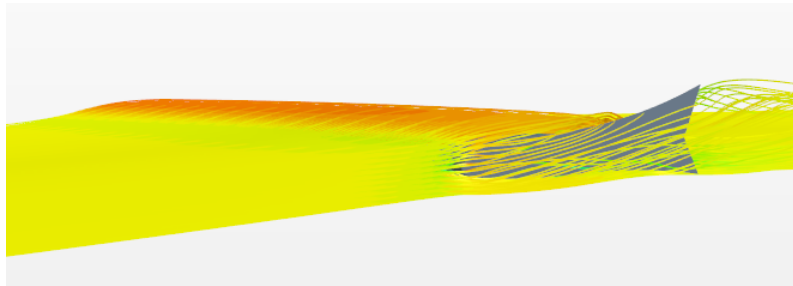


Figure 16: CFD simulation of the endplate

Table 13: Results of the CFD simulation of the endplates

Parameter	Wing with endplate	Wing without endplate
C_D	0.00101	0.00096
C_L	0.50994	0.4891
Drag [N]	4.39	4.19
Lift [N]	79.67	76.34

4.4.4 Drag Analysis

A preliminary drag estimate was obtained by summing each components' drag contribution, computed using CFD simulations and semi-empirical methods from Hoerner [11]. The drag components are normalized with the reference area of the wing. Table 14 shows the drag contributions of the major aircraft components, and Figure 18 shows the same data broken down into percentages for the third flight mission. The drag coefficient for the fuselage was determined by using Hoerner's method (Equation 4.5), which computes drag as a function of the body-fineness ratio (d/l), the Reynolds adjusted skin friction coefficient (C_{F-f}), and Prandtl-Glauert factor (P). The fuselage has a rather small contribution to the overall drag with 3% of the total drag.

$$C_{D,0} = C_{F,f} * \left[1 + 0.5 \left(\frac{d}{l} \right) + 6 * \left(\frac{d}{l} \right)^4 * P^{1,5} \right] \tag{4.5}$$

The drag coefficient for the wing was calculated using Equation 4.6. The drag for the wing includes the induced drag generated by the lift. The drag of the wing is between 21–26% and the associated induced drag is estimated to range from 23 –28% of the total drag of the aircraft.

$$C_{D,0} = 2 * C_{F,w} * \left[1 + A \left(\frac{t}{c} \right) * \cos\Lambda_{25} + B \left(\frac{t}{c} \right)^4 * P^3 * \cos\Lambda_{25} \right] \quad (4.6)$$

The drag for the landing gear was obtained through methods described by Hoerner [11, p. 251]. The landing gear contributes about 6-9% of the total drag depending on the mission. The empennage was modeled as a pair of flat plates, and their drag was determined using the same method as the wing calculation. The empennage accounts for around 30% of the total drag.

The drop mechanism was modeled as a laminar profile and analyzed by using Hoerner’s semi-empirical Equation 4.7. The drop mechanism accounts for 5% of the entire drag of the aircraft.

$$C_{D,0} = 0.33 \left(\frac{d}{l} \right) + c_{f,lam} * \left[3 \left(\frac{l}{d} \right) + 3 \left(\frac{d}{l} \right)^{\frac{1}{2}} \right] \quad (4.7)$$

The drag for the darts was obtained through CFD simulations (Figure 17). The darts account for 19% of the total drag when the aircraft is fully loaded for Mission 3.

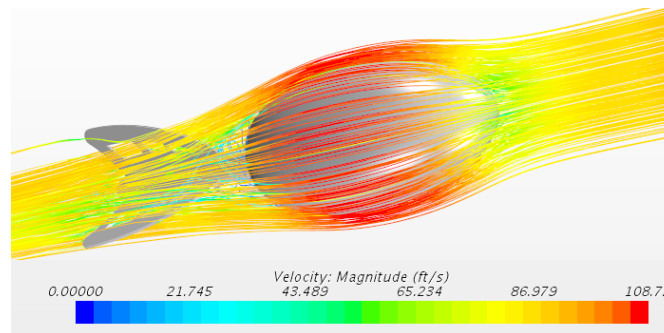


Figure 17: Result of the CFD analysis of a dart rocket

The drag coefficient for the radome includes the radome and the pylon carrying it. The drag was obtained by modeling the radome as an elliptical surface (Equation 4.8). The radome accounts for 6% of the drag in the configuration for Mission 2.

$$C_{D,0} = 2 * c_{f,lam} * \left(1 + \frac{c}{t} \right) + 1.1 \left(\frac{t}{c} \right) \quad (4.8)$$

Table 14: Aircraft zero lift drag estimates.

Component	$C_{D,0}$
Fuselage	0.00160547
Wing	0.01284189
Induced Drag (Wing)	0.01392541
Front Landing Gear	0.00124106
Rear Landing Gear	0.00302817
Horizontal Stabilizer	0.00962735
Vertical Stabilizer	0.00441254
Dart Rockets	0.01165447
Drop Mechanism	0.00250001
Radome	0.00310222
Mission 1	0.04668189
Mission 2	0.0497841
Mission 3	0.06083636

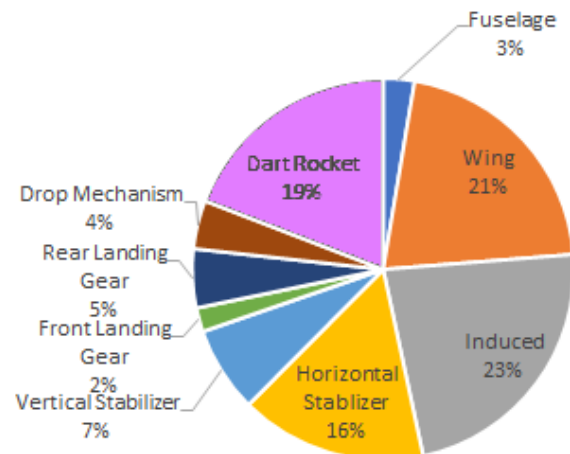


Figure 18: Graphical representation of the drag distribution for Mission 3

4.5 Stability and Control

To ensure stability and controllability of the aircraft during all flight missions, three simulation cases were determined:

- No installations
- Radome installed
- Dart rockets installed

The stability and control analysis was based on the moments of inertia, which were extracted from a preliminary CAD model. The center of gravity (CG) of the aircraft was treated as a design constraint, with the position fixed at the center line of the spar pipe, which is located at 1/3 of the chord length. The aircraft was designed in a way that small displacements of the center of gravity have no major influence on the stability. Therefore, each case was analyzed with the respective CG position. The main lifting and control surfaces were recreated in XFLR5 [12]. The analysis was conducted using the implemented vortex lattice method.

4.5.1 Longitudinal Static Stability

The initial focus of the longitudinal static stability examination was to analyze the dependency of the pitching moment coefficient (C_m) on the angle of attack (α) for each case. An aircraft can be considered stable when the corresponding C_l at $C_m = 0$ is greater than zero and $C_{m\alpha}$ is negative. For each configuration the aerodynamic center (AC) was calculated with XFLR5. After obtaining the AC position, the stability margin (SM) was computed

with Equation 4.9.

$$SM = \frac{AC - CG}{MAC} \quad (4.9)$$

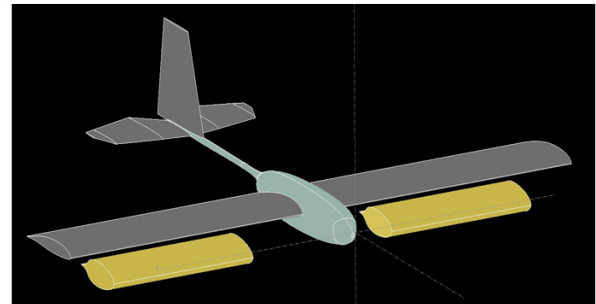
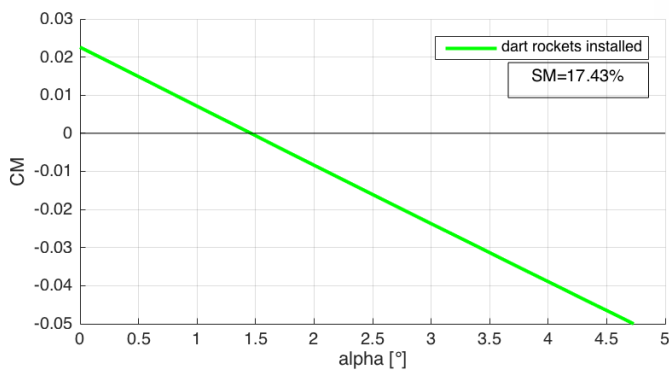
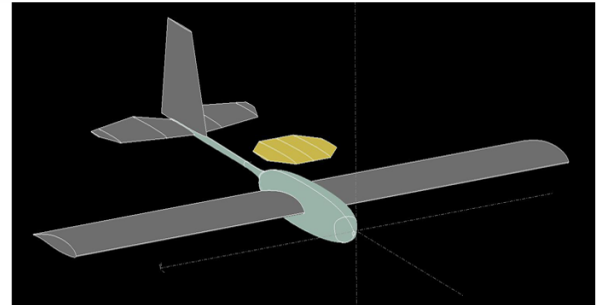
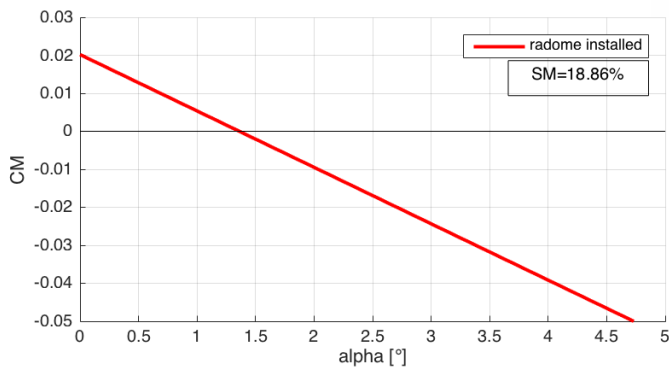
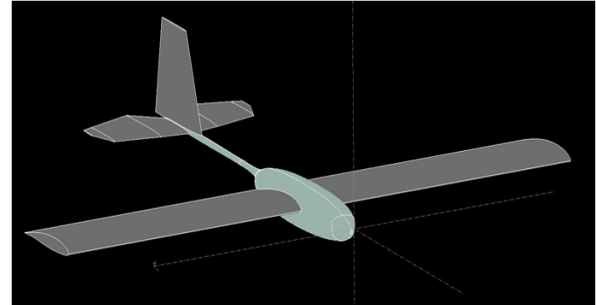
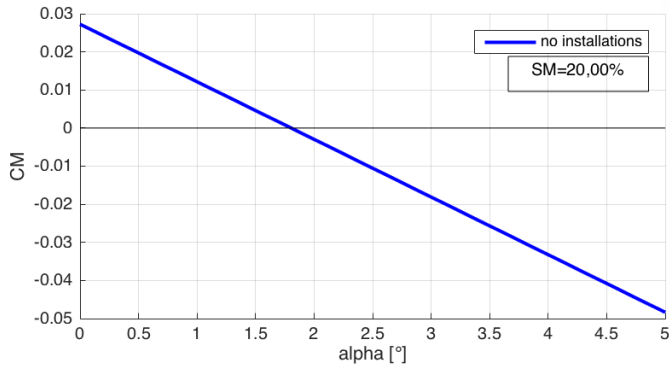


Figure 19: C_m as a function of α with the the respective payload configuration on the right side

The analysis of the three cases resulted in stability margins of 17.43%, 18.86% and 20.00% (Figure 19). For all configurations, the lift coefficient at the aircraft's operating point ($C_m = 0$) is greater than zero and therefore not indicated in Figure 19. That means that the assumption that the stability is not critically affected by the shifted CG was correct, and the aircraft has sufficient static stability.

4.5.2 Dynamic Stability

Knowing the aircraft's operating point from the static stability analysis, the next step was to investigate the dynamic behavior of the airplane. For determining the longitudinal dynamic stability, the short period and the phugoid mode were analyzed with XFLR5. The aircraft is stable in both of the longitudinal modes. Figures 20 and 21 show the time response plots of the short period and the phugoid mode respectively. For determining the lateral dynamic stability, the dutch roll, the roll and the spiral mode were analyzed. The result of the roll and dutch roll mode analysis can be seen in Figures 22 and 23. The aircraft is stable in dutch roll and roll mode and shows unstable behavior in the spiral mode. The spiral mode has a minimum doubling time of 3.207 s, which is in line with previous *jA* aircraft that flew without limitation. The root locus plot of the dynamic modes is given in Figure 24.

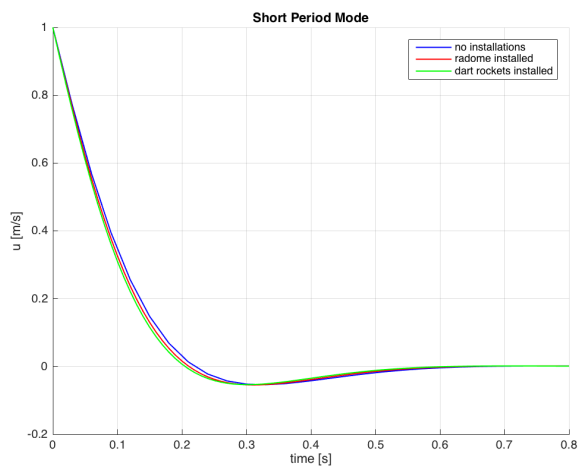


Figure 20: Time response plot of the short period mode

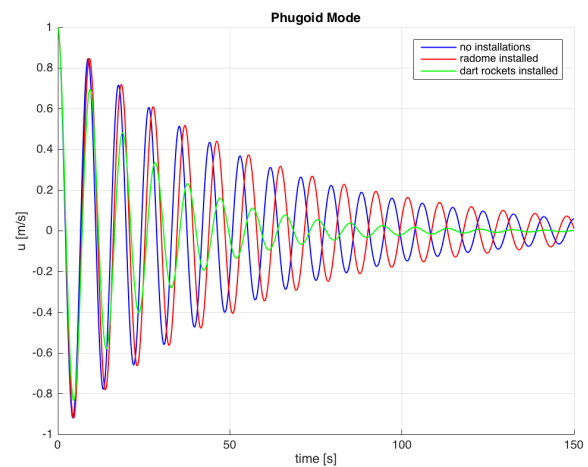


Figure 21: Time response plot of the phugoid mode

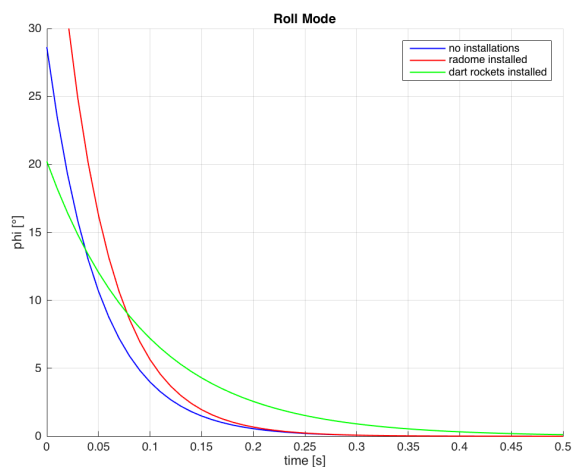


Figure 22: Time response plot of the roll mode

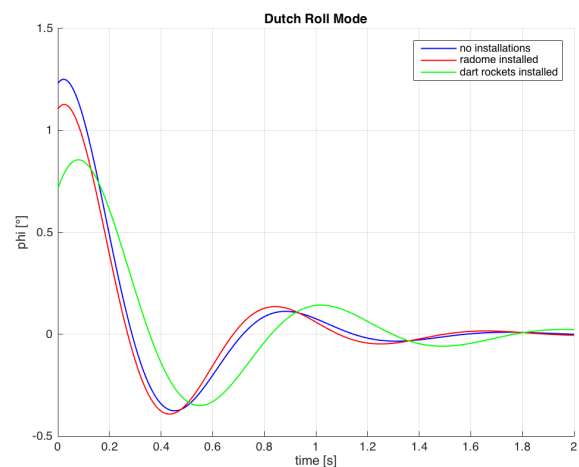


Figure 23: Time response plot of the dutch roll mode

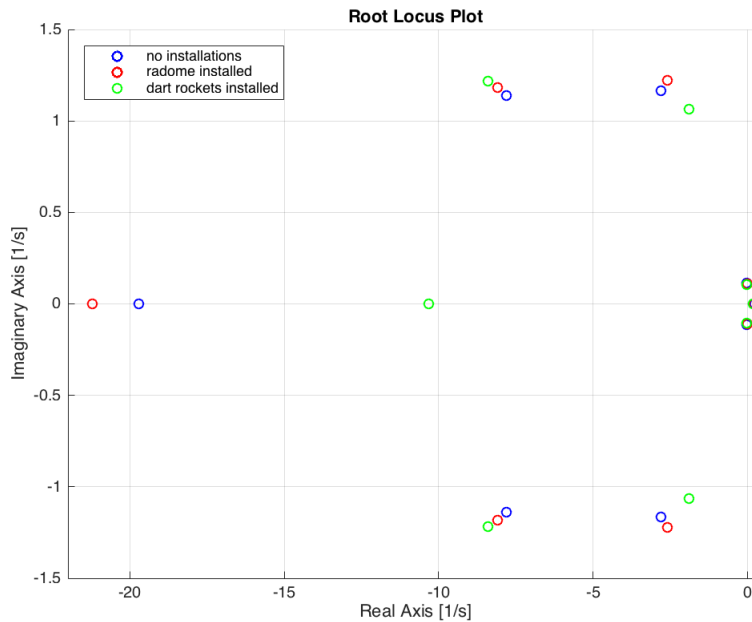


Figure 24: Root locus plot of the dynamic eigenmodes

In Table 15, the dynamic stability modes show the exact damping rates and frequencies of the longitudinal and lateral modes for the three different configurations.

Table 15: Dynamic stability modes

		Longitudinal Modes		Lateral Modes		
		Short Period	Phugoid	Dutch Roll	Roll	Spiral
No Installations	Damping Ratio [-]	0.783	0.026	0.385	-	-
	Natural Frequency [Hz]	1.168	0.113	1.246	-	-
	Time Constant [s]	-	-	-	0.035	3.207
Radome Installed	Damping Ratio [-]	0.737	0.026	0.319	-	-
	Natural Frequency [Hz]	1.751	0.108	1.291	-	-
	Time Constant [s]	-	-	-	0.033	3.511
Dart Rockets Installed	Damping Ratio [-]	0.739	0.058	0.274	-	-
	Natural Frequency [Hz]	1.810	0.106	1.106	-	-
	Time Constant [s]	-	-	-	0.067	4.006

4.6 Estimated Aircraft Performance

Based on the preliminary design of the competition aircraft, the performance for each mission was estimated. Assumptions regarding the performance of the best team for M2 were made. This preliminary estimation can be seen in Table 16. It was assumed that the aircraft would pass both M1 and the ground missions without problems. For M3 the maximum load of 14 dart rockets is to be carried, compared to 16 dart rockets for an estimated competitor.

Table 16: Preliminary aircraft performance

Performance Parameter	M1	M2	M3
Carried Darts	0	0	14
Weight [lbs]	12.94	13.56	16.31
Velocity [ft/s]	76.35	90.76	84.39
Lap Time [s]	46	38	42
Number of Laps	3	3	14

5 Detail Design

After the preliminary design had been completed, the detail design phase started. In this chapter, the detailed design and sizing of the subsystems is discussed.

5.1 Dimensional Parameters

Table 17 details the specifications for the wing and empennage for the aircraft. Table 18 states the aircraft dimension and parameters of the chosen propulsion system.

Table 17: Aircraft surface dimensions and specifications

Wing		Vertical Stabilizer		Horizontal Stabilizer	
Airfoil	HQ3.0/12	Airfoil	Flat Plate	Airfoil	Flat Plate
Span	7.05 ft	Span	12.59 in	Span	27.55 in
Area	8.09 ft^2	Area	0.96 ft^2	Area	1.61 ft^2
Incidence	+2.5°	Incidence	0	Incidence	-0.5°

Table 18: Aircraft dimensions and specification

Aircraft Dimensions		Propulsion System		Propeller	
Overall Length	5.11 ft	Motor	A50-12L Turnado V3	M1	17"x10"
Fuselage Width	0.52 ft	Speedcontrol	ROXXY BL Control 9120 - 12 Opto	M2	18"x11"
Overall Height	24.45 in	Battery	NiMH SC Akku Team Champion	M3	18"x11"
Max. Takeoff Weight	16.99 lbs	Max. Power	2750 W		

5.2 Structural Characteristics

5.2.1 Structure Layout

The main goal for the structure was to ensure that all loads can be borne. Those loads are resultants from aerodynamic forces, forces generated by the motor or the impact at landing. The loads on the aircraft need to be transferred to main load-bearing components, such as the framework of the fuselage or the root rib of the wing. Aerodynamic loads from the wings are transferred over the spar and the framework into the fuselage. Loads from the empennage were transferred over the tailboom into the fuselage. To damp the loads occurring during the landing, the point of attachment for the landing gear is reinforced.

5.2.2 Operating Envelope

The structure of the aircraft is designed to bear a load of 2.5 g at a maximum weight of 16.99 lbs. Using Equation 5.1, this results in a bank angle of around 66 degrees in a coordinated turn.

$$n = \frac{1}{\cos(\theta)} \quad (5.1)$$

Since M1 and M2 are flown with less weight, the limit load factor increases to 6.0 g. The negative load factor for M3 was set to -1.25 g to ensure that the wing attachment area will not fail under compression. In the same manner as the positive load factors for M1 and M2, the negative factors decreased to -2 g. The structural limits were combined with the aerodynamic performance of the aircraft for each mission and plotted in a velocity–load factor diagram (Figure 25).

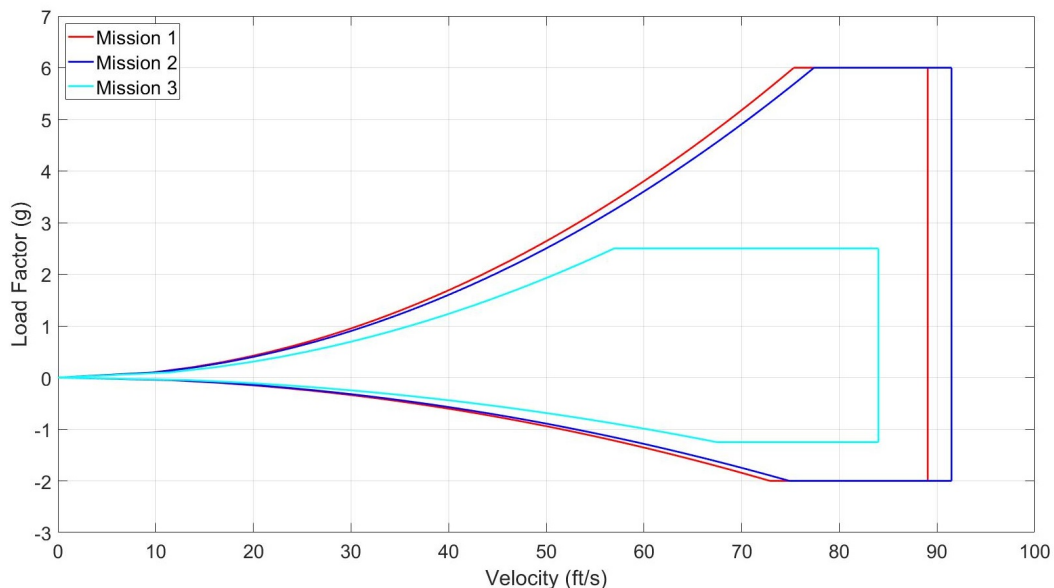


Figure 25: V-n diagram showing the load factor in dependence of the velocity for each mission

5.2.3 Fuselage

The fuselage consists of an inner framework and an outer skin. The inner framework is made of plywood. Its main purpose is to bear external loads on the fuselage. As it can be seen in Figure 26, the framework does not support the skin over the whole length of the fuselage. In the front, it acts as a support for the nose wheel and as cargo bay for the battery pack. The center section houses the folding mechanism and is also the attachment point for the radome. Since this section carries the highest loads, it is furthermore supported with a sheet of aluminium. The aft section is the attachment point for the rear landing gear and the tail boom. Figure 27 shows the fuselage with the outer skin. The skin is made of carbon fiber. Especially in the front section, the skin is designed rigid enough to carry the applied loads. The mount for the motor is glued to the skin with epoxy resin. The hook that is used to restrain the aircraft during power up is mounted at the rear end of the tail boom.

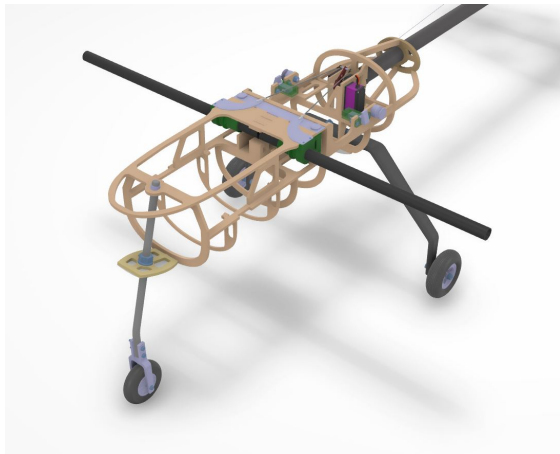


Figure 26: Plywood framework

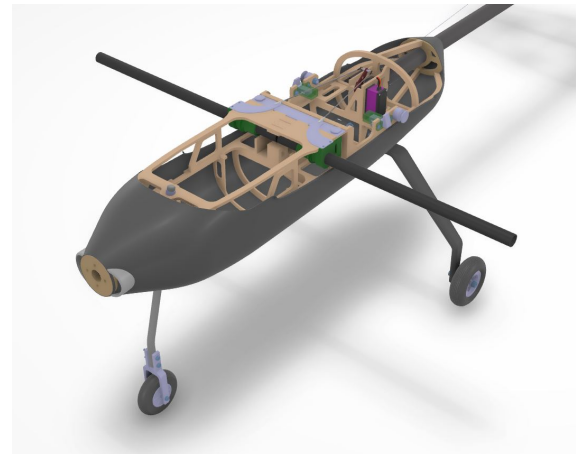


Figure 27: Carbon fiber skin of the fuselage

The interior of the fuselage is designed in such a way that every part has its own fixed place, only the different battery packs have slightly different installation positions to match the required center of gravity. The fuselage was designed with a top lid that can easily be opened and allows access to all internal components and a quick exchange of battery packs.

5.2.4 Wing

For the manufacturing of the wing a composite of different materials is used to obtain a light-weight structure with high stiffness and excellent manufacturing accuracy. The inner structure of the wing is made of Styrofoam, which has a density of 1.87 lbs/ft^3 . This material can be cut by an electrically powered hot wire which is controlled by a 4-axis computer numerical control (CNC) machine. Since the semi span of the wing is longer than the maximum airfoil size that can be cut by the CNC machine, the wing had to be produced in two parts and was glued together with an additional plywood rib in between. Once the foam is cut out in a precise way, the wing segments have to be

reinforced to obtain the required strength and stiffness. These reinforcements are a combination of a layer of glass fiber from the root rib to the additional rib, a balsa strip on the leading edge and balsa wood sheets as the skin as it can be seen in Figure 28.

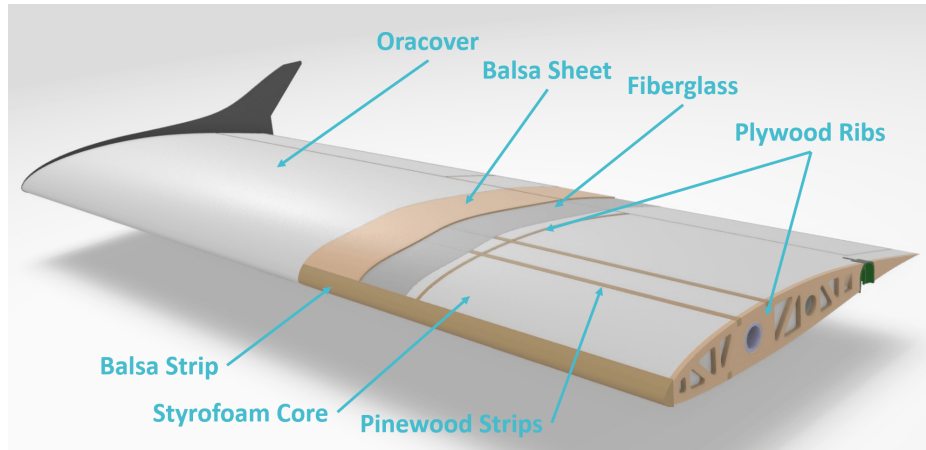


Figure 28: Main wing components

With these reinforcements the foam will fulfill its role as a core material, separate the glass fiber reinforced plastics (GFRP) structures, hold the actuators in position and introduce the loads into the spar in a uniform way. For weight saving purposes, cutouts are added to the wing at non load bearing positions. To smoothen the skin and cover the cutouts, iron-on film is used.

5.2.5 Empennage

The empennage, shown in Figure 29, was designed to be a light-weight and effective control surface. The construction uses materials such as balsa wood, carbon fiber and Oracover.

The tail was constructed as a separate unit from the fuselage and was attached to the fuselage with two balsa wood bars at the end of the tail boom. This allows the removal and replacement of the tail during the design iterations. The wiring for the control servo runs through the tail boom and into the fuselage.

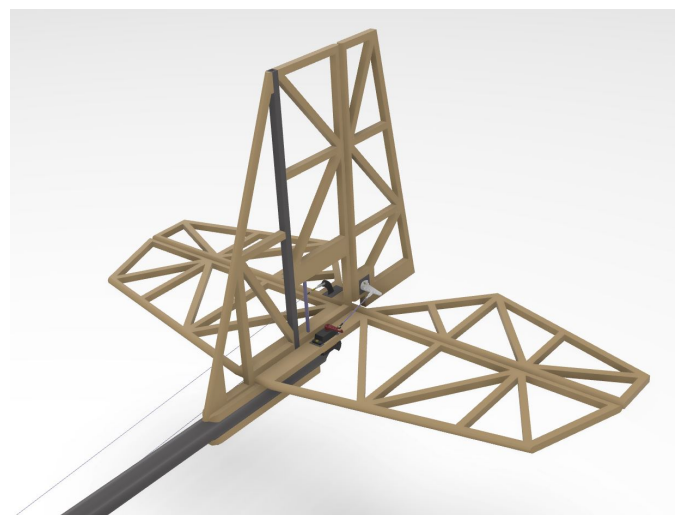


Figure 29: Empennage assembly

5.2.6 Landing Gear

The landing gear was designed as a conventional tricycle construction (Figure 30), with one nose wheel and two rear wheels. The nose gear was manufactured from an aluminium rod that was bent 15° from the vertical line. This was done to ease the transfer of the forces from the impact during the landing. Earlier designs with a damped nose wheel were discarded, as the benefits were rather small compared to the effort it would have needed to manufacture.

The rear landing gear is manufactured as one part made of carbon fiber. It offers high stability while maintaining low weight. Since it is not completely rigid, it offers some damping and, therefore, a some reduction of the force transferred to the fuselage.

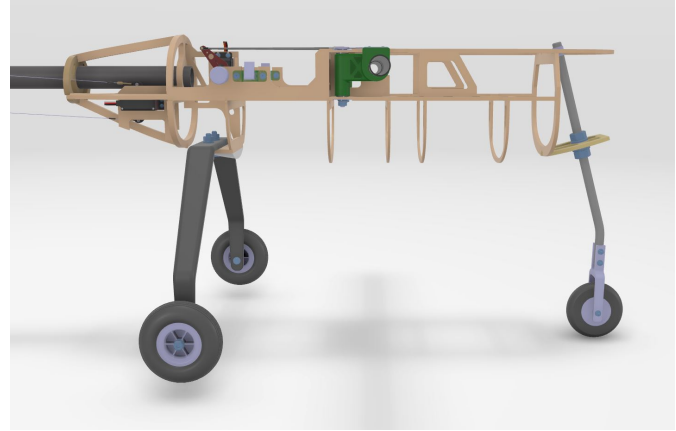


Figure 30: Landing Gear

5.3 Systems and Sub-Systems Selection, Integration and Architecture

5.3.1 Folding Mechanism

Rotation: From the initial position, the wings are rotated backwards with the leading edge facing downwards (Figure 9). A servo motor, located aft of the fuselage pulls both spars backwards until both wings have swept 90° forward around the z-axis (Figure 32). In the next step, a servo motor located in each wing rotates the wing backwards, around the y-axis until it locks mechanically (Figure 33). This rotation has been achieved by attaching the servo lever directly to the spar and the implementation of bearings in the ribs.



Figure 31: Aircraft in stowed configuration



Figure 32: Aircraft after the first sweep rotation



Figure 33: Aircraft in flight configuration

Locking: One requirement for the folding mechanism is that the wings lock mechanically without any assistance. To make sure that the wing stays in place, a groove near the trailing edge of the wing connects with a milled mushroom head attached to the fuselage (Figure 34). The wing is then mechanically locked with a snap lock at the back of the wing (Figure 35). The mushroom head prevents the wing to move in x,y and downward z-direction, whereby the snap lock prevents the leading edge from rotating upward.

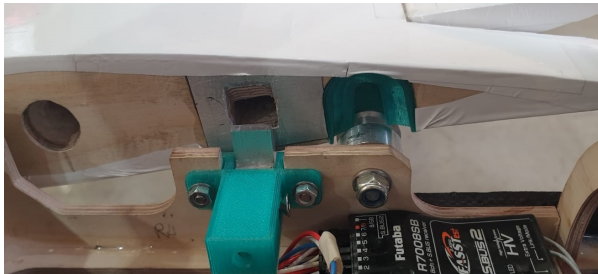


Figure 34: Unlocked Wing

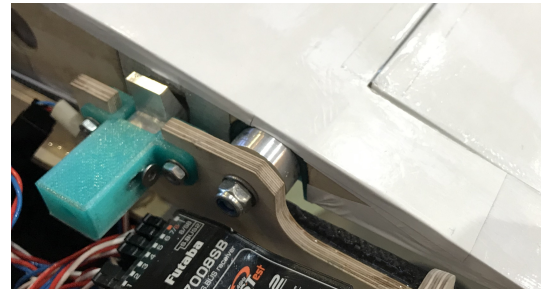


Figure 35: Locked Wing

5.3.2 Payload Drop Mechanism

The objective for designing the payload drop mechanism was to develop a light-weight, fast-to-use and reliable system to deploy the attack stores for Mission 3 without performing a maneuver dangerous to the aircraft. The structure of this system consists of a few light-weight 3D-printed parts and weighs around 0.068 lbs, including the mechanical and electrical parts. It minimizes ground handling efforts as the darts can be loaded and locked by hand by rotating only a single part. The locking works mechanically with a bolt and a spring and is unlocked with a servo motor. Therefore, there is no force on the servo in the closed position. Figure 36 shows one attack store mounted on the drop mechanism.

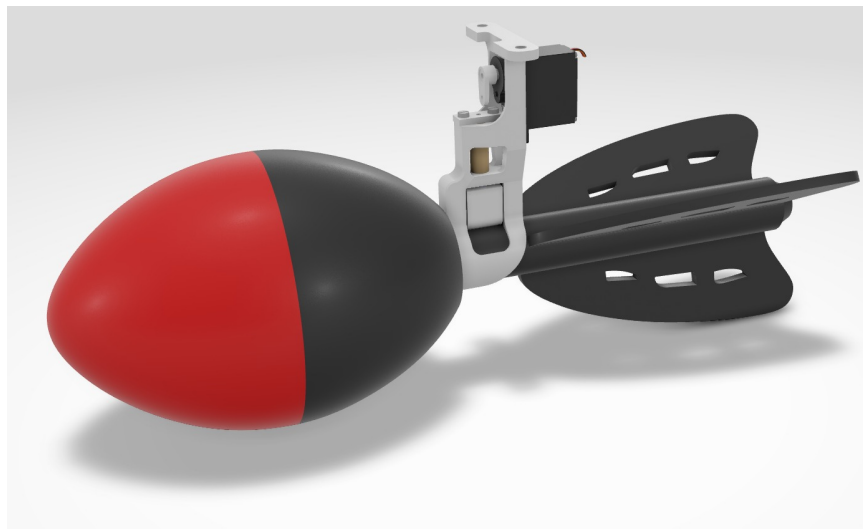


Figure 36: Attack Store drop mechanism

Figure 37 shows the principle function of the drop mechanism. Basically the structure consists of a bolt that is guided in a bushing. The bolt is pushed downwards with a spring and can be pulled upwards with a servo motor. The mechanism is divided into three stages:

- **Start:** Prior to the mission, the clamp is rotated into the open position by hand and the servo motor has to be turned into the closed position. The clamp is not able to freely rotate because the bolt is pushed downwards by the spring. Now the mechanism is ready and the darts can be attached.
- **Closed:** The darts are held in position by the clamp, which can be rotated until the bolt pushes into the groove. The mechanism is now locked.
- **Open:** In flight, the servo motor can be turned into the open position by a microcontroller. The servo motor then pulls the bolt upwards. Afterwards, the clamp can freely rotate, an elastic band pulls the clamp upward and the dart is pulled downwards by gravity.

All the servo motors are controlled by Arduino microcontroller boards. Both wing sides have an individual Arduino controller with the capacity to attach six servo motors, the innermost two servo motors are controlled by an Arduino microcontroller placed inside the fuselage, which is also responsible for the dropping sequence. The darts are dropped in a fixed sequence, starting with the outer left dart and followed by the outer right dart. This alternating sequence (left and right) continues until the last dart has been dropped.

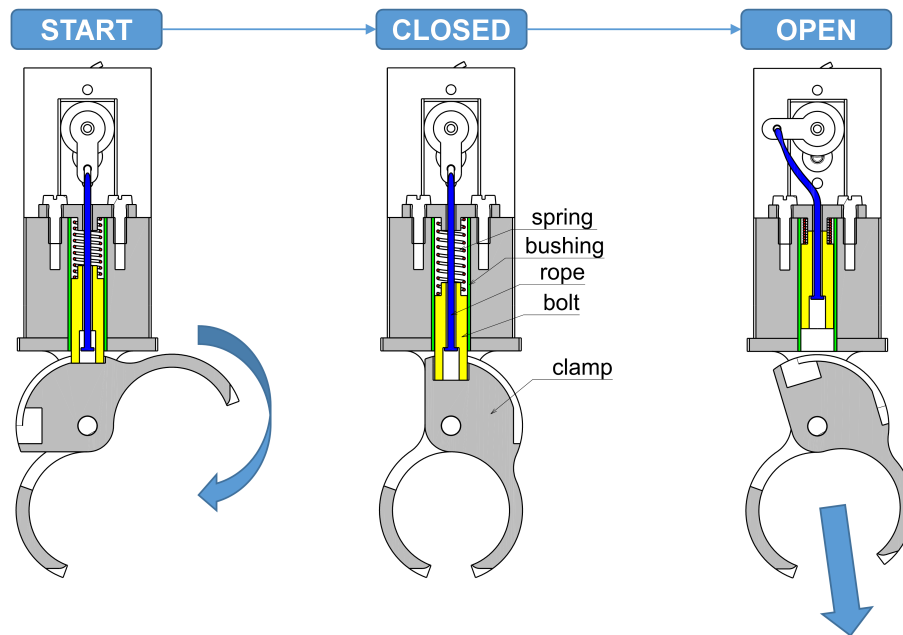


Figure 37: Lock and drop sequence

5.3.3 Radome Attachment and Rotation Mechanism

The radome attachment and rotation mechanism was designed to be mounted and removed very quickly. To achieve this, the mechanism consists of two main parts. One part is mounted on top of the fuselage and houses a speed controller for a brushed motor. The other part is fixed to the radome itself. This part houses a small electric motor which is responsible for the rotation of the radome. Both parts can be connected with a buckle like fastening. When the radome is attached, the wiring connects the motor and the receiver, and the radome is able to rotate.

5.3.4 Propulsion

Two different battery packs were chosen for fulfilling the different mission requirements. For Mission 1 and Mission 2 the propulsion battery pack consists of 40 NiMH cells with 3000 mAh and a nominal voltage of 1.2 V each. Connecting these as two 20 cell serially connected packs that are wired in parallel the battery has a nominal voltage of 24 V and a nominal capacity of 6000 mAh. For Mission 3 more capacity and more voltage is needed for a longer endurance and more static thrust. The chosen battery pack consists of 42 NiMH cells with a nominal voltage and capacity of 1.2 V and 4000 mAh each. The cells are connected to form a battery with a nominal capacity of 8000 mAh and a nominal voltage of 25.2 V. A variety of motors and propellers were analyzed using the eCalc program, as described in Section 4.2.3. The A50-12L Turnado V3 motor was chosen because of its weight, size and static thrust. A 18"x11" and a 17"x10" propeller were chosen for their desired ratio between the thrust required for cruise speed and the thrust required for takeoff. The finally selected propulsion system consists of a A50-12L Turnado V3 motor, the two mentioned battery configurations and a ROXXY BL Control 9120-12 Opto speed controller along with 18"x11" and 17"x10" propeller.

5.3.5 Controls

Various servo motors were selected for the different surfaces and moving parts on the aircraft, by analyzing hinge moments for each control surface, and then finding servos that had sufficient control power to handle the calculated moments, with the lightest weight possible. The chosen components are tabulated in Table 19.

Table 19: Selected components

Components	Description
Transmitter	Futaba T14SG
Receiver 1	Futaba R7008SB
Receiver 2	Futaba R7008SB
Aileron Servo Motor	KST DS135MG
Elevator Servo Motor	Master DS 3615
Rudder Servo Motor	Savöx SH-0263MG
Flaps Servo Motor	KST DS135MG
Folding Mechanism	
Sweep Servo Motor	Graupner DS8911
Rotation Servo Motor	KST DS125MG
Drop Mechanism	
Microcontroller	Arduino Nano
Release Servo Motor	Master mini Servo S2112
Radome	
Motor	6V 30 rpm brushed motor
Speed Control	Speed 400 motor controller

5.4 Weight and Balance

An important aspect of static and dynamic stability is the correct position of the center of gravity, which was determined in the foregoing aerodynamic calculations. In the detail design phase, all systems must be distributed correctly to balance the CG in the allowable range without the use of any additional ballast. The CG position measured from the front of the fuselage is shown in Figure 38.

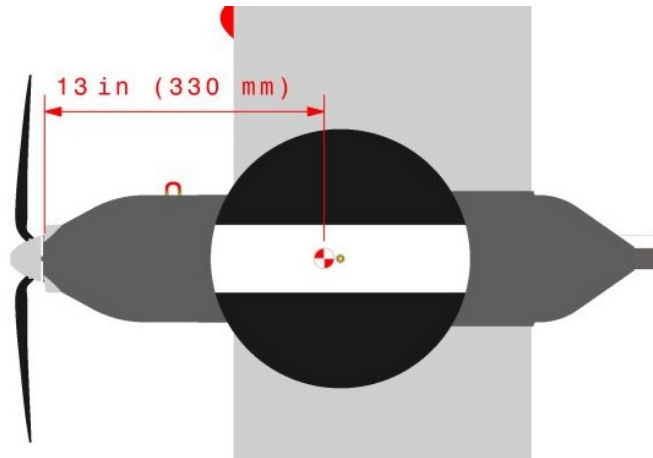


Figure 38: Center of gravity shown in the CAD model

To be able to calculate the CG position, all structural components were integrated into the CAD model of the contest aircraft *Bobby*. The CG position could then be calculated in the CAD program. Table 20 shows the calculated CG position of the final aircraft with and without payload.

Table 20: Weight and balance of *Bobby*

Component	Weight [lbs]	CG location x-axis [in]	CG location z-axis [in]
Fuselage	1.47	12.99	-0.35
Wing	2.98	15.16	0.11
Empennage	0.84	37.40	2.43
Motor & Propeller	1.05	1.42	0.00
Speed Control	0.39	8.27	1.06
Receiver Battery Management	0.09	18.11	-2.55
Receivers	0.05	20.08	1.65
Servo Motors on Wing	0.34	16.54	0.16
Rudder Servo Motor	0.04	53.15	1.18
Nose Landing Gear	0.21	3.15	-3.44
Rear Landing Gear	0.29	20.47	-4.67
Elevator Servo Motor	0.06	23.03	-0.02
Drop Mechanism	0.72	13.87	-1.51
Radome Attachment	0.07	13.78	-1.51
EW excl. Batteries	8.74	15.15	-0.06
Mission 1			
Propulsion Battery	4.74	9.04	-0.49
Receiver Batters	0.49	12.99	-2.72
Aircraft Total (EW)	13.96	13.00	-0.30
Mission 2			
Propulsion Battery	4.74	9.06	-0.49
Receiver Batters	0.49	12.99	-2.72
Radome	0.53	13.78	5.58
Aircraft Total	14.49	13.04	-0.08
Mission 3			
Propulsion Battery	5.82	9.45	-0.47
Receiver Batters	0.49	13.78	-2.69
Dart Rockets	1.94	13.39	-3.69
Aircraft Total	16.99	12.96	-0.69

5.5 Flight Performance

The flight performance of *Bobby* is described by the main flight performance parameters of velocity and stall speed. These parameters are calculated values, validated by flight test results. The turn radius was calculated under the assumptions of a constant load factor of 1.5 g and an air speed of 82 ft/s during the turn. The distance of one lap

consists of two times 1 000 ft plus one 360 degree and two 180 degree turns overall.

With the assumptions made, the resulting lap distance is 4 888 ft. With a constant speed of 84.39 ft/s the number of 14 laps is possible with enough power reserve for takeoff and a safe landing. The performance parameters presented in Table 21 apply to M3 because the aircraft has the highest takeoff weight during this missions.

Table 21: Final flight performance parameters

Parameter	Value
Maximum Takeoff Weight [lbs]	16.99
Cruise Speed [ft/s]	84.39
Stall Speed [ft/s]	32.8
C_{lmax}	1.6
Endurance [s]	720

5.6 Mission Performance

Based upon the flight performance parameters and aircraft configuration parameters, the corresponding mission results were calculated. The calculation of the mission scores and final score were made according to the formulae contained in the competition rules [13]. Because of the fact that the calculation of the flight mission score also includes the mission performance parameters from the best-performing team of each mission, estimations for these best-performing teams were made.

Table 22: Predicted flight scores

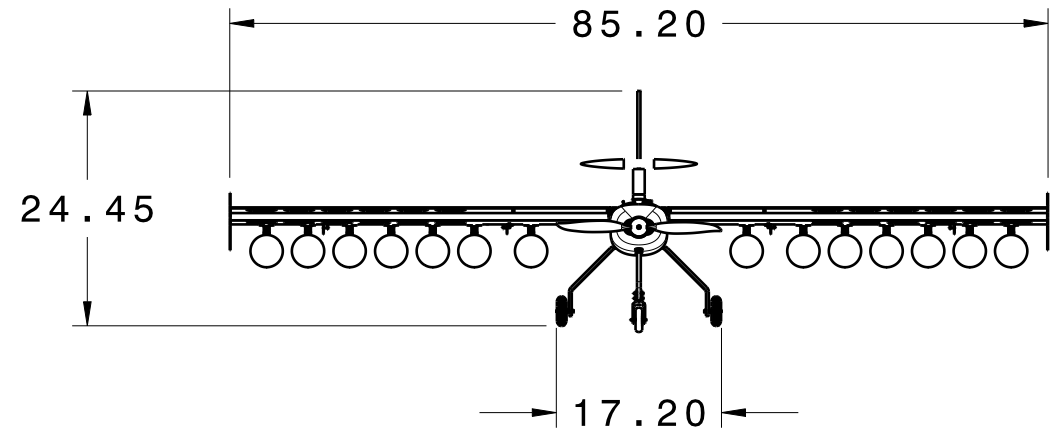
Aircraft	M1	M2	M3	GM
<i>Bobby</i>	1.0	120 s	14 Dart Rockets	40s
Assumed Best	1.0	90 s	16 Dart Rockets	30 s
Score	1.0	1.75	16	0.75

5.7 Drawing Package

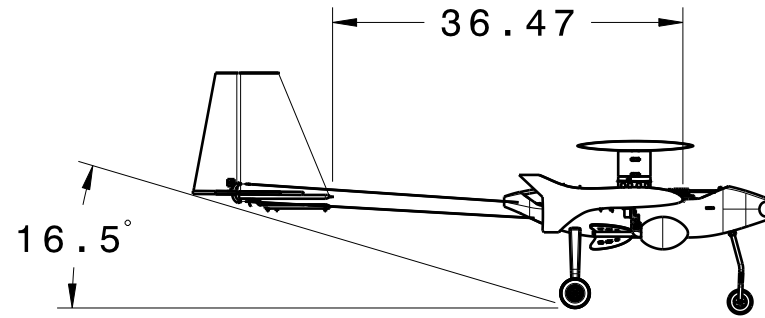
The following four pages illustrate the detailed CAD [14] drawings of *Bobby*. The first sheet has the three-view diagram with relevant dimensions. The second sheet shows the structural arrangement of all major components. The third sheet displays the systems layout and location. The fourth sheet displays the payload arrangement for the external payloads.

A

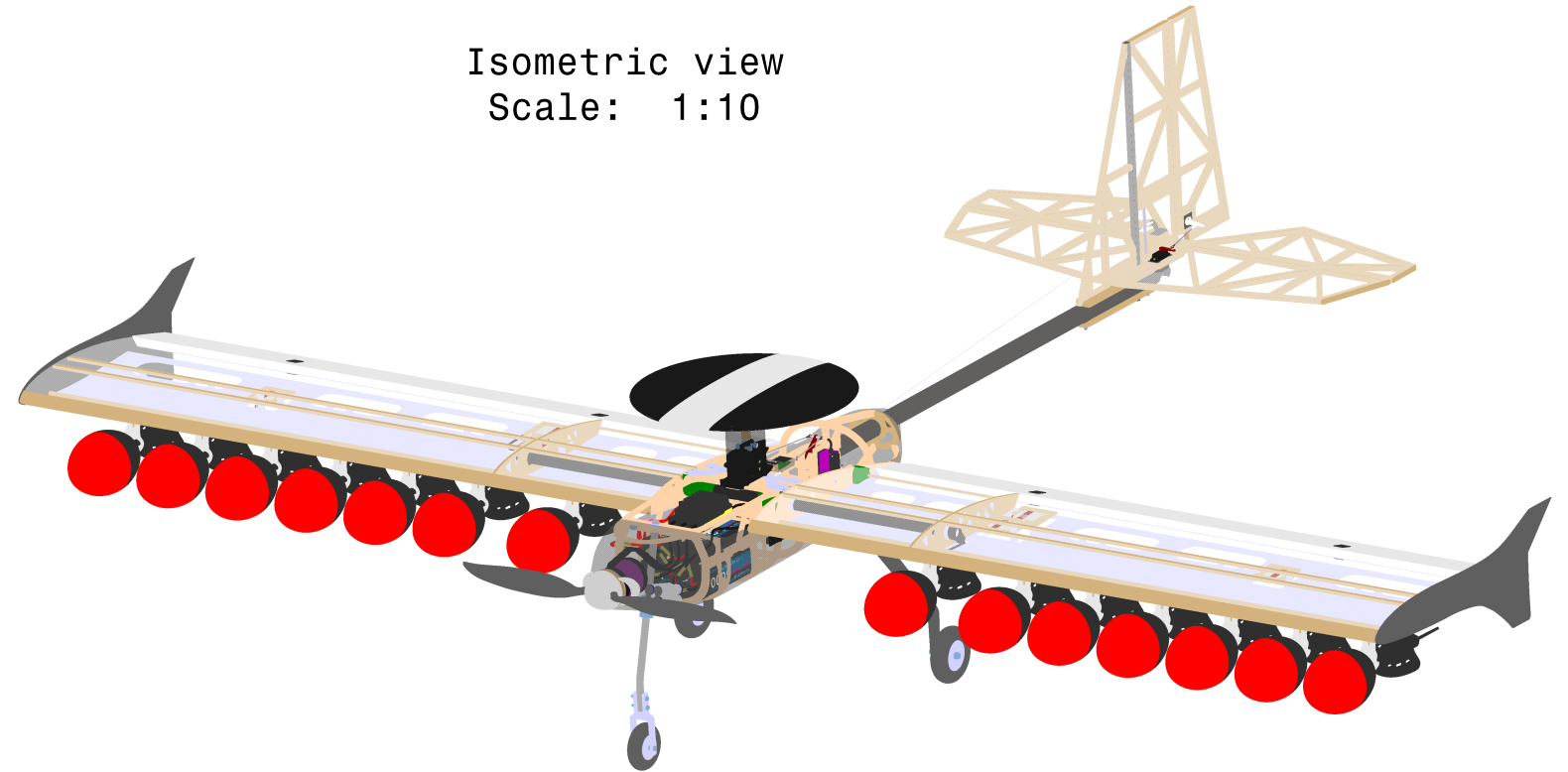
Front view



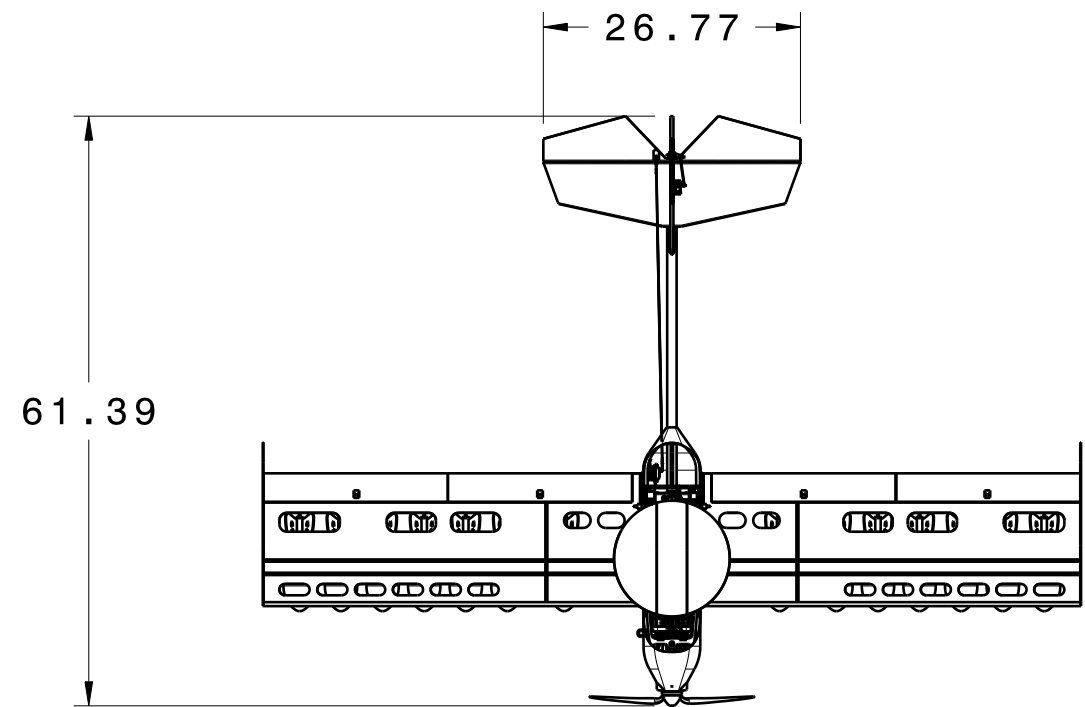
Left view



Isometric view
Scale: 1:10




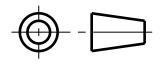
Top view

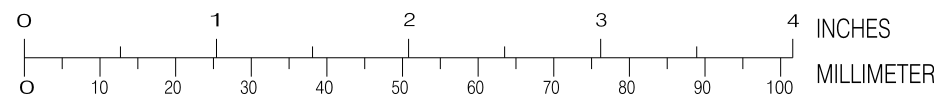


General Note:

Plastic skin on wings and empennage and fuselage top shell omitted for clarity

THIS DRAWING IS THE PROPERTY OF JOANNEUM AERONAUTICS ASSOCIATION WHICH RESERVES ALL RIGHTS

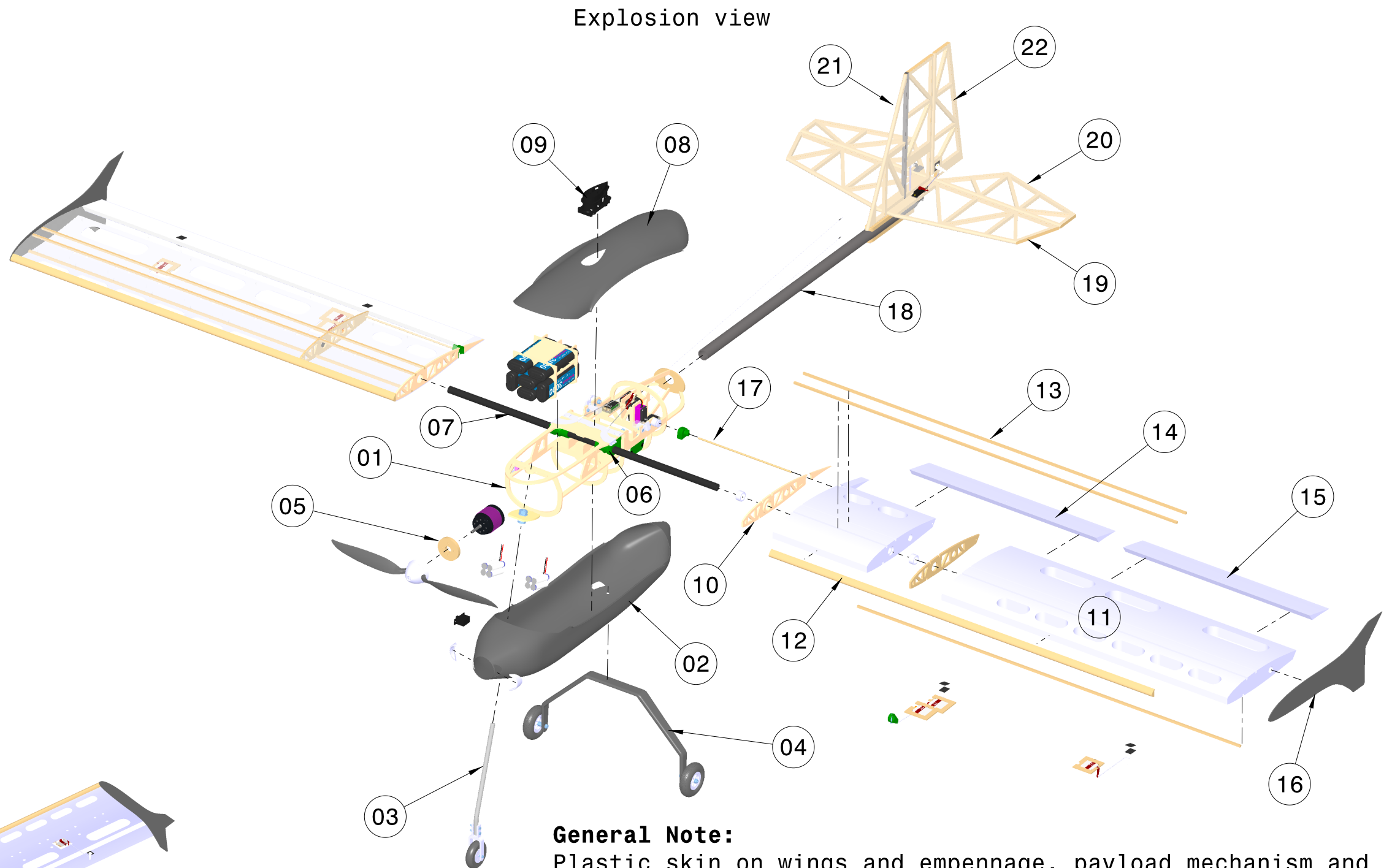
Title 3-View Drawing		AIAA DESIGN, BUILD, FLY CONTEST 2019		 joanneum Aeronautics e.V. Alte Poststraße 149 8020 Graz Austria http://joanneum-aeronautics.at/
		Date	Name	
Drawn	01.02.2019	M. Höftberger		
Chk'd	01.02.2019	M. Krampf		
App'd	01.02.2019	M. Kucera		
General Tolerances ISO 2768-1 m		Projection 		
Dimensions inches	Weight 16.99 lbs	Scale 1:20 (1:10)	Size 11" x 17"	Sheet 1 of 4



F

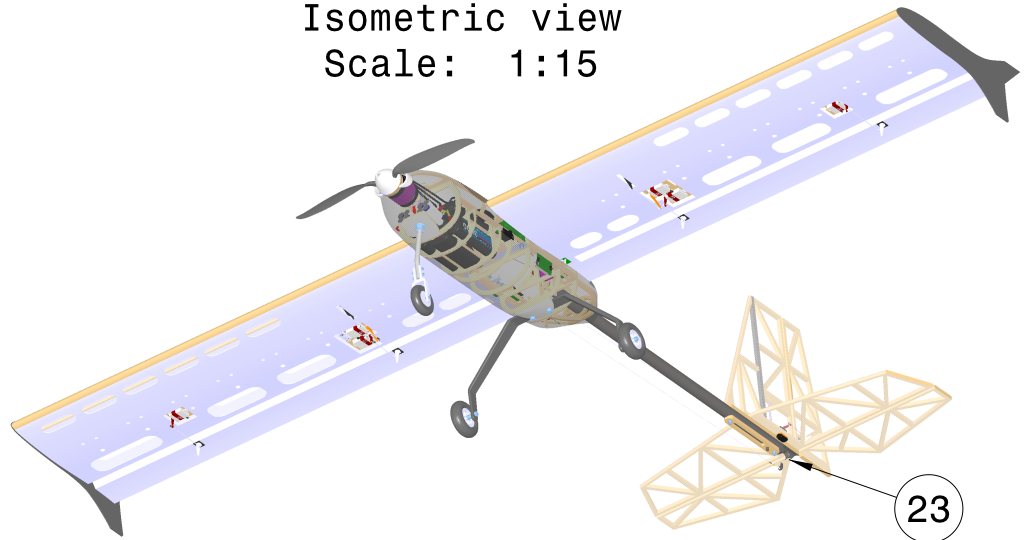
F

Item	Qty.	Part Name	Material
01	24	Fuselage Frames	Plywood
02	1	Fuselage Shell Bottom	CFRP
03	1	Nose Gear	Aluminum
04	1	Main Landing Gear	CFRP
05	1	Motor Mount	Plywood
06	2	Wing Suspension	PLA
07	2	Wing Shaft	CFRP
08	1	Fuselage Shell Top	CFRP
09	1	Radome Mount	PLA
10	4	Wing Ribs	Plywood
11	4	Wingbox	Styro
12	2	Leading Edge	Balsa
13	6	Wing Stringers	Pinewood
14	2	Flaps	Styro
15	2	Ailerons	Styro
16	2	Winglets	CFRP
17	2	Torsion Bar	Brass
18	1	Empennage Boom	CFRP
19	20	Horizontal Tail Ribs	Balsa
20	18	Elevator Ribs	Balsa
21	10	Vertical Tail Ribs	Balsa
22	10	Rudder Ribs	Balsa
23	1	Tail Hook	CFRP

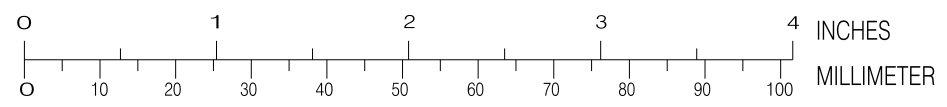


Explosion view

Isometric view
Scale: 1:15



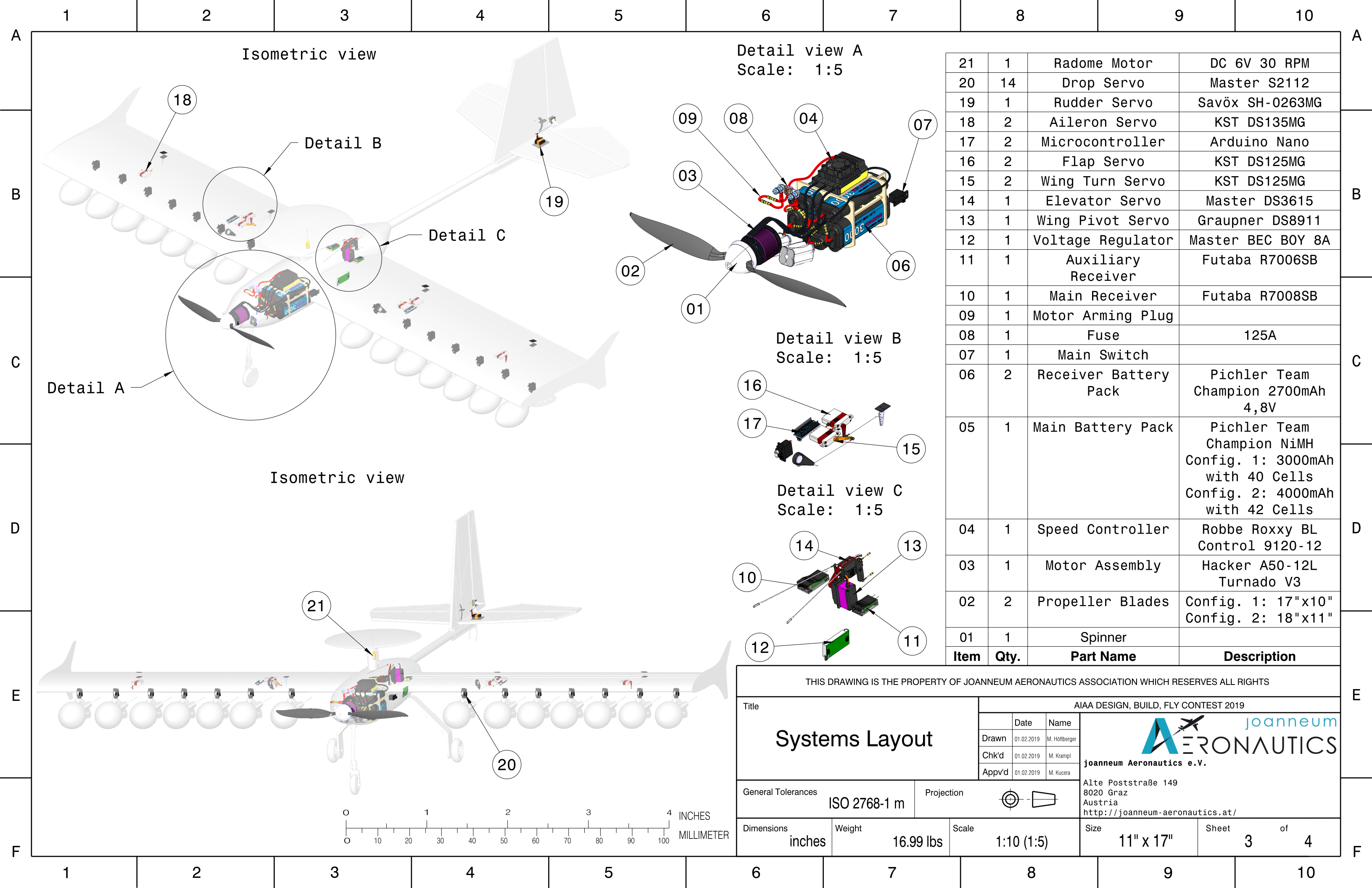
General Note:
Plastic skin on wings and empennage, payload mechanism and radome omitted for clarity



THIS DRAWING IS THE PROPERTY OF JOANNEUM AERONAUTICS ASSOCIATION WHICH RESERVES ALL RIGHTS

Title		AIAA DESIGN, BUILD, FLY CONTEST 2019	
Structural Arrangement	Drawn	01.02.2019	M. Höftberger
	Chk'd	01.02.2019	M. Krampf
	App'd	01.02.2019	M. Kucera
General Tolerances		ISO 2768-1 m	Projection
Dimensions	Weight	Scale	Size
inches	16.99 lbs	1:10 (1:15)	11" x 17"
		Sheet	of
		2	4

joanneum Aeronautics e.V.
 Alte Poststraße 149
 8020 Graz
 Austria
<http://joanneum-aeronautics.at/>



Isometric view

Detail view A
Scale: 1:5

Isometric view

Detail view B
Scale: 1:5

Detail view C
Scale: 1:5

21	1	Radome Motor	DC 6V 30 RPM
20	14	Drop Servo	Master S2112
19	1	Rudder Servo	Savöx SH-0263MG
18	2	Aileron Servo	KST DS135MG
17	2	Microcontroller	Arduino Nano
16	2	Flap Servo	KST DS125MG
15	2	Wing Turn Servo	KST DS125MG
14	1	Elevator Servo	Master DS3615
13	1	Wing Pivot Servo	Graupner DS8911
12	1	Voltage Regulator	Master BEC BOY 8A
11	1	Auxiliary Receiver	Futaba R7006SB
10	1	Main Receiver	Futaba R7008SB
09	1	Motor Arming Plug	
08	1	Fuse	125A
07	1	Main Switch	
06	2	Receiver Battery Pack	Pichler Team Champion 2700mAh 4,8V
05	1	Main Battery Pack	Pichler Team Champion NiMH Config. 1: 3000mAh with 40 Cells Config. 2: 4000mAh with 42 Cells
04	1	Speed Controller	Robbe Roxxy BL Control 9120-12
03	1	Motor Assembly	Hacker A50-12L Turnado V3
02	2	Propeller Blades	Config. 1: 17"x10" Config. 2: 18"x11"
01	1	Spinner	
Item	Qty.	Part Name	Description

THIS DRAWING IS THE PROPERTY OF JOANNEUM AERONAUTICS ASSOCIATION WHICH RESERVES ALL RIGHTS

Title		AIAA DESIGN, BUILD, FLY CONTEST 2019									
<h1>Systems Layout</h1>	Date	Name									
	Drawn	01.02.2019	M. Höftberger								
	Chk'd	01.02.2019	M. Krampf								
	App'd	01.02.2019	M. Kucera								
General Tolerances		ISO 2768-1 m	Projection								
Dimensions	inches	Weight	16.99 lbs	Scale	1:10 (1:5)	Size	11" x 17"	Sheet	3	of	4

joanneum
AERONAUTICS
joanneum Aeronautics e.V.
Alte Poststraße 149
8020 Graz
Austria
<http://joanneum-aeronautics.at/>

Radome Bill of Material

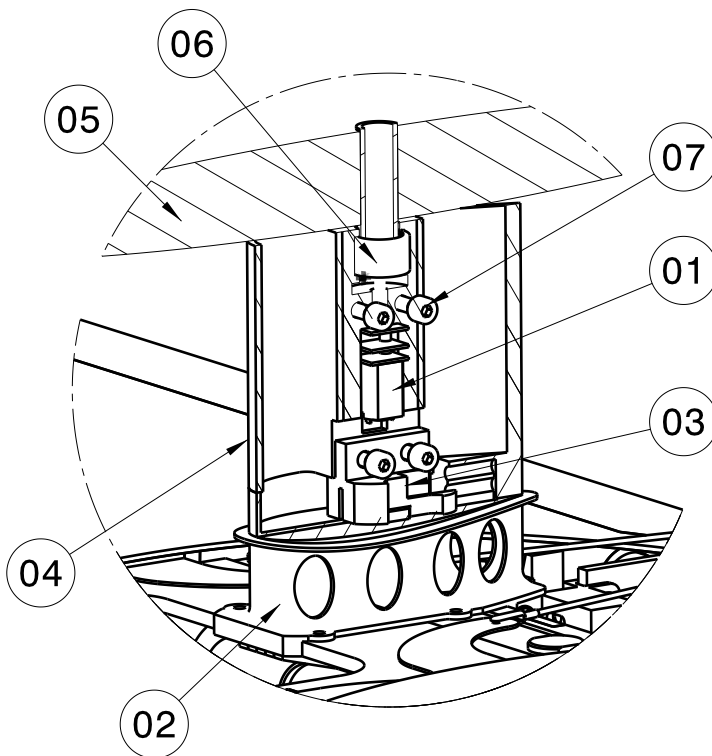
Item	Qty.	Part Name	Description
01	1	Radome Motor	DC 6V 30 RPM
02	1	Radome Mount	PLA
03	1	Radome Clip	PLA
04	1	Radome Pillar	PLA
05	1	Radome Disc	CFRP
06	1	Needle Bearing	SKF HK1210
07	4	Head Cap Screw	ISO4762-M4x20

Payload-drop Mechanism Bill of Material

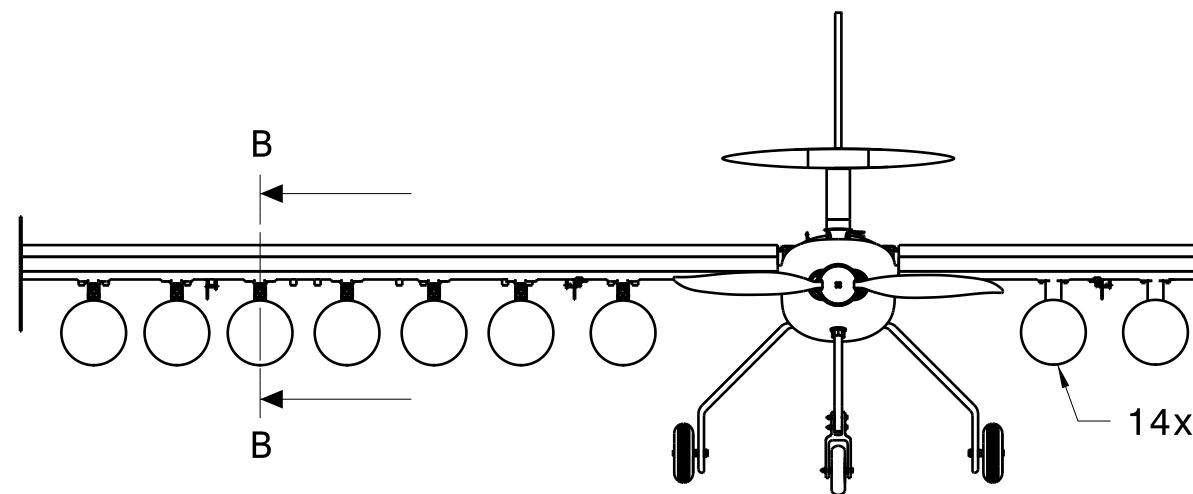
Item	Qty.	Part Name	Description
08	1	Drop Mech Mount	PLA
09	1	Clamp	PLA
10	1	Drop Servo	Master S2112
11	1	Bolt	Aluminum
12	1	Spring	Steel
13	1	Bushing	Brass

General Note:
Fuselage top shell omitted for clarity

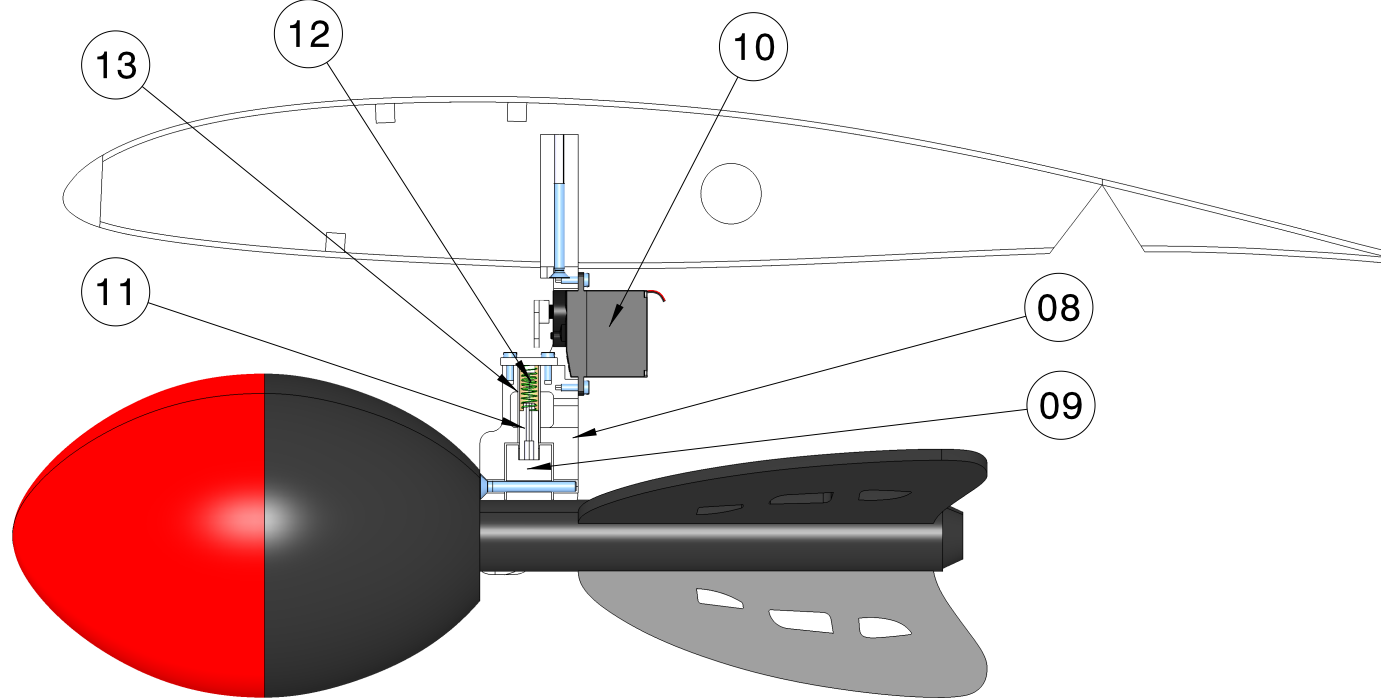
Detail view A
Scale: 1:2



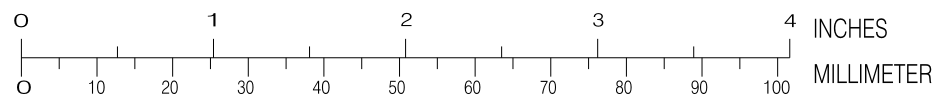
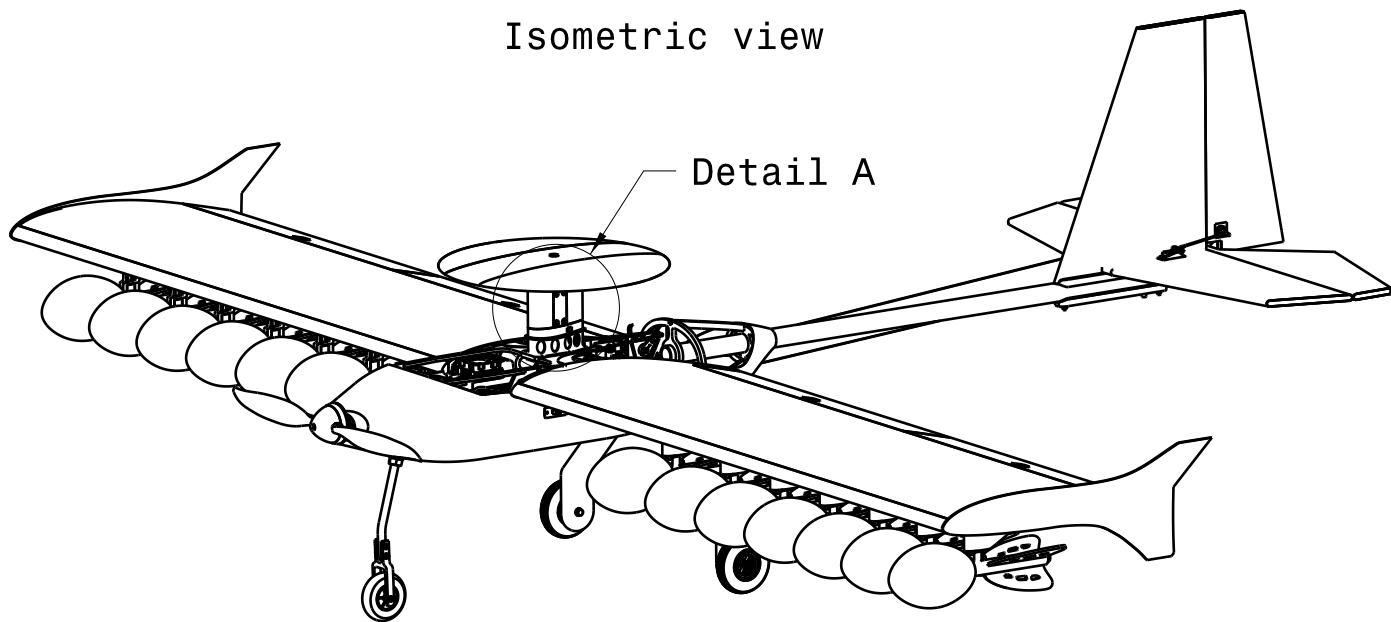
Front view



Section cut B-B
Scale: 1:2



Isometric view



THIS DRAWING IS THE PROPERTY OF JOANNEUM AERONAUTICS ASSOCIATION WHICH RESERVES ALL RIGHTS

Title
Payload Accomodation

AIAA DESIGN, BUILD, FLY CONTEST 2019

	Date	Name
Drawn	01.02.2019	M. Höftberger
Chk'd	01.02.2019	M. Krampf
App'd	01.02.2019	M. Kucera



Alte Poststraße 149
8020 Graz
Austria
<http://joanneum-aeronautics.at/>

General Tolerances ISO 2768-1 m Projection

Dimensions inches Weight 16.99 lbs Scale 1:10 (1:2)

Size 11" x 17" Sheet 4 of 4

6 Manufacturing Plan and Processes

The team considered various manufacturing processes and materials. The chosen manufacturing process for each component represented the best combination of the materials weight, repeatability, and ease of manufacturing, as well as prior experience with the process and costs.

6.1 Manufacturing Processes Investigated

The team had a wealth of experience in various manufacturing techniques. Since not every method suits every component, different methods were used and combined with each other. The techniques chosen were investigated and evaluated to optimize the manufacturing of all components of the aircraft. The main criteria for choosing the process were:

- **Weight:** Similar to the conceptual design, weight is still the most important factor.
- **Repeatability:** The process should not be too complex in order to reproduce spare parts easily.
- **Ease of Manufacturing**
- **Experience:** Prioritize methods with which team members have experience.
- **Cost:** The methods used should be in compliance with the team's limited resources.

6.1.1 Styrofoam

Styrofoam can easily be shaped by sanding or by using a hot-wire foam cutter. It is inexpensive, lightweight, and has good mechanical dampening properties. Styrofoam is ideal for non-structural parts or as a sandwich, because of its material properties.

6.1.2 3D-Printing

With 3D-printing, it is possible to manufacture complex parts as well as molds for composite manufacturing with relatively high precision on the basis of a CAD-model. Another advantage is the reduction in lead times. However, the parts which can be manufactured are limited to the size of the printing bed of the 3D-printer.

6.1.3 Composites

Carbon fiber or fiberglass composites have a high strength-to-weight ratio and are, therefore, well suited for structural elements. The downsides are the high material costs and the long lead times of the manufacturing process.

6.1.4 Balsa / Plywood Build-Up

A structure made of balsa wood provides decent strength together with low weight. The single components can be manufactured with the help of tools or by using a CNC milling machine or a CNC laser cutter.

6.2 Manufacturing Processes Selected

As already mentioned, the team used different manufacturing methods for different components. Since every method had its very unique advantage over the others for single components no FOM analysis was conducted. The following section describes the manufacturing processes selected for the major aircraft components.

6.2.1 Wings

The main structure of the wings was produced from styrofoam by means of a CNC hot-wire foam cutter (Figure 39). The cutouts for the flaps and ailerons were machined in the same CNC fashion. The holes for the control surface servomotors and M3 drop mechanisms were cut out by hand with a milling cutter. The gaps which occurred during the cutting process, were filled up with glued pinewood stringers. The leading edge of the foam was replaced with a balsa wood strip, and on the innermost position, as well as at the connection of the two styrofoam cores, the wing is reinforced with plywood ribs, which also house the needle-roller bearing enabling the wing rotation. The rib that connects both cores also connects to the main spar (Figure 40).

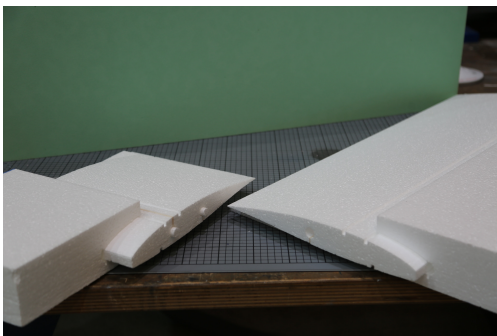


Figure 39: Styrofoam core

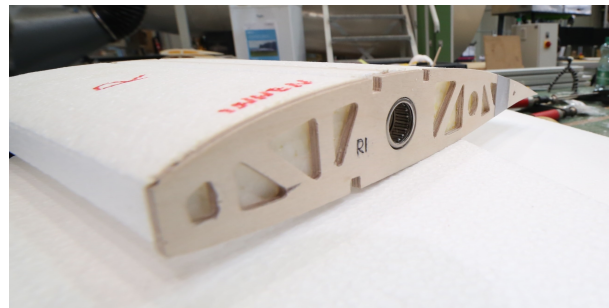


Figure 40: Balsa rib that connects both cores with bearing for folding mechanism

For additional reinforcement, one layer of fiberglass was used on the upper and lower surface of the wing, from the root up to the connection rib. This was done by laminating directly on the balsa sheets and laying the styrofoam core onto it (Figure 41). In the next manufacturing step, the wings were clad with balsa wood (Figure 42) and finally coated with Oracover.



Figure 41: Fiber reinforced Wing



Figure 42: Balsa clad wing

6.2.2 Fuselage

The fuselage consists of two main components: the outer skin and an internal framework. The skin is made of carbon fiber and manufactured using the vacuum bagging method (Figure 43). The necessary molds for this process were milled out of a SikaBlock[®] (Figure 44). The vacuum bagging manufacturing process is used to produce fiber reinforced plastic parts. The dry fabric is impregnated with an epoxy resin by hand with a brush or a roll on the mold. The open side of the mold is afterwards covered by a foil that seals the mold and the laminate from the environment. By applying a vacuum under the foil, the covered laminate gets compressed by the ambient pressure and the risk of delamination or air bubble entrapment is reduced.

The internal framework is made of plywood. Its main function is to house the folding mechanism and provide the mount for the motor. Furthermore, it supports the skin in areas of higher stress and connects the landing gear to the fuselage. The framework and carbon skin are glued together with five-minute epoxy resin.



Figure 43: Vacuum bagging method for the skin

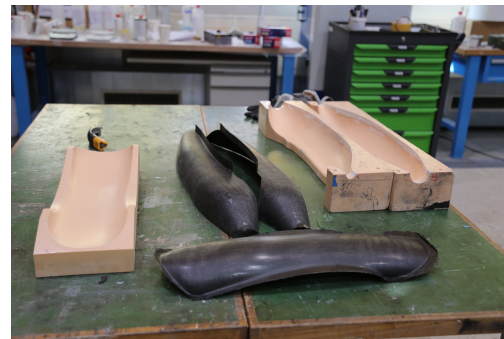


Figure 44: Finished fuselage skin

6.2.3 Empennage

Since the empennage is a rather simple part the balsa build-up method was used to minimize weight. For building the structure of the empennage, the drawing of the CAD-Model at a scale of 1:1 was printed out and used as a template for incorporating the balsa. The aircraft's wood construction was done on a pin board, so that all pieces could be precisely aligned and pinned in place to avoid wing warp. The fin and horizontal stabilizer are connected with a carbon rod. All parts of the empennage were finally coated with Oracover.

6.2.4 Folding Mechanism

The structural components of the folding mechanism were mainly 3D-printed. This was due to the fact the mechanism's geometry is rather complex and would have been too time consuming if it had been made by hand. The material of choice was Copolyester (CPE), since it is durable and tough compared to other common materials. It further demonstrates good dimensional stability. CPE is printed at a temperature of 527 °F and can be printed by any 3D-printer.

6.3 Manufacturing Milestone Plan

Figure 45 shows the manufacturing milestone chart. It is a detailed timetable of each manufacturing step, with respect to the planned and the actual time needed.

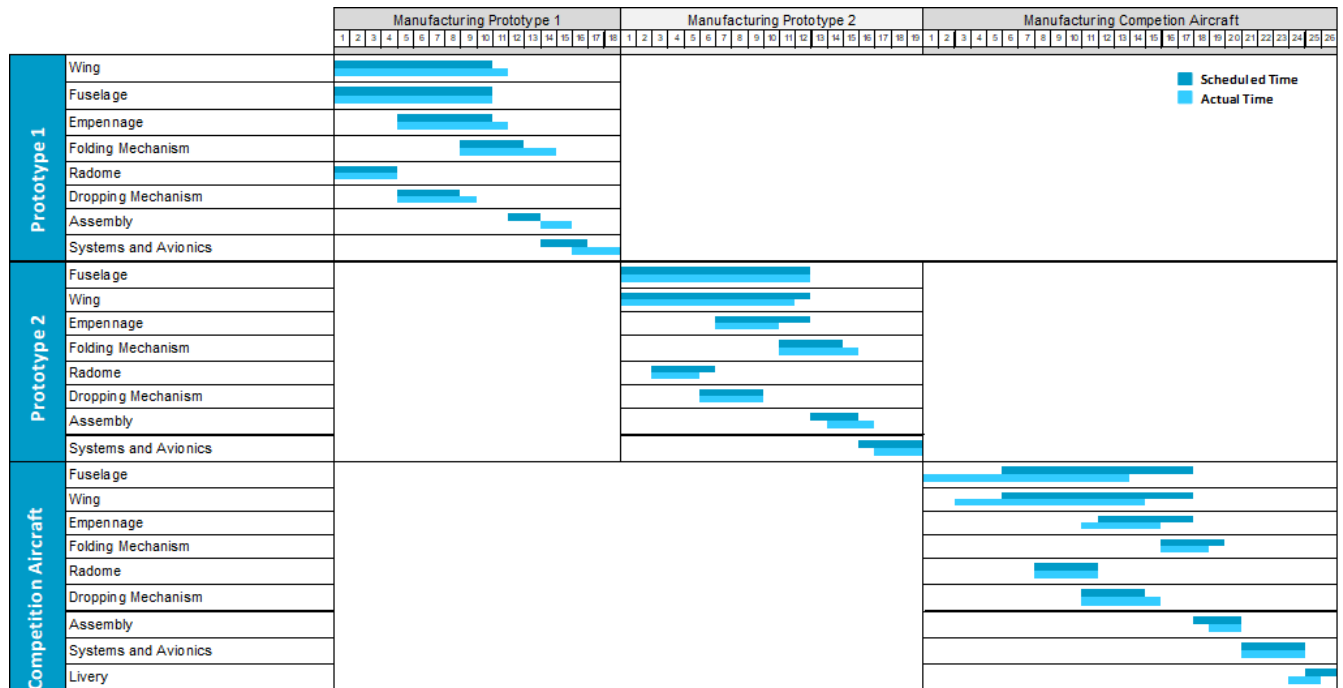


Figure 45: Aircraft manufacturing milestone chart showing planned versus actual timing

7 Testing Plan

In the flight and ground tests, the aircraft's components and mechanisms were tested to clear up the last doubts about their proper functionality and to generate profound data on their performance. Based on these data, the final design decisions were made.

7.1 Objectives and Schedule

In the test phase, several types of tests were conducted. On the one hand, ground tests like static thrust measurements, a drop mechanism test, wing folding mechanism tests and structural tests were executed. On the other hand flight tests were conducted to simulate the performance of the aircraft under contest conditions and thus predict its performance at the contest itself. A milestone chart of the testing schedule can be seen in Figure 46.

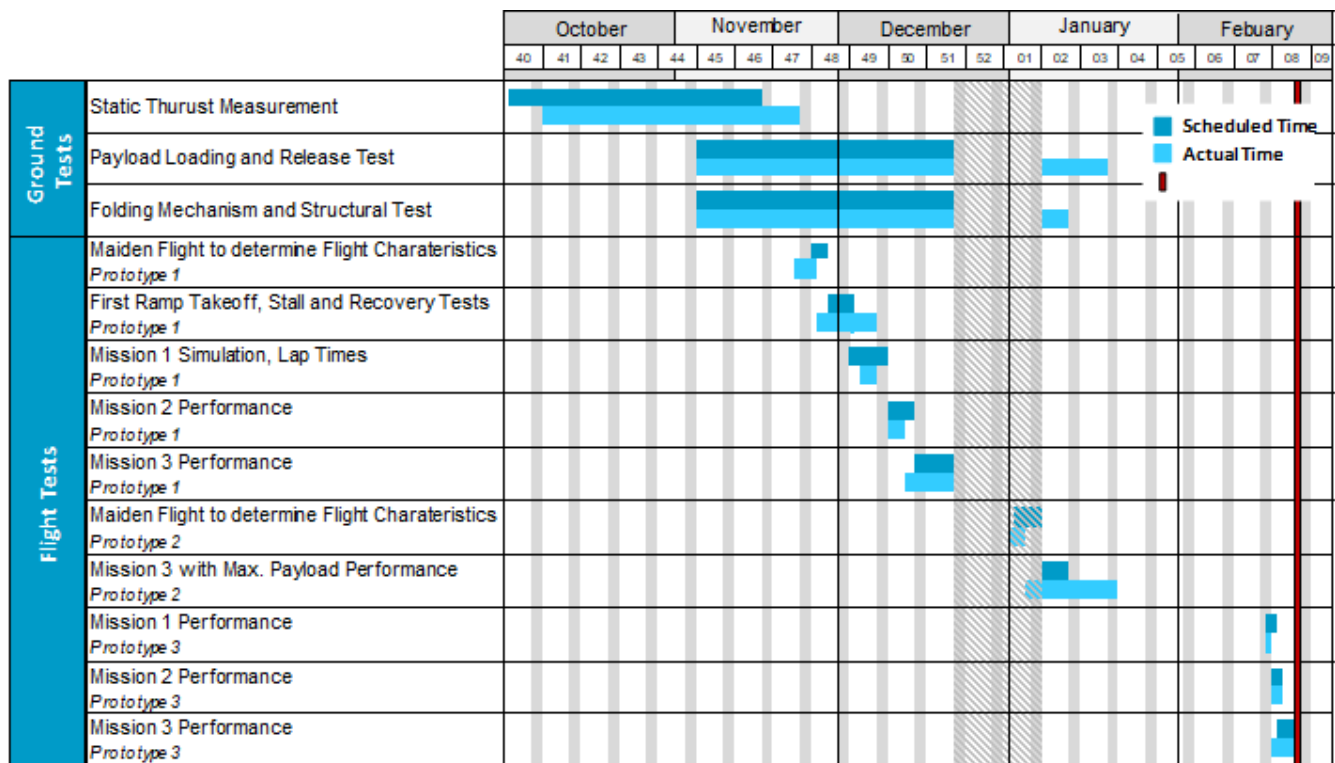


Figure 46: Aircraft and sub system testing schedule

7.2 Ground Test

The ground test included several component verification tests.

7.2.1 Static Thrust Measurement

The test objectives of the static thrust measurement were to gather data:

- the force - electric current interrelationship for different propellers. Outcome should be Newton/Ampere-curves that can be used to estimate and verify the level flight thrust or take-off thrust
- the battery pack endurance, respectively the estimated flight time
- the battery pack operating temperature
- occurring electric current peaks
- the operating voltage behavior

7.2.2 Payload Loading and Release Test

The functionality of the payload loading mechanism for the second and third missions was verified by conducting a trial ground mission. The ground mission was simulated with different individuals. Since the distance between the start/finish line and the aircraft was not specified and is unknown to the team, the double width of the mission box (20 ft) was assumed. The team conducted a timed loading sequence in which the radome was installed (4 s) and a second timed sequence in which the radome was removed (11 s) and four attack stores were installed (11 s). This test has shown that the designed mechanisms work as intended and more training is needed for a better GM score.

To gain information about the structural integrity and reliability of the mechanisms, stress tests were conducted. As the electrical components that are used to rotate the radome are integrated in its attachment, the radome was removed and attached several times to verify that the plugs do not suffer from the installation process.

The most important aspect of the drop mechanism is its reliability. The goal for the third flight mission is to drop a single dart rocket in each flown lap. If other parts than the dart rocket or a second dart rocket is dropped the lap is invalid. Therefore, the drop mechanism underwent several tests to verify its reliability. Besides inflight tests, the drop mechanism was initially tested in a controlled static environment for its proof of concept. Since no wind tunnel of sufficient size was available to the team, the drop mechanism was tested by holding it out of a car window while driving at approximately 50 kt.

7.2.3 Folding Mechanism and Structural Testing

To validate the design of the wings, the folding mechanism and the connection between the fuselage and the folding mechanism, the aircraft was subjected to a wing tip test. A wing tip test simulates the maximum loading on the wing during flight. Therefore the aircraft was loaded with the maximum weight and lifted at the wing tips. This tests simulated a loading of 2.5 g. To verify that the folded aircraft fulfills the sizing requirements, a box with the dimensions stated in the rules, was built (Figures 47 and 48).



Figure 47: Roll through test with wooden box



Figure 48: Roll through test with wooden box

7.3 Flight Test

Flight tests were conducted with three iterations of design. The first aircraft, representing the first iteration, was used to determine the flying qualities and if the desired configuration was able to take off from a ramp. Several rounds of a simulated M1 were flown. Since the concept was proven at the very first flight, the first prototype was also used for first tests with attack stores.

The second prototype incorporates some minor changes to its design. These include size and weight reduction for the empennage design and a more robust landing gear. This prototype will undergo M2 and M3 simulation.

The experience and data gained from Prototype 2 will be used to finalize the the third aircraft which will be the competition aircraft. This aircraft will then fly all three missions to determine its performance and train the pilot.

The flight order and purpose of each flight is displayed in Table 23.

Table 23: Test flight order

Flight Test	Aircraft	Purpose
1	Prototype 1	Maiden Flight, Determine Flight Characterisitcs
2	Prototype 1	First Ramp Takeoff, Stall and Recovery Tests
3	Prototype 1	Mission 1 Simulation, Lap Times
4	Prototype 1	Mission 2 Performance
5	Prototype 1	Mission 3 Performance
6	Prototype 2	Maiden Flight, Verification of Design Changes
7	Prototype 2	Mission 3 with max. Payload Performance
8	Competition Aircraft	Mission 1 Performance
9	Competition Aircraft	Mission 2 Performance
10	Competition Aircraft	Mission 3 Performance

To simulate the special takeoff scenario, the team built a takeoff ramp with the dimensions given in the rules (Figure 49). This ramp was then used for all flight tests, except for the first one.



Figure 49: Aircraft taking off the ramp

7.4 Checklists

An important measure for preventing any system from malfunctioning in flight, which could lead to a crash of the aircraft, was the checklist presented in Tables 24 and 25 . It will also be used at the competition.

Table 24: Flight checklists

Pre-Flight Checklist:		
<input type="checkbox"/>	Inspect Aircraft Exterior	NO DAMAGES
<input type="checkbox"/>	Inspect Landing Gear	FREELY MOVING
<input type="checkbox"/>	Inspect Aircraft Interior	STRUCTURE INTACT, NO CRACKS
<input type="checkbox"/>	Battery Voltages (TX, RX, Propulsion)	VERIFIED
<input type="checkbox"/>	Batteries (RX, Propulsion)	INSERTED AND ATTACHED
<input type="checkbox"/>	Mission specific Payload	PREPARED
<input type="checkbox"/>	Center of Gravity	CHECKED, WITHIN LIMITS
<input type="checkbox"/>	Canopy	CLOSED AND LOCKED
Folding Checklist:		
<input type="checkbox"/>	Wings in Stowed Configuration	CHECKED
<input type="checkbox"/>	Transmitter Switches in Stowed Configuration	CHECKED
<input type="checkbox"/>	Folding Area	CLEAR
<input type="checkbox"/>	TX Power	ON
<input type="checkbox"/>	RX Master Switch	ON
<input type="checkbox"/>	Forward Sweep	COMPLETED
<input type="checkbox"/>	Rotation	COMPLETED
<input type="checkbox"/>	Locking Device	LOCKED
<input type="checkbox"/>	Sweep Servo	RELEASED
Before Takeoff Checklist:		
<input type="checkbox"/>	Wind and Weather	FLYABLE
<input type="checkbox"/>	Air and Ground Traffic	CLEAR
<input type="checkbox"/>	TX Power	ON
<input type="checkbox"/>	RX Master Switch	ON
<input type="checkbox"/>	Control Surfaces	CHECKED, FREELY MOVING
<input type="checkbox"/>	Mission specific Payload	MOUNTED
<input type="checkbox"/>	Propeller Area	CHECKED, CLEAR
<input type="checkbox"/>	Propulsion Arming Plug	INSERTED
<input type="checkbox"/>	Propulsion	CHECKED, WORKING

Table 25: Flight checklists

After Landing Checklist:		
<input type="checkbox"/>	Propulsion Arming Plug	REMOVED AND SAFE
<input type="checkbox"/>	RX Master Switch	OFF
<input type="checkbox"/>	TX Master Switch	OFF
Post Flight Checklist:		
<input type="checkbox"/>	Top Lid	OPENED
<input type="checkbox"/>	Batteries (RX, Propulsion)	UNPLUGGED AND REMOVED
<input type="checkbox"/>	Payload	REMOVED

Separate checklists were produced for propulsion testing as well as range and fail-safe testing. These checklists are presented in Tables 26 and 27. Strict adherence to these checklists is monitored to prevent incidents and injuries to personnel.

Table 26: Test checklists

Propulsion Test Checklist:		
<input type="checkbox"/>	Motor	SECURED, ROTATES FREELY
<input type="checkbox"/>	Propeller	SECURED, NO DAMAGE
<input type="checkbox"/>	Battery	CONNECTED, CHARGED
<input type="checkbox"/>	ESC	CONNECTED, CORRECT SETTINGS
<input type="checkbox"/>	Control Unit	CONNECTED
<input type="checkbox"/>	Wiring Connected Properly	CHECKED
<input type="checkbox"/>	Measuring Instruments	CONNECTED, ACTIVE
<input type="checkbox"/>	Prop Area	CLEAR
<input type="checkbox"/>	Personal Protection Equipment	APPLIED

Table 27: Test checklists

Range and Fail-Safe Checklist:		
<input type="checkbox"/>	TX Power	ON
<input type="checkbox"/>	Range Check Mode	ACTIVATED
<input type="checkbox"/>	RX Power	ON
<input type="checkbox"/>	Controls Working	CHECKED
<input type="checkbox"/>	Propulsion Arming Plug	INSERTED
<input type="checkbox"/>	Distance to Aircraft	ACCORDING TO TX MANUAL
<input type="checkbox"/>	Controls Working	CHECKED
<input type="checkbox"/>	TX Power	OFF
<input type="checkbox"/>	Controls in Fail-Safe Position	CHECKED
<input type="checkbox"/>	TX Power	ON
<input type="checkbox"/>	Controls Working	CHECKED

8 Performance Results

The chapter Performance Results describes aircraft performance characteristics of the first prototype and the final aircraft, which includes all the final subsystems like the motor, battery pack and folding mechanism.

8.1 Performance of Key Subsystems

8.1.1 Propulsion

Batteries: Both selected battery packs were tested at their average discharge current for the most demanding mission, which is Mission 2 for the 24 V 6000 mAh configuration and Mission 3 for the 25.2 V 8000 mAh configuration. For Mission 2 the average current is around 50 A which leads to a 25 A current per parallel wired array. Mission 3 demands an average current of 44 A, which leads to a 22 A current per parallel wired pack. Tests were terminated at cut off voltage of 0.9 V per cell. The results (Figure 50) obtained show the positive influence of the battery self heating on the voltage during the discharge.

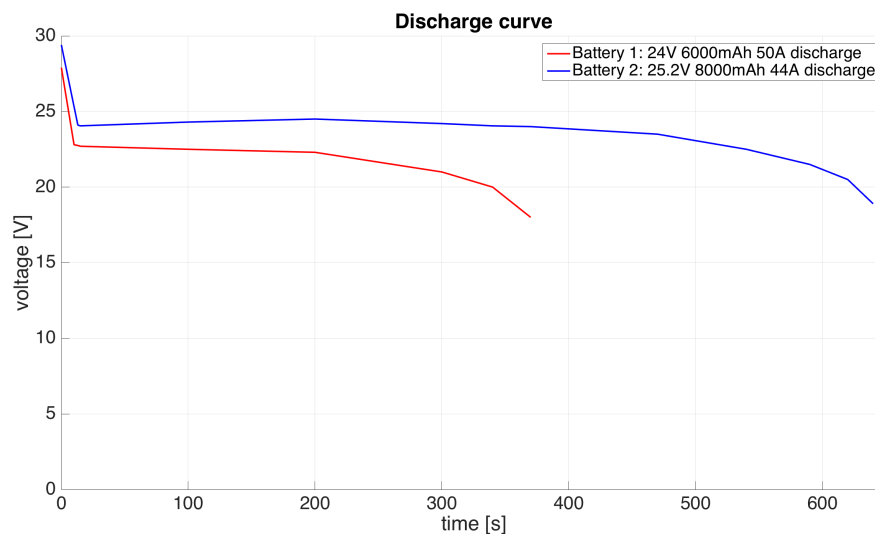


Figure 50: Battery discharge curves with different discharging currents

Motor and Propeller: The team chose the A50-12L Turnado V3 as motor for the aircraft. The most decisive factor for this choice was its high-power output and low weight. During the design phase pre-selected propellers, a 17x10" and 18x11" model, were tested on a motor test stand (Figure 51), of which both propellers are going to be used for the final design.



Figure 51: Motor testing

The maximum static thrust, the amount of current and the discharge rate were measured while using the selected battery configurations. The results for the static thrust with the different batteries can be seen in Table 28.

Table 28: Max. static thrust per battery/propeller

Propeller	Battery Pack 1 (M2)	Battery Pack 2 (M3)
17"x10"	16.86 lbs	18.21 lbs
18"x11"	18.66 lbs	20.68 lbs

8.1.2 Structural Tests

These tests were implemented to examine the strength and stability of the mechanical parts, with a focus on the wing structure and the folding mechanism.

Wing Tip Test: The wing tip test evaluated the aircraft’s ability to withstand multiple loads occurring during flight. It is also a test method which must be accomplished as part of the ground mission at the competition. To evaluate the stiffness of the prototype’s wing, this test was conducted under similar conditions in the institute’s laboratory. The aircraft was equipped with the maximum payload for Mission 3 and then lifted on both wing tips. For preventing subsequent damage to the wing, the loads were increased stepwise up to the final load of 14 dart rockets. The setup of the wing tip test with the second prototype of *Bobby* is shown in Figure 52.



Figure 52: Wing tip loading test of the final design aircraft

Folding Mechanism: The *jA Bobby* uses a folding mechanism to convert the wings into flight configuration. To ensure compliance with the competition regulations, this folding mechanism was evaluated and tested. A special focus on the development of this system was to reduce its complexity and to make it as reliable as possible. The prototype of the competition aircraft was then subjected to a folding stress test of several folding and unfolding cycles to examine the structure for any crack formation or any other signs of fatigue.

8.2 System Performance

The performance of the aircraft was validated by conducting live, timed simulations of the ground missions, the three different flight missions and a radio fail-safe check. The configuration of the aircraft used for the test can be seen in Table 29. The results of ground mission testing are documented in Table 30.

Table 29: Configuration of the final aircraft

Parameter	Specification
Battery Pack M1 & M2	40 x NiMH SC 3000 mAh
Battery Pack M3	42 x NiMH SC 4000 mAh
Receiver Battery	2 x NiMH 2700 mAh
Receiver Battery Control	Master BEC Boy 8A
Electric Motor	Hacker A50-12L
Speed Control	Roxyy BL9120-12 Opto
Propeller M1 & M2	17x10"
Propeller M3	18x11"
Empty Weight	8.74 lbs
Total Payload	16.99 lbs

Table 30: Ground mission test results

Activity	Time
Unfolding Time	10 s
Loading of Radome	4 s
Detachment of Radome	11 s
Loading of 4 Dart Rockets	11 s

A loading time test determined that the time required to run from the safe zone to the aircraft and load the M2 payload was 12 seconds. This time was assumed to be constant for each run. The M3 loading time was then timed by performing a timed trial ground mission. Initially, the time required to load a single dart rocket was 2 seconds. Flight tests with *Bobby* were performed to evaluate the performance of the aircraft and validate the performance predictions. The results indicated the performance predictions had been realistic. Further optimization steps and an increasing familiarity of the pilot with the system will improve system performance to meet or exceed the predicted performance.

Table 31: Flight test results for FM1

Flight Mission 1				Weight:
Lap	Average speed [ft/s]	Distance flown [ft]	Lap time [s]	Comment
1	69.71	2430.04	34.86	Ramp takeoff successful
2	74.71	2415.45	32.33	
3	75.51	2413.35	31.96	
Total:		7258.84	99.15	Time Below 300 s

Table 32: Flight test results for FM2

Flight Mission 2				Weight:
Lap	Average speed [ft/s]	Distance flown [ft]	Lap time [s]	Comment
1	66.38	2486.73	37.46	Ramp takeoff successful
2	67.96	2424.83	35.68	
3	69.33	2421.76	34.93	
Total:		7333.32	108.07	Time Below 300 s

Table 33: Flight test results for FM3

Flight Mission 3				Weight:
Lap	Average speed [ft/s]	Distance flown [ft]	Lap time [s]	Comment
1	53.66	2486.73	46.3	Ramp takeoff successful
2	55.69	2424.83	43.54	
3	57.35	2421.76	42.23	
4	58.23	2420.65	41.57	
5	58.69	2419.89	41.23	
6	59.01	2417.48	40.97	
7	59.76	2415.97	40.43	
8	59.57	2416.21	40.56	
9	59.32	2416.67	40.74	
10	58.21	2417.53	41.53	
11	58.70	2419.23	41.21	
12	57.74	2418.63	41.89	
13	56.48	2419.53	42.84	
14	56.02	2422.43	43.24	All Dart Rockets Dropped
Total:		33937.54	588.32	Time Below 600 s

8.3 Differences to Predictions and Improvements

The initially favored propulsion battery consisting of 36 NiMH cells did not perform sufficiently in terms of static thrust, so the team started adding cells to the battery until the desired performance was reached. The additional weight of the cells was taken into consideration for the required static thrust. The improvements resulted in the two mentioned battery configurations, one with 25.2 V and 8000 mAh and the other with 24 V and 6000 mAh. The aircraft showed better takeoff characteristics than expected, which can be explained by the negligence of the propeller stream influences on the lifting surfaces and conservative assumptions for the lift calculations.

Bibliography

- [1] Meyers, K. "Wing Cube Loading (WCL)," *SEFSD*, [online]. Available at: <http://www.sefsd.org/general-interest/wing-cube-loading-wcl/>. [Accessed February 2019].
- [2] joanneum Aeronautics Team, "Aircraft Design Report, 2015 AIAA DBF Competition", 2015
- [3] Müller, M., "eCalc" *Website* [online], Available at: <https://www.ecalc.ch/> [Accessed February 2019]
- [4] joanneum Aeronautics Team, "Aircraft Design Report, 2018 AIAA DBF Competition", 2018
- [5] Carpenter, P. (2003). *The Watts Per Pound Rule for Electric RC Planes*. [online] Rc-airplane-world.com. Available at: <https://www.rc-airplane-world.com/watts-per-pound.html> [Accessed February 2019].
- [6] Drela, M. (2019). *XFOIL*. MIT. Software. Available at: <https://web.mit.edu/drela/Public/web/xfoil/> [Accesses December 2018]
- [7] MATLAB R2018a. The MathWorks. Natick. 2014. Software. Available at: <https://de.mathworks.com/>. [Accesses November 2018]
- [8] Matthews, B. 2018. *Determining the size of flaps ailerons* [Online forum comment]. Message posted to <https://www.rcgroups.com/forums/showthread.php?3078160-Determining-size-of-flaps-aileron>
- [9] Standingford, D., "Optimal Lifting Surfaces," *Thesis submitted for the degree of Doctor of Philosophy in Applied Mathematics*, Universtiy of Adelaide, 1997, pp. 58–79.
- [10] Hoerner, S., Bosrt, H., "Fluid-Dynamic Lift," *Practical Information on Aerodynamic and Hydrodynamic Lift*, Vancouver, Washington 1985, pp. 66–69.
- [11] Hoerner, S., "Fluid-Dynamic Drag," *Practical Information on Aerodynamic Drag and Hydrodynamic Resistance*, Bakersfield, California 1965.
- [12] Deperrois, A., "XFLR5," *Website*, [online], Available at: <https://xflr5.com/xflr5.htm> [Accessed December 2018]
- [13] AIAA, "2018-2019 DBF Rules," *AIAA DBF Website* [Online]. Available: <http://www.aiaadbf.org/Rules/> [retrieved February 2019].
- [14] Dassault Systems, "CATIA V5R20," [online]. Available at: <https://www.3ds.com/de/produkte-und-services/catia/>